Use of interfaces for the formation of nanoparticulate thin films for various applications

Thesis Submitted to AcSIR

for the Award of the Degree of

Doctor of Philosophy

in

Chemical Sciences

By

Sagar Hindurao Patil

(AcSIR Roll No.: 10CC11J26081)

Under the Guidance of

Dr. Rajesh G. Gonnade

and

Dr. Kashinath R. Patil

CSIR-National Chemical Laboratory

Pune-411008, India

March 2016

सीएसआयआर–राष्ट्रीय रासायनिक प्रयोगशाला
(वैज्ञानिक तथा औद्योगिक अनुसंधान परिषद)
डॉ. होमी भाभा मार्ग, पुणे – 411 008. भारत
CSIR-NATIONAL CHEMICAL LABORATORY
(Council of Scientific & Industrial Research)
Dr. Homi Bhabha Road, Pune - 411008. India

Certificate

This is to certify that the work incorporated in this ***Ph.D. thesis*** entitled ***"Use of interfaces for the formation of nanoparticulate thin films for various applications."*** submitted by ***Mr. Sagar Hindurao Patil*** to Academy of Scientific and Innovative Research (AcSIR) in fulfillment of the requirements for the award of the Degree of ***Doctor of Philosophy***, embodies original research work under our supervision. We further certify that this work has not been submitted to any other University or Institution in part or full for the award of any degree or diploma. Research materials obtained from other sources has been duly acknowledged in the thesis. Any text, illustration, table, etc., used in the thesis from other sources have been duly cited and acknowledged.

Mr. Sagar H. Patil	**Dr. Rajesh G. Gonnade**	**Dr. Kashinath R. Patil**
(Research Student)	(Research Guide)	(Research Co-Guide)

Date: 15/3/2016

Place: Pune

Communications Channels
NCL Level DID : 2590
NCL Board No. : +91-20-25902000
Four PRI Lines : +91-20-25902000
FAX
Director's Office : +91-20-25902601
COA's Office : +91-20-25902660
SPO's Office : +91 20 25902664
WEBSITE
www.ncl-india.org

DECLARATION

I, hereby declare that all the experiments in this thesis entitled, "***Use of interfaces for the formation of nanoparticulate thin films for various applications***" submitted for the degree of ***Doctor of Philosophy*** in ***Chemical Sciences***, to the AcSIR-National Chemical Laboratory have been carried out by me at the Center for Material Characterization Division, CSIR-National Chemical Laboratory, Pune-411008, India, under the supervision of Dr. Rajesh G. Gonnade and Dr. K. R. Patil. The work is original and has not been submitted in part or full by me, for any degree or diploma to this or any other University.

Patil SH

Date: 15/03/2016

Mr. Sagar H. Patil.

Place: Pune

DEDICATED

TO

MY BELOVED FAMILY AND

RESPECTED TEACHERS

Acknowledgements

The completion of this thesis is credited to the support and encouragement of numerous people encompassing my family members, friends, colleagues and well wishers. At this point of accomplishment I am privileged to acknowledge all those people who made this thesis possible. It is a pleasant task to reciprocate to the ones who contributed in many ways to the success of this study.

First and foremost, I am extremely obliged to my guide(s) ***Dr. Rajesh Gonnade*** and ***Dr. K. R. Patil*** for being a constant source of inspiration, suggesting ideas, inspiring me for the development of logical understanding and providing me an opportunity to work on this interesting problem. His enthusiasm, sincerity and dedication towards work proved to be a self-motivator for me. I am obliged to him for showing interest in my academic as well as personal well-being. The art of writing manuscripts and to aspire for high impact factor publications is surely a gift inherited from ***Dr. K. R. Patil***. Apart from academics, he also inculcated in me the qualities required to become a good scientific manager.

I am short of words, to express my gratitude to ***Dr. S. D. Sathaye***, for his constant and tireless help in experimentation, analysis and source of innovative ideas. This Ph.D is an outcome of their conscientious efforts.

I would like to extend special thanks to My DAC members Dr. Prasad Bhagavatula, Dr. Nandini Devi, and Dr. C.V. Rode for their constant encouragements and suggestions during all my proceedings.

My special thanks to Prof. Alberto Coronos as well as Prof. Carlos Nieto De Castro and his family for giving me support when I was working with them in Spain and Portugal respectively. I am indebted to Dr. K. Sreekumar, Dr. S. Ogale, Dr. Krushnamurthy, Dr. H. Borate, Dr. C. V. Rode and Dr. Mrs. M. Shelke and their group for their resolute support during the whole course. I also extend my sincere thanks to Prof. S. W. Gosavi, Prof. S. K. Haram for constant support and encouragement during the research course. I would also like to extend my heart warming regards to the Head of the Department of CMC Prof. P.A. Joy and Director of NCL Prof. Ashwini Kumar Nangia.

I am obliged to all the staff at CMC, Dr. Mrs. S. D. Kulkarni Mr. R. S. Gholap, Mr. Shriniwas Deo, Ms. Arti Harle, Mrs. Santhakumari and Mr. Arup Gangopadhyay for constant encouragement and help.

I express my gratitude to Mrs. Rupali Waichal and Mrs. Pooja Mudellu-Kumbhar for Raman and AFM measurements. Mr. Anil Gaikwad is thanked for his help in SEM analysis and helping in my overall personal development.

I owe special thanks to my lab mates and friends Dr. Virendra, Mr. Babasaaheb, Mrs. Aarti Gaikwad, Mrs. Ashwini Bhirud, Mr. Rupesh, Dr. Bihag, Mr. Sandeep, Mr. Indrapal, Dr. Pawan, Dr. Dhanraj, Dr. Pradip, Dr. Bhausaheb, Mr. Gaikwad, Ms. Ekta, Mr. Shridhar, Mr. Sameer, Mr. Pravin, Mr. Atul, Dr. Manoj, Mr. Sanket etc. for unrelenting encouragement.

I extend my special appreciation to CSIR-NCL and UGC for their Research facility and financial help during the course.

I express my love to all my colleagues from Lisbon University, Portugal, specially Dr. Maria, Dr. Fernando, Dr. Murshed, Dr. Ana, Dr. Salome, and Mr. Luis for suitable research environment abroad. Also I feel very grateful for my colleagues from URV, Taragonna, Spain, especially, Dr. Daniel, Mr. Andry, etc. for great help in learning experimental physical chemistry.

I have no words to express my thankfulness to my family. Without their words of encouragement, support, love and patience, it would not have been possible for me to complete my Ph. D work.

Finally, I express my gratitude to all of them who have contributed directly or indirectly towards the completion of this masterpiece.

Sagar Hindurao Patil

List of Abbreviations

Abbreviation	Expansion
2-D	Two- Dimensional
CE	Counter Electrode
CNF	Carbon Nanofiber
CNT	Carbon Nanotubes
CP	Conducting Polymers
CTR	Charge Transfer Resistance
CV	Cyclic Voltammetry
CVD	Chemical Vapour Deposition
DCM	Dichloromethane
EDS	Energy-Dispersive X-Ray Spectroscopy
EDL	Electrical Double Layer
ECSA	Elctro-Chemical Active Surface Area
EDLC	Electrochemical Double Layer Capacitors
EIS	Electrochemical Impedance Spectroscopy
ESCA	Electron Spectroscopy for Chemical Analysis
ESR	Electrochemical Series Resistance
FESEM	Field Emission Scanning Electron Microscopy
FT	Fourier Transform
FTO	Fluorine doped Tin Oxide
FWHM	Full Width at Half Maximum
HOMO	Highest Occupied Molecular

	Orbital
HR-TEM	High-Resolution Transmission Electron Microscopy
IR	Infra-Red
LSV	Linear Sweep Voltammetry
LIC	Li-Ion Supercapacitor
LLIRT	Liquid-Liquid Interface Reaction Technique
NMP	N-Methyl-2-Pyrrolidone
PANI	Polyaniline
PEDOT	Polyethylenedioxythiophene
PPy	Polypyrrole
PT	Polythiophene
SAED	Selected Area Electron Diffraction
SEM	Scanning Electron Microscopy
SSA	Specific Surface Area
SLIRT	Solid-Liquid Interface Reaction Technique
TEM	Transmission Electron Microscope
TGA	Thermo Gravimetric Analysis
XPS	X-Ray Photoelectron Spectroscopy
XRD	X-Ray Diffraction

Table of Contents

Abstract

The fields of nanoscience and nanotechnology have provoked significant curiosity in the scientific organization. Solids in nanometer regime define a new group of materials exhibiting size dependant properties. Although, study on nanomaterials is centuries old, the current fever of nanotechnology is moderately determined by the ever shrinking dimension of devices in the semiconductor industry. It has been observed that all intrinsic properties of materials like mechanical strength, melting point, absorption, conductivity, magnetization etc. become a function of size. Nanoscience in general is concerned with study and manipulation of materials at a transitional scale that lies between bulk and isolated atoms. At nanometer scale, materials exhibit properties that are altogether different from the bulk as well as individual isolated atoms. This phenomenon has lead researchers to explore, design, utilize, construct and discover applications for these new sorts of materials. The last few decades have witnessed considerable surge in the understanding of these materials and their assembly. Quantum effects and surface to volume ratio dictates the optical, magnetic, electrical and structural properties for a material confined in nanometer dimensions. By virtue of their properties, nanoparticles possess a unique identity and enormous applications in the fields of electrochemical devices, catalysis, sensing, drug delivery, optoelectronic devices etc.

In order to explore novel physical properties and phenomena and realize potential applications of nanomaterials, the ability to fabricate and process nanomaterials and nanostructures is the first corner stone in nanotechnology. There are many methodologies coming under the classifications 1) top-down and 2) bottom-up approaches of synthesis of nanomaterials. Top-down processes are general extension of lithography. Bottom-up approach is known since historic times. Though materials with tailored properties can be produced, the nanometer scale possesses new challenges by virtue of its size. Doping which is a well-established phenomenon at macro scale becomes a formidable task in the nanometer regime, since self-purification is an inherent property of nanomaterials. To meet such challenges control over synthesis at atomic level is crucial.

The challenges in nanotechnology are 1) to overcome the huge surface energy that results from the enormous surface to volume ratio in nanomaterials and 2) to ensure all nanomaterials with desired size, shape, morphology, crystallinity, monodispersity, chemical composition and microstructure. To prevent nanomaterials and nanostructures from growth through either 'Ostwald' ripening or agglomeration as time passes, diverse methodologies have been studied. All these points are normally addressed by adding surfactants, capping agents during the synthesis of nanomaterials. Surfactants and capping molecules alter the optoelectronic structure of thus formed nanomaterials. Hence, a need to synthesize uncapped or surfactant-free nanoparticles becomes a pre-requisite. It has been foresaid that the properties of capped and uncapped particles will be different. The present thesis explores novel surfactant-free methodologies to make nanoparticles and subsequently, thin films of various inorganic semiconductors, metal nanoparticles and polyaniline nanocomposites. This thesis comprises of six chapters providing a systematic and coherent picture of the work done.

Chapter-1

This chapter emphasizes the need of making nanomaterials. Problems faced by the conventional silicon logic are briefly discussed with reference to the Moore's law and a short review of research methodologies developed till date towards the synthesis of nano-materials is presented. These methods are broadly classified into top-down and bottom-up approaches. The advantages and disadvantages of each approach have been summarized. The detrimental effect of surfactants/capping agents/ligands has been discussed. As many intended applications, require nanoparticulate thin films, a brief insight for the necessity of surfactant-free nanoparticles and their thin films is also put-forth.

Chapter-2

In this chapter a novel, facile, single step process is given for growing highly uniform few layer graphene nanosheets (FLGNS) thin films over a micrometer scale. Thin films are formed at liquid-liquid interface. The process is further extended to form monolayer graphene nanosheets (GNS). The films are characterized by Raman spectroscopy, Atomic force microscopy (AFM) and X-ray photoelectron spectroscopy (XPS). The results indicate that very few chemical and/or physical defects are introduced during formation of films. Further, an innovative single step method to form tin oxide (SnO_2) films at air-liquid interface is presented. A special feature of the method is that entire process is completed at room temperature. The film can be suitably transferred to the desired substrates by Blodgett technique. Characterization by various techniques such as XPS, TEM and energy dispersive spectroscopy (EDS) shows that the films are made up of uniform spherical, crystalline SnO_2 particles with the size in the range of 3-5 nm. Layer-by-layer (LbL) technique can be exploited to stack graphene and SnO_2 films alternately in a desired sequence, forming a stacked composite structure. The composite structure is subjected to characterization by XPS, FE-SEM, TEM and EDS. The results show that the structure consists of a stacking of predetermined thickness consisting of alternate layers of both the components. Such a structure is subjected to cyclic voltametry (CV) studies. The results show LbL grown SnO_2-GNS composites exhibit better electrochemical performance in terms of specific capacitance and cycling ability which are primary requirements for the supercapacitor application. The coating technique is simple, inexpensive and environmental friendly. A suitable explanation of the formation of both GNS and SnO_2 films is discussed. The proposed method extends the scope for production of high quality and defect free graphene nanosheets (GNS) and SnO_2 nanoparticulate thin films. The methods are particularly useful for LbL stacking of composite films of GNS and semiconductor nanoparticulate films.

Chapter-3

This chapter gives emphasis on the controlled synthesis of highly crystalline MoS_2 atomic layers which gives a solution to the challenges for practical applications of this emerging material. In this chapter, a facile method is demonstrated to synthesize crystalline mono-layer/few-layered MoS_2 thin films at liquid-liquid interface which can be suitably transferred on substrates. In this chapter, method of synthesis of large area (micrometer scale), monolayer/few layer and highly crystalline MoS_2 nanosheets in the form of thin films is narrated. The technique consists of intercalating bulk MoS_2 by H_2SO_4 and arranging its exfoliation process at the liquid-air interface. The film formed at interface could be transferred on a suitable substrate. A process for the synthesis of mono/few layered MoS_2 is discussed. The films are characterized for its crystal structure by XRD and for the morphology by SEM and TEM. MoS_2 nanosheet-graphene nanosheet (MoS_2-GNS) hybrid films have been developed by the application of layer-by-layer (LbL) technique. Cyclic voltammetry and other electrochemical characterization techniques reveal that the hybrid film electrode show specific capacitance of 282 Fg^{-1} at a scan rate of 20 mVs^{-1}. The as-obtained hybrid is robust and exhibits much improved cycle life (> 1000), retaining over 93 % of its initial capacitance. These results indicate that MoS_2-GNS hybrid is a promising candidate for the electrode material in supercapacitor applications.

Chapter-4

In this chapter we have given a method to form PANI nanoparticulate thin film containing highly uniform nanoparticulate size of 5 to15 nm by using modified LLIRT. Also a one step method is discussed to form a composite of polyaniline with 2D graphene nano sheets (GNS) and MoS_2 to form a robust supercapacitors by using Layer by Layer deposition technique. The composite hybrid films are formed with a well-defined architecture and tunable thickness on various substrates. The obtained hybrid films having interconnected network prevented graphene sheets from stacking

with one-another. The as prepared LbL composites are characterised by using X-ray diffraction (XRD), X-ray photoelectron spectroscopy (XPS) and high resolution transmission electron microscopy (HRTEM) which confirms uniform distribution of PANI nanoparticles over the 2D nanosheets in the composite. The electrochemical behaviour of composite was checked by cyclic voltametry (CV), electrochemical impedance spectroscopy (EIS) and galvanostatic charge discharge (GCD). The CV results indicated good capacitive behavior for PANI-GNS nanocomposites. The PANI-GNS showed the excellent improvement of specific capacitance (559 Fg^{-1}) over that of PANI-MoS_2 (413 Fg^{-1}) and PANI (185 Fg^{-1}).The stability of composite is greatly enhanced due to the LbL deposition approach. PANI-GNS showed the higher stability (94% retention of C_{sp}) that of PANI (67% retention of C_{sp}) and PANI-MoS_2 (93% retention of C_{sp}). These results are nothing but the proof of the concept that LbL composites boost the charge storage mechanism and gives robust supercapacitors. The excellent specific capacitance of 559 Fg^{-1} calculated from CV is consistent with the capacitance 549.2 Fg^{-1} calculated from charge-discharge measurement and show a very good cycling stability, is an indication that as-synthesized nanocomposite formed with the present technique is a potential candidate for super-capacitor application and in an energy storage technology in future. The excellent electrochemical performance of the composite as supercapacitor electrodes is due to the synergistic effects among the components in the composites.

Chapter-5

In this chapter, a process of formation of thin films consisting of Platinum nanoparticles (Pt NPs) with uniform size and distribution is discussed. The films are prepared at Liquid-Liquid interface. Apart from the usual substrates like glass, Si etc. the films were also deposited on the surfaces of MoS_2 thin film and graphene nanosheets (GNS), by using Layer-by-Layer (LbL) deposition technique to form Pt-MoS_2 and Pt-GNS composites respectively. The loading concentration of Pt NPs on MoS_2 and GNS can be adjusted by selecting the number and sequence of component

layers during LbL deposition. Pt thin films, Pt-MoS_2 and Pt-GNS nanocomposite thin films are characterized by transmission electron microscopy (TEM), high resolution transmission electron microscopy (HRTEM), energy dispersive X-ray spectroscopy (EDS), X-ray diffraction (XRD) and X-ray photoelectron spectroscopy (XPS). TEM results of the composites show that Pt NPs with sizes in the range of 1 to 3 nm are uniformly dispersed on MoS_2/GNS surface. The catalytic activity of Pt and Pt-composites for the reaction of methanol oxidation is studied by cyclic voltammetry and chronoamperometry. Electrochemical studies reveal that both Pt-MoS_2 and Pt-GNS nanocomposites show excellent electrocatalytic activity towards methanol oxidation. Pt-MoS_2 and Pt-GNS nanocomposite electrodes show excellent stability for reuse of catalyst. Probable mechanism of catalysis has been discussed. We propose that the similar architecture reported presently, would be promising for the synthesis of high performance catalysts for fuel cells, gas phase reactions, and other applications such as sensors.

Chapter-6

This Chapter gives an outline of the main observations and conclusions of the thesis spread in different Chapters. Initially, a concise introduction to the present thesis by emphasizing the core theme of the 2-D supported materials is presented. Later, conclusions and main findings of each Chapter are overviewed in separate sections. Final part is dedicated to the discussion on the future prospects of the present thesis. This includes importance of the present thesis in terms of materials evolved, device fabrication methodologies and their scope of improvements etc.

In summary, we have demonstrated a novel, facile approaches for surfactant free synthesis of 2D Graphene, MoS_2 and their LbL composites with semiconductor SnO_2 nanoparticulate thin films, nano-sized conducting polymer namely, polyaniline and Pt nanoparticles for the application in supercapacitors and electro catalysts.

Chapter-1

"Use of interfaces for the formation of nanoparticulate thin films for various applications"

This Chapter emphasizes the need of making nanomaterials. Problems faced by the conventional silicon logic are briefly discussed with reference to the Moore's law and a short review of research methodologies developed till date towards the synthesis of nano-materials is presented. These methods are broadly classified into top-down and bottom-up approaches. The advantages and disadvantages of each approach have been summarized. The detrimental effect of surfactants/capping agents/ligands has been discussed. As many intended applications, require nanoparticulate thin films, a brief insight for the necessity of surfactant-free nanoparticles and their thin films is also put-forth.

1.1 Introduction

The scientists are engrossed remarkably in attending the research and development in the field of Nanoscience and Nanotechnology during the last few decades. The advancement of nanomaterials science is quite fast. This Chapter gives an impending glimpse of the world of nanomaterials. The Chapter begins with the introduction to the advancement in material science offered by nanomaterials. The Chapter covers the difficulties faced by the conventional silicon based technology in light of the Moore's law. Additionally, the Chapter presents a short review of research methodologies of the synthesis of nanomaterials till date. The methods are broadly classified into top-down and bottom-up approaches. The top-down approach contains techniques like lithography, pulsed laser deposition, plasma synthesis etc. The bottom-up approach mainly consists of chemical procedures like synthesis by precipitation, micelles, reverse micelles, low temperature wet chemical synthesis, sol-gel technique etc. The advantages and disadvantages of each approach have been summarized. The process of use of surfactants to avoid aggregation of particles

sometimes becomes detrimental in several applications. It is a major disadvantage in some peculiar systems and hence discussed by giving examples. For many intended applications like sensors, solar cells and supercapacitors, nano-particulate thin film fabrication is a pre-requisite. Thus, a brief perception for the necessity of surfactant-free nano-particles and their thin films is also put-forth.

1.1.1 Nanomaterials

Nanomaterials are defined as solids having dimensions in the nanometer regime. In short, nanomaterials form a special class of materials that lie in the domain between two extremes i.e. bulk solids and molecules. Solids and molecules have been studied and understood quite well, thanks to their stability; however, nanomaterials which are relatively unstable, exhibit properties that are entirely different from these two classes. The properties of these materials are characterized by a specific length scale (less than the mean free path of electron), usually in nanometer dimensions. It is usually below ~100 nm. If the physical size of the material is reduced below this length scale, it's all properties like, mechanical, thermal, optical, magnetic and conducting etc. change and become sensitive to its size and shape. The reason for the size dependent properties arises from extremely high surface-to-volume ratio of nano-material particles.

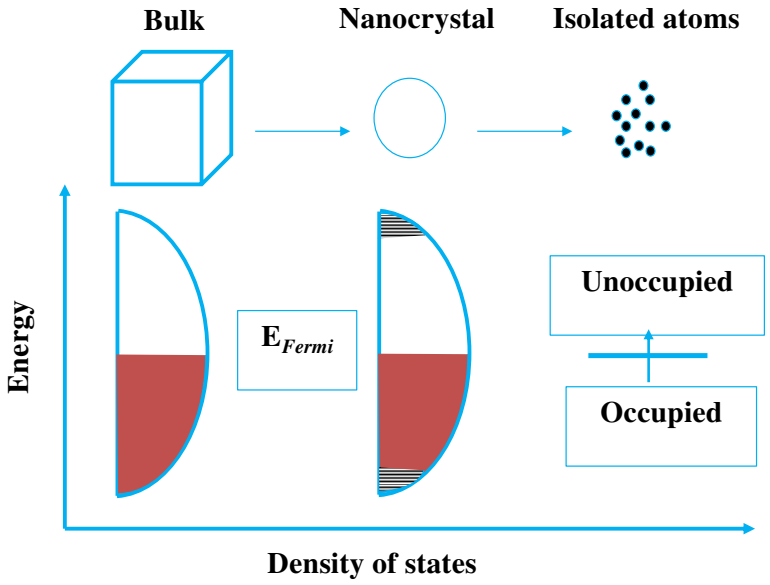

Figure 1.1. Schematic representations of changes in density of states, in case of the bulk metal, Nanocrystals and isolated atoms.

The number of surface atoms increases with decreasing particle size. In other words, nanomaterials have large number of atoms on their surfaces as compared to those in their bulk counter-part materials. The invention of special properties of nanomaterials by using various techniques and exploiting their usefulness by controlling sizes, morphologies etc. has been enlarged the scope of applications in various fields like mechanical, thermal, optical, magnetic, electronic etc.[1] Due to such size dependent physicochemical properties, nanomaterials have got potential applications in nano-sensors and nano-devices, biomedical application, novel catalysts, therapeutic uses and opto-electronic devices.[2]

Theoretically, reducing the particles sizes to nano-range have a profound effect on the energy levels spacing as the system become more confined. This effect can be explained by the 'particle in a box' model, in which energy separation between the adjacent levels increases with decreasing particle dimensions. Figure 1.1 represents a schematic diagram of changes in density of states, in case of metals, for bulk and nanocrystals (Figure 1.2). Band edges have low density of states which decreases further as the size of the particle reduces.

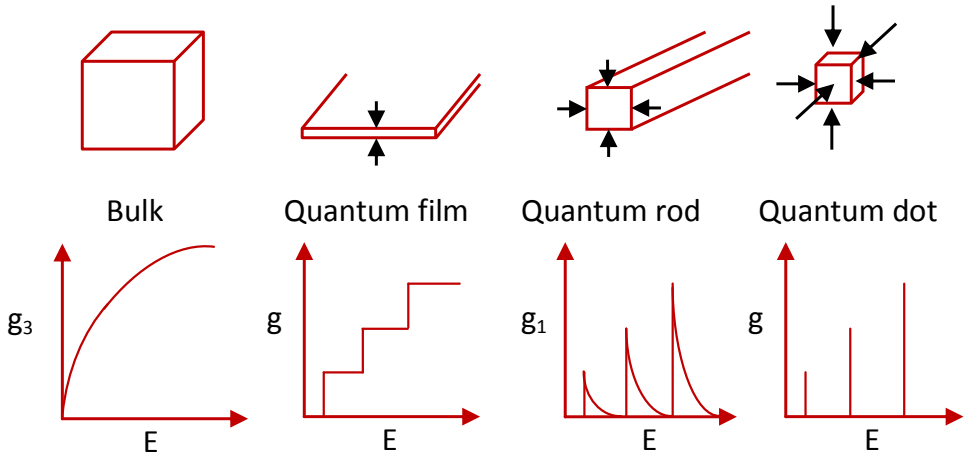

Figure 1.2. Idealized density of states versus energy for three, two, one and zero dimensional materials.

For metal nanoparticles, the relevant energy levels spacing is very small and hence in order to open up a gap between the electronic states, one should go to very small sizes (below 2 nm) for which the quantum confinement effect is observed.[3] It would be appropriate to discuss the reasons for observing so many new features of

material properties by merely reducing the particle size in nano-meter range. In fact, 'particles of materials in nano-meter range' is an unstable phase of the materials and it is the main cause of lack of research of nanomaterials in earlier developments of chemistry. Obviously, if nano-materials are to be studied, special techniques are needed to stabilize the materials. Some methods known to us from the applications of these materials in ancient times such as stabilization of nanomaterials by embedding it into glass, those get stabilized. This suggests stabilization of nanomaterials by capping or using some stable phase, by this technique Faraday prepared a very stable colloidal gold solution consisting of nanoparticles. Similarly electrical charge on particles surface can also be used to stabilize nanoparticles. Apart from these methods, particle growth can be restricted by steric hindrance, therefore, formation of sols/gels also can stabilize the nanomaterials.[4] It is known that formation of materials in 'confined' space is another method for stabilization of nanoparticles. The pores of zeolites or other porous materials are used to prepare nanomaterial; it gets stabilized as growth is restricted to the space within pores.

1.1.2 Nanoscience and nanotechnology

The nanomaterials with reduced dimensions are neither bulk solids nor like atoms or molecules. Their electronic structure differs from bulk solids and atoms or molecules. In this intermediate size regime, nanomaterials have larger percentage of atoms on their surfaces as compared to those in the interior than the similar percentage observed for corresponding bulk solids. The surface atoms are usually very reactive and are also responsible for some surface related properties. As mentioned above, nanomaterials consist of an unstable phase of a material and therefore its inherent energy structure and consequently basic properties differ from those of their bulk counterparts. The science dealing with all such materials is known as *Nanoscience*. Nanoscience is the learning of exploitation of phenomena of nanomaterials of which physical, chemical and biological properties are significantly different from those displayed by an atoms or bulk materials. This has led to a new challenge for scientists to investigate and study the nanomaterials with novel properties as well as applications in new technology. Thus, *nanotechnology* is the design, production, utilization and application of functional structures, devices and systems by controlling shape and size of materials at the nanometer scale.[4] Last few

decades have witnessed a tremendous growth of nanoscience and nanotechnology and considerable work has been carried out to understand nanomaterials and their assemblies and particles.[5]

1.1.3 Usefulness of nanomaterials

In the nanoscale regime, strictly, neither the laws of quantum chemistry nor classical physical chemistry uphold. A very strong chemical bonding leads to extensive delocalization of valence electrons in nano-materials, and the extent of delocalization is a function of size of the particles. This effect when considered along with structural changes can be explained the size dependent chemical and physical properties. Of late, it has been confirmed that a host properties such as magnetic,[6] optical,[7] melting point,[8] specific heats[9] and surface reactivity[10] are shape and size dependent in the range of nano-scale. Additionally, when nanomaterials are incorporated into host bulk materials forming composites, the resulting macroscopic solids, in some cases, display improved properties; for example, the improved plasticity.[11]

It is indisputable, that a new field of interdisciplinary science has born. The multitude of possible combinations of two, three or more materials with varying particle sizes being considered for various applications is mind blowing. It is clear that almost infinite number of possibilities of maneuvering the properties sprout-up in the nano-scale regime. This new field of clusters/nano-phase materials forms an interdisciplinary field consisting of chemistry and physics which touches upon various areas like electronics, biology, astronomy, mathematics and engineering.[6]

Additionally, it can also revolutionize various fields namely, information storage, refrigeration, chemical/optical computing, ceramics and insulators, harder metals, film precursors, solar cells, environmental remediation, water purification, destructive adsorbents, catalysts, sensors, defect-tolerant chemically assisted architectures, nanostructured electrodes, improved polymers, self-cleaning and unusual coloring paints, smart magnetic fluids and better batteries etc.[6]

1.1.4 History of nanomaterials

The first scientific paper on colloidal gold was published in the 19th century by Michael Faraday.[12] Colloidal gold sols have been studied comprehensively before the development of nanoscience and nanotechnology.[13,14] The treatment of arthritis with colloidal gold has been well-known.[15] The interaction of colloidal gold with spinal fluid of patients has been influential in disease diagnosis.[16] What has changed of late is an outburst in our ability to image, engineer and manipulate systems in nanometer regime. Figure 1.3 shows a most famous historical use of Au nanoparticles for coloring the glass and gold nanoparticles synthesized by M. Faraday.

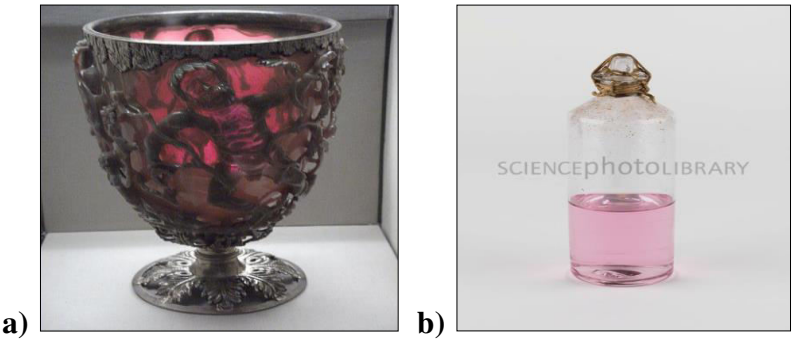

Figure 1.3. (a) Lycurgus Cup, glass, 4th century, gold and silver nanoparticles, dispersed in colloidal form, are responsible for the dichroic effect. Source: https://en.wikipedia.org/wiki/Lycurgus_Cup (b) Gold nanoparticles synthesized by M. Faraday, Source: http://www.sciencephoto.com/media/517115/view.

What is really interesting and new about nanotechnology is the amalgamation of our capability to observe and manipulate matter on nanoscale along with our understanding of atomic interactions. The continued decrease in device dimensions follows Moore's Law[17] predicted in 1970 which is illustrated in Figure 1.4. However, scaling up of number of devices leads to exponential increase in the off-currents in a metal-oxide-semiconductor field-effect transistors (MOSFET),[18] which could have become a cause of 'failure' of Moore's law. However, now it is predicted that nanomaterials might allow maintaining the trend defined by Moore's law. The invention and development of Scanning Tunneling Microscope (STM) in the early 1980s[19] and further advancement in probe microscopy such as Atomic Force Microscopy (AFM)[20] have unleashed new possibilities of material characterization and manipulation at nanometer scale.

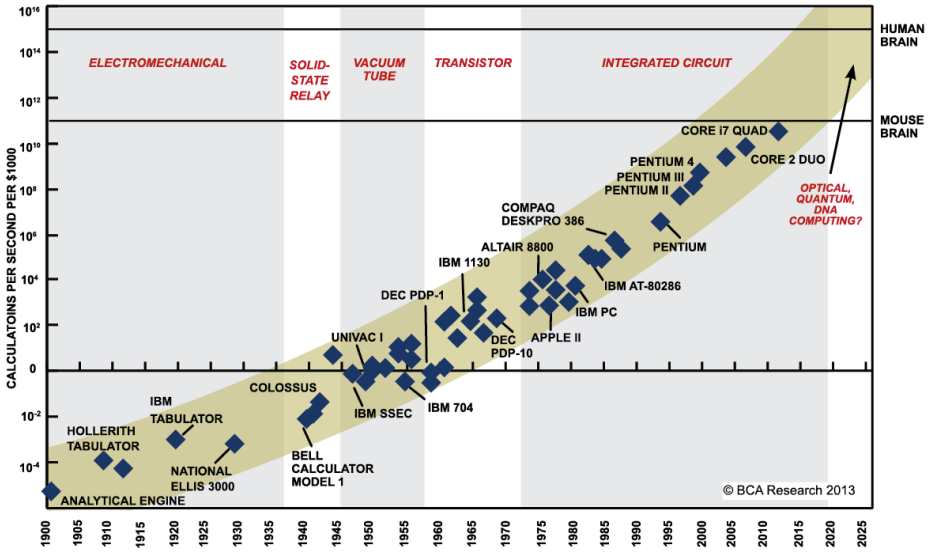

Figure 1.4. Moore's Law predicted in 1970. (http://www.extremetech.com/wp-content/uploads/2015/04/MooresLaw2.png)

Furthermore, characterization techniques like Transmission Electron Microscopy (TEM), Scanning Electron Microscope (SEM), Raman spectroscopy etc. allow investigating the intricate details of the sample down to atomic scale. All these developments are complementary to the enhanced knowledge of chemistry and physics of nanomaterials leading to the growth of nanoscience and nanotechnology.

1.1.5 Methods of synthesis of nanomaterials

Methods of synthesis and assembly strategies of nanoparticles can use precursors either from liquid, solid or gas phases by considering the thermodynamics, energetics and kinetics to obtain stable nanostructure with a desired phase and morphology required for its application. The varieties of techniques that are mainly classified in top-down and bottom-up approaches that are schematically illustrated in the following Figure 1.5. The bottom up approach of nanomaterials synthesis, initially forms the nano structured building blocks (nanoparticles) and then assemble those into the final material.[21] However, the real challenge in this approach, is to stabilize the final phase because, surface energy minimization leads to particle size growth. Therefore, it is common practice to obtain the final form of materials, dispersed in a state of matrix in solution/liquid/composite/glassy form.[22] The alternative approach is to stabilize the particles on a substrate by restricting their lateral movement required

for their aggregation/growth. In other words, it amounts to stabilize the nanomaterial on a substrate in a thin film form.

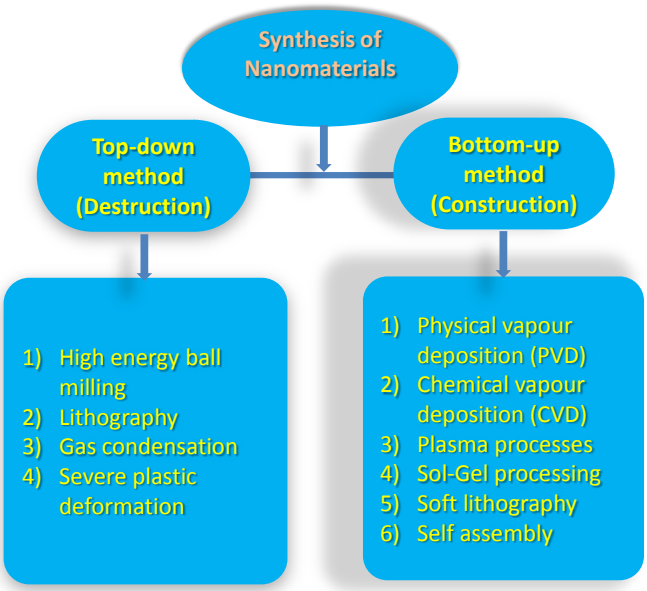

Figure 1.5 Methods of synthesis of nanomaterials.

There are enumerable techniques to convert solid/liquid precursors in to gaseous phase and allow those to nucleate and grow on the substrate; however, these techniques are usually energy intensive; and concomitantly prove to be unsuitable for large scale production. The Top-down approach is obviously 'energy intensive' as one is going from stable to neo-stable phase. Also, the problem of stabilization of nanophase persists and therefore this approach is less popular as compared to bottom-up approach.

1.2 Thin Films

As described above, the stabilization of nanomaterial on a substrate is very convenient, apart from other advantages such as less material processing, low energy requirement, large scale production, large scale device integration etc. Therefore, research in thin films of nano-materials has blossomed in to a separate branch in nano-science. A thin film of a liquid or solid can be defined such that one of its linear dimensions is very small in comparison with the other two dimensions. Usually one classifies thin films (arbitrarily) into: thick films (D > 1 micrometer, D: film thickness) thin films (D < 1 micrometer). The history of thin films begins, perhaps,

with the report by R. Boyle, R. Hooke, and I. Newton in 1650 on interference colors of thin liquid film on a liquid surface (oil on water). However, the research in thin solid films really got momentum after the developments of the technique of electrochemical deposition by M. Faraday in 1850.[7] Since then; many techniques are developed to grow thin films of solids. The real boost to the research came from the development of analytical techniques in optics, electron microscopy, diffraction techniques etc.

1.2.1 Methods of formation of thin films

Various methods of formation of thin films have been reported so far. Depending on the basic route, the methods are classified in to two major parts, namely, physical methods and chemical methods. The detailed classification is discussed in Table-1. Physical methods involve sputtering and evaporation techniques, both of which require higher energy inputs in the form of electricity, heat, etc. Moreover, vacuum is a "must" for above techniques which brings several limitations and make those techniques expensive. Chemical route of formation of thin films is further divided into gas phase and liquid phase. Several techniques like thermal evaporation, chemical decomposition are available for thin films deposition on a substrate. The evaporation of source materials or decomposition of precursor and allowing products to get condensed on substrate can be brought about by using several types of energy sources like heat, electricity, plasmas, laser or photons. In general the growth process of thin films exhibits the following features,

1. Thin films of all materials grown by any deposition technique starts with a random nucleation process followed by growth stages.

2. Nucleation and growth stages depend on various deposition conditions, such as growth temperature, growth rate, or nature of the material and the substrate and its structure.

3. The nucleation and growth parameters lead to peculiar film microstructure, associated defect structure, orientation and film stress etc.

Table 1.1. Physical and chemical methods for thin film formation.

PHYSICAL		CHEMICAL	
Sputtering	**Evaporation**	**Gas Phase**	**Liquid Phase**
Glow discharge DC sputtering	Vacuum evaporation	Chemical vapour deposition	Electro-deposition, polymer assisted deposition (PAD)
Triode sputtering	Resistive heating evaporation	Laser chemical vapour deposition	Chemical bath deposition, (CBD)/Arrested precipitation technique (APT)
Getter sputtering	Flash evaporation	Photo-chemical vapour deposition	Electro less deposition
Radio frequency sputtering	Electron beam evaporation	Plasma enhanced vapour deposition	Anodisation and Liquid phase epitaxy
Magnetron sputtering	Laser evaporation	Metal-organic chemical vapour deposition (MOCVD)	Sol- gel, Spin coating, Ion beam sputtering, Spray-pyrolysis
Ion beam sputtering			

Film composition, crystal phase and orientation, film thickness, and microstructure, are the basic properties of films, which can be controlled by the deposition conditions. Some unique features like quantum size effects, impact of strain, consequential multilayer aspects that cause variety of proximity effects are observed in thin films and cannot be realized in bulk materials.[23]

1.2.2 Physical techniques used for thin film formation and their peculiarities

1.2.2.1 Vacuum evaporative technologies

The substance of which a thin / ultrathin film is to be deposited is generated in vapour state by boiling, sublimating or vaporizing by giving sufficient energy inputs through heating, electron beam bombardment, lasers or any other energy source.

Thereafter the vapours are transported to substrate with a minimal chemical change occurring in the substance; finally, the vaporized substance is allowed to condense / deposit on substrate surface such as glass/ quartz plate, silicon wafer etc.

Peculiarities

The process needs high vacuum. Some chemical changes in substance composition are quite common such as nonstoichiometry or contamination from source container, etc. For the uniform and adherent films to be obtained the number of parameters are large and therefore process monitoring and control is needed. Molecular beam epitaxy which is an improved technology over vacuum evaporation is mainly used for growing single crystalline films (very ordered films) on single crystal substrates. The cost and number of parameters increase many folds. The operation is complex and throughput is very low. [24]

1.2.2.2 Glow discharge technologies (Sputtering)

The ejection of surface atoms from an electrode surface by momentum transfer from bombarding ion is called sputtering. In other words, during sputtering process, source of electrode material in vapor state is made available, which is used for thin film formation. There are various methods in which basic process is modified. AC sputtering, bias sputtering, magnetron sputtering are often used as modifications.

Peculiarities

The main drawback of sputtering is the contamination problem. Furthermore, the equipment is complicated and very costly.[23, 24]

1.2.2.3 Plasma processes

Some chemical reactions are accelerated in the presence of bombarding reactive ions. Therefore, the electrode material (metal) in presence of gases like O_2, N_2+H_2, CH_4 form a glow discharge thus generating a film of metal oxide, carbide, nitride on the substrate surface. The plasma can be generated by means of discharge in vacuum, electron bombardment, cyclotron resonance etc.

Peculiarities

The high cost of the equipment makes the process more expensive. Also limited number of reactions can be carried out to form thin films by this method.[23, 25]

1.2.3 Chemical methods used for thin film formation and their limitations

1.2.3.1 Sol-gel method

Conglomerates of molecule or atoms when stabilize in a suspended state in an aqueous liquid is called sol. These conglomerates or suspensions can be destabilized to generate aggregated particles or homogeneous gel by changing the conditions of solvation or suspension in sols. If the said molecular or atomic conglomerates are required to be deposited in the form of uniform films during gelation, a substrate, glass plate or quartz plate is dipped in a sol and drawn out. A thin coating of gel is formed. The substrate is then dried. The heat treatment of substrate leads to desired coating.

Peculiarities

The required conditions of sol stabilization and gelation are very critical. Also, thickness control is difficult. During the drying of gel and post deposition heat treatment, large volume changes bring about cracks in gel material and therefore it is difficult to get homogeneous, uncracked films.[26]

1.2.3.2 Chemical vapour deposition

In this method, precursors constituents in vapour phase are made to react near or on the substrate surface where the solid product is obtained in thin film form. CVD is versatile and flexible technique in producing variety of products (metals, semiconductors, and insulators, oxides, sulphides, selenides etc.) in thin film form. Metal organics are very convenient for CVD application as relatively low temperatures can transform them in vapour phase compared to pure inorganic compounds. This property is used to modify CVD called MOCVD. For increasing the reaction rates, other energy sources, assistance is taken to carry out reactions. The lasers, photons (light) are utilized for this purpose.

Peculiarities

Although the chemistry part of CVD appears to be simple, the monitoring of large number of parameters is needed to achieve reproducible films of good quality. The process, therefore, becomes technically complicated and critical. Also, thickness control of the film is difficult.[23, 24]

1.2.3.3 Spray pyrolysis

The "atomised" droplets of the solution are spread on hot substrate where pyrolysis takes place, leading to the formation of film on the substrate surface. Although versatile, this method is not useful for making ultra-thin films.[27,28]

1.2.3.4 Spin on method

In "spin on" method of depositing thin films, a drop of solution or sol is placed on rotating substrate. By centrifugal force, the solution /sol is spread on the surface of the substrate where solute separation/gelation reaction takes place as explained in the sol-gel technique. Further heating the substrate, converts the gel film in to desired film.

Peculiarities

The method can be used only for specific applications. Also, very thin film in submicron range cannot be deposited by this method with uniformity and continuity.[29]

1.2.3.5 Langmuir Blodgett method

In this method, a desired quantity ($1x10^{-5}$ to$1x10^{-4}$ M) (so as to form a mono-layer) of a solution of film forming materials such as fatty acids C_nH_{2n+1} COOH or amines C_nH_{2n+1} NH_2, dissolved in volatile solvent such as benzene, chloroform, or carbon tetrachloride and then it is delivered on a known area of clean water surface held in Langmuir trough (rectangular or circular) fitted with film pressure balance. The schematic of this method is shown in the Figure 1.6. These materials form monomolecular films at air-water interface. On lateral compression of the film with the help of barrier or oil piston (such as oleic acid), condensed solid phase is obtained which can be transferred on the substrate by dipping and withdrawing it under lateral

constant pressure at a fixed slow rate. So was the original development of monolayer formation of fatty acids.

In the subsequent modifications of formation of ultra-thin films of inorganic materials like oxides, chalcogenides, etc, the soluble metal salts are added in aqueous subphase. It allows the cations/ anions to get attached to the acid/or amine groups of spread solute in organic solvent on the surface. The monolayer is then deposited on to a solid substrate such as glass plate/ quartz plate/silicon wafer etc. The deposited films are then thermally treated/decomposed (500 -900^{o}C) to get stable ultrathin desired films. For every withdrawal or dipping of the substrate one monolayer is deposited. Usually the dipping or withdrawal is effective under constant surface pressure (15 to 35 dynes/cm.).

The nature and the amount of the species deposited from the aqueous subphase depend on deposition condition such as concentration, pH, rate of dipping and withdrawal, deposition pressure etc. By varying the deposition parameters the optimal condition for the deposition of metal ion is obtained. The deposited films are then thermally treated/decomposed (500 -900^{o}C) to get stable ultrathin desired films. The thickness of the film can be controlled by number of monolayer deposited. LB films are formed when amphiphilic molecules like surfactants interact with air at an air–water interface.[30]

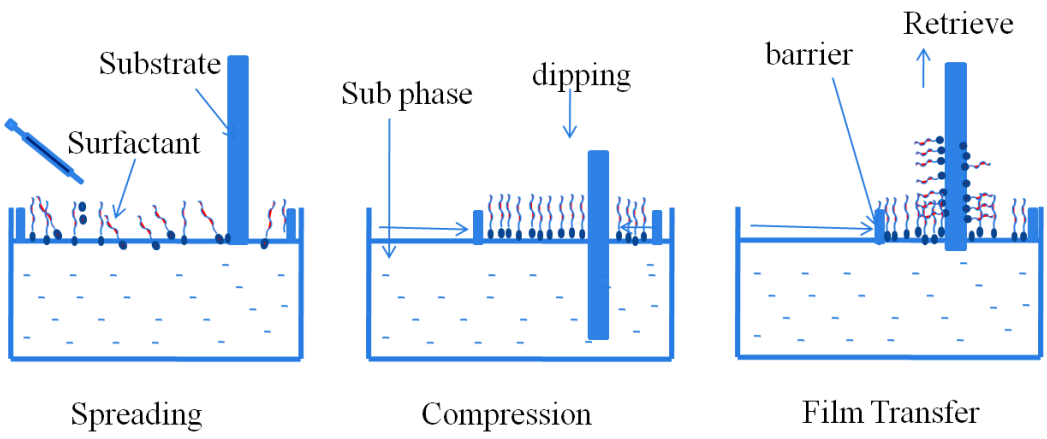

Figure 1.6. Schematic representation of hybrid film deposition process by the Langmuir–Blodgett technique.

Peculiarities

Only limited number of cation or anions could be brought in the film to react and to give desired product. Also, in the post deposition treatment, the long chain carbon containing part is to be removed mainly by burning. This leaves some chances of 'C'(carbon) contamination in the films. Also, the chemical reduction of the film material by carbon during heat treatment is possible.[31]

The section **1.2.3** described above, forms a background to emphasize the importance of the developments reported in this thesis. The general observations from the above description, it is quite clear that there is no exclusive technique which becomes 'ideal' for the growth of materials of interest in nano-science and nano-technology. Also, with the developments, the requirements of material thin films change and therefore, new developments in material preparation in general and thin film formation in particular are well acknowledged forever.

Also, other scientific and related points of concern must be in our minds during the development process are; 1) the disadvantage of dispersing agents/capping agents used in thin film formation of nanomaterials should be avoided to the maximum extent, 2) The methods of formation are preferred to be minimum cost to the possible extent, 3) To take advantages of earlier developments related to the present work, 4) Use of chemistry should dictate the developments, to justify the background of researchers and 5) The research be relevant to present day scientific developments.

1.2.4 Importance of making thin films of nanomaterials at interfaces

Nanoparticles anchored to surfaces in the form of film are considered to be important because of their potential use in nanodevices. A liquid-liquid interface offers potential to synthesize nanoparticles, as well as casting them into a film. At a liquid-liquid interface, the particles are highly mobile and rapidly achieve an equilibrium assembly. The organization of nanoparticles in a thin film form is often necessary to render those in functional and operational devices. This method involves the reaction of an inorganic/organometallic reactants dissolved in the immiscible organic layer/aqueous layer with a reducing/sulphiding/oxidizing agent dissolved in

the aqueous layer/organic layer leading to desired end product at the interface. The material formed at the interface corresponds to an ultrathin film consisting of closely-packed nanocrystals coated with the organic species present at the interface. The novelty of this method is that it involves a finite growth rate of the ultrathin nanocrystalline film with controllable parameters such as temperature and concentration.

The nanocrystalline film obtained at the interface can be easily transferred onto a solid support such as mica, quartz, glass or a polymer film. With appropriate choice of reactants, a variety of nanocrystalline films can be fabricated. This basic development can be suitably modified to make thin films of present day interest by choosing appropriate precursors/reactants and exploiting liquid-liquid interface as medium of formation. Some of the typical results obtained by this method are presented in successive Chapters to demonstrate its adaptability.

The liquid-liquid interface reaction technique is suitable for preparing films of many metal and metal compounds nanoparticles. For practical applications in the field of electronics, materials in the thin film form are desired. Hence, efforts have been made to design methodologies for synthesizing many materials into thin films.[32, 33] Semiconductor materials, mainly in the thin film form, find applications in the microelectronics, photovoltaic industry. It will be appropriate to state that all nanomaterials need to be processed in the form of thin films for applications in nanodevices. Moreover, the science of thin films is exciting as it offers properties of materials different than their bulk counterparts.[34, 35] The Interface between two immiscible phases (solid, liquid or gaseous) of matter is always of the order of few nanometers. Hence, it seems to be theoretically ideal to produce nanoparticulate thin films by exploiting the confinement provided by the interface(s). Moreover, the interface(s) is always homogenous.

1.2.5 Applications of thin films

Main fields of application are computer electronics, commercial electronics, medical electronics, space technology and energy conversion (solar cells). Optical applications of metal and dielectric films are filters, reflection coatings, optical wave guides for opto-electronic communications etc. It is, however, not only the film

structure but also the limited thickness determines the physical properties. Therefore, the geometric anisotropy and size effects also need to be studied.

In the following Chapters, we will discuss methods of film deposition with reference to basic physical phenomena, procedure of film formation, specific properties and their technical relevance.

1.3 Interfaces

The region in space where the chemical compositions as well as the physical and mechanical properties are uniform throughout is called as a phase. The homogeneous region that separates two immiscible phases is termed as interface.[32] The interface is endowed with specific physical and chemical properties which differ from those of the constituent phases. The ability of the interfaces to produce materials with tailored properties and metastable structures has attracted scientists. Interfacial interactions are the main driving force which makes atoms at the interfaces prone to react with the surrounding species and to produce materials with useful properties. In broad sense, on considering three phases of matter viz., solid, liquid and gas, we immediately arrive at three combinations of interfaces: the solid-liquid, the solid-gas, the liquid-gas interface. Interfaces are also formed between two immiscible liquids or two solid phases. The interface between two immiscible liquids is termed as liquid-liquid interface e. g. the interface between water and oil. The interface between two solids is called as solid-solid interface. Solid-solid interfaces remain crucial as far as mechanical behavior of materials is concerned. As all gases mix with each other, no gas-gas interface exists.

Interfaces that are formed between different phases of matter have been listed in Table 1.2 and 1.3. There are 5 types of interfaces possible as listed below.

1) Liquid-Liquid interface
2) Liquid-Vapor or Liquid-Gas interface
3) Liquid-Solid interface
4) Solid-Solid interface
5) Solid-Gas interface

Interfaces and colloids are often discussed together. Colloids are dispersed systems with one phase having dimensions of the order of 1nm to 1 micrometer. Colloidal dispersions are macroscopically homogenous, but not microscopically.

Table 1.2. Interfaces formed between different phases of matter

Medium		**Dispersed Phase**		
		Gas	**Solid**	**Liquid**
Continuous Phase	**Gas**	None	Solid aerosol (e.g. Smoke, Cloud, Air particulates etc.)	Liquid aerosol (e.g. Fog, mist etc.)
	Solid	Yes (e.g. Solid Foam, Areogel etc.)	Yes (e.g. Solid Sol, Canberry glass etc.)	Yes (e.g. Gel, Agar etc.)
	Liquid	Yes (e.g. Foam)	Yes (e.g. Sol)	Yes (e.g. Emulsion)

Colloids consist of grains or droplets of one phase dispersed in the matrix of another phase. Though, there exists only five types of interfaces, ten different types of dispersions can be classified based on continuous interface (dispersing matrix) and dispersed interface (grain or droplets). Materials formed at various interfaces have normally high surface area and therefore higher surface to volume ratio. Such a large surface area can be exploited for many exciting applications, for example in the field of catalysis. This is also the main reason why interfacial phenomenon forms one of the basic contributor in nanoscience and nanotechnology and many inventions in the new area of surface science. Since the research in composites is a 'hot topic' presently, interfaces research has got prominence. There are two fundamental reasons appear to be a driving force for research in this area of interfacial or colloidal science. The first reason is, it would lead to better understanding of the natural phenomena revealing the behavior of atoms/molecules in non-equilibrium state at surfaces of the phases. For example, in biology the surface tension of water leads to formation of lipid membranes.

Many natural foods like milk, butter etc. are colloidal emulsions and their properties are dominated by the liquid-liquid interfaces. The second reason is; there are many technological applications based on interfacial and colloidal science. Flotation in mineral or paper processing is one such example. Use of detergents in the washing of clothes is day-to-day experience. Often the synthesis of new materials such as composite materials involves processes at interfaces.

Table 1.3. Interfaces and their widths

Phases	**Types and Example**	**Width of interface**
Gas-Gas	No interface possible	-
Gas-Liquid	Liquid surface, body of liquid exposed to gas	0-15 Å
Gas-Solid	Solid surface, Table top	<10 Å
Liquid-Liquid	Liquid-liquid interface, Emulsion	10-50 Å
Liquid- Solid	Liquid-solid interface, Suspension	<10 Å
Solid-Solid	Solid-Solid interface, Powder particles in contact.	-

Thin films on surfaces like latex films, paints and coatings are often dominated by surface effects. The flow behavior of granular and powder media is often determined by surface forces. In triobiology, wear is reduced by the surface phenomenon which is again a surface behavior.

The interfaces being a few atoms thick have dimensions comparable to nanostructures. If the material is generated at interface, it assures realization of particle size in nm range, at least in one dimension (1D). This can be considered as an application of synthesizing nanoparticles by limiting the reaction to a confined space as mentioned earlier. Hence, dynamic processes occurring across the interface play a key-role in the growth of nanostructures. The transportation of ions, as well as, atomic species across the interface and its surroundings is determined by the organic-inorganic interface and has a major effect on the growth dynamics of nano-crystal.

Engineering of these interfaces in a precise manner remains a major challenge. If one can achieve precise control over these interfaces, the formation of nanostructures with desired morphological, structural, magnetic, electrical and optical properties as well as their combinations may be possible. Careful design of interfaces between different forms of condensed matter can be successfully exploited to synthesize a series of tailored nanostructures

1) The gas-liquid interface can be used to agglomerate or to nucleate nano-crystals.
2) The solid-solid interfaces would possibly lead to nanostructures with core-shell or nano-tape morphology.
3) The liquid-liquid interfaces can be exploited to generate mono-dispersed particles or particulate films.

1.3.1 Synthesis of nanoparticles thin films at air-water interface

The air-water interface has long been recognized as an excellent medium for the assembly of inorganic nanoparticles[36] as well as biomacromolecules like DNA[37] and proteins.[38] Hydrophobic nanoparticles can simply float on the water surface and can be compressed into a closed packed monolayer that can be subsequently transferred onto a suitable substrate by using the versatile Langmuir-Blodegett (LB) method.[39,40] Reviews by Fendler and co-workers[39] provide an excellent account on the use of the air-water interface in the assembly of hydrophobized nanoparticles as well as nanoparticles synthesized by chemical reaction of ions bound to Langmuir monolayers. The well-known Langmuir-Blodegett technique which comes under this section is discussed separately.

1.3.2 Synthesis of nanoparticles at solid-solid interface

The solid state synthesis of Zinc phosphate dehydrate,[41] Nickel ferrite,[42] Zinc oxide,[43] Zinc sulphide,[44] Indium oxide[45] nanoparticles has been well-documented in the literature. Shi et al. reported the formation of nickel phosphide (Ni_2P) nanoparticles by solid state reaction between nickel hypoposhite ($Ni(H_2PO_2)_2$) and ammonium hypophospite ($NH_4H_2PO_2$).[46] Novel polymer assisted solid state synthesis

of chalcogenides has been reported by Kanade et al.[47] Mechanically-activated solid-state synthesis of nanoparticles of Hafnium diboride (HfB_2), Hafnium (IV) carbide (HfC) and Hafnium nitride (HfN) from partially hydrated hafnium tetrachloride ($HfCl_4$) has also been reported by F. Villieras and co-workers.[48]

1.3.3 Synthesis of nanoparticles at liquid-solid-solution interface

The Liquid-Solid-Solution method (LSS) was developed by Li et al.[49] in 2005. In this approach, a water/ethanol mixed solution is used as the main continuous solution phase. Water is an ideal solvent for most inorganic species and ethanol serves as a good solvent for most surfactants including fatty acids. This approach has proved to be quite general in synthesizing nanoparticles of different types of materials with varied structure, composition and properties in the size range of 2-15 nm. The liquid-solid-solution method can be used to make nanocrystals of metals, bimetallics, oxides, composite oxides, copper pthalocyanine, polyaniline, chalcogenides and other functional materials.

1.3.4 Synthesis of nanoparticles at gas-liquid interface

The gas-liquid interfaces can be generated in situ inside a continuous solution that can serve as nucleation and growth centers for the synthesis of nanoparticles. Li et al. has successfully used this approach to synthesize hollow Zinc selenide (ZnSe) microspheres.[50] Recently, a beaker-in-autoclave set-up has been demonstrated for the successful synthesis of magnetite (Fe_3O_4) nanoparticles and subsequently transforming those into carbon coated magnetite (Fe_3O_4@C) nanoparticles[51] as an anode material for lithium ion batteries. A microplasma technique has also been reported for the synthesis of nanoparticles by using plasma irradiation in gas–liquid interfacial discharges.[52,53] Preparation of silver nanoparticles by reduction with formaldehyde gas has been reported by Liu et al.[54]

1.3.5 Aerosol synthesis of nanoparticles

Aerosol synthesis mainly deals with synthesis of nanoparticles in vapor phase.[55] In a typical procedure, a liquid or solid precursor is made to decompose or react with an appropriate gas or an appropriate counter precursor in vapor phase. Solid precursor targets are evaporated in a gaseous environment to form gas-solid interface

and are made to react by acquiring energy through inert gas condensation, thermal energy, laser ablation, spark discharge generation, ion sputtering, etc. Methods employing liquid precursors in aerosol synthesis include chemical vapor condensation, spray pyrolysis, laser pyrolysis, photothermal synthesis, flame synthesis and low temperature reactive synthesis. Metals, metal oxides, metal sulfides, metal selenides, metal carbides, metal nitrides have all been synthesized by aerosol synthesis. Owing to the required high quantum of input energy, nanoparticles prepared by using aerosol synthesis are mostly crystalline in nature.

1.4 Exploiting the Interface(s)

1.4.1 Liquid-liquid interfaces

Irwing Langmuir was the first to pioneer systematic studies on floating monolayer's on water in the late 1910's and early 1920's. He reported the transfer of fatty acid molecules from water surfaces onto solid supports in 1920.[56] However, the first detailed description of sequential monolayer transfer was given several years later by Katherine Blodgett. These built-up monolayer assemblies are therefore referred to as Langmuir-Blodgett (LB) films. The term Langmuir film is normally reserved for a floating monolayer. Today, we are in a situation where the production of ultrathin organic films with the LB technique has slowly started to find possible practical applications in many fields.[57] The methodology used in the present work also results in free-floating nanoparticulate thin films on liquid sub-phase. The Blodgett technique can be suitably used to transfer them to solid supports (substrates) for further studies and applications.

Emulsions are generally formed by robustly mixing oil and water. By such mixing droplets of oil are dispersed in a continuous phase of water or droplets of water are dispersed in a continuous phase of oil. The first form is called an oil-in-water emulsion, while the other form is called a water-in-oil emulsion.[58] Emulations form a liquid-liquid interface and are widely used in formation of nanomaterials especially in catalysis.

Micelles are an aggregate of surfactant molecules dispersed in a liquid and possess an interface. A typical micelle in aqueous solution forms an aggregate of

chemical entities wherein hydrophilic head/hydrophobic tail regions are arranged to minimize the energy. Normal micelle (oil-in-water micelle) and inverse micelles (water-in-oil micelle) formations have been exploited to form nanomaterials of various substances.[59, 60]

1.5 Need of surfactant free nanoparticles

Nanoparticles are prevented from agglomerating or aggregating mainly by two means; 1) by making them electrically charged and 2) by creating steric hindrance.

Ionic surfactants use the former technique by donating charge to concerned particle; while neutral surfactants hinder the growth of particles sterically. The long chains of surfactant cover particles' surface preventing their growth.

The term surfactant is a blend of surface active agents. Surfactants are wetting agents that lower the surface tension of a liquid, allowing easier spreading, and lower the interfacial tension between two liquids. Surfactants reduce the surface tension of water by their adsorption at the liquid-gas interface. Surfactants are usually organic compounds that are amphiphilic, meaning they contain both hydrophobic and hydrophilic groups. Therefore, they are soluble in organic solvents and water respectively. The nanoparticle-surfactant conjugates are water-free surfactant micelles filled with nanoparticles.

Capping agent is the term used for organic molecules containing a donor group with varying bulky steric substituents. The binding strength of capping agents to bind with metal nanoparticle surface is greater than its surfactants counterparts. Capping agents closely resemble complexing agents which are binding to metal atoms or ions that have pronounced covalent character. Commonly, colloidal stability with surfactants is lower as compared to that achieved with capping agents. Mass of capping agent per unit mass of nanoparticles is expected to be smaller than surfactant or polymeric stabilizers. In most cases, a monolayer of capping agent adsorbed on the nanoparticle surface is sufficient not only for its stability but also renders them isolable and re-dispersible. Inorganic capping agents are also reported in the literature.[63]

As discussed above capped nanoparticles are formed due to complexation or adsorption of surfactants or capping agents of varying concentrations on its surfaces. Due to the differences in the electronic and binding properties, they can strongly influence the optoelectronic and magnetic properties of functional monocrystalline materials.[63-65]

As capping in any form influences the true properties of nanoparticles, studying them in bare state or without capping is important. Hence, the search for surfactant-free methodologies for synthesis of nanomaterials, and or, their thin films is a subject of enormous curiosity and interest. In addition to the technological upsurge, the surfactant-free nanoparticles signify their inherent properties which will be exciting and different from their capped analogues.

Although, as stated above, the properties of nanomaterials change when capped and can be used advantageously, the capping can be detrimental also, especially while using their electrical and electronic properties. The original electrical and electronic properties of materials are circumvented and therefore the choice of material would be invalid. It is, therefore, important, at times, to synthesize surfactant-less/uncapped nanomaterials.

As discussed above, the stability of nano materials is achieved by capping the materials, covering their surface with organic moieties (micelles, polymers, etc.), charging the surface confining their growth by isolating the particles in a limited space so that the particles cannot assemble together, aggregate or agglomerate. However, the stabilizing process may make these materials unsuitable for specific applications. Therefore, the use of interfaces for confining the growth of particles of materials is a versatile option. Of course the problem of possible growth of particles during their application remains open as normally particles would come in contact with each other in the process. This issue can be resolved mostly by processing the materials in thin film form. Thus the processes of making thin films of various nanomaterials at interfaces attracted our attention. Also the work on LB technique and LLIRT in my laboratory rendered me proper guidance for the work of present thesis.

1.6 Background to the Present Work

1.6.1 Liquid-liquid interfacer technique (LLIRT)

LLIRT[66, 67] is a modification of LB technique. However the basic differences are summarized in Table-1.4. An important feature of this process is that the particle size in the nanometer range is stabilized without using the conventional methods; namely, capping the particles by chemical species[68] or polymers[69] or introducing the semiconductor particles into polymer or glass matrices.[70]

Table 1.4 Differences between LB technique and LLIRT.

Sr. No	**Langmuir-Blodgett Technique**	**Liquid-Liquid Interface Reaction Technique**
1.	Film formation mainly through phase transformation	Film formation by reaction or phase transformation, etc.
2.	Uniform mono layers	Multi layers confined to interface
3.	Ordered Films	No 'de fault' ordering
4.	Blodgett technique for transfer of film on substrate	Blodgett technique for transfer of film on substrate
5.	Confined to organic molecules	Not confined to a particular class of molecules
6.	Limited to amphiphiles	Wide applicability

This stabilization of the materials with particle size in the nanometer range is due to the conditions/parameters under which the nucleation takes place and subsequent prevention of aggregation/agglomeration which can cause particle growth. The ultimate particle size is decided by nucleation and growth processes through precipitation. It is known that if the parameters of precipitation are such that super-saturation is at a low level, and then relatively few nuclei would form that would subsequently grow. Under these conditions, the particle size is likely to be bigger. With high super-saturation, a large number of nuclei are likely to be formed. In the

competitive growth process, the particle growth would be less as compared with the case already discussed.[58]

One of the typical features of nanoparticles is their spontaneous self-aggregation into functional structures driven by the energetics of the system, which are known as self- assembling nanostructures. The assembling during non-covalent interactions (host-guest interactions, charge-transfer interactions, π-π interactions, hydrogen bonding interactions, acid/base proton transfer, van der Waals forces and electrostatic forces) is a valuable mechanism that has been proven successful in forming diverse nanoparticle assembly motifs such as 2D and 3D superlattices of nanocrystals.[71, 72]

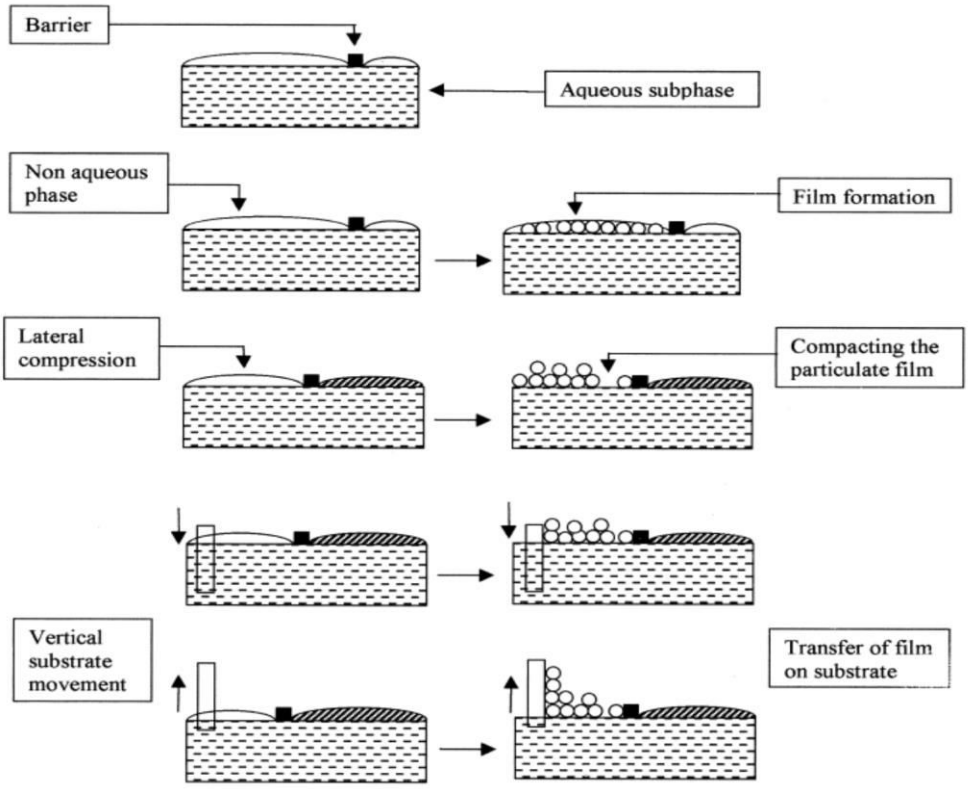

Figure 1.7 Schematic representation of LLIRT. (*Figure courtesy ref. 66*)

LLIRT is a process for the preparation of uniform and ultra-thin films of metal oxides, metal chalcogenides, metal halides, or metal compounds in general which comprises of allowing interfacial reaction, between the species contained in two immiscible solutions prepared as mentioned herein below.

With reference to Figure 1.7 the process of formation of thin films of nanomaterials is carried out in following steps. 1) In the first step we prepare an aqueous solution (10^{-4} to 10^{-6} M) of cation/anion or species of corresponding elements of interest (precursor) in Teflon tray of size (15 cm x 15 cm x 2 cm) so that it formed a meniscus at the edges. The surface of the subphase is divided into two compartments by Teflon thread barrier by fixing it at the two opposite edges of the tray so as to accommodate the expanded/contracted area of the surface. 2) In the second step we prepare non aqueous solution (volatile) of the appropriate anion/ cation species of the corresponding elements. 3) With the help of syringe a non aqueous solution formed in second step is dropped on the surface of subphase in one of the compartment in Teflon tray. After the spreading of non aqueous solution the cation/anion in non aqueous solution reacts with anion/cation in subphase which leads to the formation of solid product at the interface. 4) After the evaporation of the volatile solvent, we compress the product formed at the interface laterally which leads to the formation of thin film. 5) In the last step, we dip a desired substrate in the solution and withdraw it from the solution at a uniform rate to transfer the film on substrate surface using Blodgett technique. In case of crystallization/reaction/decomposition the films formed on the substrate are heated at high temperature.[66]

1.6.2 Synthesis of nanoparticulate films by Layer-by-Layer assembly

The Layer-by-Layer assembly (LbL) is a relatively new methodology of thin film deposition that gained popularity wherein oppositely charged polyelectrolytes are applied to stack consequent layers. The use of Layer-by-Layer assembly for nanoparticles has been described.[73-80] Layer-by-Layer technique consists of sequential adsorption of positively and negatively charged species on alternate layers by dipping the substrate alternately in the required electrolyte solvents. The charged layer is rinsed with a solvent (in most cases water) which removes the excess of the previously adsorbed electrolyte layer. This results in a thin layer of the charged species on the substrate, in turn, preparing the surface for adsorption of next layer. The major advantages of Layer-by-Layer assembly are simplicity, universality and nanometer scale thickness control.

No requirement of high purity chemicals or sophisticated set-up justifies the simplicity of Layer-by-Layer assembly method. The ability to fabricate thin films from aqueous dispersion of proteins, polymers, oligomers, nanoparticles, colloids reflects the universality of Layer-by-Layer assembly method. Since during each deposition a monolayer or a sub-monolayer is deposited, thickness of the as deposited layers in Layer-by-Layer assembly can be controlled with precision. Moreover, the optimization of sequences in which Layer-by-Layer deposition is to be carried out can be accessed by observations of UV-visible spectroscopy in most of the cases. Nanoparticulate thin films of PbS,[73] TiO_2,[74] SiO_2,[75] Au,[76] Fe_3O_4,[77] HgTe,[78] Ag,[79] CdSe,[80] ZrO_2,[81] CdTe,[82] ZnSe,[83] MoO_2,[84] polyoxometallates, [85] multilayrs or freestanding films[86] etc. have been prepared by Layer-by-Layer assembly. The assembly of clay sheets and carbon nanotubes has been demonstrated by Kotov et al. The Layer-by-Layer assembly can be considered as a very convenient tool for making both coatings and free-standing materials for a variety of most challenging applications. More detailed experimentation of our modification of Layer-by-Layer assembly is provided in the following Chapters.

1.7 Literature on Applications of Liquid-Liquid Interfaces

Like the air-water interface, the aqueous-organic (liquid-liquid) interface can be successfully exploited for nanomaterial synthesis. Rao et al.[87] have made ultrathin films of Au, Ag, Pd, and Cu,[88-90] metal chalcogenides such as CdS, CuS, CdSe, ZnS, PbS,[91-94] binary alloys like Au-Ag[69] and Au-Cu[69,76] and ternary Au-Ag-Cu alloys.[69,76] Metal sulfide bilayer films[69] such as CuS-CdS, CuS-PbS and CdS-PbS have also been reported at the toluene-water interface. Metal oxides like ZnO,[69] CuO[74] have also been synthesized at the toluene-water interface. The general experimental procedure consists of dissolving a metal-organic precursor in the organic phase and then injecting an appropriate reducing / reacting agent in the aqueous phase. For the synthesis of metal nanoparticles tetrakis-hydroxymethyl-phosphinium chloride has been used as a reducing agent. The sodium sulfide (Na_2S) has been used as sulfur source for the synthesis of metal sulfide nanoparticles. The sodium selenide (Na_2Se) or N, N-dimethylselenourea (Me_2NSeNH_2) has been used as a selenium source to synthesis metal selenides. Metal oxides were prepared by injecting NaOH in the aqueous phase at room temperature or at some elevated temperature. Formation of

substrate-free films, single-crystalline in a few cases, is an important feature of this approach. The films thus prepared can be readily transferred to any substrate. Nevertheless, the method suffers from an inherent disadvantage of nanoparticle capping as reaction of the metal-organic precursor forms nanoparticles capped with organic material. Capping is known to have adverse effect on the properties for selective applications. Paul O Brien and Co-workers have a similar strategy as reported by Rao et al. The only difference is that they use metal thio-carbamates.[95-98] Rao et al. mostly rely on metal cup-ferronates or metal phosphines or metal acetate (in case of Pd). By treating the silica precursor dissolved in an organic phase such as hexane, toluene or CCl_4 with surfactant molecules in the aqueous phase. Kleitz and co-workers were able to synthesize mesoporous silica fibres.[99] By mixing a solution of cadmium myristic acid and n-triphenylphosphine oxide in toluene with an aqueous solution of thiourea accompanied by both heating and stirring, mono disperse, luminescent CdS nanocrystals have been prepared.[100] The Se nanorods were prepared at the butanol-water interface by Song et al. [101] Single crystals of copper adipate have been reported by Cheetham and co-workers.[102]

To overcome the detrimental effect of surfactants/capping agents a different approach called Liquid-Liquid Interface Reaction Technique (LLIRT) was developed by Sathaye et al. at CSIR-National Chemical Laboratory.[66, 67] The LLIRT relies on dissolving cation or anion of the desired material in aqueous sub-phase and spreading the subsequent counter-ion in suitable organic phase on aqueous surface so that desired product is formed through ionic interaction at interface. Metal sulfides, metal selenides, metal oxides, ternary, as well as, single metal nanoparticles can be prepared by this technique. A modification of this technique for synthesis of nanoparticles of metal-organic complexes as well as organic materials termed as Liquid-Liquid Interface Recrystallization Technique (LLIRcT) was developed.[103] The most important trait of LLIRT and LLIRcT is that they achieve surfactant-free nanoparticles thin film synthesis with low cost solution processing.

1.8 Applications of Nanomaterials as Supercapacitors and Electro Catalysts

1.8.1 Supercapacitors

A supercapacitor (SC) (sometimes called ultra capacitor, formerly electric double-layer capacitor (EDLC)) is a high-capacity electrochemical capacitor with capacitance values of up to 10,000 Farads at 1.2 volt that bridge the gap between electrolytic capacitors and rechargeable batteries.[104,105] Supercapacitors store typically 10 to 100 times more energy per unit volume or mass than conventional capacitors. They can accept and deliver charge much faster than batteries. They can tolerate many more charge and discharge cycles than rechargeable batteries.[106] They are, however, 10 times larger in size than conventional batteries for a given charge. Supercapacitors are classified into a) double layers capacitors, b) pseudo capacitors and c) hybrid capacitors as given in Figure 1.8.

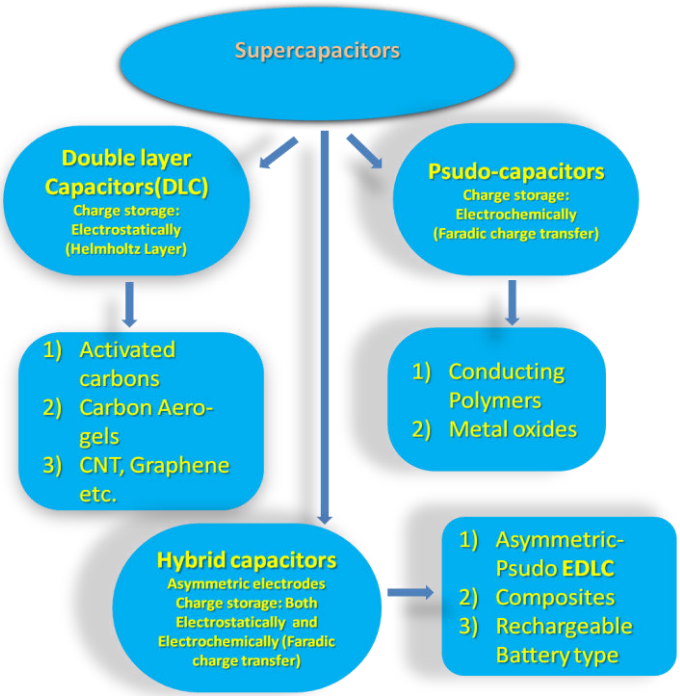

Figure 1.8 Classification of the supercapacitors.

1.8.2 Electrocatalysis

Electrocatalysis is a special field in electrochemistry that has gained a special growth after the late 1980s due to the application of new hybrid techniques wherein electrolytic and catalytic actions go together. However, most of the studies have been reported for academic purposes. An electrocatalyst is a catalyst that participates in electrochemical reactions. Catalyst materials modify and increase the rate of chemical reactions without being consumed in the process. Electrocatalysts are of specific form

of catalysts that function at electrode surfaces or may be the electrode surface itself. An electrocatalyst can be heterogeneous such as a platinum surface or nanoparticles in/on some matrix,[107] or homogeneous like a coordination complex or enzyme. The electrocatalyst assists in transferring electrons between the electrode and reactants, and/or facilitates an intermediate chemical transformation described by an overall half-reaction. There are various applications of electrocatalysis for possible technological electrochemical reactions, organic electrosynthesis, galvanoplasty, electrode sensors, fuel cells, batteries preparations, and so on.

A fuel cell is a device that converts the chemical energy from a fuel into electrical energy through a chemical reaction of fuel with oxygen or another oxidizing agent.[108] Fuel cells are different from batteries in which they require a continuous source of fuel and oxygen/air to sustain the chemical reaction whereas in a battery the chemicals present in the battery react with each other to generate an electromotive force (emf).[109] Fuel cells can produce electricity continuously as long as these inputs are supplied.[110] The composite materials of Pt nanoparticles of sizes ranging from 1.5 to 3.5 nanometer decorated over the graphene and MoS_2 is being studied in Chapter 5.

1.8.3 Electrode materials for supercapacitors and electro-catalytic oxidation

To be a good material for super capacitor or electrocatalysts, the material should have the following physical and chemical properties, namely, high surface area, flexibility to accommodate volume change, easy charge transfer (conductivity) etc. On this background, several materials used for the applications of super capacitors or electrocatalysts are as follows,

1.8.3.1 Graphene and other carbon materials

Carbon with vast number of allotropes is a marvelous element and is essential to all living systems. Further, by various synthetic strategies, carbon can be tailored in numerous structures of sizes in micro to nano regime.[111] They find wide range of applications in various fields including supercapacitors. Carbons can be classified into different types depending on their allotropic nature. Graphene is preferably used as a carbon component in carbon–nanomaterial composites because of its special properties, namely, its layer type 2D structure, high surface area, flexibility, excellent

stability and good conductivity.[112-116] These properties are mostly complimentary to the properties of other component of the composite for its application in supercapacitors which is a subject matter of front line research in recent years.[117-120] Several processes are being practiced to produce GNS such as mechanical cleavage,[121, 122] chemical cleavage of graphite, exfoliation of natural graphite in various solvents by sonication,[123, 124] acid treated pristine graphite by thermal shock[125] and electrochemical exfoliation of graphite.[126] Considering very special structural relation between graphite and graphene; it was obvious to use graphite as a precursor for the production of graphene.

1.8.3.2 Metal oxides and chalcogenides

While considering nanomaterials as a component of supercapacitor matrix, several materials are being studied, mainly, MnO_2,[127] Co_3O_4,[128] Fe_2O_3,[129] MoS_2,[130] SnO_2,[131, 132] NiO,[133] ZnO, [134] and are proven to be materials for supercapacitors, provided they have high surface area. Thus various attempts to increase the surface area of such materials have been made which includes use of 1D, 2D supporting materials and morphological modifications of active materials.

1.8.3.3 Conducting polymers

Conducting polymers like polyacetylene, polyaniline, polypyrrol, polythiopene, polyfuran and their derivatives etc. have backbones of adjacent sp^2 hybridized carbon. One valence electron on each center exists in a p_z orbital, which is orthogonal to the other three sigma-bonds. The electrons in these delocalized orbitals have high mobility. When the material is "doped" by oxidation, some of these delocalized electrons get removed. Thus the p-orbitals form a band, and the electrons in this band become mobile when it is partially filled.

In principle, these materials can be doped by reduction also, which adds electrons to otherwise an unfilled band. In practice, most organic conductors are doped oxidatively to give p-type materials. The redox doping of organic conductors is analogous to the doping of semiconductors which makes the materials conducting which are otherwise insulators. The comparison of various conductive polymers with reference to copper metal conductivity is shown in Figure 1.9.[135-139]

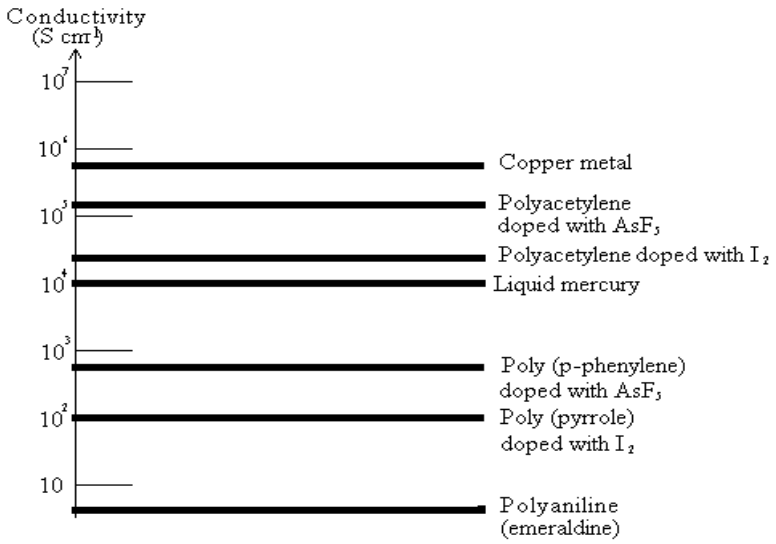

Figure 1.9 Logarithmic conductivity ladder locating some metals and conducting polymers. http://homepage.ntlworld.com/colin.pratt/cpoly1.jpg

Conducting polymers can act as a conductive support for many oxide materials to enhance the conductivities of composite in the supercapacitors.[140-143] This is also true for composites for the application of the electrocatalysts.[144-148]

1.9 Aim of the Thesis

To make use of liquid-liquid interface to synthesize nanoparticulate thin films of modern materials, namely, graphene, MoS_2, polyaniline etc. Further it is proposed to show that the thin films of composites consisting of supporting material and semiconductor/metal components can be synthesized by the above mentioned technique. Also it will be shown that such thin film composites have a potential for their applications as supercapacitor/electrocatalysts which in turn for making devices to tackle energy and environment/pollution problems.

1.9.1 Objectives of the present work

It is well accepted that nanoparticles (NPs) would enhance the scope for exploitation of materials in various new fields. However, NPs formation has inherent difficulties like spontaneous aggregation by minimizing the surface energy. To get over this problem, normally adapted procedures are: the use of surfactants, capping agents, confining the particles in nano-space etc. Among these, use of interfaces of

nano size dimensions has not been fully exploited. On this background, the broad objective of this work is to synthesize surfactant-free nanoparticles by reaction at liquid-liquid interface. The additional feature of use of interface as described herein is the formation of thin films consisting of nanoparticulate materials. Further, these films are characterized suitably for their possible applications and shown their adaptability for device formation.

In view of the above discussion, the liquid-liquid interface reaction technique (LLIRT) possesses several advantages over the conventional Langmuir-Blodgett technique. Therefore, the subordinate objective of the present thesis work is to confirm the advantage of LLIRT over LB technique; at least in some aspects of peculiarities of these otherwise similar techniques. Advantages of LLIRT deposition methods over the Langmuir-Blodgett technique have been discussed. Device quality nanoparticulate thin films of metal oxides, metal chalcogenides, metal nanoparticles and conducting polymer thin films have been produced by LLIRT.[149, 150] The objective of the present study is to understand the LLIRT to synthesize nanoparticulate thin films of inorganic semiconductors relevant to modern developments in material science and to further modify LLIRT to synthesize their surfactant-less nanoparticulate thin films.

In this thesis the limitations of the LLIRT, namely, the requirement of solubility of the reactants in aqueous or non-aqueous phase have been overcome and exploited completely.[149] Insoluble precursors are used to form nanoparticles at liquid-liquid interface by maneuvering the chemistry of those respective materials. Subsequently, these particles are transformed in a thin film form which is suitably deposited on substrates. Thus, precise objectives of the present work are three fold and can be summarized in following points,

1) To develop methods to synthesize thin films of modern nanomaterials like graphene, MoS_2 and their composites, etc.
2) To characterize and study above formed products by using modern techniques like TEM, SEM, XRD, XPS, RAMAN spectroscopy etc.
3) To show that the synthetic procedure is not only useful for objective 1 but also useful for generating special architecture for composite films by taking the

assistance of modified LbL technique. Such architectures are proved to be suitable for energy storage and energy applications.

4) To study the performances of the developed architectures as working electrodes in energy storage and elctrocatalysis.

1.9.2 The specific objectives of the present thesis

Synthesis of mono/ few layered 2D materials like graphene and transition metal di-chalcogenides e.g. MoS_2 have enormous applications in supercapacitors as well as in electrocatalysis. The formation of LbL composites of various combinations of above 2D materials with transition metal/metal-oxide nanoparticles as well as with various conducting polymers could lead to stable and robust supercapacitors or electrocatalysts for fuel cells. Thus the specific objectives of this thesis can be given as in following points,

1) To modify LLIRT suitably to synthesize mono/few layer graphene nanosheets (GNS), MoS_2 nanosheets thin films by using LLIRT.

2) To synthesize Pt metal and PANI and doped PANI, nanoparticulate thin films by LLIRT.

3) To develop LbL deposition procedure which can exploit LLIRT for synthesizing composites' thin films, making use of specific objective 1 and aiming specific applications.

4) To characterize and study the performance of composite materials prepared, for supercapacitors and electrocatalysts.

1.9.3 Organization of present thesis

Chapter 1

The Chapter 1 comprises of a brief introduction of nanotechnology, and historic background of nanotechnology. As we go on, it describes the importance of nanomaterials and the methods of preparation of nanomaterials. The importance of formation of thin films of nanomaterials and their applications have been discussed. Furthermore, the methods of formation of thin films and need of surfactant free methods of forming nanomaterials and their thin films for the specific applications are also discussed. Different kinds of interfaces and their usefulness for forming

nanoparticulate thin films are discussed. The literature study of the thin film formation is given. The brief introduction to supercapacitors and electrocatalysts and the materials used for them is given in detail at the end of this Chapter.

Chapter 2

In this Chapter a novel methods to synthesize mono/few layered graphene nanosheets (GNS) thin films and nanoparticulate SnO_2 thin films are discussed. Both the films are exhaustively characterized by various modern material characterization techniques. Atomic force microscopy (AFM) and other characterization techniques confirm formation of mono/few layered GNS. By using LbL deposition technique GNS/SnO_2 composite was formed which showed higher specific capacitance of 471 F g^{-1} with excellent durability and retention up to 72% of initial capacitance.

Chapter 3

In this Chapter we applied the similar methodology for making the mono/few layered MoS_2 nanosheets. The formation of monolayer was confirmed through Raman and AFM analysis followed by TEM analysis. Raman plays an important role in deciding the number of layers in MoS_2. The MoS_2-GNS LbL composite was formed and was characterized with the XRD analysis. Electrochemical performance of the composite was checked through cyclic voltametry and galvanostatic charge discharge. The composite showed the robust specific capacitance of 282 Fg^{-1} as compared to GNS (86 Fg^{-1}) and MoS_2 (156 Fg^{-1}). The composite showed the higher durability and excellent retention of specific capacitance of 93%. The high specific surface area and high conductivity of graphene improve the electrical conductivity of the electrode. The special architecture facilitates ion diffusion, fast charge transport and electrolyte interactions during charge and discharge. MoS_2 sheets help avoiding restacking of GNS. On the other hand, the flexibility of GNS helps accommodating volume changes in capacitors during fast charge-discharge processes which helps in the enhancement of life of super-capacitor.

Chapter 4

In this Chapter, I have focused on synthesis of conducting polymers thin films mainly 'PANI' and its LbL composites with 2D materials like GNS and MoS_2. XRD and FTIR confirm the formation of materials. The composites were checked for electrochemical performance especially for supercapacitor applications. CV measurement shows pseudo-capacitive behaviour for PANI and PANI-MoS_2 electrode. Moreover PANI-GNS electrode shows an ideal behaviour of capacitance. Pertaining to galvanostatic charge discharge PANI electrode shows drop down potential (IR drop) as expected. PANI-GNS and PANI-MoS_2 show excellent capacitive behaviour and most interestingly stability due to the LbL architecture.

Chapter 5

In this Chapter, I have reported a synthesis of thin films consisting of ultra small Pt nanoparticles. Most of the fuel cells use the Pt as electrocatalysts because of its higher activity. To reduce the cost of Pt electrode it is a need to enhance the catalytic activity and lower the amount of Pt used. LbL composites of Pt-MoS_2 and Pt-GNS show excellent enhancement in electrocatalytic activity as compared to the activity reported in other systems. Furthermore the Pt-MoS_2 composite shows higher CO tolerance than that reported for composites wherein bare Pt is a catalyst.

Chapter 6

In this Chapter the overall summary of the present thesis is given.

10. References

[1] S. Link and M. A. El-Sayed, *Int. Rev. Phys. Chem.*, 2000, **(9)3**, 409.

[2] R. W. Kelsall, I. W. Hamley and M. Geoghegan, *Nanoscale Science and Technology John Wiley and Sons Ltd.* 2005.

[3] P. Alivisator, *J. Phys. Chem.*, 1996, **100**, 13226.

[4] W. Caseri, *Encyclopedia of Nanoscience and Nanotechnology Ed. by H. S. Nawa (American Scientific Publisher, California)*, 2004, **6**, 235.

[5] S. K. Kulkarni, *Nanotechnology: Principles and Practices (Capital Books, India)* 2006.

[6] A. Roosen and H. Hausner, *Ceramic Poeders, Elsevier, Amsterdam*, 1983.

[7] H. Haug and S. W. Koch, *Quantum Theory of the Optical and Electronic Properties of Semiconductors World Scientific Publishers,* Singapore, 1990.

[8] Ph. Buffat and J-P. Borel, *Phys. Rev. A*, 1976, **13**, 2287.

[9] G. Schmid, *Dalton Trans.*, 1998, **7**, 1077.

[10] H. Fan, Y. Lu, A. Stump, S. T. Reed, T. Baer, R. Schunk, V. Perez-Luna, G. P. Lopez and C. J. Brinker, *Nature*, 2000, **405**, 55.

[11] K. Kalbunde, *Nanoscale Materials in Chemistry*, John Wiley and Sons 2001**.**

[12] M. Faraday, *Philos. Trans*., 1857,**147**, 14.

[13] J. Turkevich, *Gold. Bull.*, 1985, **18**, 86.

[14] B. E. Deal, *Interface*, 1976, **6**, 18.

[15] M. Lundstrom, *Science*, 2003, **299**, 210.

[16] R. P. Feynman, *J. Microelectromechan. Syst*., 1992, **1**, 60.

[17] G. E. Moore Electronics Magazine., 1965 p. 4. Retrieved 2006-11-11.

[18] R. Dennard, F. H. Gaensslen, H. N. Yu, L. Rideout, E. Bassous, and A. R. LeBlanc, *IEEE J. Solid State Circuits*, 1974, **SC-9**, 256.

[19] G. Binnig and H. Rohrer, *IBM Journal of Research and Development*, 1986, **30**(4), 355.

[20] G. Binnig, C. F. Quate and C. Gerber, *Physical Review Letters,* 1986, **56**, 930.

[21] P. Saravanan, R. Gopalan, and V. Chandrasekaran*, Defence Science Journal*, July 2008, **58** (4), 504-516.

[22] C. B. Murray, D. J. Norris, and M. G. Bawendi, *J. Am. Chem. Soc.*, 1993, **115**, 8706.

[23] K. Oura, V. G. Lifshits, A. A. Saranin, A. V. Zotov, and M. Katayama *Surface Science*, *Springer* 2003, chapter 14. *edition* (July 15, 2003)

[24] Hand book of thin film deposition processes and techniques. K. K. Publication, Park Ridge, New Jersey, USA, 1988.

[25] Thin film phenomenon K. L. Chopra. McGraw Hill Book Co. New York USA, 1969.

[26] Proceedings of the forth international workshop on glasses and glass ceramics from gels, *Journal of non-crystalline solids*, 1988, **7** (100), 479.

[27] R. R. Chamberlin and J. S. Skarman., *J. Electrochem Soc*., 1966, **113**(1), 86

[28] J. E. Hill and R. R. Chamberlin. *U. S. Patent,* 1964, **3**,148.084

[29] H. Schroeder, G. Hass and R. E. Thun, Physics of thin films, Acad. Press. *New York*, 1969, **5**, 87.

[30] D. E. Otten, P. R. Shaffer, P. L. Geissler and R. J. Saykally, *Proc Natl. Acad. Sci. U. S. A.,* 2012, **109(3),** 701-5.

[31] T. Nakaya, Y. Jun and K. Chakravorty, *J. Mat. Chem.*, 1996, **6(5),** 691.

[32] D. Hanaor, G Triani and C. C. Sorrell *Surface and Coatings Technology,* 2011, **205 (12)**, 3658.

[33] J. J. Richardson, M. Björnmalm, and F. Caruso *Science*, 2015, **348**, 6233.

[34] Functional Polymer Films Eds. R. Advincula and W. Knoll, *Wiley*, 2011, ISBN 978-3527321902.

[35] H. J. Butt, K. Graf and M. Kappl, Physics and Chemistry of Interfaces, 2nd Revised Edition, *Wiley-Interscience Publication*, 2003.

[36] A. Ulman, Introduction to Ultrathin Organic films from Langmuir−Blodgett to Self-assembly Academic Press, San Diego 1991.

[37] Y. Ebara, K. Mizutani and Y. Okahata, *Langmuir*, 2000, **16**, 2416.

[38] A. Boussaad, L. Dziri, N. J. Arechabaleta, N. J. Tao and R. M. LeBlanc, *Langmuir*, 1998, **14**, 6215.

[39] J. H. Fendler and F.C Meldrum, *Adv. Mater.*, 1995, **7**, 607.

[40] M. Sastry, V. Patil, K. S. Mayya, D. V. Paranjape, P. Singh and S. R. Sainkar, *Thin Solid Films*, 1998, **324**, 239.

[41] A. Q. Yuan, S. Liao, Zh. F. Tong, J. Wu and Z. Y. Huang, M*ater. Lett*., 2006, **60/17- 18**, 2110.

[42] A. Ceylan, S. Ozcan, C. Ni and S. I. Shah, *J. Magn. Magn. Mater*., 2008, **320** (6), 857.

[43] Z. Wang, H. Zhang, L. Zhang, J. Yuan, S. Yan and C. Wang, *Nanotechnology*, 2003, **14**, 11.

[44] P. Calandra, A. Longo and V. T. Liveri, *J. Phys. Chem. B*, 2003, **107** (1), 25.

[45] A. Dodd, *J. Nanoparticle Research*, 17th July, 2009.

[46] G. Shi and J. Shen, *J. Mater. Chem.*, 2009, **19**, 2295.

[47] K. G. Kanade, R. R. Hawaldar, R. Pasricha, S. Radhakrishnan, T. Seth, U. P. Mulik, B. B. Kale and D. P. Amalnerkar, *Mater. Lett.*, 2005, **59** (5), 554.

[48] E. Barraud, S. Begin-Colin, G. Le Caer, O. Barres and F. Villieras, *Int. J. Nanosci. Nanotech.*, 2008, **5**, 8649.

[49] X. Wang, Q. Peng and Y. Li, *Acc. Chem. Res*. 2007, **40** (8), 635.

[50] Q. Peng, Y, J. Dong and Y. D. Li, *Angew.Chem. Int. Ed.*, 2003, **42**, 3027.

[51] Z. M. Cui, L.Y. Jiang, W. G. Song and Y. G. Guo, *Chem. Mater.*, 2009, **21**(6), 1162.

[52] C. Richmonds and R. M. Sankaran, *Appl. Phys. Lett.*, 2008, **93**, 131501.

[53] K. Baba, T. Kaneko and R. Hatakeyama, *Appl. Phys. Express*, 2009, **2**, 35006.

[54] H. G. Liu, F. Xiao, C. W. Wang, Y. Lee, Q. Xue, X. Chen, D. J. Qian, J. Haoand and J. Jiang, *Nanotechnology*, 2008, **19**, 055603.

[55] M.T. Swihart, *Currunt Opinion in Colloid interface sci*., 2003, **8**, 127.

[56] C. N. R Rao and K. P. Kalaynikutty, *Acc.Chem. Res.*, 2008, **14** (4), 489.

[57] G. Decher, *Science*, 1997, **277**, 1232.

[58] P. Becher, ed. 1988. Encyclopedia of Emulsion Technology, **Vol. 3** Basic Theory, Measurement and Applications. New York, Dekker.

[59] J. M. Seddon, R. H. Templer. Polymorphism of Lipid-Water Systems, from the Handbook of Biological Physics, **Vol. 1**, Ed., R. Lipowsky, and E. Sackmann. 1995, Elsevier Science B.V. ISBN 0-444-81975.

[60] http://www.coatingsys.com/yahoo_site_admin/assets/docs.

[61] K. Patil, Y. Hwang, M. Kim, J-S Chang, S-E Park. *Journal of Colloid and Interface Science*, 2004, **276**, 333.

[62] K. Patil, S. Sathaye, Y. Khollam, S. Deshpande, N. Pawaskar, A. Mandale, *Materials Letters*, 2003, **57**, 1775.

[63] Y. Pei, R. V. M. Ganesh, C. Xiao, T.-W. Goh, K. Brashler, J. A. Gustafson and W. Huang, *Nanoscale*, 2015,**7**, 16721.

[64] (a) D. Kim, K-D Min, J. Lee, J. H. Park and J. H. Chun, *Mater. Sci.d Eng*. B, 2006, **131**(1-3), 13. (b) A. Quesada, M. A. Garcia, J. de la Venta, E. Ferandez Pinel, J.M. Merino and A Hernando, *Eur. Phys. J. B*, 2007, **59**, 457.

[65] M. El-Kemary, H. El-Shamy and M. M. Mosaad, *Mater. Chem. Phys*., 2009, **118**, 81-85.

[66] S. D. Sathaye, K. R. Patil, D. V. Paranjape, A. Mitra, S. V. Awate and A. B. Mandale, *Langmuir*, 2000, **16**(7), 3487.

[67] S. D. Sathaye, K. R. Patil, D. V. Paranjape, 1996, U. S. Patent No. 5549931.

[68] Y. Nosaka, K. Yamaguchi, H. Miyama, M. Hayashi, *Chem. Lett*., 1988, **17**(4), 6005.

[69] J. M. Huang, Y. Yang, B. Yang, S. Y. Liu and J. C. Shen, *Polym. Bull*., 1996, **36(3),** 337.

[70] Y. Wang and N. Herron, *J. Phys. Chem.,* 1987, **91**, 257.

[71] K. Hu, M. Brust and A. Bard, *J. Chem. Mater*., 1998, **10**, 116.

[72] L. Dong, T. Gushtyuk and J. Jiao, *J. Phys. Chem. B*, 2004, **108**, 1617.

[73] G. Decher, *Science*, 1997, **277**, 1232.

[74] N. A. Kotov, I. Dekany and J. H. Fendler, *J. Phys. Chem*., 1995, **99** (35), 13065.

[75] Y. Liu, A. Wang and R. Claus, *J. Phys. Chem*., 1997, **101**(8), 13858.

[76] M. A. Correa-Duarte, M. Giersig, N. A. Kotov and L. M. Liz-Marzan, *Langmuir,* 1998, **14**(22), 6430.

[77] W. Schrof, S. Rozouvan, E. V. Keuren, D. Horn, J. Schmitt and G. Decher, *Adv. Mater*., 1998, **10**(4), 338.

[78] F. G. Aliev, M. A. Correa-Duarte, A. Mamedov, J. W. Ostrander, M. Giersig, L. M. Liz-Marzán and N. A. Kotov, *Adv. Mater.*, 1999, **11**(12), 1006.

[79] A. Rogach, S. V. Kershaw, M. Burt, M. T. Harrison, A. Kornowski, A. Eychmüller and H. Weller, *Adv. Mater.*, 1999, **11**(7), 552.

[80] Z. L. Liu, X. D. Wang, H. Y Wu and C. X. Li, *Colloid Interface Sci.,* 2005, **287**, 604.

[81] Z. Q. Liang, K. L Dzienis, J. Xu, and Q. Wang, *Adv. Funct. Mater.,* 2006, **16**, 542.

[82] E. H. Kang, P. Jin, Y. Yang, J. Sun and J. Shen, *Chem. Commun.*, 2006, **41**, 4332.

[83] T. Franzl, D. S. Koktysh, T. A. Klar, A. L. Rogach, and J. Feldmann, *Appl. Phys. Lett.*, 2004, **84**, 2904.

[84] A. Shavel, N. Gaponik, and A. Eychmüller, *J. Phys. Chem. B*, 2004, **108**(19), 5905.

[85] I. Ichinose, H. Tagawa, S. Mizuki, Y. Lvov and T. Kunitake, *Langmuir,* 1998, **14** (1), 187.

[86] I. Moriguchi and J. H. Fendler, *Chem. Mater.,*1998, **10** (8), 2205.

[87] C. N. R Rao, G. U. Kulkarni, P. J Thomas, V. V. Agrawal and P. Saravanan, *J. Phys. Chem. B,* 2003, **107**, 7391.

[88] C. N. R Rao, G. U. Kulkarni, V. V. Agrawal, U. K. Gautam, M. Gosh and U. Tumkurkar: *J. Colloid Interface Sci.,* 2005, **289**, 305.

[89] U. K. Gautam, M. Ghosh and C. N. R. Rao, *Chem. Phys. Lett*., 2003, **381**, 1.

[90] U. K. Gautam, M. Ghosh and C. N. R. Rao, *Langmuir*, 2004, **20**, 10776.

[91] K. P. Kalaynikutty and C. N. R. Rao, *Solid State Sci*., 2008, **8**, 296.

[92] K. P. Kalaynikutty, U. K. Gautam and C. N. R. Rao, *J. Nanosci. Nanotech.*, 2007, **7**, 1916.

[93] V. V. Agarwal, P. Mahalaskhmi, G. U. Kulkarni and C. N. R. Rao, *Langmuir*, 2006, **20**, 1077.

[94] D. Fan, P. J. Thomas and Paul O'Brien, *J. Mater. Chem.,* 2007, **17**, 1381.

[95] P. J. Thomas, D. Fan and P. O'Brien, *J. Nanosci. Nanotech.***,** 2007, **7**, 1689.

[96] D. Fan, P. J. Thomas and Paul O'Brien, *Chem.Phys. Lett*., 2008, **465** (1-3), 110.

[97] D. Fan, P. J. Thomas and Paul O'Brien, *J. Am. Chem. Soc*., 2008, **130** (33), 10892.

[98] S. N. Mlondo, P. J. Thomas and Paul O'Brien, *J. Am. Chem. Soc.*, 2009, **131**(17), 6072.

[99] F. Kleitz, F. Marlow, G. D. Stucky and F. Schuth, *Chem. Mater.*, 2001, **13**, 3587.

[100] D. Pan, S. Jiang, L. An and B. Jiang, *Adv. Mater.*, 2004, **16**, 982.

[101] J. M. Song, J. H. Zhu and S. H. Yu, *J. Phys. Chem. B*, 2006, **110**, 23790.

[102] P. M. Foster, P. M. Thomas and A. K. Cheetham, *Chem. Mater.,* 2002, 14, 17.

[103] R. Hawaldar, S. Jadkar, B. Kale, U. Mulik, S. Sathaye, and D. Amalnerkar, *Chem. Lett.*, 2006, **35**, 26.

[104] S. R. Gallay, Proc. Power Conversion PCIM 1999.

[105] D. Ue, K. Ida, S. Mori, *J. Electrochem. Soc*., 1994, **141**, 2989.

[106] A. Yoshida, S. Nonaka, I. Aoki and A. Nishino, *J. Power Sources*, 1996, **60**, 213.

[107] Wang, Xin (19 January 2008). "CNTs tuned to provide electrocatalyst Support". Nanotechweb.org. Retrieved 27 February 2009.

[108] Nice, Karim and Strickland, Jonathan. "How Fuel Cells Work: Polymer Exchange Membrane Fuel Cells". How Stuff Works, accessed 4 August 2011.

[109] J. Kim, Y. Lee and S. Sun, *J. Am. Chem. Soc*., 2010, **132**, 4996.

[110] H. Lang, S. Maldonado, K. J. Stevenson and B. D. Chandler, *J. Am. Chem. Soc.,* 2004, **126**, 12949.

[111] Y. Wang, Z. Shi, Y. Huang, Y. Ma, C. Wang, M. Chen and Y. Chen, *J. Phys.Chem. C*, 2009, **113**, 13103.

[112] C. Li, Z. Yu, D. Neff, A. Zhamu and B. Z. Jang, *Nano Lett.,* 2010, **10**, 4863.

[113] T. Y. Kim, H. W. Lee, M. Stoller, D. R. Dreyer, C. W. Bielawski, R. S. Ruff and K. S. Suh, *ACS Nano*, 2011, **5**, 436.

[114] M. G. Stoller, S. Park, Y. Zhu, J.An and R. S. Ruff, *Nano Lett.,* 2008, **8**, 3498.

[115] S. Stankovich, D. A. Dikin, G. H. B. Dommett, K. M. Kohlhaas, E. J. Zimney, E. A. Stach, R. D. Piner, S. T. Nguyen and R. S. Ruoff, *Nature*, 2006, **442**, 282.

[116] Z. L. Wang, D. Xu, Y. Huang, Z. Wu, L. M. Wang and X. B. Zhang, *Chem. Commun*., 2012, **48**, 976.

[117] X. Zhou, Y. X. Yin, L. J. Wan and Y. G. Guo, *Chem. Commun*., 2012, **48**, 2198.

[118] S. Ding, J. S. Chen, D. Luan, Y. C. Boey, S. Madhavi and X. W. Lou, *Chem. Commun*., 2011, **47**, 5780.

[119] S. Ding, D. Luan, F. Y. C. Boey, J. S. Chen and X. W. Lou, *Chem. Commun.,* 2011, **47**, 7155.

[120] (a)A. L. Geim and K. S. Novoselov, *Nat. Mater*., 2007, **6**, 183. (b) K. S. Novoselov, A. K. Geim, V. Morozov, D. Jiang, Y. Zhang, S. V. Dubonos, I. V. Grigorieva and A. A. Firsov, *Science,* 2004, **306**, 666.

[121] X. Zhou, T. Wu, K. Ding, B. Hu, M. Hou and B. Han, *Chem. Commun*., 2010, **46**, 386.

[122] X. Li, X. Wang, L. Zhang, S. Lee and H. Dai, *Science*, 2008, **319**, 1229.

[123] J. Wang, K. K. Manga, Q. Bao and K. P. Loh, *J. Am. Chem. Soc*., 2011, **133**, 8888.

[124] L. Muo, K. Zhang, H. S. Chan and J. Wu, *J. Mater. Chem.,* 2012, **12**, 1845.

[125] S. Chen, J. Zhu, X. Wu, Q. Han and X. Wang, *ACS Nano*, 2010, **4**, 2822.

[126] Z. S. Wu, W. Ren, D. W. Wang, F. Li, B. Liu and H. M. Cheng, *ACS Nano*, 2010, **4**, 5835.

[127] J. Yan, Z. Fan, T. Wei, W. Qian, M. Zhang and F. Wei, *Carbon*, 2010, **48**, 3825.

[128] J. Yan, T. Wei, W. Qiao, B. Shao, Q. Zhao, L. Zhung and Z. Fan, *Electrochim. Acta*, 2010, **55**, 6973.

[129] X. Wang, L. Song, H. Yang, W. Xing, H. Lu and Y. Hu, *J. Mater. Chem.,* 2012, **22**, 3426.

[130] W. Shi, J. Zhu, D. H. Sim, Y. Tay, Z. Lu, X. Zhang, Y. Sharma, M. Srinivasan, H. Zhang, H. H. Hng and Q. Yan, *J. Mater. Chem.,* 2011, **21**, 3422.

[131] W. Wang, Q. Hao, W. Lei, X. Xia and X. Wang, *RSC Adv.,* 2012, **2**, 10268.

[132] H. Wang, Y. Liang, T. Mirfakhrai, Z. Chen, H. Casalongue and H. Dai, *Nano Res.,* 2011, **4**, 729.

[133] Z. Zhan, L. Zheng, Y. Pan, G. Sun and L. Li, *J. Mater. Chem.,* 2012, **22**, 2589.

[134] B. Zhao, J. Song, P. Liu, W. Xu, T. Fang, Z. Jiao, H. Zhang and Y. Jiang, *J. Mater. Chem*., 2011, **21**, 18792.

[135] H. Shirakawa, E. J. Louis, A. G. MacDiarmid, C. K. Chiang and A. J. Heeger, *J. Chem. Soc. Chem Comm*., 1977, 579.

[136] T. Ito, H. Shirakawa and S. Ikeda, *J. Polym. Sci.,Polym.Chem. Ed*., 1974, **12**, 11.

[137] C. K. Chiang, C. R. Fischer, Y. W. Park, A. J. Heeger, H. Shirakawa, E. J. Louis, S. C. Gau and A. G. MacDiarmid , *Phys. Rev. Letters,* 1977, **39**, 1098.

[138] C. K. Chiang, M. A. Druy, S. C. Gau, A. J. Heeger, E. J. Louis, A. G. MacDiarmid, Y. W. Park and H. Shirakawa, *J. Am. Chem. Soc*.,1978, **100**, 1013.

[139] A. R. Blythe and D. Bloor, *Electrical Properties of Polymers*, Cambridge University Press, 10-Jun-2005-Science-480.

[140] S. Bhadra, D. Khastgir, N.K. Singha and J. H. Lee, *Progress in Polymer Science*, 2009, **34**, 783.

[141] K. Zhang, L. L. Zhang, X. Zhao and J. Wu, *Chem. Mater.*, 2010, **22**, 1392.

[142] Y. Li, X. Zhao, Q. Xu, Q. Zhang and D. Chen, *Langmuir*, 2011, **27**, 6458.

[143] J. Yan, T. Wei, B. Shao, Z. Fan, W. Qian, M. Zhang and F. Wei, *Carbon*, 2010, **48**, 487.

[144] Y. Liu, N. Lu, S. Poyraz, X. Wang, Y. Yu, J. Scott, J. Smith, M. J. Kim and X. Zhang, *Nanoscale*, 2013, **5**, 3872.

[145] S. K. Ghosh and T. Pal, *Chem. Rev*., 2007, **107**, 4797.

[146] C. Y. Kang, C. H. Chao, S. C. Shiu, L. J. Chou, M. T. Chang, G. R. Lin and C. F. Lin, *J. Appl. Phys.,* 2007, **102**, 073508.

[147] X. Zhang and S. K. Manohar, *J. Am. Chem. Soc*., 2004, **126**, 12714.

[148] Y. Borodko, S. E. Habas, M. Koebel, P. Yang, H. Frei and G. A. Somorjai, *J. Phys. Chem. B*, 2006, **110**, 23052.

[149] S. Patil, V. Patil, S. Sathaye and K. Patil, *RSC Adv*., 2014, **4**, 4094.

[150] S. Patil, A. Harle, S. Sathaye and K. Patil, *CrystEngComm*., 2014, **16**, 10845.

Chapter-2

Facile room temperature methods for growing ultrathin films of graphene nanosheets and nanoparticulate tin oxide composite structure for supercapacitor application

This chapter gives a novel, facile, single step process for growing highly uniform few layer graphene nanosheets' (FLGNS) thin films over a micrometer area scale, initially formed at liquid-liquid interface and subsequently transferred on desired substrate. The process is further extended to form "monolayer" graphene nanosheets (GNS). The films are characterized by Raman spectroscopy, atomic force microscopy (AFM) and X-ray photoelectron spectroscopy (XPS), etc. The results indicate that very few chemical and/or physical defects are introduced during formation of the films. Further, an innovative single step method to form tin oxide (SnO_2) films at air-liquid interface is presented. A special feature of the method is that entire process is completed at room temperature. The film can be suitably transferred to the desired substrates by Blodgett technique. Characterization by various techniques such as XPS, TEM and energy dispersive X-ray spectroscopy (EDS) shows that the films are uniform, made up of spherical, crystalline SnO_2 particles with the size in the range of 3-5 nm. Layer-by-Layer (LbL) technique is exploited to stack graphene and SnO_2 films alternately, in a desired sequence, forming a stacked composite structure. The composite structure is subjected to characterization by XPS, FE-SEM, TEM and EDS. The results show that the structure consists of a stacking of predetermined thicknesses consisting of alternate layers of both the components. Such a structure is subjected to cyclic voltammetry (CV) studies. The results suggest that LbL grown SnO_2-GNS composites exhibit better electrochemical performance in terms of specific capacitance and cycling ability which are primary requirements for the supercapacitor application. The coating technique is simple, inexpensive and environmental friendly. A suitable explanation of the formation of both GNS and SnO_2 films is discussed. The proposed method extends the scope for production of high quality and defect free graphene nanosheets (GNS) and SnO_2nanoparticulate thin

films. The methods would be particularly useful for LbL stacking of composite films of GNS and other semiconductor nanoparticulate films.

RSC Advances, 2014, **4** (8), 4094.
(http://pubs.rsc.org/en/content/articlelanding/2014/ra/c3ra46576d#!divAbstract)

2.1 Introduction

Composites of nanomaterials are becoming an important area of research in view of value addition to the unique properties of constituent materials for their applications.[1] In this respect, polymer-nanomaterial composites,[2] porous matrix-nanomaterial composites,[3] and carbon-nanomaterial composites[4] are being studied prominently. Graphene is preferably used as a carbon component in carbon-nanomaterial composites because of its special properties, namely, its layer type 2D structure Figure 2.1, high surface area, flexibility, excellent stability and good conductivity.[5] These properties are mostly complimentary to the other component of the composite for its application in supercapacitors which is a subject matter of front line research in recent years.[6] While considering nanomaterials as a component of supercapacitor matrix, several materials are being studied, mainly, MnO_2,[7] Co_3O_4,[8] Fe_2O_3,[9] MoS_2,[10] SnO_2,[11] NiO,[12] ZnO[13] etc. Several processes are being practiced to produce GNS such as mechanical cleavage,[14] chemical cleavage of graphite,[15] exfoliation of natural graphite in various solvents by sonication,[16] acid treated pristine graphite by thermal shock[17] and electrochemical exfoliation of graphite.[18] Considering very special structural relation between graphite and graphene; it was obvious to use graphite as a precursor for the production of graphene. There are two major problems to obtain graphene from graphite. 1) Exfoliation of graphite and 2) avoiding restacking of exfoliated layers. The scientific community has accepted an answer to the first problem, i.e. by weakening of van der Waals bonds in graphite through surface oxidation or introducing intercalating species in between graphite layers. The oxidized graphite, called graphite oxide (GO) gets dispersed in water on sonication which can be subsequently reduced to graphene by common reducing agents, forming graphene dispersions. However, dispersing agent is needed to stabilize graphene dispersions. Therefore, one can alternatively design and develop binder-free method

to obtain GNS which can be handled to form the hybrid structure for desired application such as supercapacitor.[19] Many intercalating agents or other species have been studied by introducing those in graphite layers to weaken van der Waals bonds. Thus, subsequent process of sonication can break stacked graphite structure to form graphene dispersions. The requirement of dispersing agent, however, persists. In some applications, the presence of dispersing agent, even in trace amount, becomes detrimental.

To make thin films of graphene is an important issue scientifically, as for some applications, it is a prerequisite. Once the dispersion of graphene is formed, known processes like spin casting and Langmuir-Blodgett assembly can be employed to get thin films of graphene. Chemical vapor deposition (CVD), using variety of carbon precursors, has been reported to give monolayer/few layer graphene films.[20] However, these methods suffer from the need of expensive equipment/high vacuum.

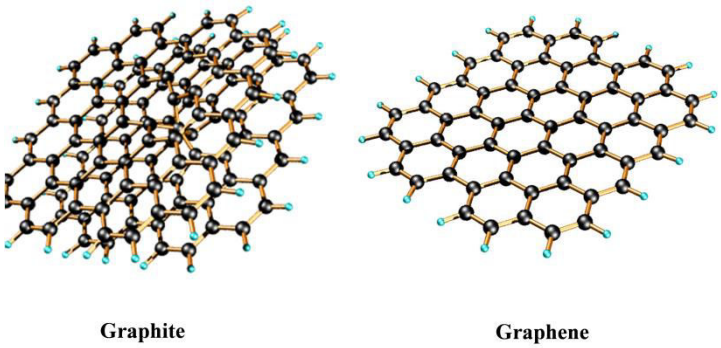

Figure 2.1. Crystal structure of graphite and graphene.

Image courtesy http://www.chm.bris.ac.uk/webprojects2001/may/grappic.gif, http://cnx.org/resources/bac5ec5fc6a10f049e0f85c5470c7d24/graphene.jpg

In this present Chapter, we are going to discuss a novel method to grow thin film of monolayer/few layer graphene. The method, instead of using dispersing agent to arrest restacking of dispersed graphene layers, confine the exfoliation and/or dispersion reaction to air-water interface. These dispersed GNS are, later, compressed laterally and transferred to the suitable substrates to form uniform films.

To effectively overcome the shortcoming of limited specific capacitance of graphene and other nanomaterials, their composites have been considered for the supercapacitor application.[21] Till date, there have been numerous reports on preparing graphene supported Sn-based materials to improve their separate electrochemical

performance.[22] Moreover, in one of the applications it has been reported that Sn-based nanoparticles could be easily peeled off from the graphene leading to failure of its performance in concerned application.[23] Therefore; it is of great interest to develop a facile and reliable structure to bind Sn-based nanomaterials on the graphene surface. There is still a requirement for an efficient and facile route to achieve satisfactory control of such architecture with graphene supported nanocomposites.[24]

Tin Oxide (SnO_2) having special properties, namely, wide band gap (3.6 eV), ease of maneuvering conductivity from metallic to insulating, optical transparency, low cost, chemical stability, suitability for forming thin films on common substrates like glass is studied presently to form a composite with graphene. Considering its high theoretical capacity, recently it has been studied as an anode materials in Li-ion batteries.[25] Most of the methods of formation of SnO_2; namely, sol-gel,[26] spray pyrolysis[27] electron-beam plasma-deposition,[28] sputtering,[29] chemical vapor deposition,[30] atomic layer deposition,[31,] etc; involve a step requiring high temperature or use of costly equipment.

Taking these limitations in to account, we have developed a method using the same equipment that is used to grow graphene thin films, to form nanoparticulate SnO_2 thin films which involve only room temperature processing steps. Thus, the second attractive aspect of this chapter is that we report a versatile method to grow thin film of nanoparticulate crystalline SnO_2. The particle size in these films is in the range of 3-5 nm which is an achievement, rarely reported.[32] Also; the method neither employs any dispersing agent to arrest the particle growth nor any capping agent. Instead, the reaction of formation is confined to air-water interface. Procedurally, the methods to grow thin films of GNS and SnO_2 are very similar.

The special features of this method are 1) room temperature reactions, 2) making use of the liquid-liquid interface for the confinement of particle size of the desired material in the film, 3) formation of a thin film of end product in a single step etc. Applying the above mentioned method to grow thin films of presently 'hot' material, namely graphene, needed a modification, involving use of solid material in the reaction for the first time. Also, similar reaction was conceived to grow thin films of SnO_2, a material with wide range of applications presently and in the future. Apart from these developments, it was thought that the formation of ultrathin film of the

desired materials could be exploited to form a composite with uniform distribution along its thickness by employing layer by layer deposition of the components.

Another feature of the present research is that the GNS and SnO_2 layers can be grown over each other in a desired sequence using LbL assembly, forming a matrix of the composite. One can decide the sequence so as to maximize the synergetic effect of components in the desired electrochemical application. Such architectural structures would be useful in other applications such as, optoelectronic devices, dye-based solar cells, catalysts, gas sensors, electronic devices and electrode materials.[33]

2.2 Experimental Section

All chemicals were analytical grade and used without any further processing. Conc. Sulfuric acid (H_2SO_4, 98%), Oleic Acid (99% by GC), Hydrogen per oxide (H_2O_2, 35%), Ethylene diamine (EDA, 99%), were purchased from Merck chemicals. Carbon tetrachloride (CCl_4 99.5%) was purchased from Loba Chemie. Tin metal (99.998%) and graphite rod (99.99%) were purchased from Sigma-Aldrich. Water used in this process was doubly distilled de-ionized.

2.2.1 Preparation of graphene film on a suitable substrate via air-water interface reaction.

2.2.1.1 Rationale

LLIRT has been employed for the deposition of many semiconductor films. Further, it is suitably modified to grow organic materials, complexes like copper phthalocyanine and polymer films. Mostly, these films were polycrystalline in nature and having 3D structure. Later, yet another modification of LLIRT is reported to grow 0D films of semiconductors (CdS).[34] With the progress in modern materials, there was a need to grow thin films of 2D layered structured materials like graphene, MoS_2, etc. One needs to imagine a reaction which may exfoliate bulk graphite/MoS_2 at liquid-liquid interface. Incidentally, the literature on the subject gives intercalation processes which on sonication resulted in exfoliation of respective materials. It was rather difficult to sonicate bulk materials at liquid-liquid interface without disturbing the interface itself where formation of thin film is expected. Therefore, it was decided to try other source of energy to exfoliate solids without disturbing the interface itself. It

occurred to us that heat of reaction of intercalated species could be used for the purpose. Therefore, graphite was intercalated by H_2SO_4 and spread on subphase water as in a step of LLIRT. The exothermic reaction resulted in exfoliation of graphite to graphene which was of course reported in the literature as shown in following reaction,

$$H_2SO_4\,(l) \longrightarrow 2H^+\,(aq) + SO_4^{2-} \quad -96.2\ kJ/mol\ (aq) \quad (1)$$

The energy is briskly released in this reaction and it is sufficient to overcome the bond strength of van der Waal bonds (0.4-4.1 kJ/mol), holding graphene layers together, as well as facilitates exfoliation.

Thus, we could successfully grow graphene films without disturbing the interface. Encouraged by this result, we adapted same methodology to grow thin films of layered graphene successfully which becomes a major contribution from this thesis work.

Our approach was to use intercalated graphite/expanded graphite as a precursor to graphene as it gets easily exfoliated during film formation procedure. Natural graphite rod which is tapered at one end is used as a starting material. The tapered end was converted to expanded graphite by treating it with 98% concentrated sulphuric acid for 30 hrs at room temperature.

2.2.2 Optimisation of synthesis of graphene films by LLIRT

The interaction/intercalation time of sulphuric acid is a very important factor. The number of layers in graphene was always more than one when intercalation time was less than 24 hrs. Thus, after the careful observations it was optimized that the process needs the dipping time up to 30 hrs.

The choice of H_2SO_4 was done apart from possible acids viz. HNO_3, $HClO_4$ and HCl and the respective heat of solution are -33.3 kJ/mol, -88.8 kJ/mol, -74.8 kJ/mol respectively.

Thus, sulphuric acid with heat of solution of -96.2 kJ/mol was more suitable for the exfoliation process as the reaction with water would be exothermic and kinetically fast. Further the purification process of end product is easier when H_2SO_4 is used. Another consideration was to find a suitable spreading solvent for this process. The solvent must not react with the acid present in the intercalated graphite.

The different solvents viz. n-hexane, chloroform, carbon tetrachloride (CCl_4), DCM and NMP were studied. Each spreading solvent/s has its own cons and pros. In order to fit in LLIRT, the solvent must spread spontaneously over the subphase and also it must have low boiling point for its fast evaporation. CCl_4 was found to be the best amongst the studied spreading solvents.

In a typical experiment, intercalated graphite was exfoliated as narrated above. It led to the formation of layered graphene on aqueous surface. The graphene layers were laterally compressed by using an oleic acid piston to form a film. The procedure of formation and transferring the film to a substrate is described in the chronological steps as follows.

The general method of the formation of graphene thin films at air-water interface is based on earlier reported procedure for deposition of cadmium sulphide.[35] However; some modifications were introduced for the present purpose of formation of graphene film at air-water interface.

In a typical procedure,[35] deionised water (sub phase) was placed in a Teflon tray (15 cm x 15 cm x 2 cm) so that it formed a meniscus at the edges. The surface of the subphase is divided into two compartments by a Teflon thread barrier (Scheme 2.1). The tapered tip of the expanded graphite rod was arranged in such a way that it just touches the meniscus of the sub-phase in one of the compartment. A few drops of carbon tetrachloride were allowed to slide on expanded graphite rod which spread on entering the water surface. Along with it, GNS formed at the tip, touching water, also spread on the surface forming GNS/few layer graphene (FLGNS) on the subphase surface. After allowing all CCl_4 spread on the surface to evaporate naturally, the GNS/FLGNS film was then compressed laterally via a teflon thread barrier by spreading a drop of oleic acid on the surface of subphase in the other compartment of the tray. The spreading oleic acid (pressure 30 dynes cm^{-1}) acts as a piston. The as formed compressed film on the subphase surface (water) was transferred on a glass/quartz or silicon wafer substrate by immersing the substrate vertically in the subphase where the compressed GNS/FLGNS film floats, at a constant rate of 0.5 cm/min. and lifting it vertically at the same rate so that the film covers the dipped area of the substrate (Langmuir Blodgett technique).

A similar procedure was adapted to deposit the film on the TEM grid. If a few layered graphene thin films are used as a precursor, in place of graphite initially used,

it is transformed in intercalated film by treating it with sulphuric acid and then used as a starting material for film formation; we call it as double exfoliation. The operation was repeated many times to get a large film thickness when desired.

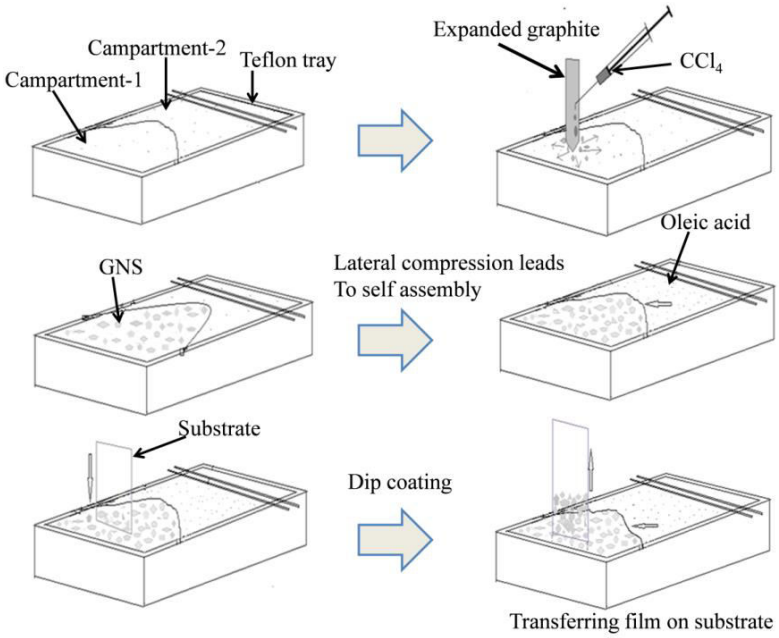

Scheme 2.1 Schematic illustration of self-assembly of graphene films.

The film was then washed with deionised water several times until it turned out to be of neutral pH. This film was then used for characterization. Calibration of the mass with respect to number of dips at a fixed dipping area was established by using quartz crystal microbalance (QCM-200).

2.2.3 Preparation of SnO_2 nanoparticulate film

Deng et. al.[36] reported the procedure of formation of SnO_2 nanoparticles and the chemistry involved in it. The multiple steps procedure was modified, making it suitable for the application of Liquid-Liquid Interface Reaction Technique (LLIRT) which makes it a 'one step method'. The procedure is based on LLIRT reported earlier.[35]

The actual procedure is comparable to the procedure to form GNS film as described in Scheme 2.2. The chronology of formation of thin film of tin-oxide is as follows.

In a typical procedure, deionized water was placed in a Teflon tray (15 cm x 15 cm x 2 cm) so that it formed a meniscus at the edges (sub phase). The surface of

the subphase was divided into two compartments by a Teflon thread barrier.

In one of the compartments, a tip of tin metal was arranged so as to touch the meniscus of subphase (water). Successively, 0.2 mL ethylene diamine (EDA) and 0.2 mL of hydrogen peroxide were allowed to pass over metal, drop by drop by using a micro syringe, resulting in the spreading of the mixture over the surface. When Teflon thread barrier gets fully stretched, oleic acid was allowed to spread in the second compartment so that the film formed in the first compartment gets laterally compressed by the pressure of 30 dynes cm^{-1}. Then the substrate was allowed to dip vertically at the constant speed of 0.5 cm. min^{-1} and retrieved at the same rate during which film formed on the surface of subphase gets transferred to the substrate by a well known Langmuir Blodgett technique. The dried film was washed with distilled water several times. The films formed by this procedure were used for the characterization.

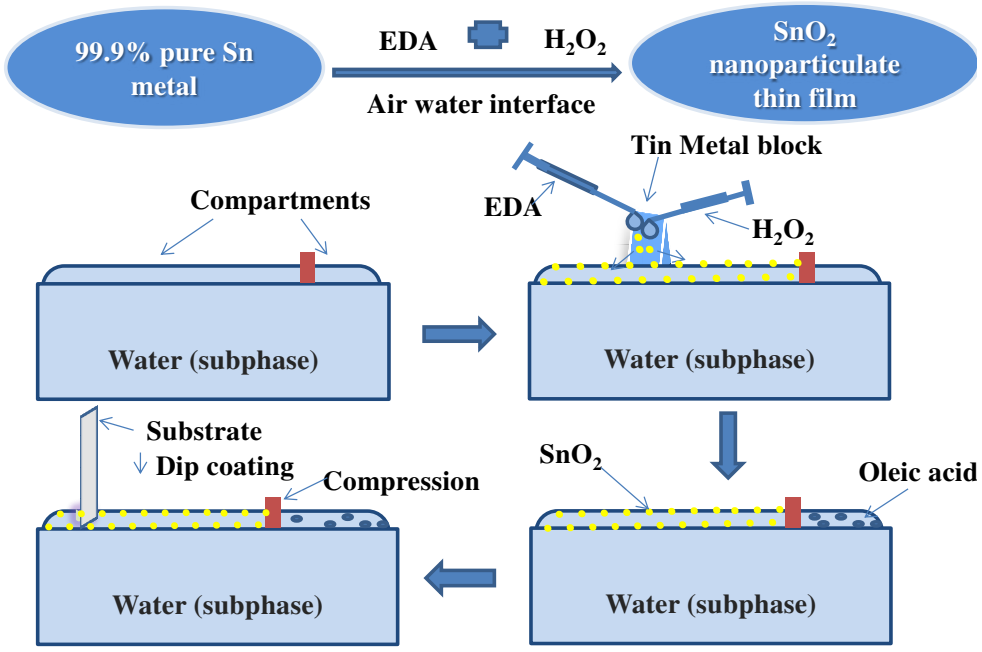

Scheme 2.2 Schematic illustration of formation of SnO_2 nanoparticulate thin film

Thus, during this thesis work, two procedurally similar but otherwise independent and novel techniques are developed, to form graphene and SnO_2 films respectively, by modified LLIRT at room temperature. Moreover, we point out that the techniques can be useful for the growth of the composite matrix consisting of graphene and SnO_2 by the application of modified conventional LbL technique using

a desired sequence which might become important for some specific applications. In fact, such sandwich structure is reported to have an advantage over the use of composite film of same constituents in supercapacitor application.[37]

In the conventional technique, the use of chemical is made which gives a typical charge to the earlier deposited film surface; followed by the use of chemical which gives apposite charge, is made in a subsequent step. This particular procedure increases the number of steps as well as the use of typical chemicals becomes essential. We would like to point out that the above described limitations are overcome in the modified process.

Thus, the above described procedures are put into practice to form the composite film of SnO_2/GNS, by forming the film of each component in two independent trays. By dipping the substrates in one of the trays, a film of GNS/SnO_2 with desired thickness is deposited on the substrate. Then the same substrate is dipped in the other tray to deposit the film SnO_2/GNS with desired thickness and so on. The structure formed by repeating the procedure is shown in Scheme 2.2. The SnO_2/GNS hybrid electrode of desired thickness is obtained by deciding number of bilayers. Thus, $(SnO_2/GNS)_{60}$ assembly indicates 60 alternate dips of each components in hybrid electrode for which the electrochemical study has been done.

Scheme 2.2 Schematic representation of SnO_2/GNS composite.

2.2.4 Sample characterization

For TEM and HRTEM analysis, samples were prepared on a carbon-coated copper grid that was temporarily fixed on the glass substrate. The grid fixed substrate was then coated by the film by the above-described procedure by dipping it twice in the solution containing GNS film on the surface. The film-coated grid was processed for TEM analysis. The electron diffraction facility was employed during the morphological characterization of the film for the assessment of the structure and the phases present. The morphology and size of as-prepared products were observed by

transmission electron microscopy (TEM), carried out on a JEOL 1200-EX transmission electron microscope with an accelerating voltage of 100 kV, and high-resolution transmission electron microscopy (HRTEM) (JEOL 2010F) at an acceleration voltage of 300 kV.

The surface species were analyzed using X-ray photoelectron spectrometer (XPS, VG Micro Tech ESCA-3000). The chamber pressure was about 1 x 10^{-9} Torr under testing condition. Peak deconvolution of C1s was accomplished using XPS Peak 4.1.

Atomic force microscopy is considered as an effective tool for the characterization of mono- or few-layer graphene. The morphology and microstructure of the casted film was examined by an atomic force microscope (AFM, Digital Instrument Environ Scope) using a tapping mode. FE-SEM (Hitachi, S-4800), is used to get additional information of morphology and microstructure. Raman spectroscopy is accepted as a reliable tool to decide the formation of mono/few layer graphene structures and hence used to characterize graphene (HR-800, Horiba Jobin Yvon) by using an excitation at 632 nm. The absorption in the UV-Vis region was studied on the films deposited on the quartz substrate using a JASCO dual-beam spectrophotometer (Model V-570) operated at a resolution of 1 nm. FTIR spectra were collected with a Nicolet Magna 550 spectrometer. Cyclic voltammetry and constant current charge/discharge test were performed on an electrochemical workstation (CHI 660C) at varying potentials ranging between -0.7 and 1.2 V and 0 to 1V respectively in 0.1 M H_2SO_4 aqueous solution at room temperature.

2.3 Results and Discussion

2.3.1 Synthesis and characterization of GNS

Expanded graphite obtained by the intercalation of sulphuric acid between the graphite layers is used as a graphene precursor.

2.3.1.1 XRD analysis

The XRD analysis of the precursor reveals that as a result of intercalation, it does not deviate from the basic structure of pure graphite as shown in Figure 2.2.
The only difference observed is that the full width at half maxima (FWHM) is slightly increased from 0.23 to 0.28^o as measured for graphite (002) peak. This shows that

there is no damage of the graphite crystalline structure. Expanded graphite is thus, a readily available source for exfoliation, resulting in GNS.

The formation of GNS layer can be understood by considering the chemistry that occur at the tip of graphite rod after it touches the meniscus of sub phase water. The intercalated sulphuric acid would react violently with water which is an exothermic reaction. The large amount of energy released during the reaction is sufficient to break van der Waals bonds between graphite layers, resulting in exfoliation of graphite. After the exfoliation, carbon tetrachloride is allowed to spread from the graphite tip over the whole area of the tray compartment.

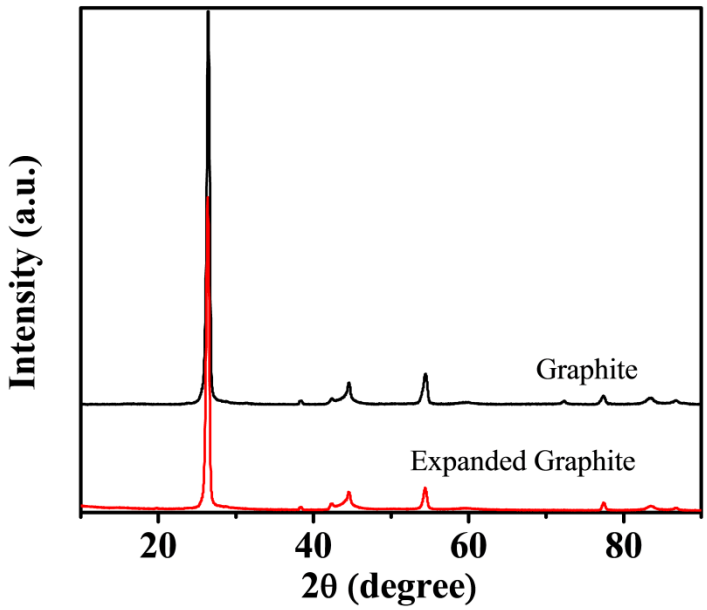

Figure. 2.2 XRD pattern of (a) natural flake graphite and (b) expanded graphite.

Along with carbon tetrachloride, exfoliated graphene layers also occupy the surface of the subphase. Further, the lateral compression results in the compaction of GNS layer which is later transferred to a suitable substrate.

2.3.1.2 Raman Spectroscopy

The formation of GNS film at air-water interface and subsequently transferred on glass substrate was investigated by Raman and XPS studies. The Raman spectroscopy is extensively employed to characterize carbon materials. The characteristic G-band (~ 1580 cm^{-1}) and D-band (~ 1350 cm^{-1}) in the Raman spectrum are assigned to the E_{2g} phonon of C-sp^2 atoms, and breathing mode of k-point

phonons of A1g symmetry mode, activated by the presence of disorder respectively.[38] The nature of these two bands is known to be indicative of defects/disorders in carbon materials.[39] Raman spectrum of the GNS film is depicted in Figure 2.3.

A key structural parameter, the Raman intensity ratio of the D-band to G-band (I_D/I_G), can index the degree of disorder in sp^2 bonded carbon. The two major components of the spectrum consisted of peaks at 1570 cm^{-1} and 2645 cm^{-1} which are commonly designated as the G-band and the 2D-band respectively.

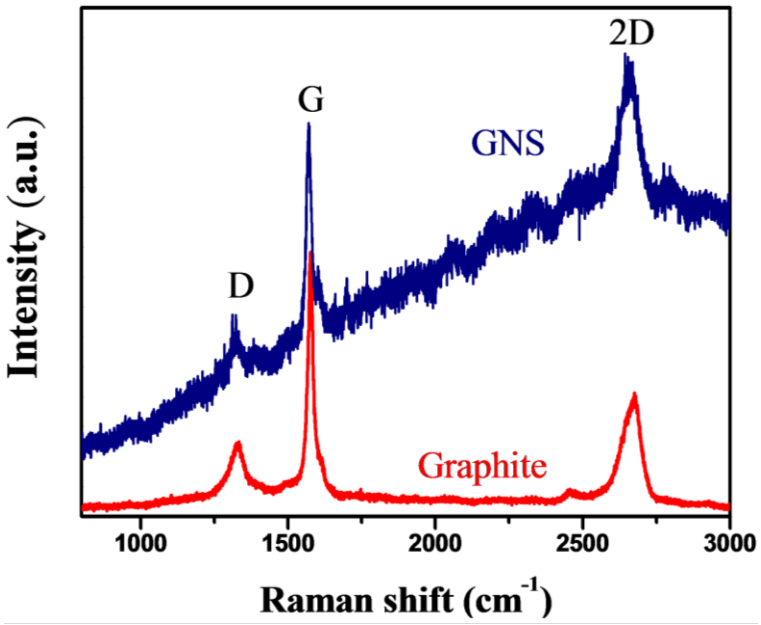

Figure 2.3 Raman spectra recorded for graphene nanosheets (GNS) and Graphite.

It was demonstrated that not only graphite can be easily distinguished from graphene but also the number of layers in graphene could be determined from Raman spectra.[40] Also, the position of D and G-band respectively indicate, the presence and number of layers of graphene. Higher intensity of G-band than that of D-band (I_D/I_G = 1/5) is indicative of number of layers in graphene sheets.[41] However, in the present case, the ratio I_D/I_G is 0.3, suggests that the product could be few-layers of graphene (FLGNS). The D-band found in the spectrum at 1323 cm^{-1} which is of significantly lower intensity, can be attributed to lattice defects formed in the structure during the processing.[42] It is also reported that the 2D-band at ~ 2700 cm^{-1} is sensitive to the number of layers. Also a shift to higher wave number indicates increasing number of layers. Chen et. al, [43] reported that the 2D band occur at ~ 2645 cm^{-1} for one layer of graphene. Further, it is mentioned that 2D band shifted to ~ 2750 cm^{-1} for 20 layers of

graphene. The Raman spectroscopy study of the films formed by the present procedure shows that 2D band occurs at ~2645 cm^{-1}, a shift to a much lower frequency than 2700 cm-1, which is in close agreement with the value reported for single layer graphene.[41]

2.3.1.3 Fourier transform infra red (FTIR) spectroscopy

The FT-IR of graphene film clearly shows (Figure 2.4) the absence of bands at (~1700-1800 cm^{-1}) which is expected for C=O functionality and therefore it is inferred that the oxide formation is absent in the present GNS product.

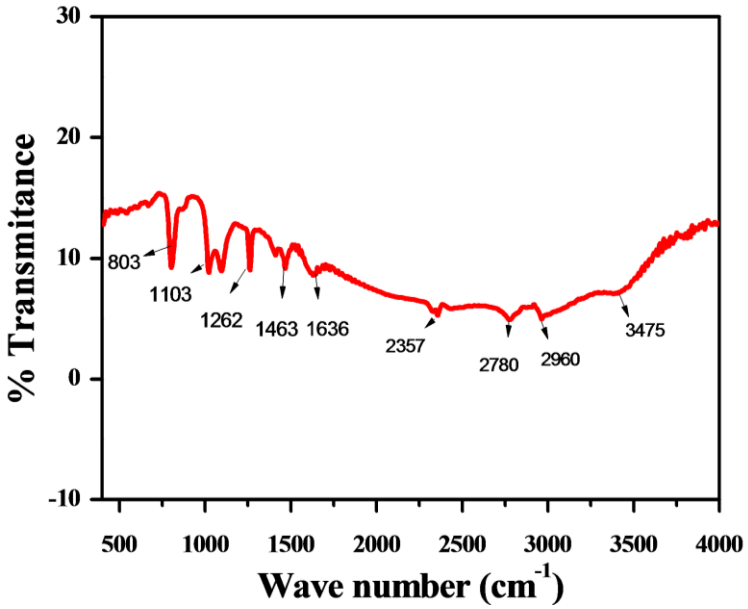

Figure 2.4 FTIR spectra for exfoliated graphene nanosheets (GNS).

However, band at ~3475 cm^{-1} attributable to C-OH functionality is found to be present in low intensity suggesting the OH bonding to graphene, most probably at the edges of the sheet. Bands at ~2700-2900 cm^{-1} are due to sp^3 carbon atoms, and intense band at ~1636 cm^{-1} indicates sp^2 hybridized carbon.

2.3.1.4 X-ray photoelectron spectroscopy (XPS)

The surface chemical composition of the graphene nanostructure is further characterized by XPS. XPS spectrum depicts a survey scan of GNS which shows the presence of two elements, namely, C and O with the relative atomic percentage of (94.2) and (5.8) respectively as shown in Figure 2.5a. It is significant to note that S2p

is not indicated to be present from XPS analysis, on the background that H_2SO_4 intercalated graphite has been used as precursor for growing GNS films. Judging from these data, it could be noted that while precursor graphite was transformed into graphene nanosheets (GNS), very few impurities are retained or newly introduced. The high resolution C1s XPS shown in Figure 2.5b shows a single peak at 284.6 eV with an asymmetrical tail at higher energies.

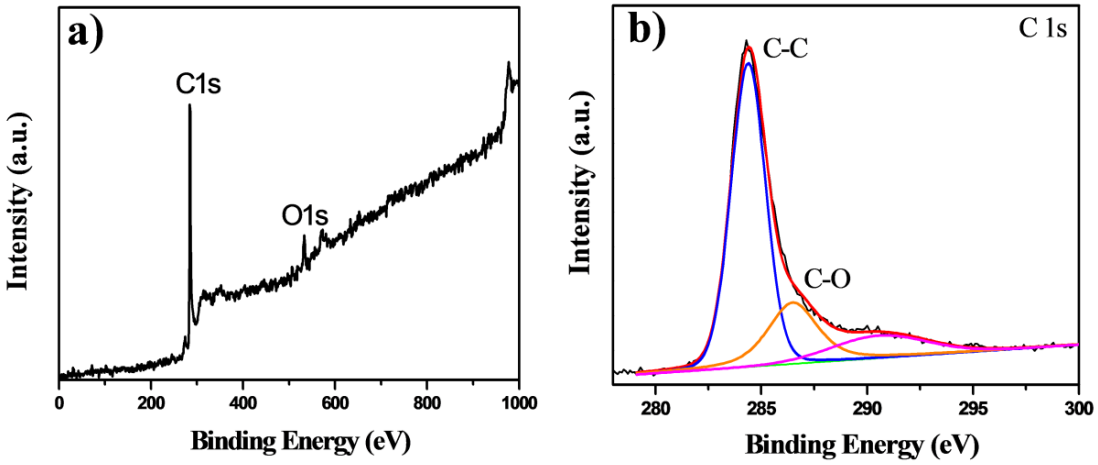

Figure 2.5 General XPS spectra for GNS (a) and C1s for GNS (b).

The main component of deconvoluted peak represents graphitic carbon (C-C) while the remainder (286.4 eV) components are attributed to be made up of a very low amount of C-O derived from graphite stacking material[43] as well as $\pi - \pi^*$ shake-up signal (290.1 eV) which is typical for sp^2 hybridized carbon.[44]

2.3.1.5 Scanning electron microscopy (ESEM) and transmission electron microscopy (TEM)

The morphologies and microstructures of the FLGNS and GNS were characterized by FESEM and TEM. As illustrated in Figure 2.6 FE-SEM of the GNS possesses an ideal layer structure over a micrometer scale. Figure 2.7 shows the TEM images of GNS film. Figure 2.7a shows that the FLGNS film consists of transparent layers forming sheets with a very few dark ripples. The transparency reveals that the sheets contain only a few graphene layers. The few dark ripples could arise from the scrolling and crumpling of nanolayers during the formation of sheet.

The inset image of few-layer graphene in Figure 2.7a shows a spot diffraction pattern with hexagonal symmetry which indicates monocrystalline nature of resulting

layers. Transmission electron microscopy (Figure 2.7a) and selected area electron diffraction pattern (SAED inset of Figure 2.7a) were used to characterize the single layer GNS.

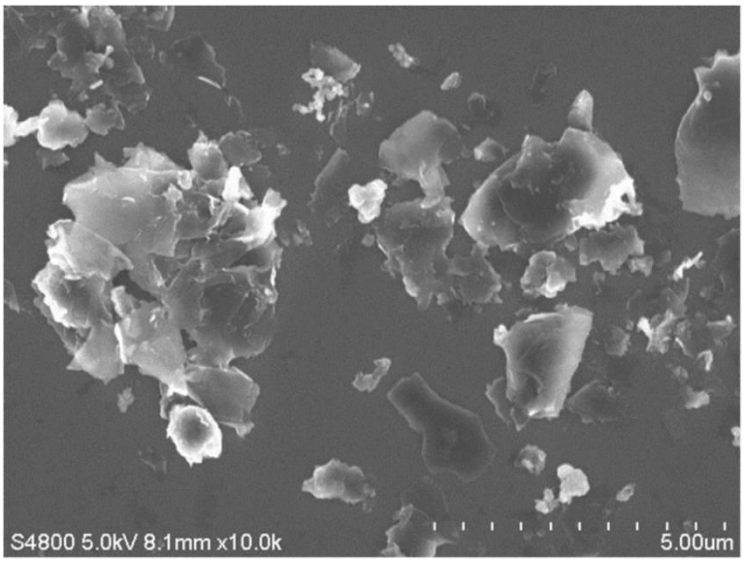

Figure 2.6 FESEM image of graphene sheet indicating the graphene sheets are continuous over micrometer scale area.

The intensity of the spots (SAED profile in inset of Figure 2.7 a) on inner hexagon is higher than that of outer hexagon, is an indication of a single layer GNS. The SAED pattern of GNS was similar to that reported for graphene sheet, confirming a single-layer graphene film formation.[45, 46]

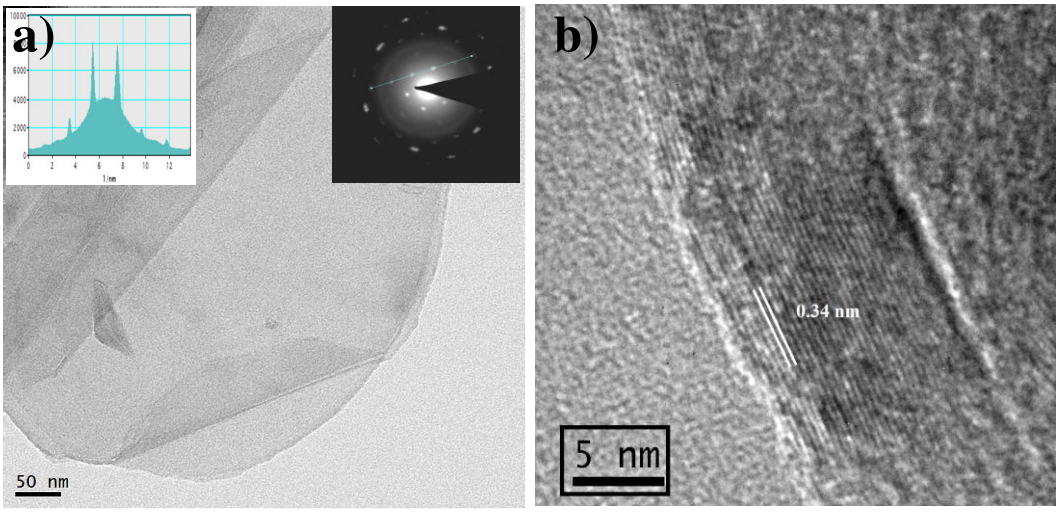

Figure 2.7 TEM images of GNS (a) the inset is the corresponding SAED pattern and SAED profile. (b) HR-TEM of GNS.

Figure 2.8 shows TEM image of the few-layer graphene, wherein graphene sheets with length in micrometer range is clearly seen. The HRTEM image of stacked graphene layers where the fringes are clearly displayed in Figure 2.7b. The distance between the lattice fringes measures to be about 0.34 nm which is corresponds to the spacing of the (002) planes of graphite structure. The characterization of films by TEM, FESEM, SAED and HRTEM infers that the method of formation of thin films results in the product, namely, FLGNS crystalline film with a very few defects. Also, by following proper procedure, a single layer graphene film can be achieved without any complicated and cumbersome procedure.

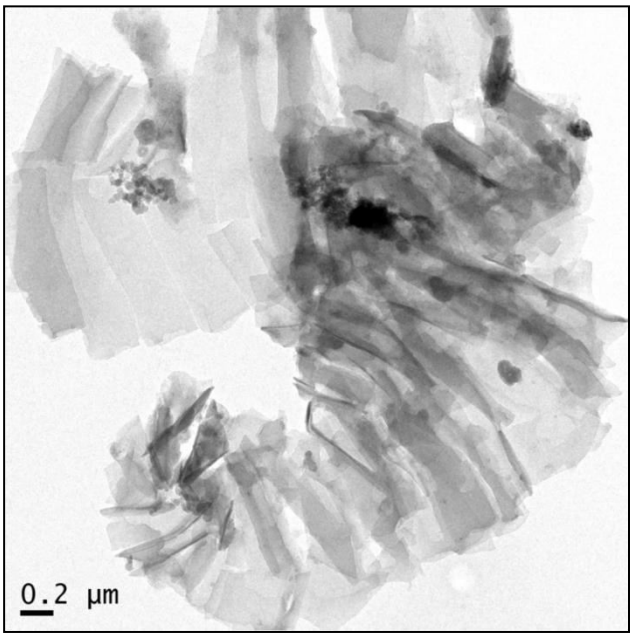

Figure 2.8 The TEM image of graphene sheets with varying length.

These results indicate that the sheet structure of graphene is well retained even after double exfoliation.

2.3.1.6 Atomic Force Microscopy (AFM)

AFM was employed to confirm that graphene sheets are indeed formed by the present method. The AFM morphological images and the corresponding cross-section analysis of GNS on the silicon wafer substrate are shown in Figure 2.9. It can be seen that the FLGNS possesses an average thickness of ~4 nm which indicates that graphene sheet is formed by stacked 4-5 graphene layers.[47] When the exfoliation process is repeated twice, the resulting film shows the average thickness of ~0.8 nm

which is close to the thickness of single layer of graphene[48] indicating that a single layer GNS has been obtained successfully by the present simple method.

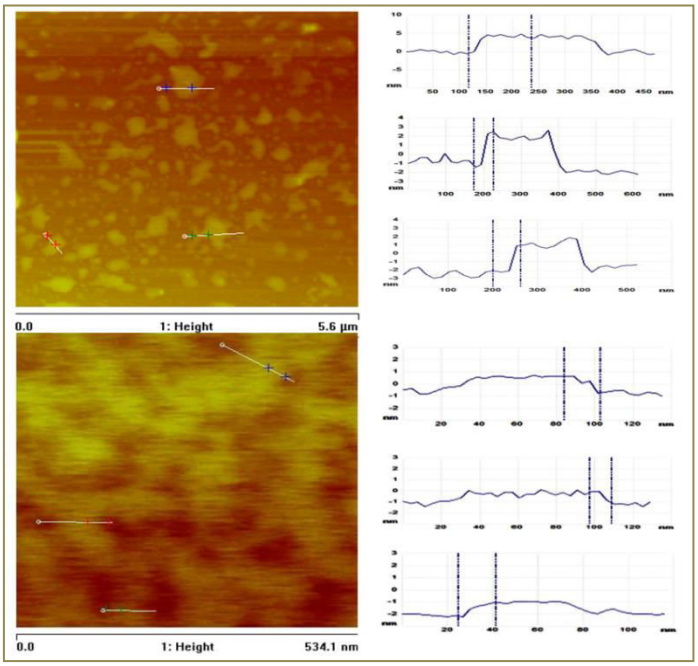

Figure 2.9 AFM images of GNS and its cross section.

2.3.2 Synthesis and characterization of SnO_2 nanoparticulate films

The basic reaction of tin oxide formation[49] occurring at the interface would be,

$$Sn_{(S)} + 2\ EDA \longrightarrow [Sn(EDA)_2]^{2+} + 2e^-$$

$$[Sn(EDA)_2]^{2+} + 2\ H_2O_2 \longrightarrow SnO_2 + 2\ EDA$$

EDA plays a double role in the reaction. Sn precursor is in the form of a solid metal. Moreover, oxidation of tin metal by hydrogen peroxide is slow. EDA forms a complex with metallic tin and thus, transforms it into solution form. Also, it acts as a catalyst, accelerating oxidation of tin metal by hydrogen peroxide.[36] Thus, in the presently reported procedure, formation of tin oxide at the interface is well justified. Since the reaction is confined to air-water interface, the aggregation of tin oxide particles is controlled as against the use of PVP as capping agent.[36]

2.3.2.1 Electron dispersive x-ray spectroscopy (EDS) and XPS analysis

To establish, chemical identity of the samples, XPS study was employed as shown in Figure 2.10. EDS facility in SEM was employed to obtain the atomic ratio of Sn-O which found in agreement with XPS analysis as shown in Figure 2.11.

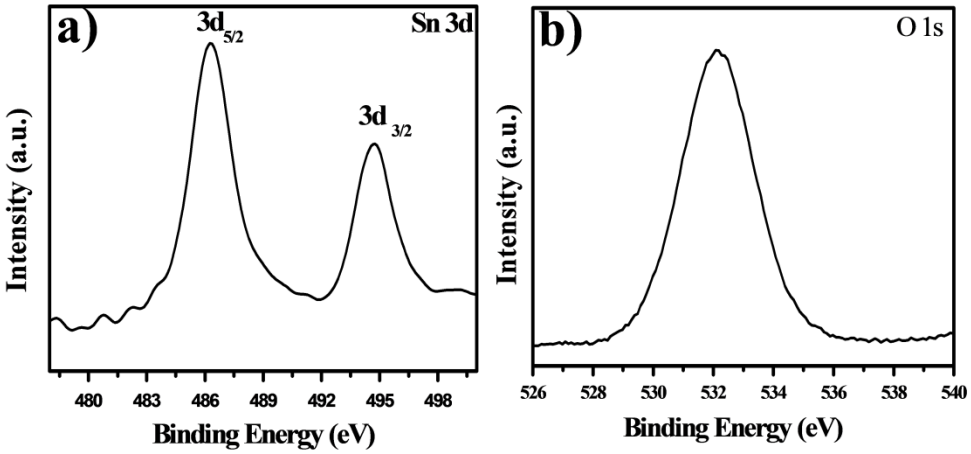

Figure 2.10 Characterization of SnO_2 nanoparticulate thin film a) XPS spectra of SnO_2; b) 3d and O 1s;

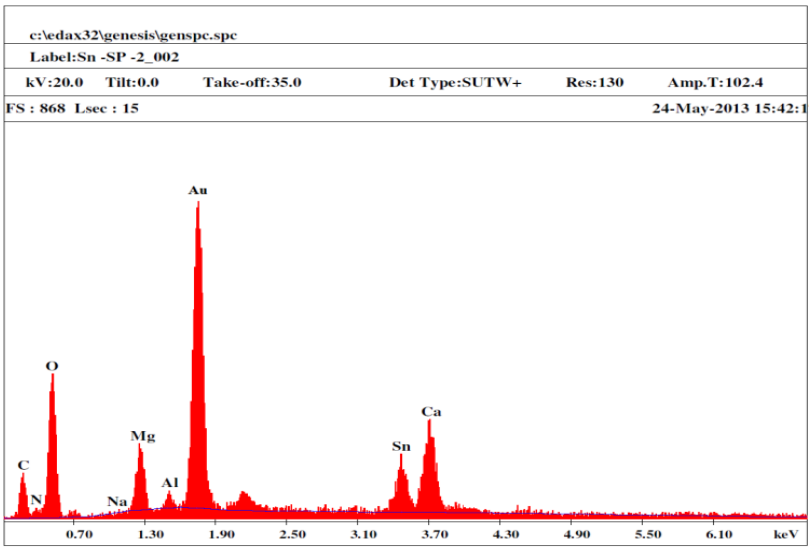

Figure 2.11 EDS of SnO_2 thin film over the glass substrate coated with gold.

The X-ray photoelectron spectroscopic (XPS) measurements were performed to investigate the chemical composition of the surface of SnO_2. XPS survey scan shows C, O and Sn without any other impurities. Figure 2.10 presents the high resolution XPS of Sn3d and O1s spectra of the SnO_2. Figure 2.10a gives the Sn3d spectrum in which the peaks of $Sn3d_{5/2}$ and $Sn3d_{3/2}$ are located at 486.5 and 495.1 eV,

respectively, with an energy separation of 8.6 eV, confirming the formation of SnO_2.[49] The peak of O1s (530.5 eV) is attributed to Sn-O. The atomic ratio of the Sn and O was estimated by considering the intensities of the $Sn3d_{5/2}$ and O1s levels and their corresponding photoionization cross sections. The ratio was found to be close to 0.5, supporting the formation of SnO_2. Further, after confirming the chemical identity of the samples, to envisage the morphology and structure the SnO_2 films were characterized by TEM and HRTEM as shown in Figure 2.12.

2.3.2.2 Transmission electron microscopy (TEM) of SnO_2 nanoparticulate thin film

TEM image demonstrates that the resulting nanoparticles are well separated and do not agglomerate. The average particle size of SnO_2 is in the range of 3-5 nm as illustrated in the histogram plot as shown in Figure 2.12a lower inset.

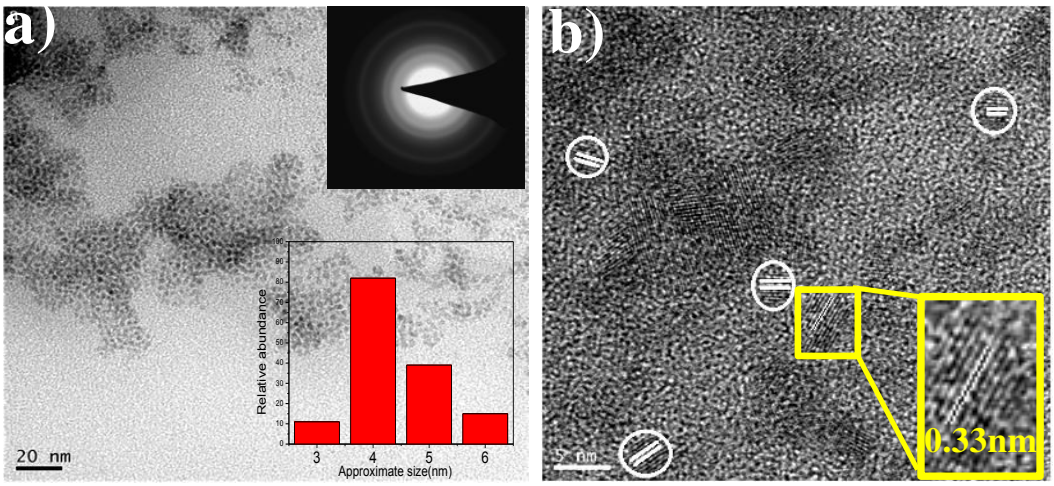

Figure 2.12 Transmission electron microscopy image of SnO_2 nanoparticles (a) inset shows SAED (upper right) and histogram of particle size distribution (lower right), (b) High resolution TEM of SnO_2 nanoparticles inset shows lattice fringes for SnO_2 particles.

The HRTEM image of SnO_2 nanoparticles exhibits clear lattice fringes with lattice spacing of 0.33 nm corresponding to the interplaner distance of (110) lattice planes of tetragonal SnO_2 (JCPDS no. 41–1445) as shown in Figure 2.12b. Selected area electron diffraction (SAED), shown in the upper inset of Figure 2.12a, proves that the SnO_2 has a polycrystalline structure and the observed rings could be ascribed to (110), (101) and (211) planes of the tetragonal SnO_2 (JCPDS no. 41–1445).

2.3.2.3 UV-Visible spectroscopy (UV-Vis)

UV-vis absorption spectrum of SnO_2 as shown in Figure 2.13 was recorded to elucidate information on the band gap energy. The cut-off wavelength in the films formed by the present process is at 329 nm, much lower wavelength than at 340 nm, reported for bulk tin oxide, indicating a significant blue shift which can be ascribed to the quantum confinement effect of nanoscale particles.[50]

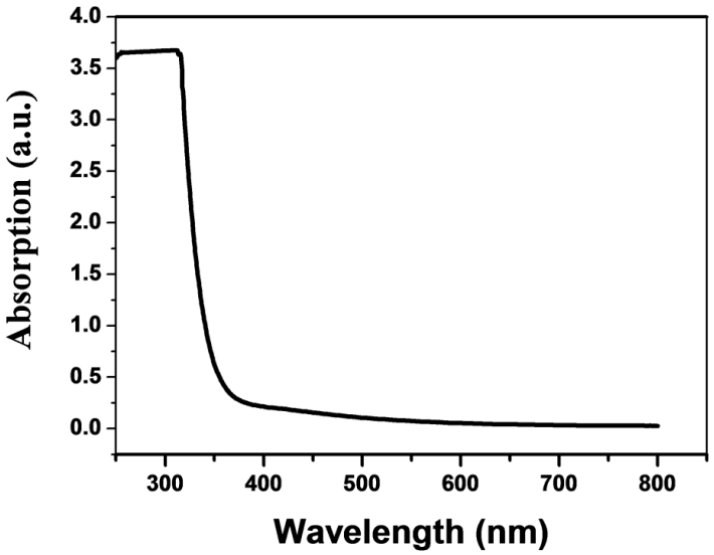

Figure 2.13 UV-Vis. Spectra for pure SnO_2 nanoparticulate thin film.

2.3.3 Characterization and physicochemical properties of SnO_2/GNS composite

The films of composite deposited by the procedure described in the experimental section are characterized as given below. The composite had a composition $(SnO_2/GNS)_{60}$ as explained in experimental section.

2.3.3.1 RAMAN spectroscopy

In order to verify the formation of the SnO_2/GNS composite, the samples were studied by Raman spectroscopy (Figure 2.14). Apart from usual graphene peaks, the two peaks are observed at about 431 and 710 cm^{-1} for SnO_2/GNS composite.

The peak at 431 cm^{-1} corresponds to the high frequency E_2 modes of SnO_2. The peak at 710 cm^{-1} may be caused by the combination of transverse optical (TO) and longitudinal optical (LO) phonon mode.[51]

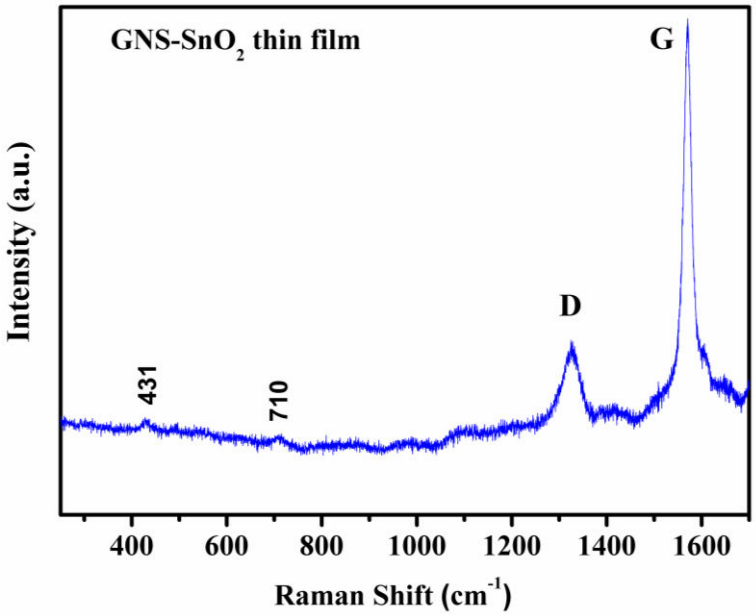

Figure 2.14 RAMAN spectra of SnO_2/GNS composite.

Such a result demonstrates that the layer by layer deposition followed in the present work has successfully synthesized SnO_2/GNS composite films.

2.3.3.2 Transmission electron spectroscopy (TEM) and EDS.

TEM studies accompanied by SAED and EDS were performed to characterize the morphology, structure and chemical composition of the SnO_2/GNS composites, as depicted in Figure 2.15.

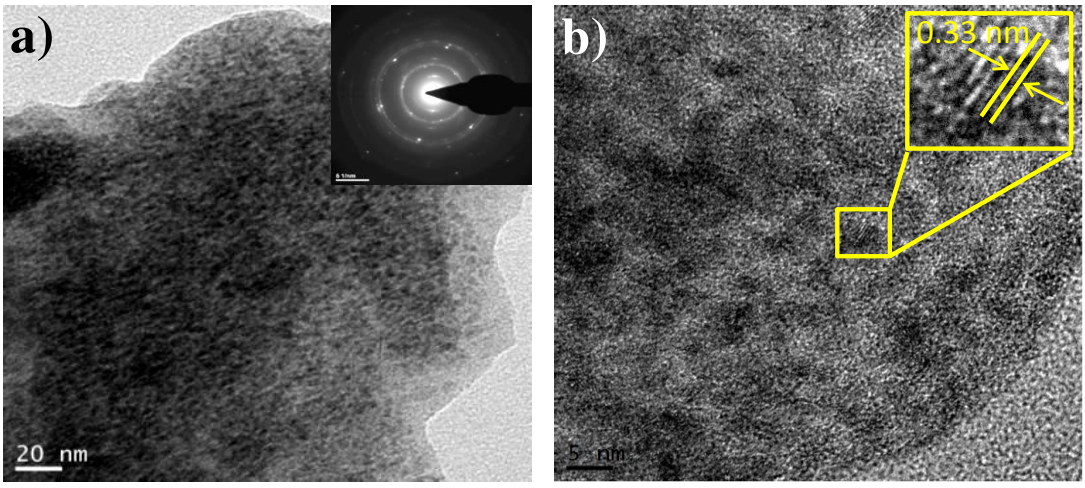

Figure 2.15 a) TEM image of SnO_2/GNS composite, inset shows SAED, b) HRTEM image, and inset showing lattice fringes at 5 nm scale.

TEM image in Figure 2.15a shows many well dispersed SnO_2 nanoparticles with a uniform size of around 3-5 nm coated on GNS surface. The HRTEM image of SnO_2/GNS as shown in Figure 2.15 shows the clear lattice fringes of SnO_2 with a spacing of 0.335 nm corresponding to (110) plane[52] of standard SnO_2 (JCPDS card No. 41-1445). The SAED pattern of the composite (inset of Figure 2.15a) confirms the presence of polycrystalline SnO_2, in the hybrid SnO_2/GNS structure.

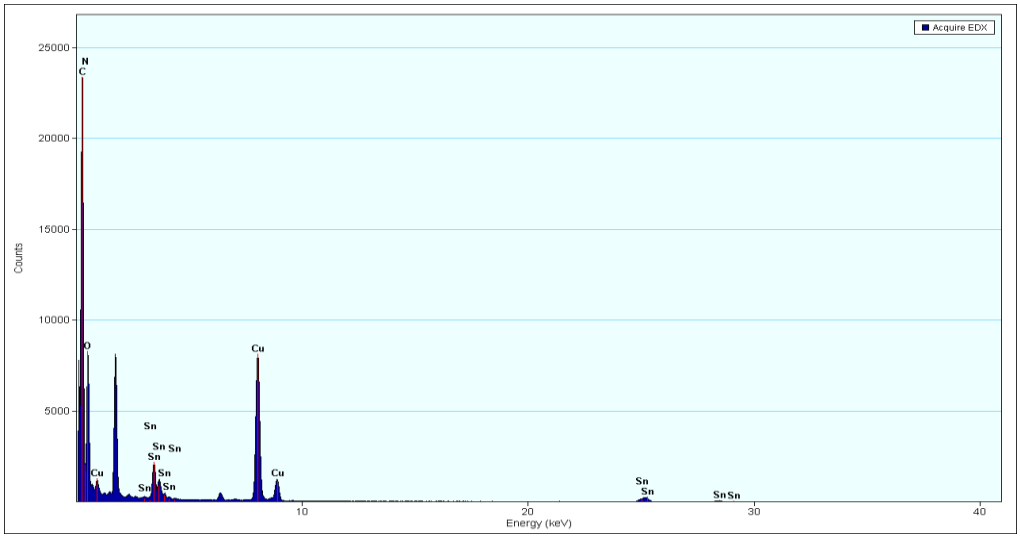

Figure 2.16 Energy-Dispersive X-ray spectrum (EDS) of SnO_2/GNS composite.

The energy-dispersive X-ray spectrum (EDS) from composite product (Figure 2.16) shows an intense peaks of C, Sn and O, displaying the composite consisting of GNS and SnO_2. The Cu and C signals came from the supporting TEM grid.

2.4 Electrochemical characterization

2.4.1 Cyclic voltammetry (CV)

The performance of nanostructured GNS and (SnO_2/GNS) composite as an electrode material for super capacitor was investigated by standard cyclic voltammetry (CV) and galvanostatic charge-discharge technique. The thin film was coated over ITO glass. The cyclic voltammetry measurements were done in 0.1 M H_2SO_4 electrolyte. In order to ensure adhesion of film, electrodes were heated at 70^0 C for 15 hours. The CV curves of SnO_2/GNS composite are obtained within a large potential window from -0.3 to 1.2 V and for GNS, -0.7 to 0.3 V at various scan rates

(50, 100, 150 and 200 mVs^{-1} respectively) are shown in Figure 2.17. All curves show a nearly rectangular shape, which is considered as an ideal capacitive behavior of the materials.[7, 53] The specific capacitance values of the samples are calculated from the CV curves using following equation, [11, 54]

$$Csp = \frac{\int I dV}{v m V} \qquad (1)$$

Where, C_{sp} is the specific capacitance in farads per gram (Fg^{-1}), m is the active mass of the electrode material (g) obtained from quartz crystal microbalance (QCM-200) , *I* is the response current density (A g^{-1}) and *v* is the potential scan rate in (Vs^{-1}) V is potential (V).

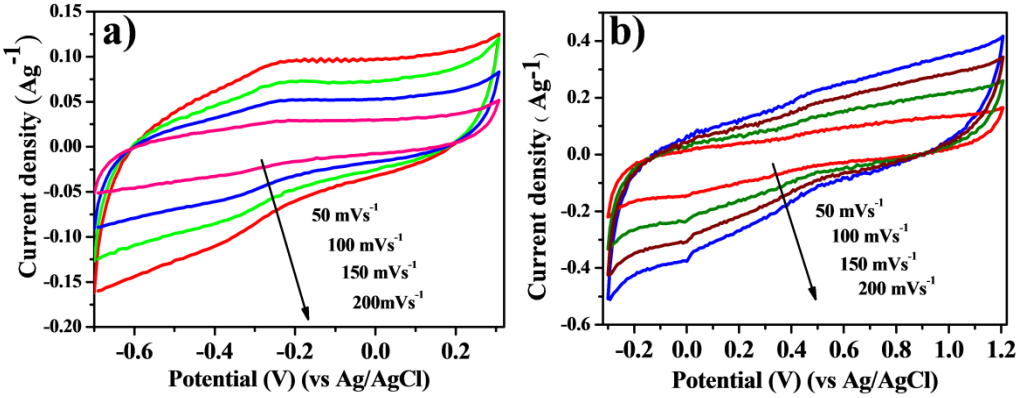

Figure 2.17 Typical CV curves of GNS (a) and SnO_2/GNS (b) at different Scan Rates 50- 200 mVs^{-1}.

2.4.2 Detailed procedure for mass measurement

The quartz crystal is first cleaned by using isopropyl alcohol (IPA), and then distilled water alternately followed by sonication in IPA for 10 minute, and finally washed by using distilled water. After drying crystal in vacuum oven for 30 min at 90^0 C, it is placed in a groove of machine (QCM-200) and blank run is taken. This crystal is then used to deposit GNS and SnO_2/GNS thin film over it and it is kept to dry in vacuum oven for the same time and temperature as for the blank; after drying, it is kept for measurement in the machine and the difference in frequency (Δ freq) is calculated.

The mass (m) is calculated by using Sauerbrey equation 2, [55]

$$m = \frac{-\Delta\, freq. \times A \times \sqrt{(\mu q \times \rho q)}}{2 \times Fq^2} \qquad (2)$$

Where, Δ mass is the mass change, Δ freq is the resonant frequency change (Hz), μ_q is AT-cut quartz crystal constant, ρ_q is the quartz crystal density, F_q is the reference frequency, and A is the surface area of the electrode (cm^2)

The calibration plot is obtained by measuring the mass of the material for number of dips taken as shown in Figure 2.18. GNS electrode is made by taking 200 dips, and calculated mass is 7.8±0.05 µg and for SnO_2/GNS the same mass is used for ease of comparison.

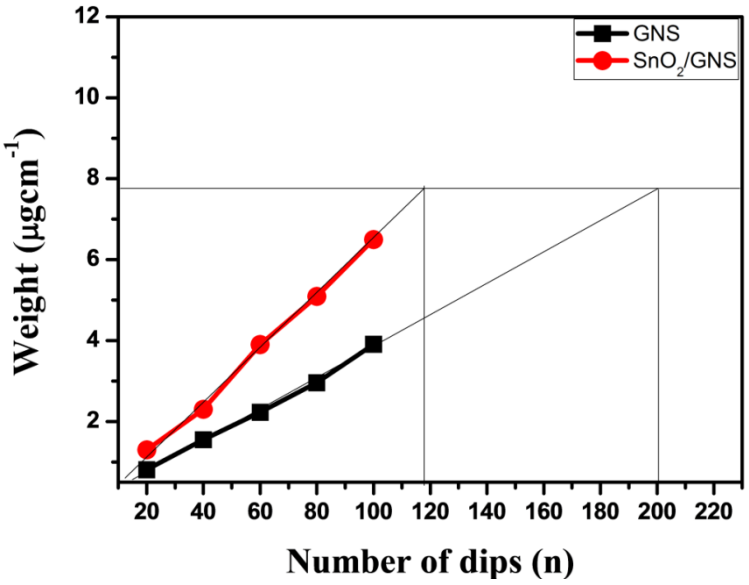

Figure 2.18 Calibration plot for the measurement of active mass of the electrode (obtained by Quartz Crystal Microbalance) as a function of number of dips taken.

Based on the above equation we found C_{sp} to be 472 and 122 Fg^{-1} respectively for the SnO_2/GNS and GNS electrodes at the scan rate 50 mVs^{-1}, while at the scan rate of 200 mVs^{-1} the respective values are 321 and 86 Fg^{-1} (the details are tabulated in Table-2.1) However, the details of change of C_{sp} with scan rates are shown in the Figure 2.19.

Wang and co-workers,[56] reported on microwave assisted one-pot synthesis of SnO_2/GNS nanocomposites, which gave rise to the specific capacitance of 99.7 Fg^{-1}. Li et. al.[57] prepared SnO_2/graphene using one-step synthesis approach, which showed a specific capacitance of 34.6 Fg^{-1}. Recently, Lim et. al.[58] synthesized SnO_2/graphene nanocomposite using solvothermal method showed a specific capacitance 363.3 Fg^{-1}

using CV measurement at 10 mVs^{-1}. Pure SnO_2 nanoparticles reach a reversible capacitance of 96.6 Fg^{-1}. Despite of various studies on SnO_2-Graphene have been reported so far[59-62] present work gives very easy and inexpensive means of formation of composites.

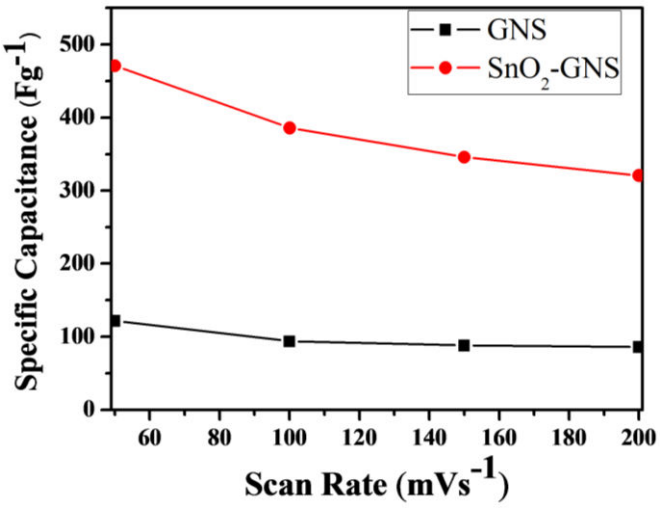

Figure 2.19 Specific capacitance values calculated from equation (1) for GNS and SnO_2/GNS as a function of Scan Rates mVs^{-1}.

2.4.2 Electrochemical Impedance spectroscopy (EIS)

To know more about the impedance at the interface of the electrode, an electrochemical impedance spectroscopy was employed as shown in Figure 2.20. The solution resistance (Rs) for the GNS, SnO_2/GNS and SnO_2 was found to be 0.43, 5.15 and 20.3 Ω respectively.

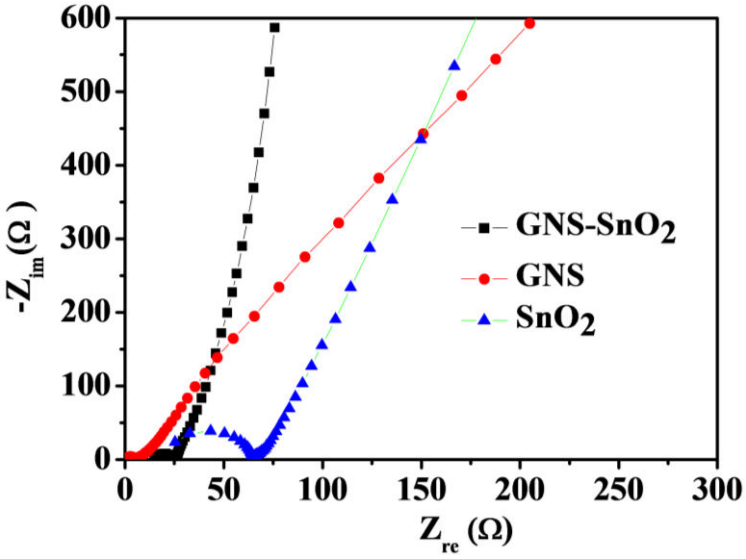

Figure 2.20 Electrochemical Impedance spectroscopy (EIS) for GNS and SnO_2/GNS.

The charge transfer resistance (Rct) was measured to be 6.11, 11.3 and 45.4 Ω for GNS, SnO_2/GNS and SnO_2 respectively. The decrease in impedance in case of SnO_2/GNS is responsible for the increase in rapid charge transfer at the interface of electrolyte and electrode which has led to increase in capacitance and proper charge discharge.

Table 2.1 Specific capacitance at different scan rates for GNS and GNS+ SnO_2 composite.

	Specific capacitance Fg^{-1} from Cyclic Voltametry.				**Retention (%)**
Scan Rate	**50 mVs^{-1}**	**100 mVs^{-1}**	**150 mVs^{-1}**	**200 mVs^{-1}**	
GNS	122	93.84	88.2	86.15	70.61%
GNS+SnO_2	472	386	346	321	68.1%

The capacitance (472-321 Fg^{-1}) obtained in the present study is considerably higher than those of Sn-based graphene composites mentioned above. The higher capacitance obtained is due to layer-by-layer structure of composite,[59] and having conducting and high surface area graphene in close contact with SnO_2 as one of the components, facilitating rapid charging and discharging at the electrode. These results indicate the exciting potential for the use LbL SnO_2/GNS film in high-performance supercapacitor. The percent retention of C_{sp} in case of composite is 68% at the high capacitance value of C_{sp} = 472 Fg^{-1}.

2.4.3 Galvanostatic charge-discharge

To evaluate real applicability of the SnO_2/GNS composite, we also measured the charge/discharge behavior of both the electrodes by using two electrode systems in 0.1 M H_2SO_4 as electrolyte at different current densities ranging from 10 μA to 100 μA. The specific capacitance was calculated by using the equation 3,

$$Csp = \frac{(i \times \Delta t)}{\Delta E \times m} \qquad (3)$$

Where, i is current density Ag^{-1}, Δt is discharge time (s), ΔE is a voltage difference in (V) and m is an active mass of electrode derived from quartz crystal microbalance[55, 63] (7.8±0.05µg for both GNS and SnO_2/GNS electrode. As calculated from the above equation-3 high values in the range of 471 to 234 Fg^{-1} are obtained for C_{sp} at the high current densities in the range of 10 µA to 100 µA, (Table 2.2) which is consistent with the results of CV studies.

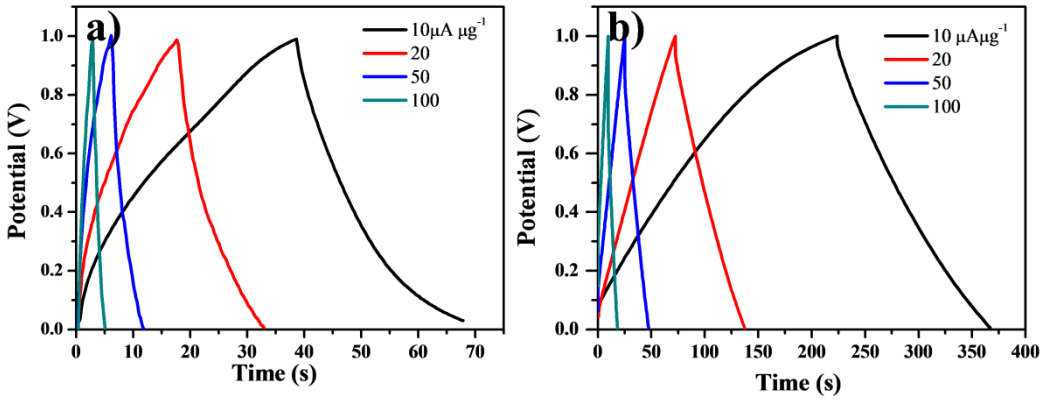

Figure 2.21 Typical galvanostatic charge discharge profile of GNS (a) and SnO_2/GNS (b) device at different current densities.

The charge-discharge curves (Figure 2.21a, b) are observed to be nearly symmetric, revealing a good capacitive behavior. In addition, the voltage drop is observed to be very small, which indicates that the electrode has low internal resistance.

Table 2.2 The specific capacitance of GNS and SnO_2/GNS as a function of current density.

	Specific capacitance Fg^{-1} From Charge/Discharge.				**Retention (%)**
Current	10µA	20 µA	50 µA	100 µA	
GNS	87.17	85.02	73.06	69.1	79.27%
GNS+SnO_2	471	352	299.48	233.97	49.57%

It is found that there is a significant value addition by making an LbL composite of SnO_2/GNS in terms of obtaining higher capacitance at high current density with good retention over the individual components of the composite.

The observed C_{sp} from the calculations of both CV and Charge/Discharge study are comparable and than that for exclusive GNS and to the best of our knowledge, SnO_2-GNS composites reported in literature. It is proposed[63] that this improvement arises from LbL stacking of GNS and SnO_2. 1000 cycles of Charge-discharge processes (inset of Figure 2.22b) have been studied to establish the stability of the performance of the composite and it is found that there is retention of C_{sp} up to 72% at high current density of 2.56 Ag^{-1} (20µg/7.8µg). From the durability study of hybrid electrode it is seen that specific capacitance decreases at higher rate up to 250 cycles and it remains constant afterwards; so that the retention of specific capacitance is up to 90% from 250 to 1000th cycle (Figure 2.22b)

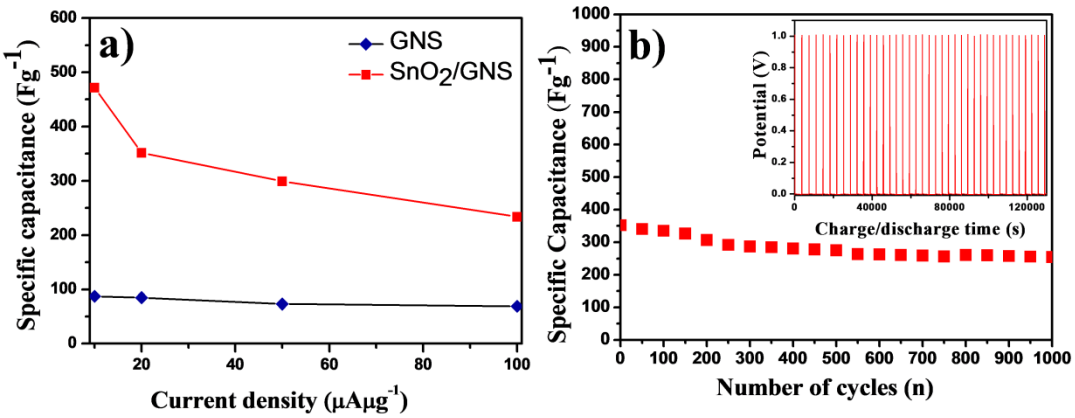

Fig 2.22 (a) The specific capacitance of GNS and SnO_2/GNS as a function of current density. (b) Cycle performance of SnO_2/GNS at current density of 2.56 Ag^{-1}, inset shows 1000 cycles.

Also, it can be seen that in case of SnO_2/GNS composite, the specific capacitance is rapidly decreasing (26%) at current density 20 µA and then at noticeably lower rate of decrease at 50 and 100 µA (Figure 2.22a); thus it may be relatively more stable at higher current density as well as at higher number of cycles, and can be useful for specific applications. It is suggested that the large capacitance for SnO_2/GNS can be rationally explained by the complete separation of GNS sheets from SnO_2 as a spacer in the composite, fast charge transfer at the interface between the electrode and electrolyte ions and large surface area due to GNS.

2.5. Conclusions

A simple, facile and a single step method to synthesize 4-5 monolayer graphene film and highly uniform nanoparticulate SnO_2 thin film with an average particle size of 3-5 nm on various substrates for applications such as supercapacitorsis established by using modified LLIRT. An additional feature of the present technique is the applicability of LbL technique to fabricate SnO_2/GNS composite hybrid films with a well-defined architecture and tunable thickness on various substrates for applications such as supercapacitors. The obtained hybrid films having interconnected network prevented graphene sheets from restacking with one-another, thus assisting in the formation of suitable nanocomposites.

This is the proof of the concept of forming graphene semi-conductor composite by the reported technique and opens a new area for forming better capacitors. The CV results indicated good capacitive behavior for SnO_2/GNS nanocomposites. The excellent specific capacitance of 472 Fg^{-1} calculated from CV and 471 Fg^{-1} calculated from charge-discharge measurement and very good cycling stability is an indication that as-synthesized nanocomposite formed with the present technique is a potential candidate for super-capacitor application and in an energy storage technology in future. The excellent electrochemical performance of the composite as supercapacitor electrodes is due to the synergistic effects among the components in the composites.

2.6 References

[1] (*a*) S. Ikeda, S. Ishino, T. Harada, N. Okamoto, T. Sakata, H. Mori, S. Kuwabata, T. Torimoto and M. Matsumura, *Angew. Chem., Int. Ed*., 2006, **45**, 7063; (*b*) R. M. Rioux, R. Komor, H. Song, J. D. Hoefelmeyer, M. Grass, K. Niesz, P. Yang and G. A. Somorjai, *J. Catal*., 2008, **254 (1)**, 1; (*c*) T. Harada, S. Ikeda, H. Ng, Y. T. Sakata, H. Mori, T. Torimoto and M. Matsumura, *Adv. Mater*., 2008, **18**, 2190; (*d*) J. Okal, *Catal. Commun*., 2010, **11**, 508; (*e*) P. Simon and Y. Gogotsi, *Nat. Mater*; 2008, **7**, 845.

[2] S. He, X. Hu, S. Chen, H. Hu, M. Hanif and H. Hou, *J. Mater. Chem*., 2012, **22**, 5114.

[3] (*a*) Y. G. Wang and Y. Y. Xia, *Electrochim acta*, 2006, **51**, 3223; (*b*) M. Y. Cheng and B. J. Hwang, *J. Power sources*, 2010, **195**, 4977; (*c*) M. Boutros, A. Denicourt-Nowicki, A. Roucoux, L. Gengembre, P. Beaunier, A. Gedeon and F. Launay, *Chem, Commun*., 2008, 2920.

[4] (*a*) S. Yoon, B. H. Ka, C. Lee, M. Park and S. M. Oh, *Electrochem. Solid-State Lett*., 2009, **12** (2) A28; (*b*) Z. Yang, G. Du, Q. Meng, Z. Guo, X. Yu, Z. Chen, T. Guo and R. Zeng, *J. Mater. Chem*., 2012, **22**, 5848-5854; (*c*) J. Xu, Y. Wang, Z. Li and W. Zhang, *J. Power Sources*, 2008, **175** (2), 903.

[5] (*a*) C. Li, Z. Yu, D. Neff, A. Zhamu and B. Z. Jang, *Nano Lett*., 2010, **10**, 4863; (*b*) Y. Wang, Z. Shi, Y. Huang, Y. Ma, C. Wang, M. Chen and Y. Chen, *J. Phys. Chem. C*, 2009, **113**, 13103; (*c*) T. Y. Kim, H. W. Lee, M. Stoller, D. R. Dreyer, C. W. Bielawski, R. S. Ruff and K. S. Suh, *ACS Nano*, 2011, **5**, 436; (*d*) M. G. Stoller, S. Park, Y. Zhu, J. An and R. S. Ruff, *Nano Lett*., 2008, **8**, 3498.

[6] (*a*) X. Zhou, Y. X. Yin, L. J. Wan and Y. G. Guo, *Chem. Commun*., 2012, **48**, 2198; (*b*) Z. L. Wang, D. Xu, Y. Huang, Z. Wu, L. M. Wang and X. B. Zhang, *Chem. Commun*., 2012, **48**, 976; (*c*) S. Stankovich, D. A. Dikin, G. H. B. Dommett, K. M. Kohlhaas, E. J. Zimney, E. A. Stach, R. D. Piner, S. T. Nguyen and R. S. Ruoff, *Nature*, 2006, **442**, 282; (*d*) S. Ding, J. S. Chen, D. Luan, Y. C. Boey, S. Madhavi and X. W. Lou, *Chem. Commun*., 2011, **47**, 5780; (*e*) S. Ding, D. Luan, F. Y. C. Boey, J. S. Chen and X. W. Lou, *Chem. Commun*., 2011, **47,** 7155.

[7] (*a*) Q. Cheng, J. Tang, J. Ma, H. Zhang, N. Shinya and L. Qin, *Carbon*, 2011, **49**, 2917; (*b*) S. Chen, J. Zhu, X. Wu, Q, Han and X. Wang, *ACS Nano*, 2010, **4**, 2822; (*c*) Z. S. Wu, W. Ren, D. W. Wang, F. Li, B. Liu and H. M. Cheng, *ACS Nano*, 2010, **4**, 5835; (*d*) J. Yan, Z. Fan, T. Wei, W. Qian, M. Zhang and F. Wei, *Carbon*, 2010, **48**, 3825; (*e*) B. Wang, J. Park, C. Wang, H. Ahn and G. Wang, *Electrochim. Acta*, 2010, **55**, 6812; (*f*) L. Muo, K. Zhang, H. S. Chan and J. Wu, *J. Mater. Chem.*, 2012, **12**, 1845.

[8] (*a*) J. Yan, T. Wei, W. Qiao, B. Shao, Q. Zhao, L. Zhung and Z. Fan, *Electrochim. Acta,* 2010, **55**, 6973; (*b*) X. Wang, L. Song, H. Yang, W. Xing, H. Lu and Y. Hu, *J. Mater. Chem.*, 2012, **22**, 3426.

[9] W. Shi, J. Zhu, D. H. Sim, Y. Tay, Z. Lu, X. Zhang, Y. Sharma, M. Srinivasan, H. Zhang, H. H. Hng and Q. Yan, *J. Mater. Chem*., 2011, **21**, 3422.

[10] X. Zhou, L-J. Wan and Y-G. Guo, *Chem. Commun*., 2013, **49**, 1838.

[11] (*a*) W. Wang, Q. Hao, W. Lei, X. Xia and X. Wang, *RSC Adv*., 2012, **2**, 10268-10274; (*b*) F. Li, J. Song, H. Yang, S. Gan and Q. Zhang, *Nanotechnol.*, 2009, **20**, 455602.

[12] 12 (*a*) H. Wang, Y. Liang, T. Mirfakhrai, Z. Chen, H. Casalongue and H. Dai, *Nano Research*, 2011, **4**, 729-736; (*b*) B. Zhao, J. Song, P. Liu, W. Xu, T. Fang, Z. Jiao, H. Zhang and Y. Jiang, *J. Mater. Chem*., 2011, **21**, 18792.

[13] Z. Zhan, L. Zheng, Y. Pan, G. Sun and L. Li, *J. Mater. Chem*., 2012, **22**, 2589.

[14] (*a*) A. L. Geim and K. S. Novoselov, *Nat. Mater*., 2007, **6,** 183; (*b*) K. S. Novoselov, A. K. Geim, V. Morozov, D. Jiang, Y. Zhang, S. V. Dubonos, I. V. Grigorieva, and A. A. Firsov, *Science*, 2004, **306**, 666.

[15] (*a*) S. Park and R. S. Ruoff, *Nat. Nanotechnol*., 2009, **4(4)**, 217; (*b*) I. Jung, D. A. Dikin, R. D. Piner and R. S. Ruoff, *Nano Lett*., 2008, **8**, 4283.

[16] (*a*) X. Zhou, T. Wu, K. Ding, B. Hu, M. Hou and B. Han, *Chem. Commun*., 2010, **46**, 386; (*b*) X. Wang, P. F. Fukvio, G. A. Baker, G. M. Veith, R. R. Unocic, S. M. Mahurin, M. Chi and S. Dai, *Chem, Commun*., 2010, **46**, 4487.

[17] (*a*) G. Chen, W. Weng, D. Wu, C. Wu, J. Lu, P. Wang and X. Chen, *Carbon*, 2004, **42**, 753; (*b*) X. Li, X. Wang, L. Zhang, S. Lee and H. Dai, *Science*, 2008, **319**, 1229.

[18] J. Wang, K. K. Manga, Q. Bao, and K. P. Loh, *J. Am. Chem. Soc*., 2011, **133**, 8888.

[19] (*a*) A. P. Yu, I. Roes, A. Davies and Z. W. Chen, *Appl. Phys. Lett*., 2010, **96**, 3; (*b*) H. R. Byon, S. W. Lee, S. Chen, P. T. Hammond and Y. Shao-Horn, *Carbon*, 2011, **49**, 457; (*c*) X. J. Lu, H. Dou, B. Gao, C. Z. Yuan, S. D. Yang, L. Hao, L. F. Shen and X. G. Zhang, *Electrochim. Acta*, 2011, **56**, 5115; (*d*) X. W. Yang, J. W. Zhu, L. Qiu and D. Li, *Adv. Mater*., 2011, **23**, 2833.

[20] (*a*) P. W. Sutter, J. I. Flege and E. A. Sutter, *Nat. Mater*., 2008, **7,**406; (*b*) X. Li, W. Cai, J. An, S. Kim, J. Nah, D. Yang, R. Pinner, A. Velamakanni, I. Jung, E. Tutuc, S. K. Baberjee, L. Colombo and R. S. Ruff, *Science*, 2009, **324**, 1312; (*c*) K. S. Kim, Y. Zhao, H. Jang, S. Y. Lee, J. M. Kim, K. S. Kim, J. H. Ahn, P. Kim, J. Y. Choi and B. H. Hong, *Nature*, 2009, **457**, 706; (*d*) S. Bae, H. Kim, Y. Lee, X. Xu, J. S. Park, Y. Zheng, J. Balakrishnan, T. Lei, H. R. Kim, Y. I. Song, Y. J. Kim, K. S. Kim, B. Ozyilmaz, J. H. Ahn, B. H. Hong and S. Lijima, *Nat. Nanotechnol*., 2010, **5**, 574.

[21] (*a*) S. Chen, J. Zhu, X. Wu, Q. Han and X. Wang, *ACS Nano*, 2010, **4**, 2822; (*b*) R. B. Rakhi, W. Chen, D. Cha and H. N. Alshareef, *J. Mater. Chem*., 2011, **21**, 16197; (*c*) X. Dong, H. Xu, X. Wang, Y. Huang, M. Chan-Park, H. Zhang, L. Wang, W. Huang and P. Chen, *ACS Nano*, 2012, **6**, 3206; (*d*) D. Chen, L. Tang and J. Li, *Chem Soc. Rev*., 2010, **39**, 3157; (*e*) D. Wang, R. Kou, D. Choi, Z. Yang, Z. Nie, J. Li, L. V. Saraf, D. Hu, J. Zhang, G. L. Graff, J. Liu, M. A. Pope and I. A. Aksay, *ACS Nano*, 2010, **4**, 1587.

[22] (*a*) S. Liang, X. Zhu, P. Lian, W. Yang and H. Wang, *J. Solid State Chem*., 2011, **184**, 1400; (*b*) G. Wang, B. Wang, X. Wang, J. Park, S. Dou, H. Ahn and K. Kim, *J. Mater. Chem*., 2009, **19**, 8378.

[23] (*a*) D. Larcher, S. Beattie, M. Morcrette, K. Edstroem, J.-C. Jumas and J.-M. Tarascon, *J. Mater. Chem*., 2007, **17**, 3759; (*b*) H. K. Liu, G. X. Wang, Z. P. Guo, J. Z. Wang and K. Konstantinov, *J. Nanosci. Nanotechnol*., 2006, **6**, 1.

[24] (*a*) S. Chen, P. Chen, M. Wu, D. Pan and Y. Wang, *Electrochem. Commun*., 2010, **12**, 1302; (*b*) X. Zhu, Y. Zhu, S. Murali, M. D. Stoller and R. S. Ruoff, *J. Power Sources*, 2011, **196**, 6473; (*c*) B. Li, H. Cao, J. Shao, G. Li, M. Qu and G. Yin, *Inorg. Chem*., **50**, 1628; (*d*) Y. Li, X. Lv, J. Lu and J. Li, *J. Phys. Chem. C*, 2010, **114**, 21770.

[25] L. S. Zhang, L. Y. Jiang, H. J. Yan, W. D. Wang, W. Wang, S. G. Song, Y. G. Guo and L. J. Wan, *J. Mater. Chem*., 2010, **20**, 5462.

[26] (*a*) A. Maddalena, R. D. Maschio, S. Dire and A. Raccanelli, *J. Non-Cryst. Solids*, 1990, **121**, 365; (*b*) M. Arienzo, L. Armelao, A. Cacciamani, C. Mari, S. Polizzi, R. Ruffo, R. Scotti, A. Testino, L. Wahba and F. Morazzoni, *Chem. Mater*., 2010, **22**, 4083.

[27] J. Bruneaux, H. Cachet, M. Froment and A. Messad, *Thin Solid Films*, 1991, **197**, 129.

[28] T. Isono, T. Fukuda, K. Nakagawa, R. Usui, R. Satoh, E. Morinaga and Y. Mihara, *J. SID,* 2007, **15**, 161.

[29] (*a*) M. S. Huh, B. S. Yang, J. Lee, J. Heo, S. J. Han, K. Yoon, S. H. Yang, C. S. Hwang and H. J. Kim, *Thin Solid Films*, 2009, **518**, 1170; (*b*) R. P. Howson, H. Barankov and A. G. Spencer, *Thin Solid Films*, 1991, **196**, 315.

[30] (*a*) R. D. Tarey and T. A. Raju, *Thin Solid Films*, 1985, **128**, 181-189; (*b*) J. Sundqvist, J. Lu, M. Ottosson and A. Hasta, *Thin Solid Films*, 2006, **514**, 63.

[31] (*a*) X. Du and S. George, *Sens. Actuators*, B 2008, **135**, 152; (*b*)H. Virola and L. Niinisto, *Thin Solid Films*, 1994, **251**, 127; (*c*) G. Choi, L. Satyanarayana and J. Park, *Appl. Surf. Sci*., 2006, **252**, 7878; (*d*) J. Heo, A. S. Hock and R. G. Gordon, *Chem. Mater*., 2010, **22**, 4964.

[32] S. Mao, S. Cui, G. Lu, K. Yu, Z. Wen and J. Chen, *J. Mater. Chem*., 2012, **22**, 11009.

[33] (*a*) S. Yang, I. Kim, M. Jeon, K. Kim, S. Moon, H. Kim and K. An, *Ind. And Engng. Chem. Res*., 2008, **14**, 365; (*b*) S. Das, S. Chaudhari and S. Maji, *J. Phys. Chem.* C, 2008, **112**, 6213.

[34] A. Jadhav, S. Patil, S. Sathaye, K. Patil, *Journal of colloid and interface science*, 2015, **439**, 121.

[35] S. D. Sathaye, K. R. Patil, D. V. Paranjape, A. Mitra, S. V. Awate and A. B. Mandale, *Langmuir*, 2000, **16**, 3487.

[36] Z. Deng, B. Peng, D. Chen, F. Tang and A. J. Muscat, *Langmuir*, 2008, **24**, 11089.

[37] (*a*) W. Yue, S. Jiang, W. Huang, Z. Gao, J. Li, Y. Ren, X. Zhao and X. Yang, *J. Mater. Chem*., A, 2013, **1**, 6928; (*b*) D. Yu, L. Dai, *J.Phys. Chem. Lett*., 2010, **1**, 467.

[38] X, Li, G. Zhang, X. Bai, X. Sun, X. Wang, F. Wang and H. Dai, *Nat. Nanotechnol.*, 2008, **3**, 538.

[39] Y. X. Wang, L. H. Li, C. Sun, S. Y. Xie, G. L. Xu, S. R. Chen, Y. F. Xu, J. T. Li, S. L. Chou, S. X. Dou and S. G. Sun, *J. Mater. Chem*., 2012, **22**, 4744.

[40] (*a*) A. C. Ferrari, *Solid State Commun*., 2007, **143**, 47; (*b*) A. C. Ferrari, J. C. Meyer, V. Scardaci, C. Casiraghi, M. Lazeri, F. Mauri, S. Piscanec, D. Jiang,

K. S. Nevoselov, S. Roth and A. Geim, *J. Phys. Rev. Lett*., 2006, **97**, 187401; (c) Y. Zhu, S. Murali, W. Cai, X. Li, J. W. Suk, J. R. Potts and R. S. Ruoff, *Adv. Mater.,* 2010, **22**, 3906.

[41] A. Gupta, G. Chen, P. Joshi, S. Tadigadapa and P. C. Eklund, *Nano Lett*., 2006, **6**, 2667.

[42] J. H. Chen, W. G. Cullen, C. Jang, M. S. Fuhrer and E. D. Williams, *Phy. Rev. Lett***.,** 2009, **102**, 236805.

[43] A. Safavi, M. Tohidi, F. A. Mahyari and H. J. Shahbaazi, *J. Mater.Chem*., **2012**, *22*, 3825.

[44] H. L. Poh, F. Sanek, A. Ambrosi, G. Zhao, Z. Sofer and M. Pumera, *Nanoscale*, 2012, **4**, 3515.

[45] Z. Deng, D. Chen, F. Tang, X. Meng, J. Ren and L. Zhang, *J. Phys.Chem. C,* 2007, **111**, 5325.

[46] Y. Hernandez, V. Nicolosi, M. Lotya, F. M. Blighe, Z. Sun; S. De, I. T. Mcgovern, B. Holland, M. Byrne, Y. K. Gunko, J. J. Boland, P. Niraj, G. Duesberg, S. Krishnanurthy, R. Goodhue, J. Hutchison, V. Scardaci, A. C. Ferrari and J. Coleman, *Nat. Nanotechnol.*, 2008, **3**, 563.

[47] (*a*) A. K. Geim., *Science*, 2009, **324**, 1530; (*b*) A. K. Geim and K. S. Novoselov, *Nat. Mater*., 2007, **6**, 183.

[48] S. Stankovish, D. A. Dikin, R. D. Piner, K. A. Kohlhaas, A. Kleinhammes, Y. Jia, Y. Wu, S. T. Nguyen and R. S. Ruff, *Carbon*, 2007, **45**, 1558.

[49] Y. Li, Z. Wang and Y. Ding, *Inorg. Chem*., 1999, **38**, 4737.

[50] M. Batzill, U. Diebold, *Prog. Surf. Sci.* 2005, **79**, 47.

[51] L. Shi and H. Lin, *Langmuir*, 2010, **26(24)**, 18718.

[52] (*a*) Y. Li, S. Zhu, Q. Liu, J. Gu, Z. Guo, Z. Chen, C. Feng, D. Zhang and W. Moon, *J. Mater. Chem*., 2012, **22(6),** 2766; (*b*) K. N. Yu, Y. H. Xiong, Y. L. Liu and C. S. Xiong, *Phys. Rev. B: Condens. Matter*, 1997, **55**, 2666.

[53] C. Zhu, S. Guo, Y. Fang, S. Dong, *ACS Nano*, 2010, **4**, 2429.

[54] Z. Xin, T. C. Bryan, B. Belen, W. Weiliang, J. Colin, S. John and M.S.G. Patrick, *Nanotechnology*, 2009, **20(6),** 065605.

[55] T. Lee, T. Yun, B. Park, B. Sharma, H. K. Song and B-S. Kim, *J. Mater. Chem*., 2012, **22**, 21092.

[56] S. Wang, S. P. Jiang and X. Wang*, Electrochim. Acta*., 2011, **56**, 3338.

[57] F. Li, J. Song, S. Gan, Q. Zhang, D. Han and L. N. Ari Ivaska, *Nanotechnology*, 2009, **20**, 455602.

[58] S. P. Lim, N. M. Huang and H. N. Lim, *Ceramic International*, 2013, **39**, 6647.

[59] F. Li, J. Song, H. Yang, S. Gan and Q. Zhang, *Nanotechnology*, 2009, **20**, 455602

[60] Y. Li, X. Lv, J. Lu and J. Li, *J. Phys. Chem., C*, 2010, **114**, 21770.

[61] X. Wang, X. Zhou, K. Yao, J. Zhang and Z. Liu, *Carbon*, 2011, **49**, 133.

[62] J. Liang, W. Wei, D. Zhong, Q. Yang, L. Li and L. Guo, *ACS Appl. Mater. Interfaces,* 2012, 4, 454.

[63] S. Patil, V. Patil, S. Sathaye, K. Patil, *RSC Advances*, 2014, **4 (8)**, 4094.

Chapter-3

Development of a novel method to grow MoS_2 mono/few-layer films and MoS_2-graphene hybrid films for supercapacitor applications

The controlled synthesis of highly crystalline MoS_2 layers remains a challenge for the practical applications of this emerging material. We have established a facile method to synthesize crystalline mono/few-layered MoS_2 thin films at liquid-liquid interface with low defect concentration. Number of layers formed is analyzed by Raman spectroscopy as well as atomic force microscopy which clearly show that as formed product has 2-4 layers of MoS_2. Morphology of the product is checked by FE-SEM and TEM which depicts transparent 2D sheets. XRD pattern of film confirms highly oriented MoS_2 nanosheets. This simple approach opens an avenue on the synthesis of high quality crystalline MoS_2 layers on suitable substrates, accessible for studies of the fundamental aspects and its various applications. Also, synthesis of exfoliated MoS_2 nanosheets-graphene nanosheet (MoS_2-GNS) hybrid thin films has been developed by the application of layer by layer (LbL) technique. The maximum specific capacitance of this MoS_2-graphene hybrid thin film electrode was 282 Fg^{-1} at a scan rate of 20 mVs^{-1}. The as-obtained hybrid thin film electrode exhibits more robust cycling performance (> 1000 cycles), retaining over 93 % of its initial capacitance. These results indicate that MoS_2-graphene hybrid thin film is a promising candidate for the electrode material in supercapacitor applications.

Content in this chapter is published in the following article,

CrystEngComm, 2014, **16** (47), 10845.

(http://pubs.rsc.org/en/content/articlelanding/2014/ce/c4ce01595a#!divAbstract)

3.1 Introduction

Encouraged by previous results (Chapter-2), we adapted a similar methodology to grow thin films of layered MoS_2 successfully which is a major contribution from this thesis work. Layered materials have been studied intensively, considering their special properties. Layered hydroxides were the subject matter of

research for a long time earlier and it was mainly for the application in the field of catalysis. The importance of other layered materials like graphene, hexagonal boron nitride (h-BN),[1] transition metal sulphides (MS_2, where M = Mo, Sn, W), etc. was revealed later, not only for the applications in isolated field of catalysis but also in the field of nano-electronics, containing energy storage devices, solar cells, Lithium/Sodium ion batteries, capacitors etc. Two important points may be mentioned here namely, 1) these materials have more applications as a component in composites than in their singular devices, exploiting their distinct inherent exclusive properties, and 2) the devices using them in thin film form outnumber the devices in bulk form. Super capacitor is one such device which is under the development by researchers with intensive inputs. High energy and power density, fast charge-discharge ability and long cycle life are crucial properties for energy-storage devices such as supercapacitors that can meet the ever-increasing energy demands in various applications such as hybrid electric vehicles, mobile electronic devices and memory backup systems.[2-5] Graphitic materials are intensively used as commercial electrode materials because of their flat potential profile and good structural stability during cycling.

Graphene has found enormous research interest and number of applications in materials science and physics due to its unique properties such as superior electrical conductivity, excellent mechanical flexibility, larger surface area, and high thermal and chemical stability.[6-10] These properties can complement metal oxide properties to improve its performance in electrochemical devices if their composite is formed. Such a composite may be consisting of metal oxide film between the graphene nano sheets/layers or metal oxides nanoparticles dispersed on the surface of graphene layers.[11-13] Inspite of versatile properties of graphene, its zero energy-gap restrict its applications in logic electronics. Also, inherent capacitance of graphene layers is not high so as to be suitable for high power device applications. Researchers, therefore, focused their search for other graphene-like 2-D layered semiconducting materials with appropriate band gaps to complement layered graphene in a composite for high power device applications.[14-16] Recently it is investigated that the use of two-dimensional semiconducting materials having a band gap of 1.2 – 1.8 eV, such as MoS_2, that has layered structure (Figure 3.1) similar to graphene and therefore is complementary to zero-band gap graphene.[17-21] Surfactant assisted self-assembly of

graphene-metal oxide nano composites have been reported to form sandwich structures. However for the final electrode formation, an additional step of removing surfactants would be needed.[17,18] As against this; if the final product is retained with surfactants their presence may limit many applications of the composites. The large band-gap (1.2-1.8 eV) and flexibility of MoS_2 atomic layers allow for their applications in nano-electronic and optoelectronic devices.[22-24] Soon and Lohz[25] reported that the MoS_2 is used as an electrode material for capacitor due to its sheet-like morphology, which provides large surface area for charge storage.

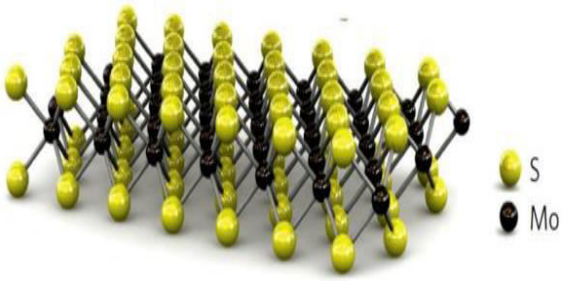

Figure 3.1 MoS_2 crystal structure.

https://www.utwente.nl/.system/dl/ic~AQLrVA0BEeECAoU4CwBfzMsCBwHERALkAIA6CIo

Researchers have achieved the growth of large, high quality MoS_2 sheets and have proposed possible applications, such as low power transistors,[26,27] complex electronic circuits,[28,29] hydrogen evolution reaction, and energy storage.[30,31] MoS_2 is also used in petrochemical process.[32] For the electronic device applications, it is a critical prerequisite to produce high-quality MoS_2 thin films with controlled number of MoS_2 layers.[20] Recently, single and few-layered graphene have been reported by both 'top down' exfoliation of graphite and 'bottom-up' sp^2 carbon assembly synthesis. Similar to graphene, MoS_2, exfoliated by mechanical cleavage showed the high quality layered structure, but their size, thickness and shape were not controllable.[20] To obtain layered MoS_2 on large scale, the methods reported are solution phase exfoliation of MoS_2 in liquids[33-37] and also hydrothermal synthesis.[38, 39] However the quality of the product is not assured for their applications. The method to synthesize large-area and high quality MoS_2 films has been reported by spin-coating and also by thermolysis of alkyl-diammoniumthiomolybdate in solvents.[40, 41] However, the carbon contaminations from the solvent molecules were suspected to

cause sulfur deficiency in the composition, apart from amorphous structure of films. Thermally decomposed ammonium thiomolybdate layer forming MoS_2, when annealed in sulphur atmosphere can produce large area MoS_2 thin layers with superior electrical performance on insulating substrate. This is a two-step process requiring H_2 atmosphere and high temperature. Recently, chemical vapor deposition (CVD), was successful in growing high-quality graphene, has been applied to obtain MoS_2 thin films on the substrate.[42, 43] However, it is difficult to obtain crystalline MoS_2 thin films with controlled number of layers by CVD as against it, the geometry, thickness and crystallinity of graphene could be monitored by using a suitable catalyst. Also, to obtain two-dimensional growth of MoS_2, precursors such as Mo[43], MoO_2,[44] and MoO_3[45] were first deposited on the substrate as thin films which on sulfurization leads to final product. Alternatively, thermal decomposition of $(NH_4)_2MoS_4$[46] precursors at elevated temperature is also reported to give MoS_2. Thus, obtained films were polycrystalline with small crystal size; as a result, number of layers was not controllable. The grain boundaries in these polycrystalline films could be greatly detrimental to the electrical performance of MoS_2 on graphene.[47]

In general, it can be inferred from the available literature that bottom up methods of forming layered MoS_2 thin film processes are energy intensive while top down processes are mostly two step processes, apart from their other pros and cons mentioned above. Therefore, a 'top-down' single step process would be a desirable step forward for the applications of layered MoS_2 thin films.

So far, many research groups have devoted their efforts to exploit MoS_2 through its electrochemical performance. However, stacked MoS_2 would have very little space between the layers which would not suit electrochemical applications apart from unfavorable inefficient charge transport. The clue is to form an electrode of a material/composite made up of enlarged interlayer distance of MoS_2 as one of the constituents, example, constructing carbon-MoS_2 composites wherein carbon occurs between the layers of MoS_2.[48-51] Layered MoS_2-graphene composite was synthesized by solution phase method and the specific capacitance of the hybrid reaches up to 243 Fg^{-1} at a discharge current of 1 Ag^{-1}.[51] A cationic surfactant-assisted hydrothermal route was developed for synthesis of MoS_2/graphene composites for reversible lithium storage.[52] A facile method has been developed for stable lithium storage wherein

MoS_2-graphene hybrid in the form of nanosheets is synthesized using lithiation assisted exfoliation process.[53] In this process, the subsequent template elimination without destruction of morphology and structure is difficult.

Despite the great improvement that has been achieved on the electrochemical performance of MoS_2 or MoS_2 containing composite electrodes, the cycle life is still not satisfactory for their practical applications. Therefore, achieving a composites formation, combining the unique properties of graphene, like fast electron transfer, along with its 2D structure and MoS_2 having layered structure but semiconducting properties opens new avenues for research in energy conversion and storage.

Thus, for a simple method, capable of producing MoS_2 layers in a controlled manner is still desirable. Taking these requirement into account, we have developed a 'top down' method, using the same equipment that is used to grow graphene films reported earlier.[54] The method reports the formation of MoS_2 nanosheets in the form of thin films at room temperature at liquid-liquid interface, which can be suitably transferred on the substrates. The resulting MoS_2 nanosheet film can be deposited on the surface of graphene nanosheet/s by layer-by-layer (LbL) assembly. The as-prepared MoS_2-GNS hybrid nanosheets not only prevent the agglomeration of MoS_2 nanosheets but also restrict the growth of MoS_2 during LbL by the bond formed (Van der Waal) between MoS_2 nanosheets and graphene. Remarkably, the MoS_2–GNS hybrid demonstrates high capacitance and outstanding cycle life when evaluated as an electrode material for supercapacitor, showing a synergistic effect between MoS_2 nanosheets and graphene nanosheets.

3.2 Experimental Methods

3.2.1 Chemicals

All of the reagents used herein were of analytical grade and used as received without any further purification. Molybdenum disulfide (MoS_2, 99.9%) and graphite rod (99.99 %) were purchased from Sigma-Aldrich Ltd. Conc. Sulfuric acid (H_2SO_4, 98%), Sodium Sulphate (Na_2SO_4) and oleic acid (99% by GC) were purchased from Merck chemicals, carbon tetrachloride (CCl_4, 99.5%) was purchased from Loba Chemie and water used in this process was doubly distilled de-ionized.

Rationale of MoS_2 film development

We adopted the same rational as reported from graphene in Chapter 2.

3.2.2 Preparation of MoS_2 films, graphene films, and MoS_2-graphene composite films.

The intercalated MoS_2/graphite was used to form the few-layered nanosheets in the form of thin film using chemical exfoliation process. The MoS_2 in the form of pallet/graphite rod was intercalated by treating with 98% of concentrated sulphuric acid for 24 hrs at room temperature in a closed vessel. MoS_2 palette was prepared from hydraulic palette machine at 150 kg/cm^2 pressure using MoS_2 powder. The intercalated MoS_2 gets easily exfoliated at the interface during film formation procedure to form single-layer/few-layered MoS_2 thin films. Although, a detailed process of formation[54] and transferring[55] the film to a suitable substrate was described in earlier chapter, for a better conception, a short schematic of MoS_2 film formation is given in Scheme. 3.1a. In a typical procedure, deionised water was taken in a Teflon tray (15 cm x 15 cm x 2 cm) so that it forms a meniscus at the edges of the tray (sub phase). The surface of the subphase deionised water was divided into two compartments by a Teflon thread barrier which was conveniently fixed on the opposite edges of the tray. The intercalated MoS_2 was arranged in such a way that it just touches the meniscus of the subphase in one of the compartment. Few drops of carbon tetrachloride were dropped with the help of syringe over intercalated MoS_2 pallet which slides down over it on the surface of subphase (water). The exfoliation in the present case is due to effect of exothermic reaction between an intercalated sulphuric acid and subphase water as shown in following equation,

$$H_2SO_4\,(l) \longrightarrow 2H^+\,(aq) + SO_4^{2-}(aq) \qquad -96.2\ kJ/mol \qquad (1)$$

The energy is aggressively released in this reaction and it is sufficient to overcome the bond strength of van der Waal bonds (0.4-4 kJ/mol), holding MoS_2 layers together, as well as facilitates exfoliation. The surface tension of water makes MoS_2 layers thus formed to float on the surface while CCl_4 helps to spread it occupying whole subphase in the compartment. After allowing all CCl_4 spread on the surface to evaporate, the single-layer/few-layer MoS_2 film was then compressed laterally *via* a teflon thread barrier by spreading a drop of oleic acid on the surface of subphase in the other

surface compartment of the tray. The spreading oleic acid exerts a lateral pressure 30 dynes cm^{-1}, on the film formed on the surface. The as-formed compressed film on the subphase surface (water) was transferred on a glass, quartz or silicon wafer substrate by immersing the substrate vertically in the subphase where the compressed MoS_2 film floats, at a constant rate of 0.5 cm min^{-1} and lifting it vertically at the same rate with the help of coating unit, so that the film covers the dipped area of the substrate (Langmuir-Blodgett technique).

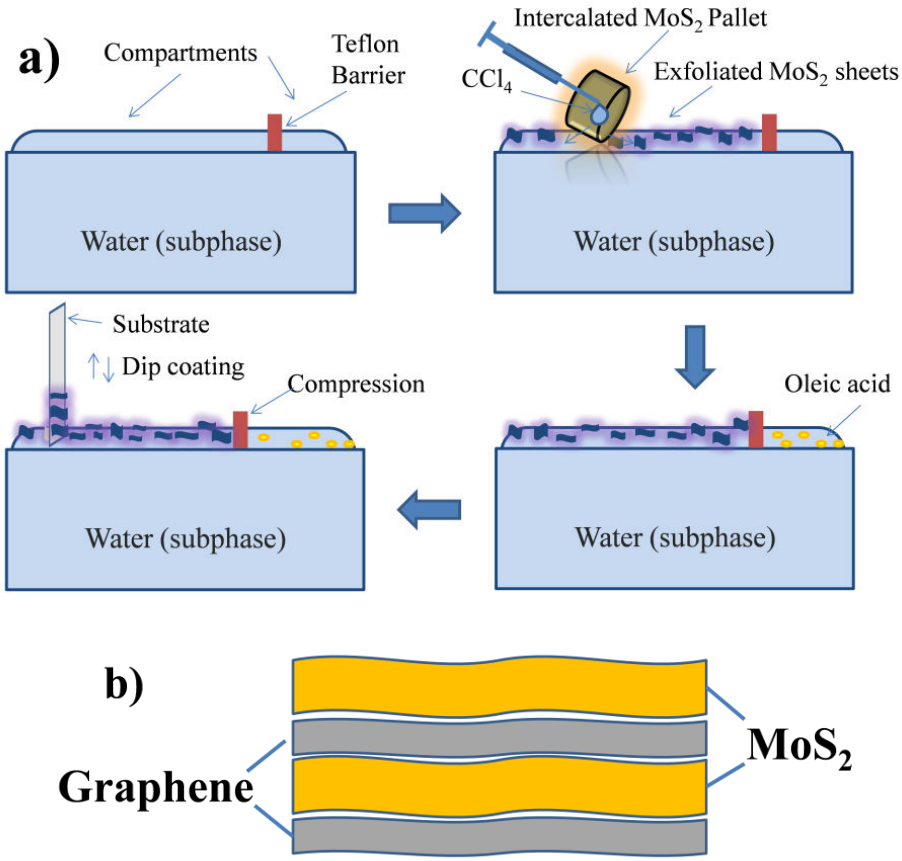

Scheme. 3.1 Schematic illustration of formation of a) MoS_2 nanosheets thin film and b) LbL composite of graphene and MoS_2.

A similar procedure was adapted to obtained graphene film.[54] The operation of transferring the film from subphase surface to substrate was repeated many times to get a desired film thickness/mass for specific applications and characterization. The film was then washed with deionised water several times until it turned out to be of neutral pH. This film was then used for characterization. Calibration of the mass with respect to number of dips at a fixed dipping area was established by using quartz crystal microbalance (QCM-200). Moreover, as shown in Scheme 3.1b this technique

can be useful for the growth of the composites consisting of MoS_2 and graphene by LbL technique using desired sequence which might become important for some specific applications such as supercapacitor.[14] A few-layered graphene nanosheets were obtained on the surface of water in a separate tray as described in previous report.[54] Stacked composite film of MoS_2-GNS is deposited on the substrate by forming a film of each component in two independent trays. By dipping the substrate in one of the trays, a film of MoS_2-GNS with desired thickness/mass was deposited on the substrate. Then the same substrate was dipped in the other tray to deposit the film of MoS_2-GNS with desired thickness and so on. Scheme.3.1b gives the schematic of desired composite layer film formation.

The MoS_2-GNS hybrid electrode of the desired thickness is obtained by deciding the number of layers of each component in a sequence for which the electrochemical study has been performed. Here it may be noted that alternate deposition of single dip of MoS_2 and GNS on the substrate would establish a close contact between MoS_2 layer and graphene layer. Graphene being good electronic conductor, such an arrangement is proposed to be suitable to get better capacitance for the composite.

Here we would like to note some of the observations on resulting film formation due to experimental parameters.

(i) It is important to wipe out H_2SO_4 adhered to MoS_2 pallet carefully so that only intercalated H_2SO_4 reacts with subphase water. This helps efficient exfoliation of MoS_2. (ii) Intercalation period of MoS_2 Pallet is critical and 24 h period was found to be suitable for better exfoliation. (iii) We studied the effect of lateral pressure on the final nature of the film with respect to number of layers in it. It was thought that lower lateral pressure than the one exerted by oleic acid (30 dynes/cm) would increase the proportion of monolayers in resulting film. However it was observed that there was no significant improvement in obtaining higher proportion of monolayers in the film at lower lateral pressure; instead there was deterioration in film quality in terms of uniformity and continuity.

3.3 Characterization.

The crystal structure of the material was determined using Cu Kα radiation (λ=1.54A^{o}) (PAN analytical X'Pert pro X-ray diffractometer). The X-ray tube was operated at 40 kV and 30 mA. Transmission electron microscopy (TEM) images were taken on a JEOL 1200-EX instrument with an accelerating voltage of 100 kV and high-resolution transmission electron microscopy (HRTEM-JEOL 2010F) at an acceleration voltage of 300 kV. The morphologies and microstructure of the dip coated films were examined on an atomic force microscope (AFM, Digital Instrument Environ Scope,) using a tapping mode, with a tip of phosphorus (n) doped silicon and the frequency of cantilever was 237-326 kHz. Environ- SEM (E-SEM, Quanta 200 3D) was used to get the additional information of morphology. FTIR spectra were collected using a Nicolet Magna 550 spectrometer. XPS analysis was performed on a ESCA-3000 VG Scientific UK, using non-monochromatic, AlKα radiation (1486.6 eV) operating at 150 W with a spectral resolution of 0.2 eV. Raman spectra of the samples were obtained using a HR800 micro-Raman spectroscope (Horiba Jobin-Yvon, France) by using an excitation at 632 nm. The photoluminescence spectra of the films were recorded on an F-2500 Fluorescence spectrophotometer at 375 nm excitation source with UV blocking filters to cut down the scattered light from the sample. Cyclic voltammetry and constant current charge/discharge tests were performed using an Autolab PGSTAT 30 (Ecochemie) electrochemical workstation at varying potentials in 1M Na_2SO_4 aqueous solution at room temperature. Electrochemical impedance spectroscopy (EIS) was carried out in the frequency range from 0.1 Hz to 100 kHz and AC bias voltage of 10 mV.

3.4 Results and Discussion

MoS_2 nanosheet thin films were synthesized by making acid intercalated bulk MoS_2 to exfoliate and spread at liquid-liquid interface, laterally compressing it and then transferring it on Si wafer substrate. The procedure is similar to the one reported earlier for GNS thin film formation from bulk graphite.[54]

3.4.1 X-Ray diffraction (XRD), fourier transform infra red spectra (FTIR), scanning electron microscopy (SEM) and high-resolution transformation electron microscopy (HRTEM).

The crystal structure, orientation and morphologies of the samples were characterized by using XRD, scanning electron microscopy (SEM) and high-resolution transformation electron microscopy (HRTEM). Figure 3.2 shows XRD patterns of the as-prepared MoS_2 and MoS_2–GNS hybrid thin films prepared by acid intercalated exfoliation route at room temperature.

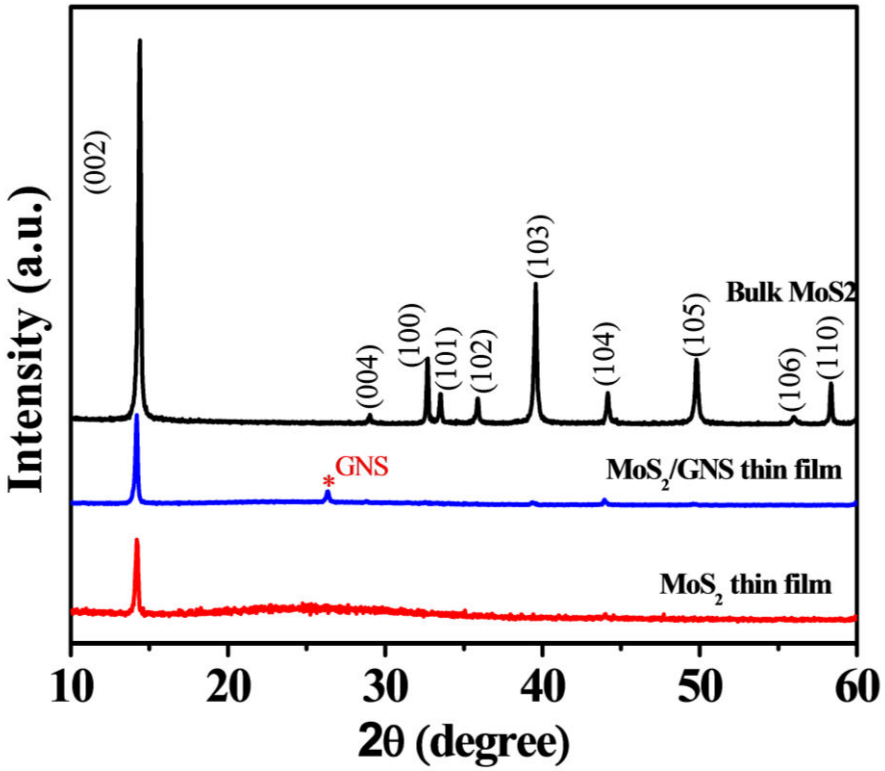

Figure 3.2 XRD patterns of as-prepared MoS_2 thin film, MoS_2-GNS hybrid film and bulk MoS_2.

XRD of MoS_2 bulk pallets is also given for comparison. One sharp and narrow diffraction peak at 14.30 degree attributed to (002) plane of MoS_2 is observed. The presence of exclusive high intensity diffraction peak due to (002) plane of MoS_2 suggests highly oriented thin film of hexagonal MoS_2. Further, the shift of (002) peak in thin film of MoS_2 to lower 2θ when compared to the corresponding peak of the bulk MoS_2, confirms that the product is having Mono/few-layers of MoS_2.[56] For MoS_2-GNS layered composite, the presence of peak at $2\theta = 27^0$ which corresponds to the (002) diffraction peak of GNS, gives the evidence that the graphene is incorporated in composites. The presence of other characteristic peaks in XRD correspond to (103),

(104) and (105) reflections of hexagonal MoS_2 with the intensity much lower than that reported for standard MoS_2 pattern (PDF # 77-1716).

It supports the suggestion of highly oriented few-layered structure for MoS_2 film is formed. Thus, it can be inferred that the composite is made up of alternate hexagonal few-layered MoS_2 and few-layered graphene oriented structures wherein (002) planes of both components lye parallel to each other.

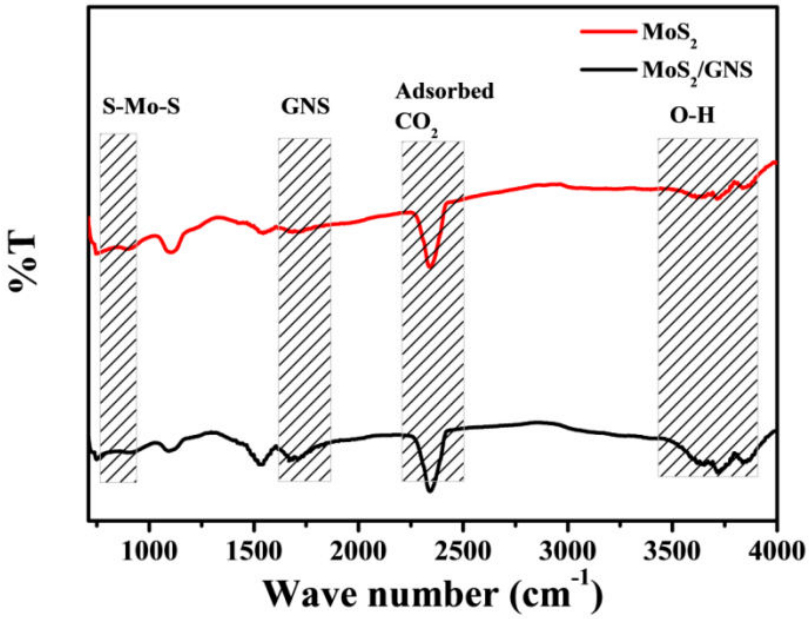

Figure 3.3 Fourier transform infrared spectra (FTIR) of MoS_2 nanosheets and MoS_2 – GNS composites.

The FTIR results also support the formation of MoS_2-GNS composites as shown in Figure 3.3. The frequency region between 400-4000 cm^{-1} was considered for comparison of FT-IR spectra of MoS_2-GNS composites with that of singular constituents of the composite. As shown in Figure 3.3, in the FT-IR spectra, the bands between 3400 to 3700 cm^{-1} are attributed to the oxygen containing functional groups of graphene.[1] The peak at 2260 cm^{-1} were caused by CO_2 absorbed in the sample.[2] Furthermore, the observed absorption band between "1620-1730 cm^{-1}" for MoS_2-GNS, indicates the skeletal vibration of graphene sheets.

SEM image shows that MoS_2 possesses sheet-like structure (Figure 3.4. The size of the sheets ranges from 200 nanometres to 2 micrometers.

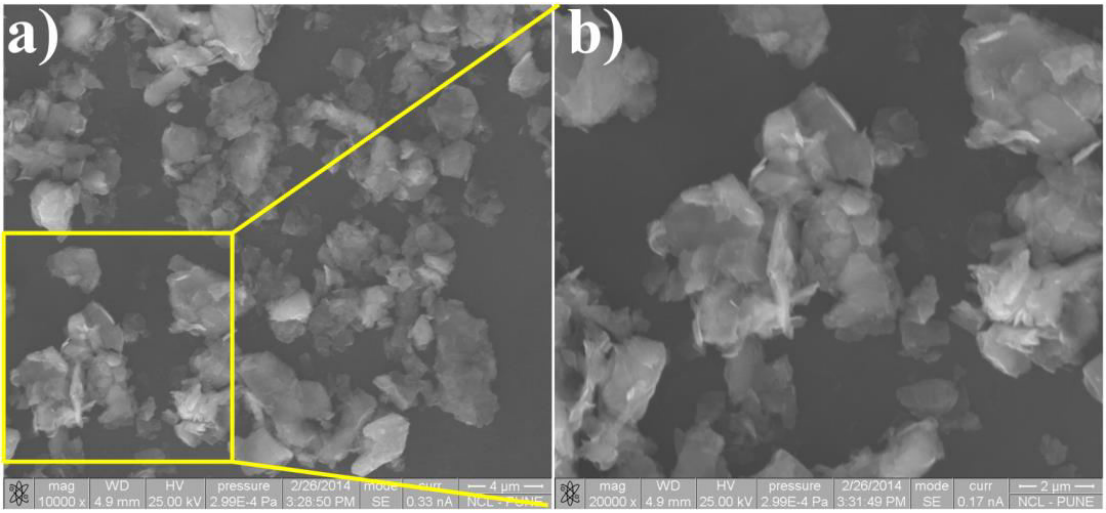

Figure 3.4 SEM image of acid-intercalated exfoliated MoS_2 nanosheets deposited on Si wafer.

High resolution transmission electron microscopic (HRTEM) analysis was performed to explore the structural changes that occur during film formation. The low magnification HRTEM image exhibits film of continuous large areas on the copper grid (Figure3.5a, b&c, Figure 3.6). At the edges of broken regions, some folding of the film could be clearly distinguished. In general, edge folding is a common phenomenon in two-dimensional materials like graphene, which could be effectively utilized to determine the number of layers.[57]

A single dark line at the folded edge could be correlated to a monolayer. The corresponding SAED pattern (an inset of Figure 3.5a) of the area under consideration shows spot diffraction pattern, indicating a single crystal nature of the film. Moreover, high-resolution transmission electron microscopy image of the edge areas of the MoS_2 nanosheet shows fringes, identified by their interlayer distance of 0.61 nm (Figure 3.5d), which is in agreement with XRD analysis as well as earlier reports.[53, 57] The TEM results thus signify that the MoS_2 prepared in this study is a monolayer/few layered film having insignificant defects.

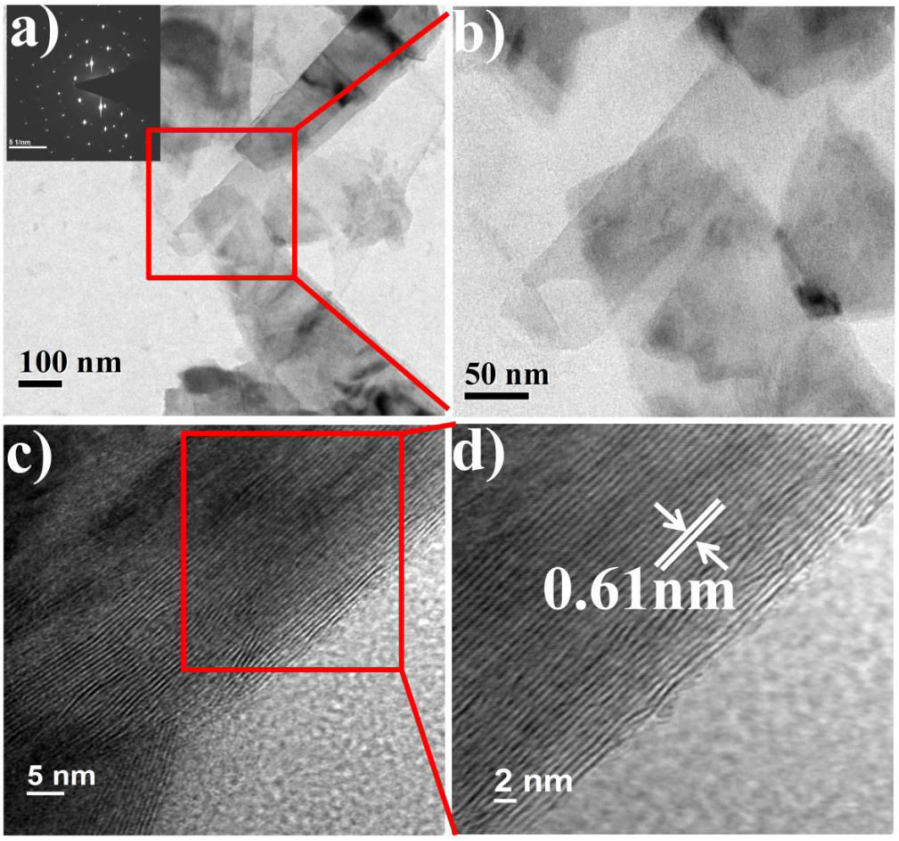

Figure 3.5 TEM characterizations of MoS_2 sheets (a) low-magnification TEM image of MoS_2 sheets supported on carbon grid. Inset: SAED patterns. (b) enlarged TEM image marked in a (c) enlarged high-resolution TEM image of MoS_2 resolved at film edge showing hexagonal lattice and (d) HRTEM image of enlarged portion of 'c'.

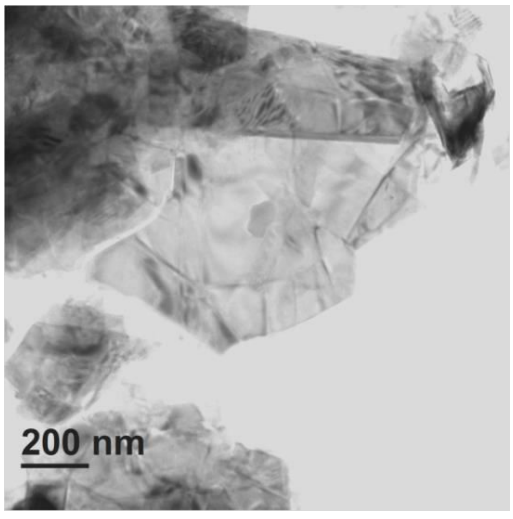

Figure 3.6 HRTEM of MoS_2 image display the curved graphene like morphology at low magnification.

3.4.2 X-ray photoelectron spectroscopy (XPS)

XPS was used to measure the binding energies of Mo and S in the MoS_2 film (Figure 3.7) and to find any impurity occurring during preparation. The XPS spectrum depicts a survey scan (not shown) of bare MoS_2nanosheets which shows the presence of two elements, namely Mo and S. Judging from this data, it could be noted that while multi-layered precursor i.e. bulk MoS_2 was transferred into few-layered MoS_2nanosheets, no impurities are introduced proving the cleanliness of the present method. The Mo3d shows two peaks at 229.3 and 232.5 eV, attributed to the doublet $Mo3d_{5/2}$ and $Mo3d_{3/2}$ respectively as shown in Figure 3.7a. The peaks, corresponding to the $S2p_{1/2}$ and $S2p_{3/2}$ orbital of divalent sulphide ions (S^{-2}) are observed at 163.7 and 162.5 eV as shown in Figure 3.7b. These results are consistent with the reported values for MoS_2 crystal.[37]An atomic ratio of Mo and S estimated from XPS is ~1:2, further confirming the stability of MoS_2 phase during the preparation of the film, although bulk gets transformed in mono/few layered structure. It may be noted that although, H_2SO_4 is used for the intercalation of bulk MoS_2, XPS peak corresponding to SO_4^{2-} species is not observed.

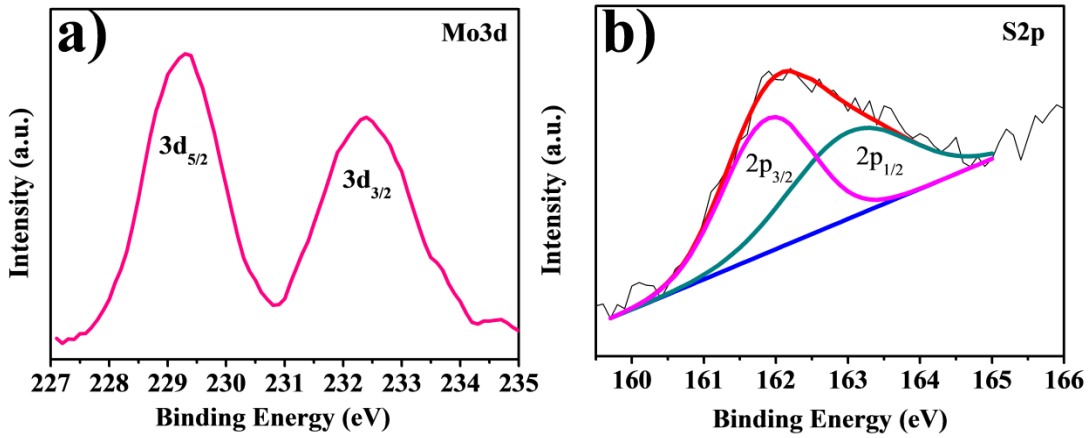

Figure 3.7 XPS spectra of MoS_2 nanosheets (a) Mo 3d and (b) S 2p.

3.4.3 Atomic force microscopy, Raman spectroscopy and photoluminescence spectroscopy

Atomic force microscopy, Raman spectroscopy and photoluminescence spectroscopy were used to identify the monolayers nature of the products.[58] Figure 3.8 shows a typical AFM topographic image of thin MoS_2 layers supported on Si wafer followed by annealing at 100° C for 4 hours. From AFM studies, the thickness is

shown to be 0.8 nm, typical for a MoS_2 monolayer on Si substrate.[59] A statistical analysis based on AFM measurements indicates that the 2D nanosheets have predominant area, having a thickness in the range of 0.8 nm to 1.6 nm corresponding to 1 to 2 layers (Figure 3.9) of MoS_2, although, in other parts varied thicknesses is observed. MoS_2 samples with varied thickness were also investigated using Raman spectroscopy and photoluminescence (PL) spectroscopy.

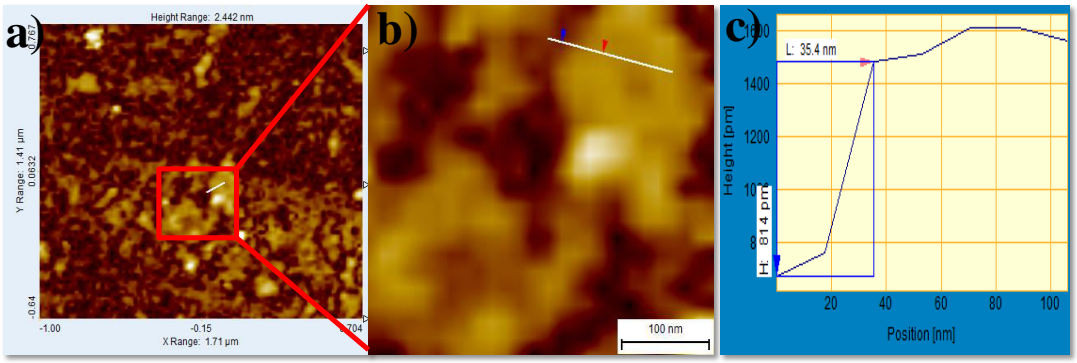

Figure 3.8 (a) AFM image of a typical layered MoS_2 (b) magnified image of the area indicated by the square in (a) and (c) height profile for the marked area.

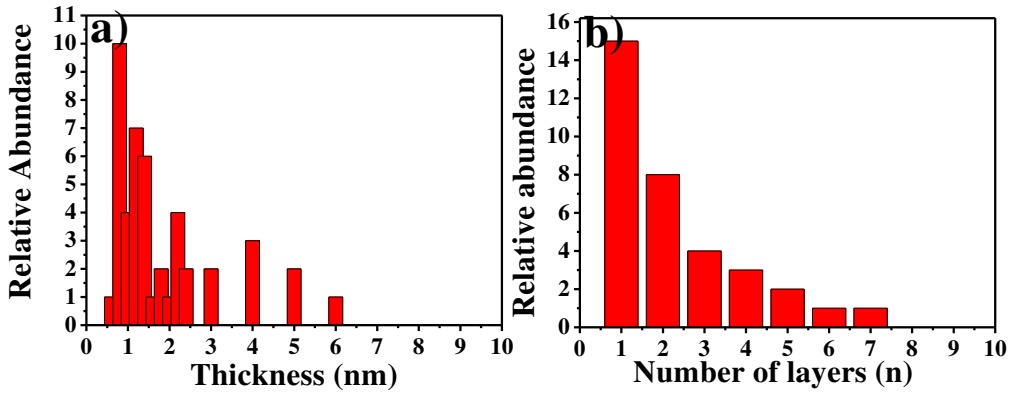

Figure 3.9 Thickness distribution based on 50 randomly selected 2D nanosheets of MoS_2 in the AFM topographic image, Figure 3.8a.

Raman measurements performed on the sample (Figure 3.10) for various layers of MoS_2, exhibited two characteristic peaks, corresponding to two phonon modes, A_{1g} and E_{2g}. The A_{1g} Raman mode is very sensitive to number of layers, and the peak frequency difference between E_{2g} and A_{1g} modes can be used to identify the number of layers of MoS_2.[60]

Figure 3.10 a and b show the variation of wave number difference between Raman E_{2g} and A_{1g} peaks observed for the film tested at different places on the substrate. It is noted that A_{1g} peak shifts are more (6 wave numbers) than corresponding shifts observed for E_{2g} peaks at a particular location of the sample. It implies that the number of layers formed at different locations varies. The exact relation of the frequency difference between two Raman modes for layers of MoS_2 is reported in the literature.[61] The peak shifts in Raman spectra of MoS_2 with the number of layers is 18 cm^{-1}, 21.9 cm^{-1}, and 23.4 cm^{-1} for number of 1, 2, and 4 layers respectively.[62, 63] Therefore, it can be concluded that MoS_2 layer on the substrate consists of a mix up of areas of monolayer, bi-layer and multilayer. This observation is consistent with the conclusions of HRTEM and AFM. The statistical analysis of the shifts in the Raman peaks at various locations on a sample of MoS_2 formed by the present method shows that the predominant area is made up of monolayer. Two independent characterization tools, namely, AFM and Raman show that the film formed is mostly of a monolayer nature which is an important feature of the present method.

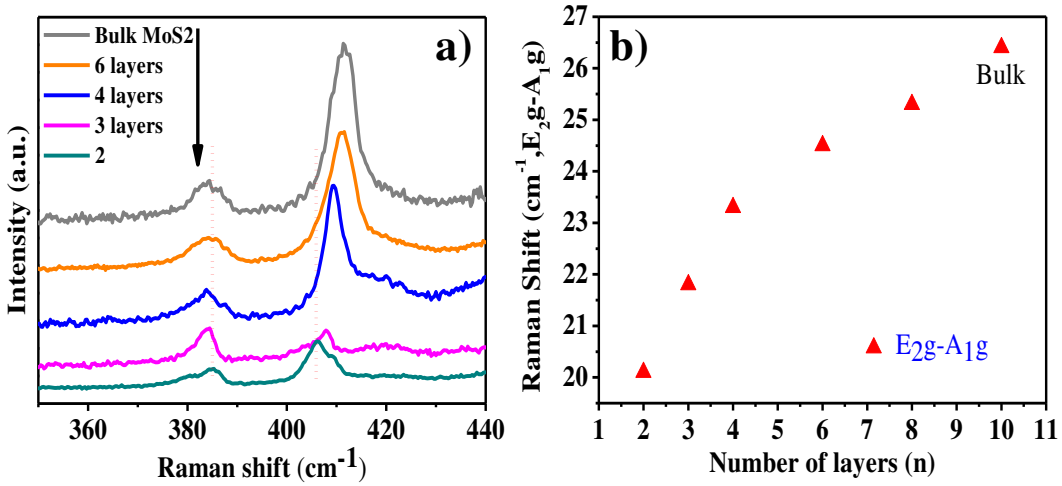

Figure 3.10 (a) Raman spectra of MoS_2 monolayer's on glass substrate and bulk MoS_2. (b) Peak energy difference between A_{1g} and E_{2g} of transferred MoS_2 as a function of layer number.

Apart from Raman peaks, characteristics of MoS_2 at ~384 and ~404 cm^{-1}, the peaks corresponding to D, G and 2D bands of graphene are observed in MoS_2-GNS hybrid shown in Figure 3.11 confirming the formation of stacked composites.

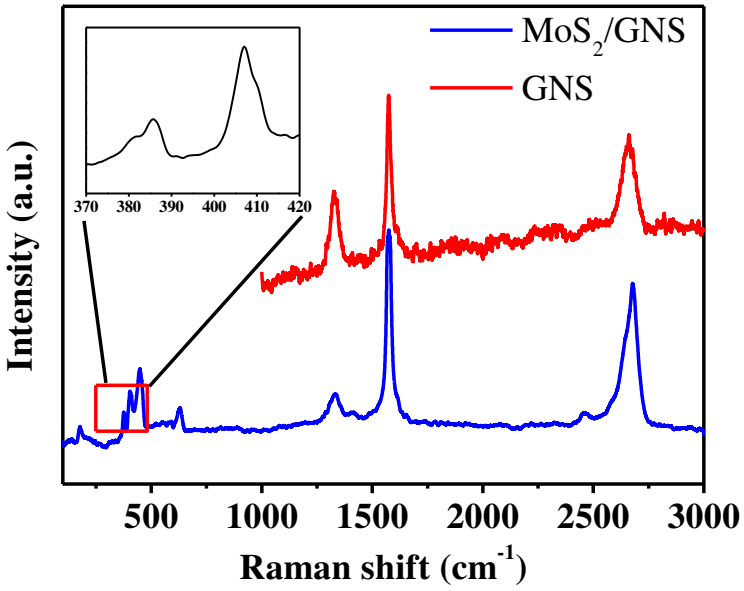

Figure 3.11 Raman spectra of GNS and MoS_2-GNS composite

We further recorded the PL spectra of mono/few layersMoS_2 on quartz plate. As reported earlier, the bulk MoS_2 possesses an indirect band gap of 1.2 eV.[64] For two dimensional monolayer sheets, the band gap becomes direct and wider (1.8 eV). This transition from indirect band gap to direct band gap shows its effect in terms of strong PL of single layer MoS_2 and low intensity or absence of PL for multilayer films. In the bulk MoS_2, no photoluminescence is observable due to its indirect band gap like silicon.[64] PL spectra in Figure 3.12 show PL intensity for the sample prepared by one dip as well as multi dips during the deposition.

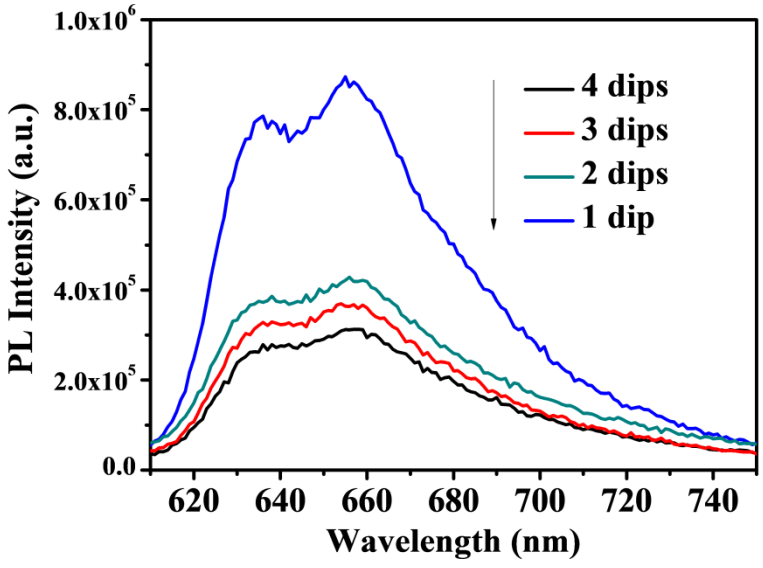

Figure 3.12 Photoluminescence spectra of MoS_2 for different layers.

The strong PL is indicative of monolayer MoS_2 formed by one dip during the deposition. As the number of dips increases, the PL intensity goes down as the nature of the sample tends to its bulk properties. The PL peaks of as-grown one dip MoS_2 on quartz substrate are approximately located at 660 and 633 nm, which can be attributed to excitonic transition of monolayer MoS_2 which is in close agreement with earlier reports. [64, 65]

3.4.4 Electrochemical Characterization

3.4.4.1 Cyclic voltammetry (CV)

The electrochemical performance of the as-prepared MoS_2 and MoS_2-GNS films on conducting glass as electrodes was evaluated by using a standard cyclic voltammetry (CV) with a two electrode system. To check stability and recycling of electrodes, galvanostatic charge-discharge technique was used. The thin film was coated over FTO glass. The CV measurements were done in 1 M Na_2SO_4 as an electrolyte. In order to ensure the adhesion of film, electrodes were heated at 70^o C for 15 hours. No binder material like nafion is necessary for fabrication of electrode which is another advantage of the present method. Figure 3.13 a, b show typical CV curves of MoS_2 and MoS_2-GNS composites. Data are obtained between -0.4V to 0.6 V at a scan rates 20, 50, 100 and 150 mV s^{-1}.

The CV of the MoS_2-GNS electrode approximates an ideal rectangle with a greater area and a more symmetrical shape than CV acquired for MoS_2 thin film. This indicates the enhanced capacitance of the hybrid matrix. All curves show nearly rectangular shape, even at scan rates, as high as 150 mVs^{-1} which is considered as an ideal capacitive behavior of the materials. The specific capacitance values of the samples are calculated from the CV curves using following equation, [66]

$$C_{sp}=/IdV/V\Delta m \quad \text{---------- (2)}$$

where, C_{sp} is a specific capacitance of the electrode (Fg^{-1}), m is an active mass of the electrode material (g) which was obtained from quartz crystal microbalance (QCM-200) in the present study, I is the response current density (A g^{-1}) and v is the potential scan rate in (V s^{-1}) and V is potential (V).

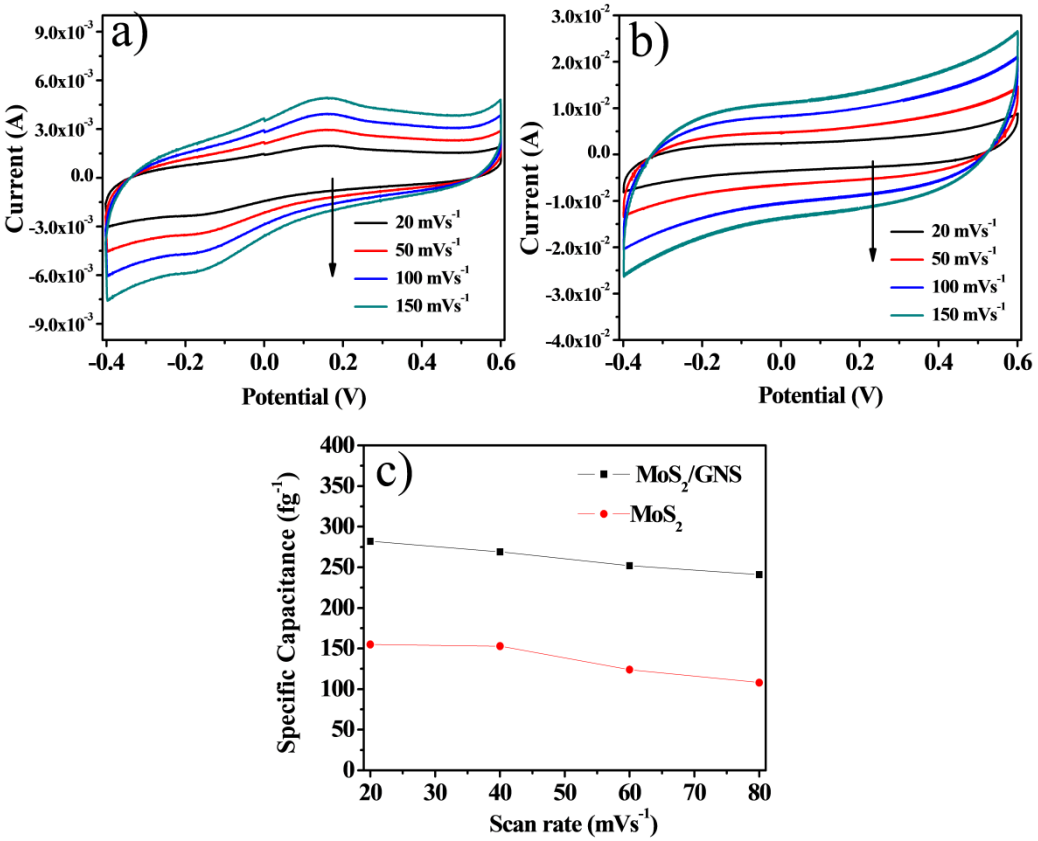

Figure 3.13 CV curves of MoS_2 (a) and MoS_2-GNS composites (b) at different scan rates 20, 50, 100 and 150 mVs^{-1}. (c) Specific capacitance values calculated from eqn. (1) for MoS_2 and MoS_2-GNS as a function of scan rates mVs^{-1}.

The calculated C_{sp} values of the MoS_2-GNS and MoS_2 electrodes were 282 and 156 Fg^{-1} at the scan rate 20mVs^{-1} and 241 and 108 Fg^{-1} at the scan rate of 150 mVs^{-1} respectively (Table 3.1). C_{sp} of bare GNS electrode is obtained to be 122 and 88 Fg^{-1} respectively at the scan rate 50 and 150 mVs^{-1}. Also, on the basis of charge/discharge results, C_{sp} of bare GNS at 20 and 50 µA is 87 and 73 Fg^{-1} repectively.[54] Figure 3.13c shows the variation in specific capacitance as a function of scan rate. The hybrid nanostructure electrode demonstrated that the specific capacitance was higher than those of observed for MoS_2 and graphene at the scan rates from 20 to 150 mVs^{-1}.

Moreover, C_{sp} decreased with increasing scan rate. The decrease in C_{sp} at higher scan rates was attributed to the presence of inner active sites that cannot sustain the redox transitions due to less diffusion of ions in the electrode matrix. The

decreasing C_{sp} indicates that the parts of the electrode surface becomes inaccessible at high charging-discharging rates.[67]

So far, Huang, Ke-Jing et.al.[68] reported MoS_2-graphene composite synthesized by a modified l-cysteine-assisted solution phase method, which gave rise to the specific capacitance of 243 F g^{-1} at a discharge c.d. 1 A g^{-1}.

Table 3.1: Comparison of specific capacitance calculated for MoS_2 and MoS_2-GNS electrode by cyclic Voltammetry.

	Specific capacitance Fg^{-1} from Cyclic Voltametry				**% Retention**
Scan Rate	**20mVs-1**	**50 mVs-1**	**100 mVs-1**	**150 mVs-1**	
MoS_2	155	153	124	108	69%
MoS_2/GNS	282	169	152	141	85%

Alkali metal cations play an important role in the charge-discharge electrochemistry of MoS_x coating. A mechanism based on a surface adsorption of electrolyte cation such as Na^+ on MoS_x can be proposed as follows, [69]

$$(MoS_x/GNS)_{surface} + Na^+ + e^- \leftrightarrows ((MoS_x/GNS)^- Na^+)_{surface} \quad (3)$$

$$MoS_x/GNS + H^+ + e^- \leftrightarrows (MoS_x/GNS)H \quad \text{(intercalation)} \quad (4)$$

Where, equation (3) represents the surface adsorption of Na^+ on MoS_2-GNS composite, equation (4) represents the reversible intercalation/de-intercalation of protons in MoS_2 crystal. It may be noted that the shape of CV curves do not change with frequency, implying that the mechanism of electrochemical activity is same throughout the frequency range of study. It is well established that the contribution of capacitance is due to reversible intercalation process. Therefore, the improvement in the overall capacitance of composite can be mainly attributed to reversible proton intercalation.

The other factor that causes improvement in capacitance is use of mono/few layers of MoS_2 and mono/few layers of graphene in the composite. The layer thicknesses are small; so that quantum confinement effects become apparent. Very large areas are available for adsorption of ions (equation 3). Also, as per the expected design of the composite, (scheme 1b), MoS_2 sheets are in close contact with graphene sheets. Graphene is known to be good electronic conductor, it provides high rate capability for charge/discharging process in the composite. The flexibility of graphene sheets provide accommodations for the possible volume changes occurring during charge-discharge processes, thus avoiding the degrading of capacitance properties. The presence of graphene sheets between two neighboring MoS_2 sheets do not allow agglomeration/stacking of MoS_2. The total sum effect of all the aspects mentioned above (synergistic effect) is reflected in the enhancement shown in the capacitance performance of MoS_2/GNS composite over bare MoS_2 or graphene capacitance.

An alternate single layer is being reported as it is proposed to be most suitable for capacitive storage as protons enter in the matrix; the charge would be transported through the electronic circuit through the conducting layer (GNS) in close contact with MoS_2. We would like to indicate that in any other sequence of deposition of MoS_2 and GNS, the contact between the layers would be inferior to the one discussed above which does not suit obtaining high capacitance.

The capacitance (282-241 F g^{-1}) obtained in the present study is considerably higher than those of MoS_2/graphene composite mentioned reported earlier.[68] The higher capacitance obtained is due to layer-by-layer structure of composite, and having conducting and high surface area graphene in close contact with similar structured MoS_2 as one of the components facilitating rapid charging and discharging of the electrode. These results indicate the exciting potential for the use of LbL MoS_2/GNS film in high performance supercapacitor. The percent retention of specific capacitance (C_{sp}) in case of composite is 85% at the high value of C_{sp} = 282 F g^{-1}, while in case of MoS_2 alone, it is 69%.

3.4.2.2 Electrochemical impedance spectroscopy (EIS)

Electrochemical Impedance Spectroscopy (EIS) gives information regarding the internal resistance of an electrode material as well as the resistance between the

electrode and electrolyte. Impedance spectra for MoS_2-GNS and MoS_2 are shown in Figure 3.14.

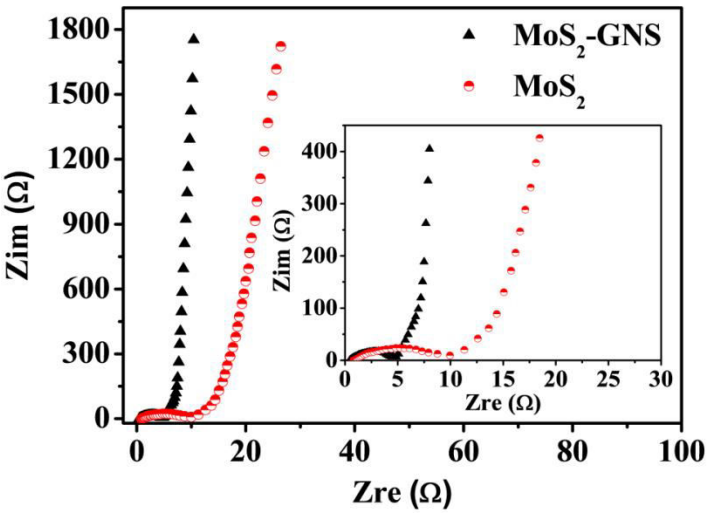

Figure 3.14 Electrochemical Impedance Spectroscopic results for MoS_2-GNS and MoS_2 electrode. Inset shows magnified portion in the high frequency region.

The spectra are analyzed using Nyquist plots. A semicircle in high frequency region is related to the charge transfer resistance and a straight line in low frequency region represents an ideal capacitive behavior. The diameter of the fitted circle is equal to the electrode resistance arising from the charge transfer resistance (Rct) in the cell.[70] The solution resistance (Rs) for the MoS_2-GNS composite and MoS_2 was found to be 0.4 and 0.94 Ω respectively.

The charge transfer resistance (Rct) was measured to be 4.1 and 12.1 Ω respectively. This indicates that MoS_2-GNS electrode possesses low charge transfer impedance and therefore the composite shows higher capacitance than shown by the bare MoS_2 electrode. These results are consistent with those obtained in the CV results.

3.4.4.3 Galvanostatic charge discharge

Figure 3.15 a, b shows the constant current charge/discharge curves obtained with MoS_2 and MoS_2-GNS composite electrodes by using two electrode systems in 1 M Na_2SO_4 at different current densities ranging from 20 µA to 80 µA between -0.4 to 0.6 V. The curve is nearly symmetric and the time required for discharging is higher than that of charging revealing a good capacitive behaviour. The voltage drop is

observed to be very small, which indicates that the electrode has low internal resistance.

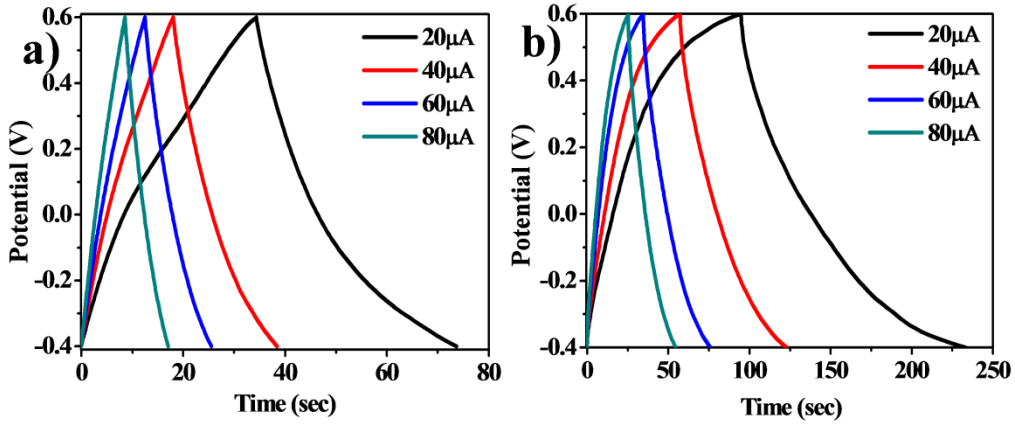

Figure 3.15 Galvanostatic charge-discharge curves of MoS_2 (a) and MoS_2-GNS (b) at different current densities (20, 40, 60 and 80 µA.

Using the charge/discharge curve, the specific capacitance of the electrode can be calculated by the following equation,[71-73,]

$$C_{sp} = ((i \times \Delta t))/(\Delta V \times m) \qquad (5)$$

where, 'i' is current density Ag^{-1} , Δt is discharge time (s), ΔV is a voltage difference in (V) and m is an active mass of electrode derived from quartz crystal microbalance directly and was found to be 10.50 ±05 µg for MoS_2/GNS and 5.05 ±05 µg for MoS_2 electrode. The calculated C_{sp} from the above equation shows high values of 255 Fg^{-1} to 236 Fg^{-1} at the high current densities from 20 µA to 80µA (Table 3.2).

Table 3.2. Calculated Specific capacitance Fg^{-1} from Galvanostatic charge discharge at varying current density.

	Specific capacitance Fg^{-1} from Galvanostatic charge discharge				**% Retention**
Current Density	**20 µA**	**40 µA**	**60 µA**	**80 µA**	
MoS_2	156	152	147	144	92.3%
MoS_2/GNS	255	243	240	236	92.5%

The cycle stability of MoS_2 and MoS_2-GNS composites was evaluated by repeating the constant current charge/discharge test between -0.4 and 0.6 V at a current density 3.6 and 2 Ag^{-1} for 1000 cycles respectively. Figure 3.16a shows rate performance of the MoS_2 and MoS_2-GNS electrodes at various current densities. Figure 3.16b shows that for MoS_2-GNS composite the specific capacitance retention is up to 93% at high current density of 2 Ag^{-1} (20 µA / 10.05 µg) as against 83% for MoS_2 alone at 3.6 Ag^{-1}(20 µA / 5.50 µg). Thus MoS_2-GNS composite is relatively more stable even at higher current density as well as higher number of cycles.

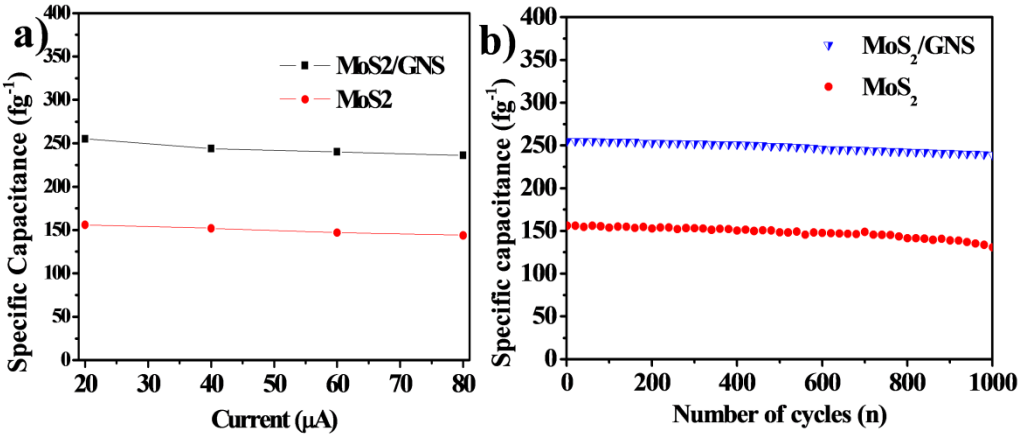

Figure 3.16. (a) Specific capacitance of the MoS_2 and MoS_2-GNS composites at different current densities. (b) Cyclic performance of MoS_2 and MoS_2-GNS composites electrode at current density of 3.6 Ag^{-1} and 2 Ag^{-1} respectively.

The specific capacitance of MoS_2-GNS composites after 1000 cycles remains as high as 243 Fg^{-1} even at high discharge current density of 2 Ag^{-1}. The results indicate that the MoS_2-GNS composites have high rate of capacitance, which is recognized as one of the most important electrochemical property in the application of capacitor electrodes and batteries. The robust composite structure and synergistic interaction between graphene and few-layered MoS_2 sheets are believed to be the main reasons for the superior performance of MoS_2-GNS composites.

The other important features that contribute for enhanced performance of the presented composite matrix films are (1) the high specific surface area and high conductivity of graphene improve the electrical conductivity of the electrode and facilitate ion diffusion, fast charge transport and electrolyte interactions during charge and discharge (2) aggregation of graphene/MoS_2nanosheets was prevented by

MoS_2/graphene nanosheets forming alternate layers in the matrix by using LbL technique used in the present work. It is reported that restacking of 2D nanosheets was one of the main reasons for the capacity loss[74] (3) in addition, the flexibility of GNS could enhance the stability of the composite electrode structure during repeat charging/discharging process. (4) MoS_2 (002) planes and graphene (002) planes stack together in the composite. Such an arrangement is thought to be the best for deriving the advantages mentioned above, especially when composites from the same components have been reported in the literature where such an arrangement is not realized.[69] Therefore, the perfect match between the morphology and crystal structure of MoS_2nanosheets and GNS maximizes the synergistic interaction between both, resulting in significant improvement in the electrochemical performances of MoS_2-GNS composites.

3.5 Conclusions

In conclusion, we have successfully synthesized large area (micrometer scale), monolayer/few layer and highly crystalline MoS_2nano sheets in the form of thin films by a novel technique. The technique consists of intercalating bulk MoS_2 by H_2SO_4 and arranging its exfoliation process at the liquid-air interface. The film formed at interface could be transferred on a suitable substrate. The present method forms monolayer MoS_2 in the predominant area of the film with enhanced crystallinity of MoS_2, as evidenced by various microscopic and spectroscopic characterizations including XRD, TEM, SAED Raman and PL.

The work is extended to synthesize MoS_2-GNS composites thin films via LbL technique for super-capacitor applications. When tested as an electrode material, the as-obtained MoS_2-GNS exhibits high capacity, excellent rate capability, and long cycle life. The maximum specific capacitance achieved as calculated from CV is 282 Fg^{-1} at the scan rate 20 mVs^{-1} for MoS_2-GNS electrode and for MoS_2 156 Fg^{-1}. C_{sp} calculated from galvanostatic charge discharge is 255 F g^{-1} at a current density 2 Ag^{-1} compared to 150 Fg^{-1} at current density 3.6 Ag^{-1} for MoS_2. Thus synergistic effect in MoS_2-GNS composite is revealed through the improved capacitance, better cycle life as shown by the studies of CV, galvanostatic charge discharge characterization and EIS.

By selecting other layered transition metal dichalcogenides, we believe that this approach can produce a variety of new nanosheet hybrids for the application in a broad range consisting of lithium ion batteries, electrochemical capacitors, sensors and catalysis.

3.6 References

[1] G. Shi, Y. Hanlumyuang, Z. Liu, Y. Gong, W. Gao, Bo. Li, J. Kono, J. Lou, R. Vajtai, P. Sharma and P. M. Ajayan, *Nano Lett*., 2014, **14**, 1739.

[2] J. Yang and S. Gunasekaran, *Carbon*, 2013, **51**, 36.

[3] I. Zhu, S. Zhang, Y. Cui, H. Song and X. Chen, *Electrochim. Acta*, 2013, **89**, 18.

[4] P. Simon and Y. Gogotsi, *Nat. Mater*., 2008, **7**, 845.

[5] J. R. Miller and P. Simon, *Science*, 2008, **321**, 651.

[6] S. Stankovich, D. A. Dikin, G. H. B. Dommett, K. M. Kohlhaas, E. J. Zimney, E. A. Stach, R. D. Piner, S. T. Nguyen and R. S. Ruoff, *Nature*, 2006, **442**, 282.

[7] Z. L. Wang, D. Xu, Y. Huang, Z. Wu, L. M. Wang and X. B. Zhang, *Chem. Commun*., 2012, **48**, 976.

[8] M. D. Stoller, S. Park, Y. Zhu, J. An and R. S. Ruoff, *Nano Lett*., 2008, **8**, 3498.

[9] Y. Wang, Z. Shi, Y. Huang, Y. Ma, C. Wang, M. Chen and Y. Chen, *J. Phys. Chem. C*, 2009, **113**, 13103.

[10] Y. Bai, R. B. Rakhi, W. Chen and H. N. Alshareef, *J. Power Sources*, 2013, **233**, 313.

[11] X. Zhou, Y.–X. Yin, L.–J. Wan and Y.-G. Guo, *Chem. Commun*., 2012, **48**, 2198.

[12] S. Ding, J. S. Chen, D. Luan, F. Y. C. Boey, S. Madhavi and X. W. Lou, *Chem. Commun*., 2011, **47**, 5780.

[13] S. Ding, D. Luan, F. Y. C. Boey, J. S. Chen and X. W. Lou, *Chem. Commun*., 2011, **47**, 7155.

[14] W. Yue, S. Jiang, W. Huang, Z. Gao, J. Li, Y. Ren, X. Zhaoa and X. Yang, *J. Mater*, *Chem*, *A,* 2013, **1**, 6928.

[15] W. Lv, F. Sun, D. M. Tang, H. T. Fang, C. Liu, Q. H. Yang and H.-M. Cheng, *J. Mater. Chem*., 2011, **21**, 9014.

[16] S. B. Yang, X. L. Feng and K. Mullen, *Adv. Mater*., 2011, **23**, 3575.

[17] D. Wang, D. Choi, J. Li, Z. Yang, Z. Nie, R. Kou, D. Hu, C. Wang, L. V. Saraf, J. Zhang, I. A. Aksay and J. Liu, *ACS Nano*, 2009, **3-4**, 907.

[18] D. Wang, R. Kou, D. Choi, Z. Yang, Z. Nie, J. Li, L. V. Saraf, D. Hu, J. Zhang, G. L. Graff, J. Liu, M. A. Pope and I. A. Aksay, *ACS nano*, 2010, **4 (3),** 1587.

[19] D. Chen, L. H. Tang and J. H. Li, *Chem. Soc. Rev.*, 2010, **39**, 3157.

[20] Q. H. Wang, K. Kalantar-Zadeh, A. Kis, J. N. Coleman and M. S. Strano, *Nat. Nanotechnol*., 2012, **7**, 699.

[21] X. Huang, Z. Y. Zeng and H. Zhang, *Chem. Soc. Rev*., 2013, **42**, 1934.

[22] J. Q. Liu, Z. Y. Zeng, X. H. Cao, G. Lu, L. H. Wang, Q. L. Fan, W. Huang and H. Zhang, *Small*, 2012, **8**, 3517.

[23] Q. Y. He, Z. Y. Zeng, Z. Y. Yin, H. Li, S. X. Wu, X. Huang and H. Zhang, *Small*, 2012, **8**, 2994.

[24] Z. Yin, H. Li, I. Jiang, Y. M. Shi, Y. H. Sun, G. Lu, Q. Zhang, X. D. Chen and H. Zhang, *ACS Nano*, 2012, **6**, 74.

[25] J. M. Soon and K. P. Loh, *Electrochem. Solid-state Lett*., 2007, **10**, A250.

[26] B. Radisavljevic, A. Radenovic, J. Brivio, V. Giacometti and A. Kis, *Nat. Nanotechnol*., 2011, **6**, 147.

[27] Y. J. Zhang, J. T. Ye, Y. Matsuhashi and Y. Iwasa, *Nano Lett*., 2012, **12**, 1136.

[28] B. Radisavljevic, M. B. Whitwick and A. Kis, *ACS Nano*, 2011, **5**, 9934.

[29] H. Wang, L. Yu, Y.-H. Lee, Y. Shi, A. Hsu, M. L. Chin, L.-J. Li, M. Dubey, J. Kong and T. Palacios, *Nano Lett*., 2012, **12**, 4674.

[30] M. Chhowalla, H. S. Shin, G. Eda, L. J. Li, K. P. Loh and H. Zhang, *Nat. Chem.*, 2013, **5**, 263.

[31] A. B. Laursen, S. Kegnaes, S. Dahl and I. Chorkendorff, *Energy Environ. Sci*., 2012, **5**, 5577.

[32] J. V. Lauritsen, M. Nyberg, J. K. Norskov, B. S. Clausen, H. Topsoe, E. Laegsgaard and F. Besenbacher, *J. Catal*., 2004, **224**, 94.

[33] J. N. Coleman, M. Lotya, A. O'Neill, S. D. Bergin, P. J. King, U. Khan, K. Young, A. Gaucher, S. De, R. J. Smith, I. V. Shvets, S. K. Arora, G. Stanton, H. Y. Kim, K. Lee, G. T. Kim, G. S. Duesberg, T. Hallam, J. J. Boland, J. J. Wang, J. F. Donegan, J. C. Grunlan, G. Moriarty, A. Shmelio, R. J. Nicholls, J. M.

Perkins, E. M. Grieveson, K. Theuwissen, D. W. McComb, P. D. Neelist and V. Nicolosi, *Science*, 2011, **331**, 568.

[34] Z. Y. Zeng, Z. Y. Yin, X. Huang, H. Li, Q. Y. He, G. Lu, F. Boey and H. Zhang, *Angew. Chem. Int. Ed.*, 2011, **50**, 11093.

[35] K. G. Zhou, N. N. Mao, H. X. Wang, Y. Peng and H. L. Zhang, *Angew. Chem., Int. Ed.*, 2011, **50**, 10839.

[36] C. Altavilla, M. Sarno and P. A. Ciambelli, *Chem. Mater.*, 2011, **23**, 3879.

[37] Y. Li, H. Wang, L. Xie, Y. Liang, G. Hong and H. Dai, *J. Am. Chem. Soc.*, 2011, **133**, 7296.

[38] H. S. S. R. Matte, A. Gomathi, A. K. Manna, D. G. Late, R. Datta, S. K. Pati and C. N. R. Rao, *Angew. Chem. Int. Ed.*, 2010, **49**, 4059.

[39] Y. Peng, Z. Meng, C. Zhong, J. Lu, W. Yu, Y. Jia and Y. Qian, *Chem. Lett.*, 2001, **8**, 772.

[40] A. M. Seayad and D. M. Antonelli, *Adv. Mater.*, 2004, **16**, 765.

[41] J. Putz and M. A. Aegerter, *J. Sol-Gel Sci. Technol.*, 2000, **19**, 821.

[42] Y. H. Lee, X. Q. Zhang, W. J. Zhang, M. T. Chang, C. T. Lin, K. D. Chang, Y. C. Yu, J. T. W. Wang, C. S. Chang, I. J. Li and T. W. Lin, *Adv. Mater.*, 2012, **24**, 2320.

[43] Y, J, Zhan, Z. Liu, S. Najmaei, P. M. Ajayan and J. Lou, *Small*, 2012, **8**, 966.

[44] X. Wang, H. Feng, Y. Wu and L. Jiao, *J. Am. Chem. Soc.*, 2013, **135**, 5304.

[45] Y. C. Lin, W. J. Zhang, J. K. Huang, K. K. Liu, Y. H. Lee, C. T. Liang, C. W. Chu and L. J. Li, *Nanoscale*, 2012, **4**, 6637.

[46] K. K. Liu, W. J. Zhang, Y. H. Lee, Y. C. Lin, M. T. Chang, C. Su, C. S. Chang, H. Li, Y. M. Shi, H. Zhang, C. S. Lai and L. J. Li, *Nano Lett.*, 2012, **12**, 1538.

[47] Y. M. Shi, W. Zhou, A. Y. Lu, W. J. Fang, Y. H. Lee, A. L. Hsu, S. M. Kim, K. K. Kim, H. Y. Yang, L. J. Li, J. C. Idrobo and J. Kong, *Nano Lett.*, 2012, **12**, 2784.

[48] H. Hwang, H. Kim and J. Cho, *Nano Lett.*, 2011, **11**, 4826.

[49] H. Liu, D. Su, R. Zhou, B. Sun, G. Wang and S. Z. Qiao, *Adv. Energy Mater.*, 2012, **2**, 970.

[50] C. Zhang, Z. Wang, Z. Guo and X. W. Lou, *ACS Appl. Mater. Interfaces*, 2012, **4**, 3765.

[51] S. Ding, D. Zhang, J. S. Chen and X. W. Lou, *Nanoscale*, 2012, **4**, 95.

[52] G. Huang, T. Chen, W. Chen, Z. Wang, K. Chang, L. Ma, F. Huang, D. Chen and Y. Lee, *Small*, 2013, **9**, 3693.

[53] X. Zhou, L.-J. Wan and Y.-G. Guo, *Chem Commun*., 2013, **49**, 1838.

[54] S. Patil, V. Patil, S. Sathaye and K. Patil, *RSC Adv*., 2014, **4**, 4094.

[55] S. D. Sathaye, K. R. Patil, D. V. Paranjape, A. Mitra, S. V. Awate and A. B. Mandale, *Langmuir*, 2000, **16**, 3487.

[56] B. Lei, G. R. Li and X. P. Gao, *J. Mater. Chem., A,* 2014, **2**, 3919.

[57] J. C. Meyer, A. K. Geim, M. L. Katsnelson, K. S. Novoselov, T. J. Booth and S. Roth, *Nature*, 2007, **446**, 60.

[58] D. J. Late, B. Liu, H. S. S. Mate and C. N. R. Rao, *Adv. Funct. Mater*., 2012, **22**, 1894.

[59] J. Z. Ou, A. F. Chrimes, Y. Wang, S.-Y. Tang, M. S. Strano and K. Kalantar-zadeh, *Nano Lett*., 2014, **14**, 857.

[60] Y.-H. Lee, L. Liu, H. Wang, W. Fang, X. Ling, Y. Shi, C.-T. Lin, J.-K. Huang, M.-T. Chang, C.-S. Chang, M. Dresselhaus, T. Palacios, L.-J. Li and J. Kong, *Nano Lett*., 2013, **13**, 1852.

[61] H. Li, Q. Zhang, C. C. R. Yap, B. K. Tay, T. H. T. Edwin, A. Olivier and D. Baillargeat, *Adv. Funct. Mater*., 2012, **22**, 1385.

[62] C. Lee, H. Yan, I. E. Brus, T. F. Heinz, J. Hone and S. Ryu, *ACS Nano*, 2010, **4**, 2695.

[63] S.-L. Li, H. Miyazaki, H. Song, H. Kuramochi, S. Nakaharai and K. Tsukagoshi, *ACS Nano*, 2012, **6**, 7381.

[64] A. Splendiani, L. Sun, Y. Zhang, T. Li, J. Kim, C.-Y. Chim, G. Galli and F. Wang, *Nano Lett*., 2010, **10**, 1271.

[65] K. F. Mark, C. Lee, J. Hone, J. Shan and T. F. Heinz, *Phys. Rev. Lett*., 2010, **105**, 136805.

[66] T. Lee, T. Yun, B. Park, B. Sharma, H. K. Song and B.-S. Kim, *J. Mater. Chem*., 2012, **22**, 21092.

[67] J. Wang, Z. Gao, Z. Li, B. Wang, Y. Yan, Q. Liu, T. Mann, M. Zhang and Z. Jiang, *J. Solid State Chem*., 2011, **184**, 1421.

[68] K. J. Huang, L. Wang, Y. J. Liu, Y. M. Liu, H. B. Wang, T. Gan and L. L. Wang, *Int. J. Hydrogen Energy*, 2013, **38**, 14027.

[69] C. D. Lokhande, D. P. Dubal and J. Oh-Shim, *Curr. Appl. Phys*., 2011, **11**, 255.

[70] Z. Wang, T. Chen, W. Chen, K. Chang, L. Ma. G. Huang, D. Chen and J. Y. Lee, *J. Mater. Chem. A*., 2013, **1**, 2202.

[71] K. Zhang, Li. Li. Zhang, X. S. Zhao and J. Wu, *Chem. Mater*., 2010, **22**, 1392.

[72] W. Wang, Q. Hao, W. Lei, X. Xia and X. Wang, *RSC Advances*, 2012, **2**, 10268.

[73] D. P. Dubal and R. Holze, Energy, 2013, **51**, 407.

[74] J. W. Lee, A. S. Hall, J. D. Kim and T. E. Mallouk, *Chem. Mater*., 2012, **24**, 1158.

Chapter-4

Polyaniline (PANI)-Graphene, PANI-MoS_2LbL composites for durable supercapacitors.

In this Chapter, a method to form robust supercapacitors based on Layer by Layer (LbL) deposited composites of polyaniline (PANI)and graphene nanosheets (GNS) and PANI-MoS_2 is described. Layers of the basic components were formed by LLIRT (PANI) and composites were formed by applying LbL method developed recently and fully elaborated in earlier Chapters (GNS and MoS_2). A special feature of the development is the architecture which is very rarely found in the literature by which composite is formed. As prepared LbL composites were characterized by using X-ray diffraction (XRD), X-ray photoelectron spectroscopy (XPS) and high resolution transmission electron microscopy (HRTEM). The characterization confirms the formation of composites having uniform distribution of PANI nanoparticles over the 2D nanosheets of GNS and nanosheets of MoS_2 respectively. The electrochemical behavior of composites is studied by cyclic voltammetry (CV), electrochemical impedance spectroscopy (EIS) and galvanostatic charge discharge (GCD). The PANI-GNS showed an excellent specific capacitance (Csp) of 549 Fg^{-1} while PANI-MoS_2 and PANI singularly showed Csp to be (413 Fg-1) and (185 Fg-1) respectively. It is the proposed that Csp stability of the composites is greatly enhanced by the architecture of composite formation through LbL deposition approach. PANI-GNS showed high stability (94% retention of Csp), PANI-MoS_2 (93% retention of Csp) as against single component capacitance of PANI (67% retention of Csp). The results reveal the usefulness of the proposed architecture of composite formation through modified LbL method. Presently, we show its application as nothing but a proof of the concept that thus formed LbL composites boost the charge storage mechanism as well as gives stable robust supercapacitors.

Partial content in this chapter is published in the following article, *Colloid and Polymer Science*, 292 (5), 2014, 1079-1089.
(http://link.springer.com/article/10.1007/s00396-013-3150-3)

4.1 Introduction

Supercapacitors are a set of the devices which can accumulate the electric energy. The storage capacity is mainly derived from the surface structural modifications and with different composite formations. Supercapacitors have emerged as appealing energy storage devices for systems requiring speedy charge-discharge cycles and high power densities. Electrical charge is accumulated in supercapacitors according to two primary mechanisms. 1) Physical charge separation across an interface as in the case of electrical double layer capacitors (EDLC), and 2) through a Faradaic reaction between an electrolyte and an electrode, either metal oxide or conducting polymer, as in the case of redox capacitors.

Electrical charge is accumulated in supercapacitors according to two primary mechanisms. 1) Physical charge separation across an interface as in the case of electrical double layer capacitors (EDLC), typically observed in porous carbon,[1-3]and 2) through a Faradaic reaction between an electrolyte and an electrode, either metal oxide or conducting polymer, as in the case of redox capacitors. Conducting polymers (CPs) offer a unique combination of both the mechanisms, while providing low cost alternative to the often expensive and rare materials employed in other devices. The feasibility of energy storage in conducting polymers occurs mainly due to the highly porous nature of the synthesized material and the redox activity of polymer backbone.[4]The requirement to sustain an acidic aqueous electrolyte contact for operation, limits the integration of polyaniline with most metal oxides in asymmetric supercapacitors. Also, the overall power is limited by the operative voltage window of water i.e. (1V).

Continuing advancement in electrode performance demands new materials that can assemble into three-dimensional structures and maintain transport pathways for the electrolyte and counter-ions.[1, 2] The Faradaic storage mechanism through (redox activity) depends on the chemical/physical structure of the polymer. The porosity and structure of the material determine EDLC contributions and mass transport properties of the electrodes. Electronically, conducting polymers is an interesting class of materials, which have received important attention because of its potential relevance in the development of super capacitor electrodes, battery cathodes,[5-8]inelectronic devices,[9] in electrochromic displays, etc.[10,11]Use of

conducting polymers in electrochemical supercapacitors value adds in high specific capacitance and specific energy of the device.[12]In the middle of the range of conducting polymers, polyaniline, poly (pyrrole) and poly (thiophene) must be mentioned for their promising applications,[13-18] due to their superb capacity for energy storage, straightforward synthesis, suitable conductivity and minor cost.[19]

Hybrid capacitors make a unified supercapacitor by combining the best features of electric double layer capacitors (EDLCs) and pseudocapacitors. Thus, they utilize both physical and chemical charge storage mechanisms together in a single electrode. The major advantage of these hybrid electrodes over the bare conducting polymer electrodes is that these composites have been able to accomplish superior cycling stability than that of EDLCs while holding the high storage capacity of faradaic electrodes. The carbon based materials afford a capacitive double layer intended for charge storage and also offer a high surface area backbone so as to increase the interface between the deposited pseudo-capacitive materials and electrolyte.[20]

Conducting polymers with superior electrochemical activity[21] and their composites are potential candidates as hybrid capacitor electrodes.[22] Usually, when conducting polymer is synthesized, the energy gap between the conduction and valence bands (LUMO and HOMO) is typically of order of 1-3 eV.[21] Conducting polymers can be chemically or electrochemically synthesized as p-doped, n-doped, or un-doped.[23] In the oxidized or 'p-doped' state, the polymer backbone is positively charged and has high electronic conductivity, normally in the range of l-100 S/cm. The polymer doping may or may not be reversible. The p-doped polymer can generate the 'undoped' state or neutral state which is typically insulating, or semi-insulating, depending on the extent of achievement of the undoping process.[24] Charging or discharging for the non-conducting state of the polymer generates portable electronic charge carriers in the polymer at electrode-electrolyte interface, and such charging process is referred to as 'chemical doping'. In present work the polymer is being doped by HCl i.e. with H^+ ions (P-type).

Inspite, it can conduct electrical charges through π-bond network. Therefore, the process of 'Doping" becomes possible. On doping, the charge neutrality is maintained by the formation of local defects. Such defects include micropores and/or

nanopores. Eventually, these defects prove to be useful to accommodate electrolyte in the composite matrix wherein ions provide the charge for effectively storing the energy. The mobility of the 'free' electronic charges in conducting polymers is insignificant when compared to the mobility of charges in semiconductor materials because of the absence of good long range order. However, a workable electronic conductivity of the order 1-100 S/cm is normally obtained for the 'doped' state of a conducting polymer.

The mechanical stress (due to intercalation and de-intercalation) in the polymer thin film depends on the number of charge-discharge cycles of capacitors. However, the protracted-time stability throughout the cycling is a most important prerequisite for the exploitation of capacitors based on conducting polymers.

The carbon based materials provide a capacitive double layer for charge storage and also provide a high surface area support that increases the contact between the deposited pseudo-capacitive materials and electrolyte. It is already proved[25,26] that the composites of polymers with variety of carbon forms show better stability. A high surface area and flexibility of graphene in the composite matrix is able to adapt the volume change. Therefore such an arrangement accommodates contraction and thus an extra stable capacitance with cycling can be obtained.

In the present thesis work the polymer thin film synthesis route is liquid-liquid interface reaction technique (LLIRT) is an easy and inexpensive process. Here, we also deal with the synthesis of polyaniline and their LbL composites with 2D structured graphene and MoS_2 as the electrode materials for the development of supercapacitors. The raw material is a monomer of the polymer i.e. Aniline. Polymerization is carried out with an oxidizing agent i.e. ammonium persulphate. To increase the conductivity, the polymer is doped with H^+ ions by using dil. HCl. During the oxidation process the presence of acid is likely to form doped polyaniline which was confirmed from the characterization. Subsequently these polyaniline films were used for composite formation through LbL technique wherein the other component was graphene/MoS_2.

In chapter 2 and 3, the suitable features of GNS and MoS_2 are described. Moreover, graphene consists of a two dimensional sheet structure made up of

covalently bonded carbon atoms and finds a multitude of applications in devices. The special characteristics of this material such as high electronic conductivity, low mass density and very high specific surface area etc. make it suitable for various applications especially for supercapacitors.[27] The very high in-plane conductivity and surface area makes it an attractive material for use in dye sensitized solar cells[28] supercapacitors[29] and other high technology functional areas. An authoritative review on graphene and its composites, their electronic structure, synthesis methods, characterization etc. is available in the literature.[30] Electrochemical double layer capacitors show properties of very high power density, energy density and long cycle life.[31] Graphene as a constituent of the electrode material overcomes many of the limitations of activated carbon. Graphene based electrodes benefit from improved mechanical integrity, higher electronic and ionic conductivity and larger electrode specific capacitance and greater stability in charge-discharge cycling compared with the pure conducting polymers.[32] On the other hand MoS_2 has similar structure to that of graphene with comparatively lower surface area. Having low intrinsic capacitance for singular MoS_2, its combination with PANI could lead to enhanced capacitance.

By considering the properties of PANI, 2D graphene/MoS_2 and the available tool of their composite formation through LbL as described in earlier Chapters, it occurred to us that the composite of PANI and GNS/MoS_2 could be tested for their capacitive properties. An important point to be considered in this respect is that perhaps the cost of the device would be much lower as PANI would be cheaper than MoS_2.

4.2. Materials and Methods

4.2.1 Chemicals

Aniline (99.9%), Molybdenum sulphide (MoS_2), graphite rod and ammonium per-sulphate were purchased from sigma-Aldrich, Hydrochloric acid (HCl), sulfuric acid (H_2SO_4), sodium sulphate (Na_2SO_4) were purchased from Merck chemicals. Carbon tetrachloride (CCl_4, 99.5 %) was purchased from Loba chemicals. All the chemicals used were of analytical grade and used as received without further purification. Double distilled water has been used for all the experiments.

4.2.2 Preparation of doped polyaniline (PANI), PANI-GNS and PANI-MoS_2 thin films

4.2.2.1 Thin film formation

The technique LLIRT has been fully described in earlier Chapter and therefore, presently we have briefly described the procedure to avoid repetition.

1) 10^{-4} M solution of ammonium persulphate (APS was prepared by dissolving 18.25 mg in 800 ml of double distilled water. In same solution 10^{-6} M Hydrochloric acid (HCl) was added. 2) A dilute solution of aniline was prepared in 5 mL glass vial by adding 4 drops (~50 mg) of aniline in 5mL CCl_4. 3) The above 10^{-4} M ammonium persulphate solution was poured in the Teflon through of size 15cm x 10 cm x2 cm so that the meniscus formed above the edge. 4) The surface of the solution was cleaned (for removal of dust or floating contaminants) with usual practice in LLIRT that is by wiping the surface by a Teflon barrier. 5) Teflon thread barrier was fixed on the edges of the trey such that surface of the solution is divided in two compartments as shown in following Scheme 4.1 6) By using 1 mL glass syringe, aniline in carbon tetrachloride was dropped on the surface of the subphase in one of the compartment so that it spreads over the surface.[33] 7) The aniline solution was dropped until it forms the lens over the subphase. After this step the thread gets stretched completely. 8) The CCl_4 is allowed to evaporate. 9) A drop of oleic acid is carefully dropped on the other compartment subphase surface so that the polyaniline film gets compressed laterally by the thread barrier which can be seen by the movement of Teflon thread. The lateral pressure exerted by an oleic acid is 30 dynes cm^{-1}which exerts the lateral pressure on the PANI film 10) Cleaned glass substrate was prepared with treatment of freshly prepared piranha solution (3:1 of conc. H_2SO_4 /30% H_2O_2, heated at 70^0C for 15 min and subsequently rinsed by distilled water. 11) The film was transferred on the substrate by using Blodgett Technique. The substrate was vertically dipped and withdrawn in the polyaniline film compartment at a constant rate of 0.5 cm/min. In this process, the film gets deposited on the substrate. By repeating the above procedure, desired thickness can be obtained. A similar procedure was adapted to obtain graphene film[34]and MoS_2 films.[35]The operation of transferring the film from subphase surface to substrate was repeated many times to get a desired film thickness/mass for specific applications

and characterization. 12) The film was then washed with deionized water several times until it turned out to be of neutral pH.

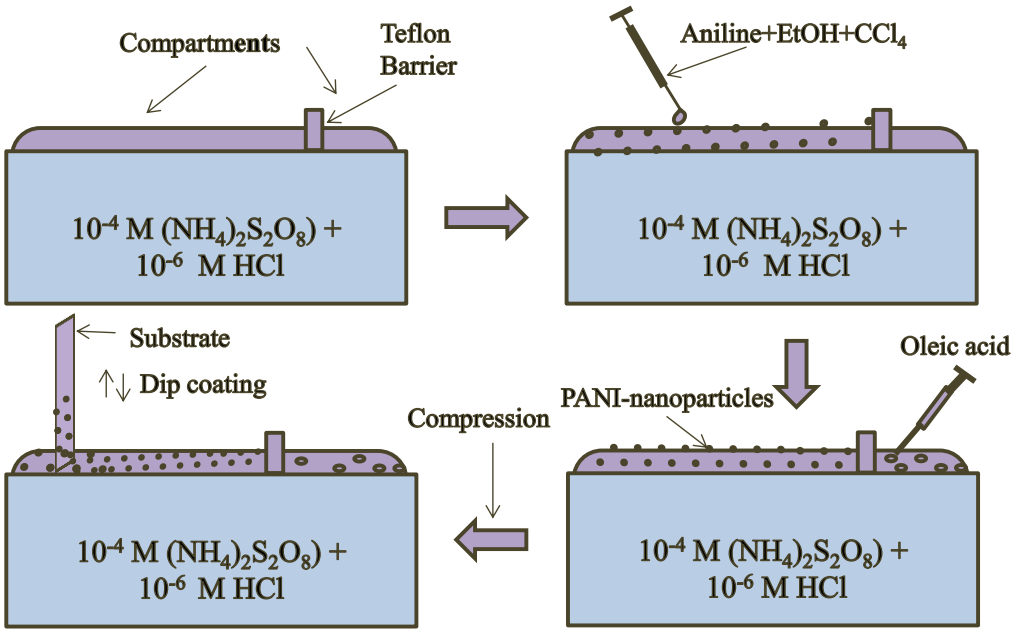

Scheme 4.1. Schematic representation of the steps involved in the formation of polyaniline (PANI) nanoparticulate thin film.

4.2.3 Preparation of LbL composite of PANI-GNS and PANI-MoS_2

Furthermore, this technique can be useful for the synthesis of the composites consisting of PANI-graphene by modified LbL technique using desired sequence which might become important for some specific applications such as supercapacitor.[35] A few-layered graphene nanosheets were obtained on the surface of water in a separate tray as given in previous Chapters. Stacked composite films of PANI–GNS and PANI-MoS_2 are deposited as described in Chapter 2. Scheme 4.2 gives the schematic of desired composite layer film formation.

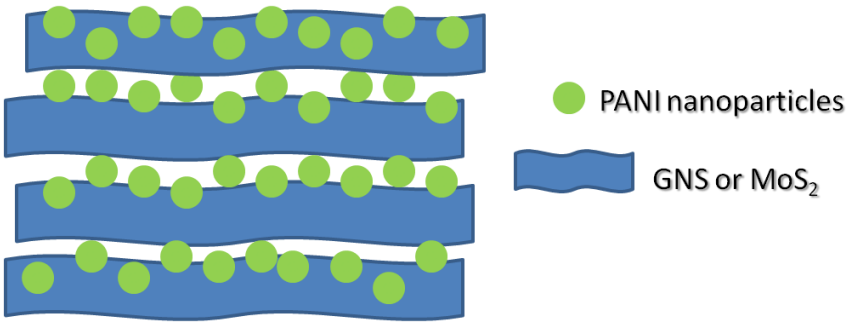

Scheme 4.2. Schematic representation of PANI-GNS and PANI-MoS_2LbL composite.

4.3. Results and Discussion

The formation of PANI at the liquid-liquid interface takes place through the reaction of interfacial polymerization between, aniline monomers in the organic phase and the ammonium per sulphate (APS) in aqueous phase is shown in Figure 4.1

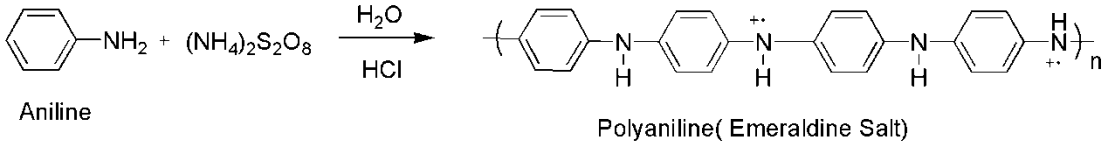

Figure 4.1 Oxidation of aniline by ammonium persulphate.

The formation of PANI was confirmed by characterizing the PANI film by Fourier transform infra red spectroscopy (FT-IR), X-ray diffraction (XRD), Raman spectroscopy, X-ray photoelectron spectroscopy (XPS) and energy dispersive x-ray spectroscopy (EDS) analysis. The morphological changes observed in the process, were studied by SEM and TEM.

4.3.1 FT-Infrared spectroscopic study of PANI, PANI-GNS and PANI-MoS_2 hybrid films

FTIR spectra of the PANI and PANI composites were recorded with the ATR mode for the thin films of PANI and PANI composite i.e. PANI-GNS and PANI-MoS_2 hybrid films coated over the Si wafer. Figure 4.2 shows the FTIR spectra for polyaniline (PANI), PANI-GNS and PANI-MoS_2 thin films.

The FTIR of PANI and its LbL composite suggest the formation of composites. The peaks at ~1545 and ~1470 cm^{-1} are attributed to quinone and benzene ring deformation respectively.[36a] The broad peak in the range of 3650 to 3000 cm^{-1} corresponds to the presence of interstitial water and hydroxyl groups. Two peaks at ~2800 and ~ 2930 $cm^{-1}$are due to C-H stretching. Peak at ~2350 is attributed to adsorbed CO_2.

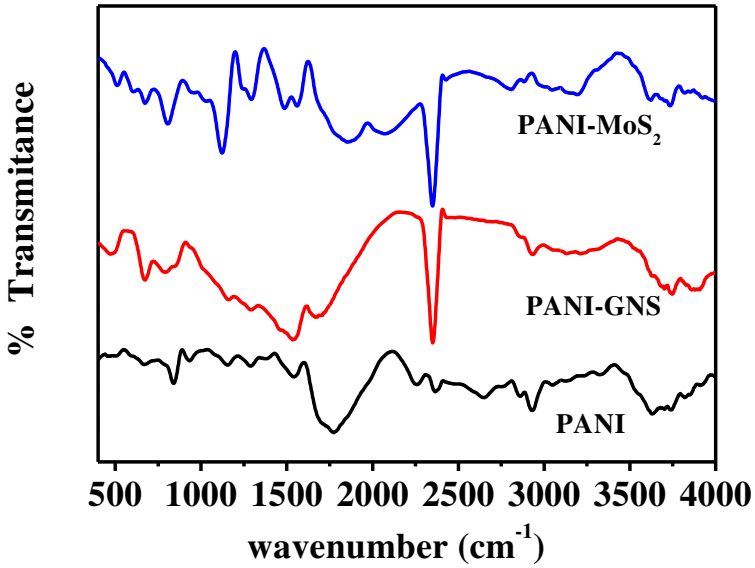

Figure 4.2 Fourier transform infrared spectra for polyaniline (PANI), PANI-GNS and PANI-MoS_2.

4.3.2Raman spectroscopic study

The Raman spectroscopy is a useful analytical tool to investigate PANI. It distinguishes between the modes and excitation line wavelength originating from the vibrations from benzenoid and quinoid segments in the polymer. Moreover for GNS, as discussed in chapter-2, D, G and 2D bands are observed at ~1320, ~1500 and ~2600 cm^{-1} respectively.

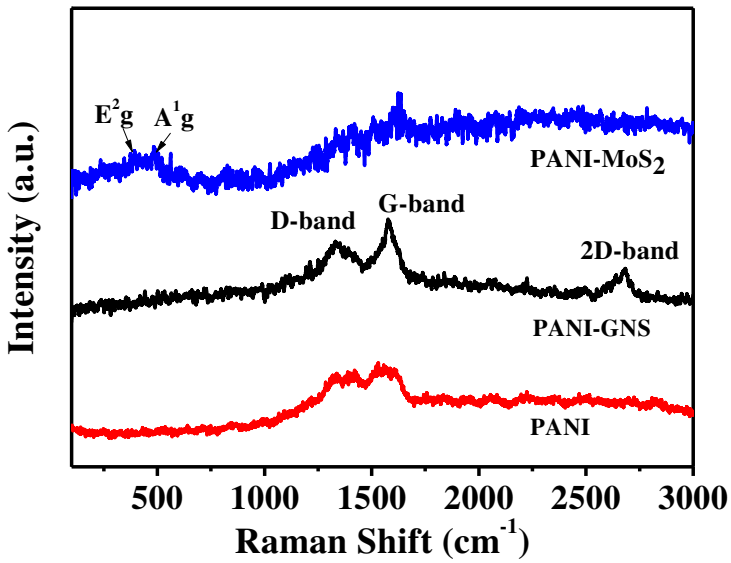

Figure 4.3 Raman spectrums of Polyaniline (PANI) film, PANI-GNS and PANI-MoS_2 LbL hybrid films coated over Si wafer substrate.

For MoS_2 two important bands for E^2g and A^1g are observed at ~384 and ~404 cm^{-1} respectively. As shown in Figure 4.3, three Raman bands, 1284, 1422 and 1615

cm^{-1} are identified as characteristics of the quinoid structure of PANI. The bands from 1329 to 1387 $cm^{-1}$are associated with stretching of C-N bonds with different conjugation length and with the presence of charged phenazine-like or oxazine like rings in PANI-emeraldine salt (ES). The formation of cross linking structure is associated with the ES form of PANI. The bands from 1490 to 1550 cm^{-1} are associated with the stretching C=N modes of the quinoids unit having different conjugation length. The PANI-GNS LbL hybrid shows PANI peaks along with GNS. Peak at 1320, 1574 and 2680 cm^{-1} are due to the GNS present in the composite thin film. Moreover, the PANI-MoS_2 composite thin film shows peaks for PANI along with main peaks for E^2g and A^1g mode observed in MoS_2 at 386 and 415 cm^{-1} having difference in energy of 29 cm^{-1} suggesting the multilayered MoS_2 composite formation.

4.3.3 X-ray diffraction

The XRD pattern of polymer generally differs because of uncertainty in polymer chains. It depends on the synthetic routes, solvent and ionized state. For example, the XRD patterns of PANI prepared by different methods have been reported to have amorphous to crystalline nature with different percentage.[36a]

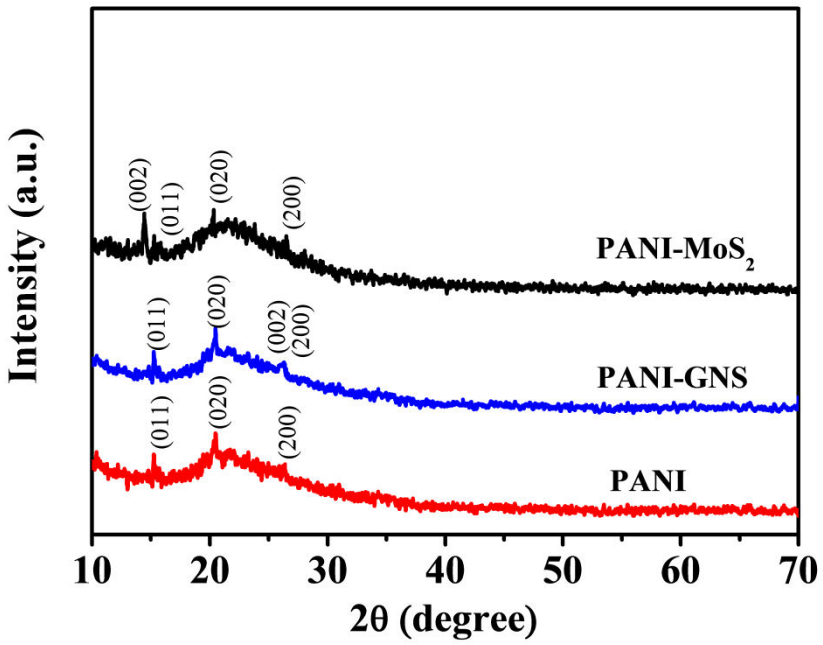

Figure 4.4 XRD spectra for Polyaniline (PANI) PANI-GNS and PANI-MoS_2 electrode.

The XRD characterization have been done by using computer controlled XRD system of PAN analytical Powder XRD instrument at an operating rate of 40 KV and 30 mA (Cu Kα radiation λ=0.1548 nm) in the 2θ range 15-35 degrees for a measuring times of 5 sec per step. Figure 4.4 shows XRD spectra for Polyaniline (PANI) PANI-GNS and PANI-MoS_2 electrode. The XRD pattern of PANI shows a peak at 2θ = 15.1, 20.3 and 26.3; these peaks can be attributed to the (011), (020) and (200) planes respectively which are characteristics of the emeraldine salt phase of PANI.[36b] PANI-GNS composite shows signature peaks of PANI as mentioned above along with a broad peak at 26.1 for the (002) plane of graphene.[37a] A similar signature peaks can be seen in PANI-MoS_2. A peak at 14.4 can be attributed to (002) plane of the MoS_2.[35]Thus; the overall XRD study reveals that the hybrid films can be successfully fabricated by this technique.

4.3.4 X-ray photoelectron spectroscopic (XPS) study

The formation of polyaniline at the interface was examined by X-ray Photoelectron Spectroscopy (XPS) and also studied the electronic structure of it[37b] Figure 4.5 shows the XPS spectrum of the as prepared PANI thin film.

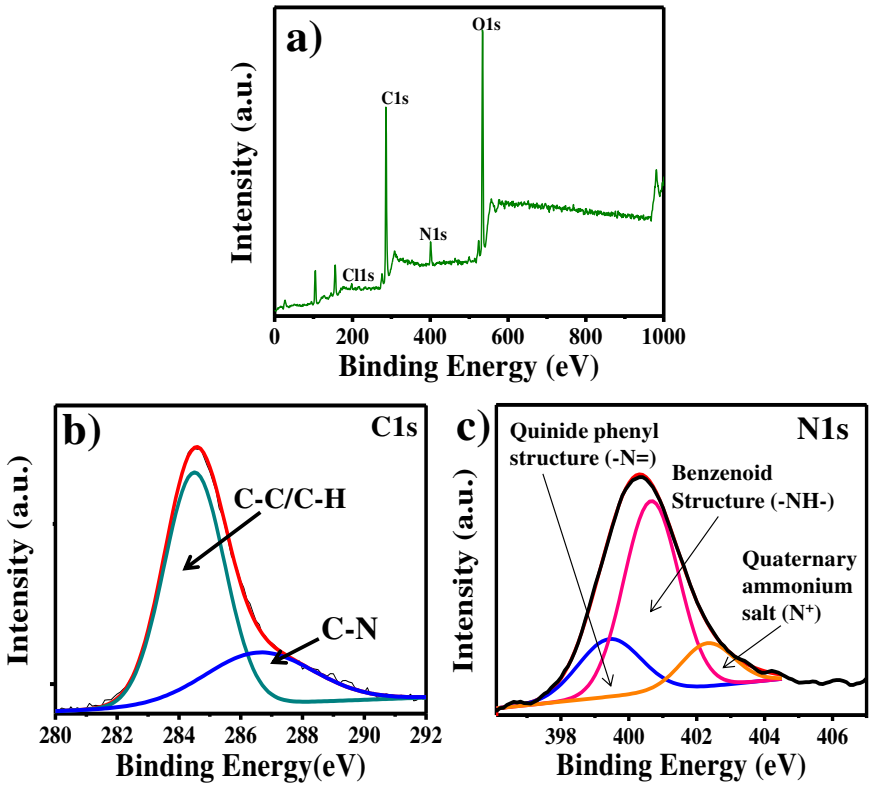

Figure4.5 XPS spectra of PANI thin film a) General spectra, b) C1s and c) N1s.

The typical XPS survey scan of the PANI (Figure 4.5) shows the presence of Nitrogen (N), Oxygen (O), Silicon (Si), along with Carbon (C). Si was detected from the glass substrate. The O1s at 531 eV shows the presence of oxygen and the Cl1s at 200 eV shows the presence of chlorine due to HCl /treatment/doping with PANI.

The C1s spectrum consists of broad peaks at 284.6 eV and 286.8 eV. C1s core level at 284.6 eV is attributed to the presence of quinoid structure and benzenoid rings. The C1s binding energy is in good agreement with that of reported values.[38,39] The N1s spectra has shown one broad asymmetrical peak at 400.4 eV which signifies the presence of more than one type of nitrogen. Peak at 400.6 eV can be attributed to benzenoid structure. Peaks appeared at 399.3 eVand 402.3 eV are due to the quinoid phenyl structure and quaternary ammonium salt structure respectively. Thus, in oxidized polyaniline, quinoid and benzenoid structure exist in the carbon backbone and electronic charges resides on nitrogen atoms. A shift towards higher binding energy of N 1s shows that electronic charges do occur on N. Figure 4.6 shows the XPS survey spectra of PANI-GNS. Survey spectra shows the presence of Cl1s at 201 eV, C1s at 284.6 eV, N1s at 401 eV and O1s at 532 eV.

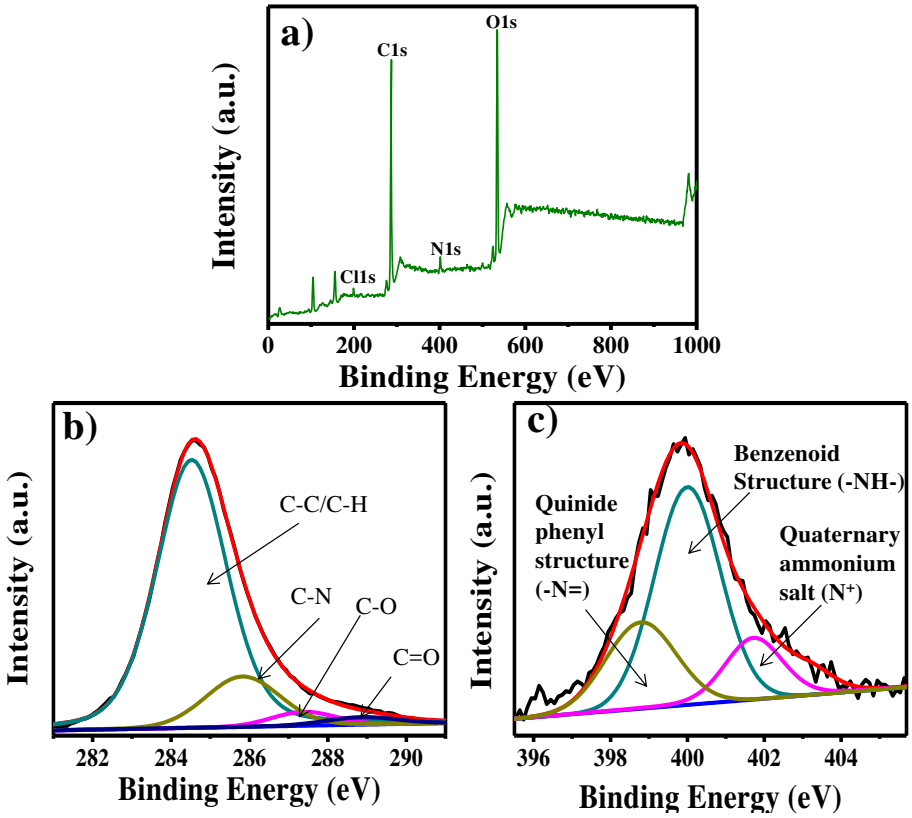

Figure 4.6 XPS spectra of PANI-GNS, a) General spectra b) C1s and c) N1s.

The ratio of C1s/O1s is found to be higher in PANI-GNS as compared to that shown in the samples of either PANI or PANI-MoS_2 thin film. C1s peak is further deconvoluted for the possible presence for C-C, C-N, C-O and C=O etc. as shown in figure.

On deconvolution the respective binding energy values for Cs1obtained are, 284.6, 285.8, 287.4 and 289 eV. N1s peak is observed at 399.8 eV which is quite asymmetric and needs to be deconvoluted. After the deconvolution, N1s shows three peaks namely, quinoide phenyl structure (-N=), benzenoid structure (-NH-) and quaternary ammonium structure (N+) at 398.7, 400.1 and 401.9 eV respectively as shown in the Figure 4.6. It shows that there are no structural changes occurring in PANI on composite formation.

Pertaining to PANI-MoS_2, we found that the survey spectra contain Cl1s, Mo3d, S2p, C1s and O1s which is consistent with the EDS study. Compared to PANI-GNS composite C1s of PANI-MoS_2 is more symmetric. However, it shows presence of one more species namely C-N. Figure 4.7b shows the C1s spectra for PANI-MoS_2 hybrid thin film. Peak at ~284.7 is attributed to the species C=C or C-H functional carbon.

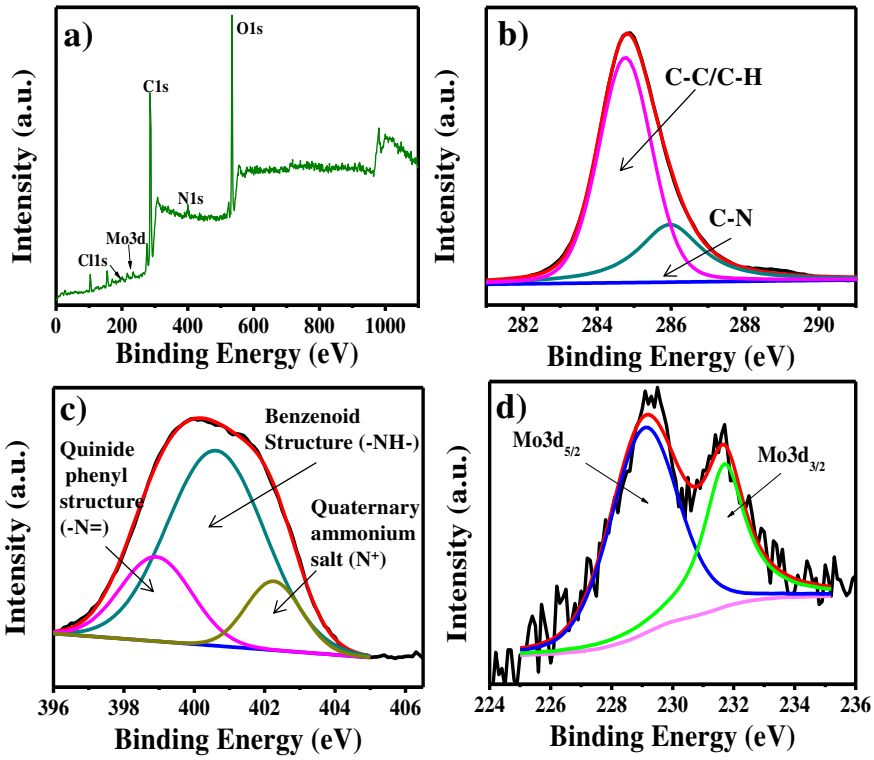

Figure 4.7 XPS spectra of Pani-MoS_2 a) General spectra, b) C1s c) N1s and d) Mo 3d.

Peak at 286.2 eV can be attributed to C-N functional moiety. N1s as shown in the Figure 4.7b is more asymmetric as compared to the corresponding peak in PANI and PANI-GNS. There are again three species of N containing functional groups (Figure 4.7c), namely, quinoide phenyl structure (-N=) at 398.8 eV, benzenoid structure (-NH-) at 400.5 e) and quaternary ammonium structure (N+) at 402.2 eV. Figure 4.7d shows the Mo3d spectra. It shows two peaks attributed to $Mo3d_{5/2}$ and $Mo3d_{3/2}$ at binding energy 229.1 eV and 232.3 eV respectively. Thus an XPS study reveals the formation of composite hybrid thin films.

Furthermore, to study the morphology of the composite thin films we used transmission electron microscopy (TEM) and scanning electron microscopy (SEM).

4.3.5 Transmission electron microscopy studies of PANI, PANI-GNS and PANI-MoS_2

The TEM images were taken with electron microscope (JEOL, Technai F20-200 kV) and High resolution TEM images on JEOL 300 kV FEI Technai F30. The TEM samples were prepared by dipping the carbon coated TEM grid twice through films formed at respective interfaces.

The PANI films were examined by high resolution transmission electron microscopy (HRTEM) to investigate the size shape and morphology of the thin films.

4.3.5.1 Formation of PANI nanoparticles by self assembly of nanoparticles at room temperature

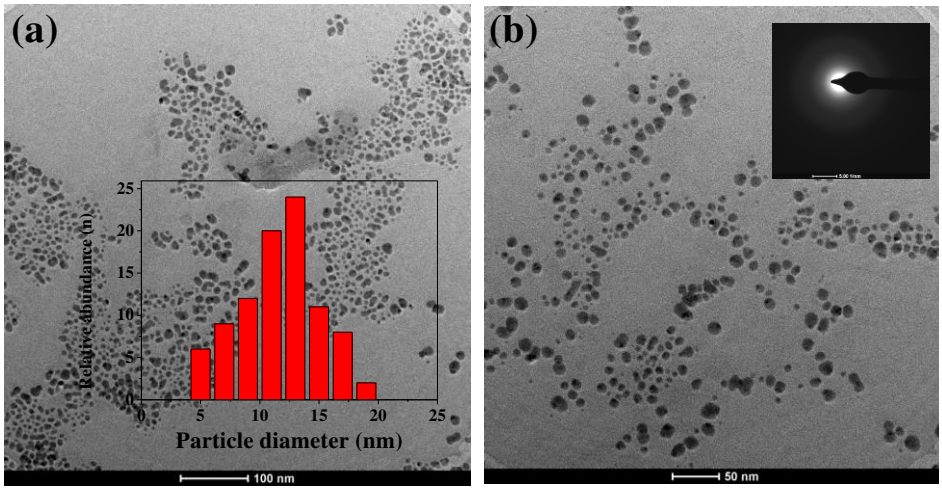

Figure 4.8 (a) TEM image for the polyaniline (PANI) nanoparticulate thin film, (b) magnified image of 'a' inset shows the SAED pattern suggesting the crystalline as well as amorphous nature of the film.

From the micrograph (Inset of Figure 4.8a) it can be seen that the average nanoparticles size is nearly equal to 14 nm Figure 4.8. The SAED pattern of polymer generally differs because of uncertainty in polymer chains (Inset of Figure 4.8b). It depends on the synthetic routes, solvent and ionized state.[17, 22] from the histogram it is seen that the nanoparticles are having various sizes (between 5-18 nm).

4.3.5.2 Formation of PANI-GNS hybrid thin film electrode

Figure 4.9 shows the TEM images of the LbL composite i.e. PANI-GNS. From the Figure it can be seen that the PANI nanoparticles are uniformly decorated over the graphene nanosheets. The inset of Figure 4.9b shows the SAED pattern for the hybrid composite electrode. SAED tells us that the film is composed of mixture of crystalline and amorphous materials.

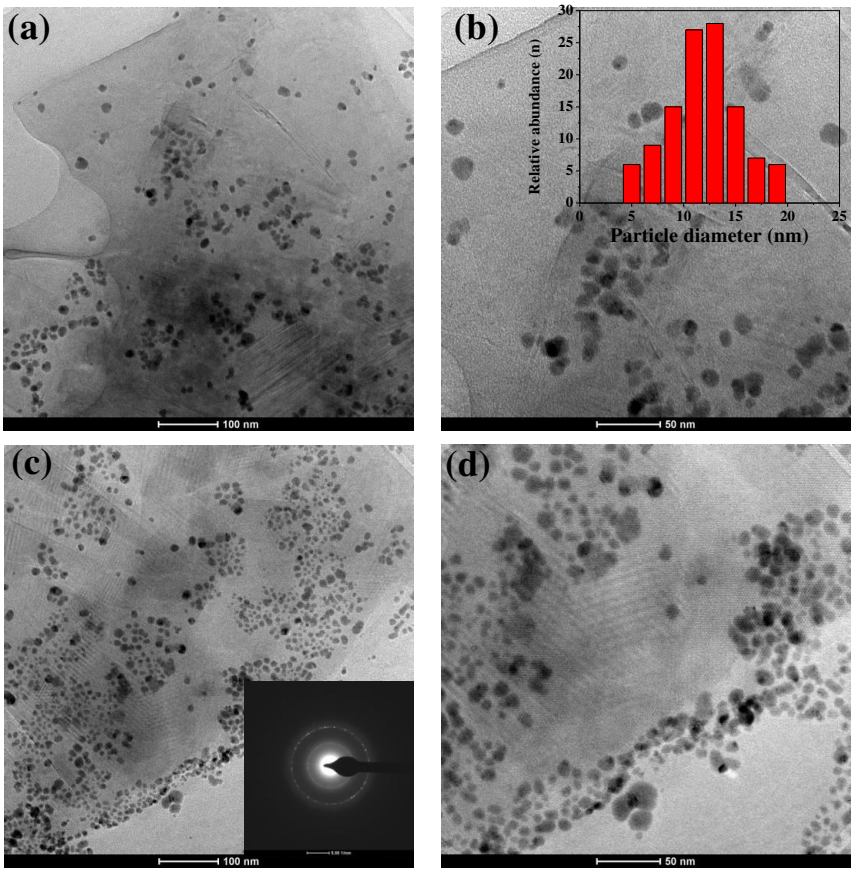

Figure 4.9 (a & c) TEM image for the PANI-GNS LbL composite thin film, (b & d) magnified images of 'a & c' inset shows the SAED pattern showing rings as well as spot pattern suggesting the crystalline as well as polycrystalline nature of the film.

The spot pattern suggests the presence of the GNS. The diffused rings pattern is due to the PANI incorporation as shown 4.9c. Histogram drawn from the Figure

4.9a is shown in Figure 4.9b. An average size of particles can be seen from it. The average size was found to be 13.5 nm and the range of particle size was between 5-20 nm. Micrograph shown in the inset of Figure 4.9b shows the nanoparticles of various sizes (between 5 to 20 nm).Inset of Figure 4.9c shows the SAED pattern which confirmed the crystallinity of nanoparticles.

4.3.5.3 Formation of PANI-MoS_2 hybrid composite

Figure 4.10 shows the TEM images for the formation of PANI-MoS_2. Inset of figure 4.10d shows the SAED pattern for the hybrid thin film. It is evident from SAED that the 2D MoS_2 shows the spot pattern having perfect hexagonal symmetry, suggesting the crystalline nature of MoS_2 nanosheets.[36b]

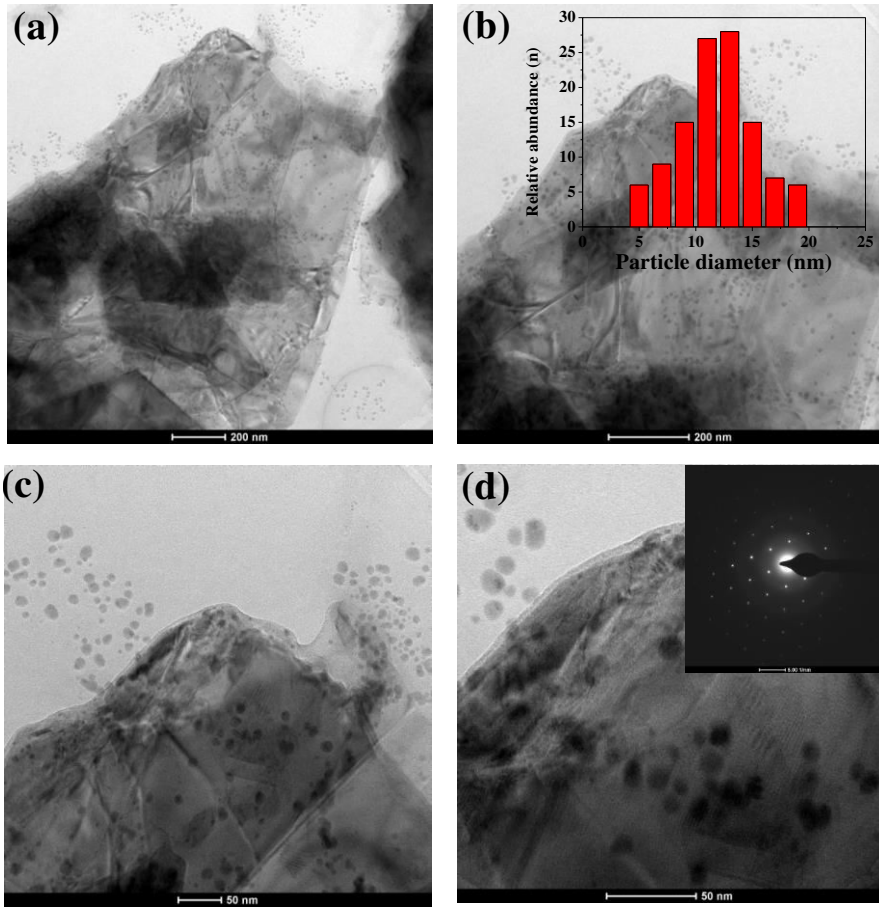

Figure 4.10 (a) TEM image for the PANI-MoS_2 LbL composite thin film, (b- d) magnified images of 'a' inset'd' shows the SAED pattern shows rings as well as spot pattern suggesting the single crystalline as well as Polycrystalline nature of the film.

The hexagonal spots observed on the SAED are in agreement with reported for (002), (104) and (105) plane of the MoS_2, and (020) of PANI confirming the crystallinity and formation of the hybrid thin film.

The PANI nanoparticles are uniformly spread over the MoS_2 nanosheets. The average particle size of the PANI nanoparticles is 12 nm and it is in the same range to that of rest of the electrodes studied earlier that is PANI and PANI-GNS. Figure 4.10b shows the histogram of the PANI nanoparticle distribution over the MoS_2 nanosheets. The particle size is in the range of 5-20 nm.

The interactions between the primary nuclei decide the plane of growth. Neither surfactants nor any other additives are used in the present study, the phenomenon of preferential growth of planes i.e. orientation of structure does not occur. Especially, it occurs owing to the fact that growth in the present experiment takes place at the interface (2 Dimensional) as against the growth in solution (3-dimensional). The van der Waal attractive forces can be a cause of self assembly.[24-26] This 2D arrangement of interface facilitate the growth of GNS and MoS_2 within the interface. LbL deposition again leads to 2D composites thin film formation giving compact devices.

4.3.6 Scanning electron microscopy (SEM)

SEM study was employed to get the information of surface morphology and surface modifications after the LbL assembly of the PANI nanoparticulate thin film with Graphene (GNS) and MoS_2nanosheets. Figure 4.11 shows the SEM images for the PANI-GNS.

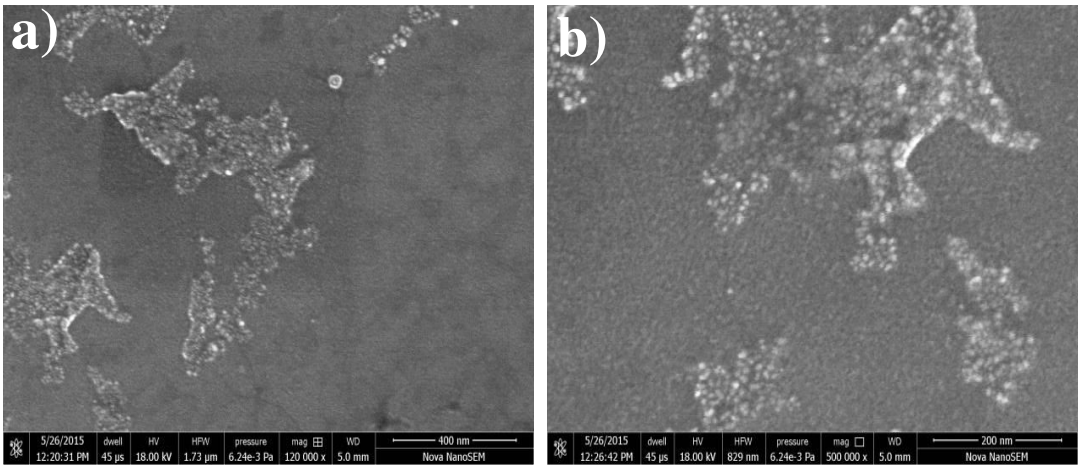

Figure 4.11 FE-SEM images for the PANI-GNS, at varying magnification

Following figure 4.12 shows SEM image of PANI-MoS_2 hybrid thin film. Figures 4.11 and 4.12support the observations obtained from the TEM analysis.

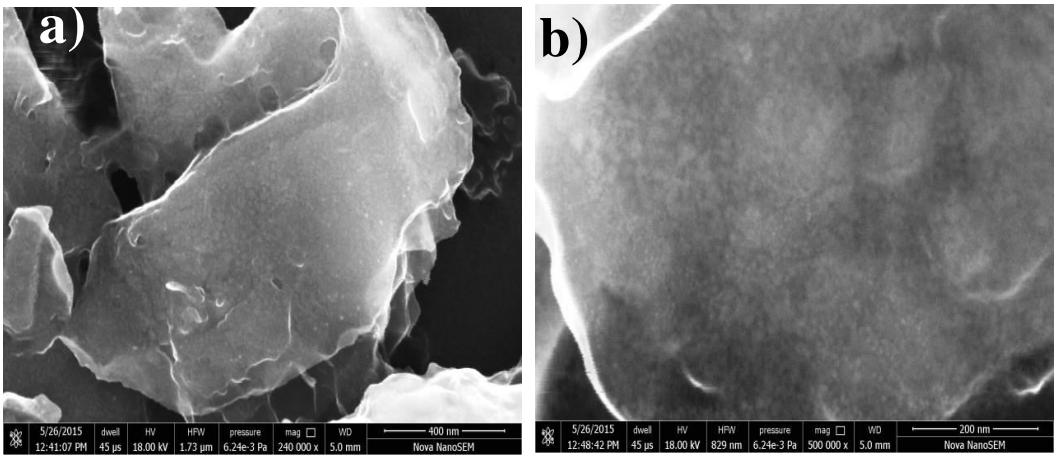

Figure 4.12 SEM images for the PANI-MoS_2.

4.3.7 Energy dispersive x-ray spectroscopy analysis (EDS)

To establish the chemical composition of the films, energy dispersive X-ray spectroscopy, (EDS) facility in Scanning electron microscopy (SEM) has been exploited. Figures 4.13-4.15 shows the energy dispersive *X*-rays spectroscopic analysis (EDS) spectra of as deposited film.

As seen from the EDS spectra, Carbon and Nitrogen signals are observed on particles of film formed. This is clearly indicating the formation of emeraldine form of PANI. No other impurities have been observed except the signals of Si, which arise from the Si wafer substrate. Thus, the EDS analysis is in consistency with the observations of XPS analysis.

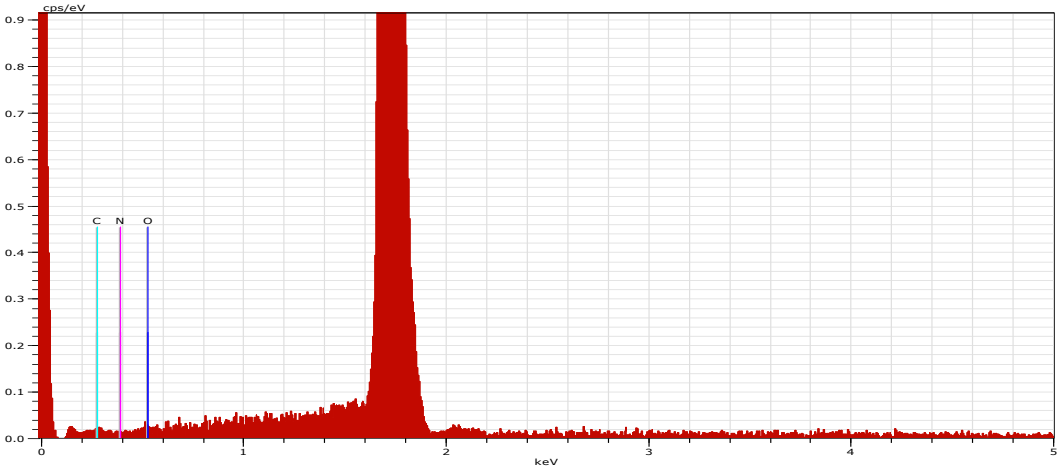

Figure 4.13. EDS spectra of PANI thin film.

EDS spectra obtained for the PANI-GNS shows the presence of Carbon, Oxygen and Nitrogen. EDS spectra of PANI and PANI-GNS is in agreement with XPS.

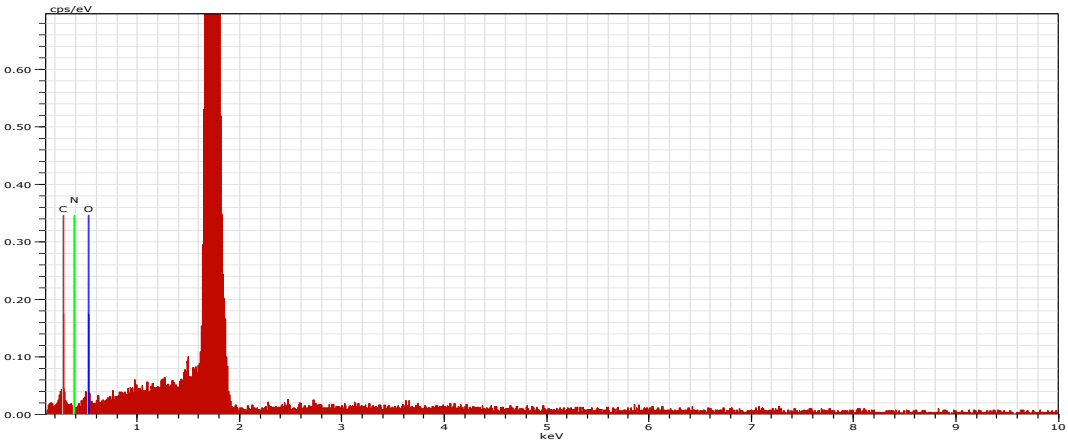

Figure 4.14. EDS spectra forPANI-GNS hybrid thin film.

The composite PANI-MoS2 shows the presence of carbon, Nitrogen, Oxygen, Molybdenum and Sulfur.

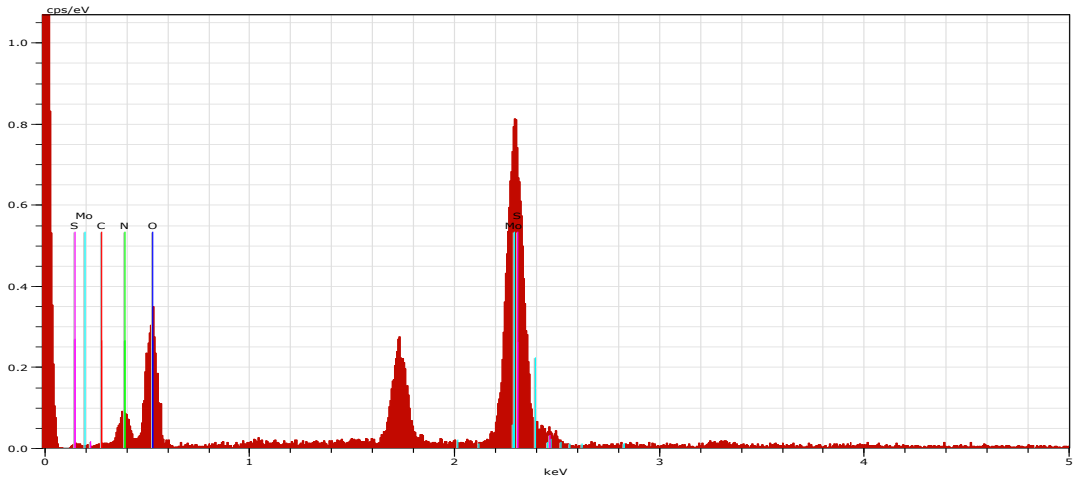

Figure 4.15 EDS spectra forMoS2-PANI hybrid thin film.

4.4 Electrochemical performance of PANI, PANI-GNS and PANI-MoS_2 hybrid thin films as supercapacitor electrodes

4.4.1 Cyclic voltammetry

The performance of nanostructured PANI and its composites (PANI-MoS_2/GNS) as an electrode material for super capacitor application was investigated by standard cyclic voltammetry (CV) and galvanostatic charge-discharge technique. The thin films of respective materials were coated on FTO glass. The cyclic voltammetry measurements were done in 0.5 M H_2SO_4 electrolyte. In order to ensure adhesion of

film, electrodes were heated at 70^0C for 15 hours. The CV curves of PANI and PANI-MoS_2/GNS composites are obtained within a potential window from -0.4 to 0.6 V and at various scan rates (20, 50, 100, 150, 200 and 250 mVs^{-1} respectively) which are shown in Figure 4.16.

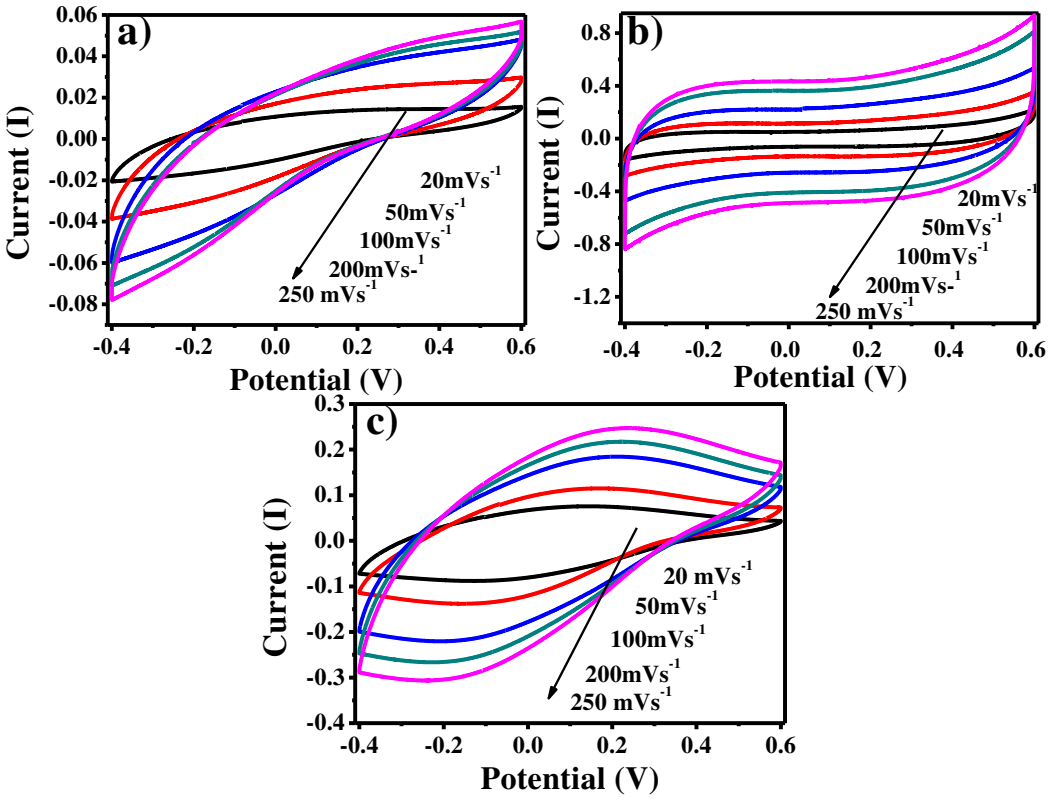

Figure 4.16 Cyclic voltammograms of a) PANI thin film, b) PANI-GNS and c) PANI-MoS_2, composite thin films deposited over FTO microelectrode in aqueous 0.5 M H_2SO_4 solution at scan rates varying from 20 to 250 mVs^{-1}.

All curves show a nearly rectangular shape, which is considered as an ideal capacitive behavior of the materials. The specific capacitance values of the samples are calculated from the CV curves using following equation, given in Chapter 1,

$$\text{Csp} = \frac{\int I \mathrm{d}V}{v \mathrm{m} V} \qquad (1)$$

Where, C_{sp} is the specific capacitance in farads per gram (Fg^{-1}), m is the active mass of the electrode material (g), I is the response current density (A g^{-1}) and v is the potential scan rate in (Vs^{-1}), V is potential (V). Based on the above equation-1, we found C_{sp} to be 192, 559and 426 Fg^{-1} respectively for the PANI, PANI-GNS and PANI-MoS_2 electrodes at the scan rate 20 mVs^{-1}. Furthermore at the scan rate of 200 mVs^{-1}, the respective values were 105, 515 and 381 Fg^{-1}. The detailed calculated

values are tabulated in following Table-1. The details of changes of C_{sp} with all the studied scan rates are shown in the Figure 4.17. The capacitance (559-515 Fg^{-1}) obtained in the present study is considerably higher than most of PANI-based graphene composites reported elsewhere.[40-45] The higher capacitance obtained is attributed to layer-by-layer structure of composite,[35, 36] resulting in conducting and high surface area graphene in close contact with PANI, facilitating rapid charging and discharging of the electrode. These results indicate the exhilarating potential for the use LbL PANI-GNS film in high-performance supercapacitor.

Table 1 Comparison of Specific capacitance Fg^{-1} obtained from cyclic voltammetry.

	Specific capacitance Fg^{-1} from Cyclic Voltammetry.					**Retention (%)**
Scan Rate mVs^{-1}	**20**	**50**	**100**	**150**	**200**	
PANI	192	186	154	136	105	54.6
PANI-GNS	559	544	530	523	515	92.1
PANI-MoS2	426	416	401	394	381	89.4

The conspicuously good charge discharge behavior of both PANI/GNS and PANI/MoS_2 is due to the fast adsorption and desorption of ions at the interface of PANI/GNS or PANI/$MoS_2$from the electrolyte used. The ionic interactions of H^+ ions in electrolyte further increase the conductivity of PANI and hence the fast electron transfers between the PANI-GNS and PANI-MoS_2. The mechanism of charge storage[35] can be explained by using following equations (2-5),

$$(PANI\text{-}GNS)_{surface} + H^+ + e^- \leftrightarrows ((PANI\text{-}GNS)^- H^+)_{surface} \quad (2)$$

$$MoS_x/GNS + H^+ + e^- \leftrightarrows (MoS_x/GNS)H \quad \text{(adsorptive intercalation)} \quad (3)$$

$$(PANI\text{-}MoS_x)_{surface} + H^+ + e^- \leftrightarrows ((PANI\text{-}MoS_x)^- H^+)_{surface} \quad (4)$$

$$PANI\text{-}MoS_x + H^+ + e^- \leftrightarrows (PANI\text{-}MoS_x)H \quad \text{(adsorptive intercalation)} \quad (5)$$

As discussed in our earlier report[33] and in experimental section, the PANI films are doped with H^+ ions to increase the conductivity; the H^+ ions saturate the doping level in PANI, and hence would show more improvements in the conductivity. This can be explained in following equations,[35]

$$(PANI/GNS) + H^+ \leftrightarrows ((PANI\text{-}H/GNS)^+)_{ionic} \text{ (Ionic Intercalation)} \quad (6)$$

$$((PANI\text{-}H/GNS)^+)_{ionic} + e^- \leftrightarrows (PANI\text{-}H/GNS) \quad (7)$$

$$(PANI\text{-}MoS_x) + H^+ \leftrightarrows ((PANI\text{-}H/MoS_x)^+)_{ionic} \text{ (Ionic Intercalation)} \quad (8)$$

$$((PANI\text{-}H/MoS_x)^+)_{ionic} + e^- \leftrightarrows (PANI\text{-}H/MoS_x) \quad (9)$$

Thus, in this process, both chemical as well as the electrochemical doping can occur which leads to again boost up the charge storage mechanism in the composite. According to this proposal, the charging and discharging could be the result of a synergistic effect of the both adsorption/desorption of the ions on the surface and ionic intercalation of H^+ over the N species of PANI surface.

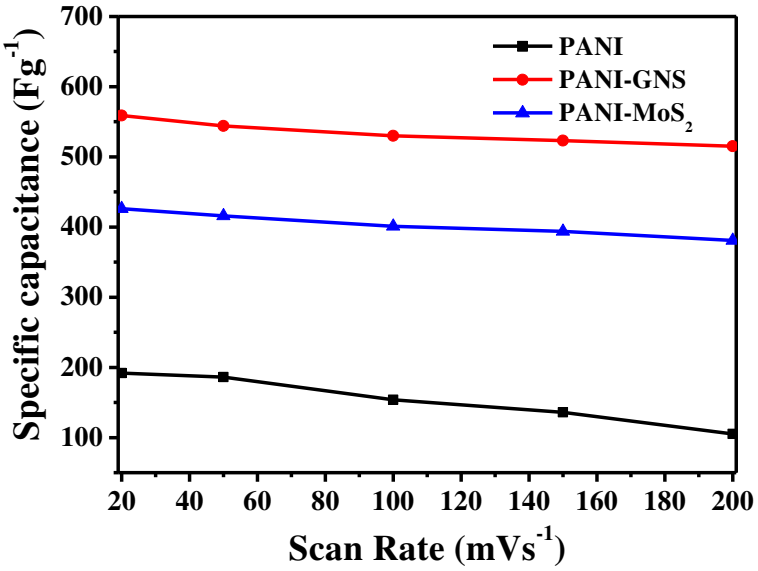

Figure 4.17 comparative study of specific capacitance calculated from CV for PANI and PANI-GNS/MoS_2 as a function of scan rate.

In comparison with PANI-GNS, lower specific capacitance was observed for the PANI-MoS_2 composite. The values for specific capacitance were 426-381 Fg^{-1}at the

scan rate of 20 and 200 mVs^{-1} respectively. The percent retention of C_{sp} in case of composite PANI-GNS was superior to the PANI-MoS_2 and PANI electrodes. PANI-GNS electrode showed about 92.1% retention even at the high scan rate of $200mVs^{-1}$. PANI and PANI-MoS_2 electrodes showed 54.6 and 89.4 % retention of specific capacitance at the 200 mVs^{-1}scan rate. The detailed comparison of specific capacitance as a function of scan rate is given in Figure 4.17.

4.4.2 Electrochemical impedance spectroscopy (EIS)

Electrochemical impedance spectroscopy (EIS) gives information regarding the internal resistance of an electrode material as well as the resistance between the electrode and electrolyte. Impedance spectra for PANI, PANI-GNS and PANI-MoS_2 are shown in Figure 4.18. The spectra are analyzed using Nyquist plots. A semicircle in high frequency region is related to the charge transfer resistance and a straight line in low frequency region represents an ideal capacitive behaviour. The diameter of the fitted circle is equal to the electrode resistance arising from the charge transfer resistance (Rct) in the cell.[36]

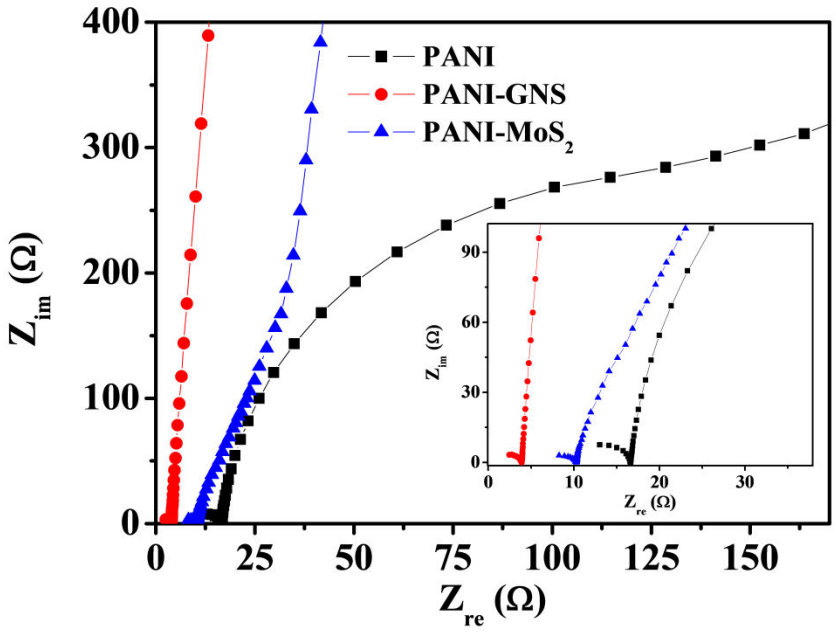

Figure 4.18 Nyquist plot for PANI, PANI-GNS and PANI-MoS_2electrode.

The solution resistance (Rs) for was found to be 16.58, 10.26 and 3.85 Ω respectively. Also, the charge transfer resistance (Rct) was measured to be 6.48, 3.4 and 2.48 Ω respectively for PANI, PANI-GNS and PANI-MoS_2 composite electrode. This

indicates that PANI-GNS electrode possesses low charge transfer impedance and therefore the composite shows higher capacitance than shown by the bare PANI electrode. These results are consistent with those obtained in the CV results.

4.4.3 Galvanostatic charge discharge profile

To evaluate the applicability of the PANI-GNS and PANI-MoS2 composite, we measured the charge/discharge behavior of both the electrodes by using two electrode systems in 0.5 M H_2SO_4 as electrolyte at different current densities ranging from 20 µA to 100 µA. The specific capacitance was calculated by using the equation

$$Csp = \frac{(i \times \Delta t)}{\Delta E \times m} \qquad (10)$$

Where, i is current density Ag^{-1}, Δt is discharge time (s), ΔE is a voltage difference in (V) and m is an active mass of electrode derived from quartz crystal microbalance[35, 36] (detailed procedure of estimation of mass is given in Chapter-1), The calculated C_{sp} from the above equation shows high values of 549.2 to 458.9 Fg^{-1} at the high current densities from 20 µA to 100 µA, for PANI-GNS and 413.6 to 297.3 Fg^{-1} at the high current densities from 20 µA to 100 µA, for PANI-MoS_2 which is consistent with the results of CV studies. The obtained values are higher and comparable to most of the reports on PANI-GNS[45-47] and PANI-MoS_2.[48]

The charge-discharge curves as shown in Figure 4.19 are nearly symmetric, revealing a good capacitive behavior. In addition, the voltage drop is observed to be 0.48V for the PANI electrode and 0.22 V for PANI-MoS_2 electrode whereas most interestingly in case of PANI-GNS it is negligible which indicates that the electrode has low internal resistance. It is found that there is a significant value addition by making an LbL composite of PANI-GNS in terms of obtaining higher capacitance at high current density with good retention over the individual components of the composite. Figure 4.20shows Change of specific capacitance with current density for PANI thin film, PANI-GNS and PANI-MoS_2 hybrid thin films and Table 2 shows corresponding values.

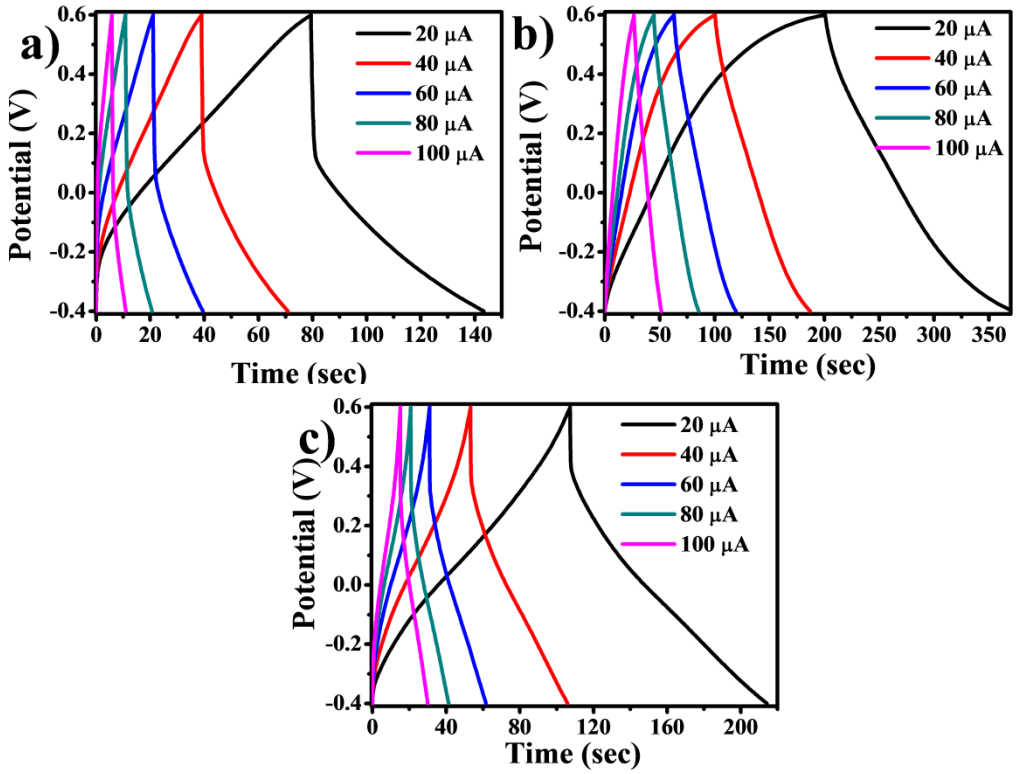

Figure 4.19 Charge-discharge curves for a) PANI electrodes, b) PANI-GNS and c) PANI-MoS_2 in a 0.5 M H_2SO_4 electrolyte within the potential window of -0.4 V to 0.6 V.

The PANI-MoS_2 composites, reported in literature show good capacitive behavior[49] and specific capacitance up to 390 F/g and 86% retention of specific capacitance for 1000 cycles.

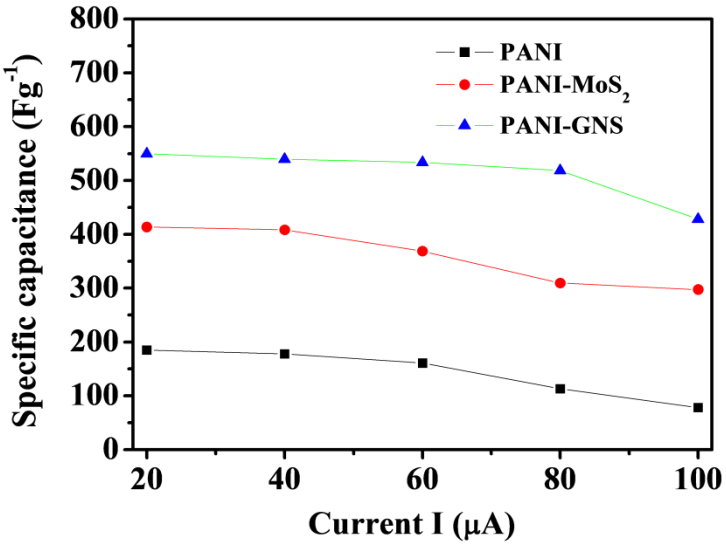

Figure 4.20 Change of specific capacitance with current density for PANI thin film, PANI-GNS and PANI-MoS_2 hybrid thin films.

Table 2 Comparison of specific capacitance Fg^{-1} obtained from galvanostatic charge discharge at elevated current density.

	Specific capacitance Fg^{-1} from Galvanostatic charge discharge.					Retention (%)
Current Density	**20 µA**	**40 µA**	**60 µA**	**80 µA**	**100 µA**	
PANI	185	178	161.2	113.5	78.26	42.3
PANI-GNS	549.2	539.6	533.7	518.2	458.9	83.4
PANI-MoS2	413.6	408.1	368.8	309.6	297.3	71.9

The observed C_{sp} from the calculations of both CV and charge/discharge study are comparable for exclusive PANI. For PANI-GNS composites, C_{sp} turns out to be higher than those reported in literature. It is proposed that this improvement arises from LbL stacking of GNS and PANI.

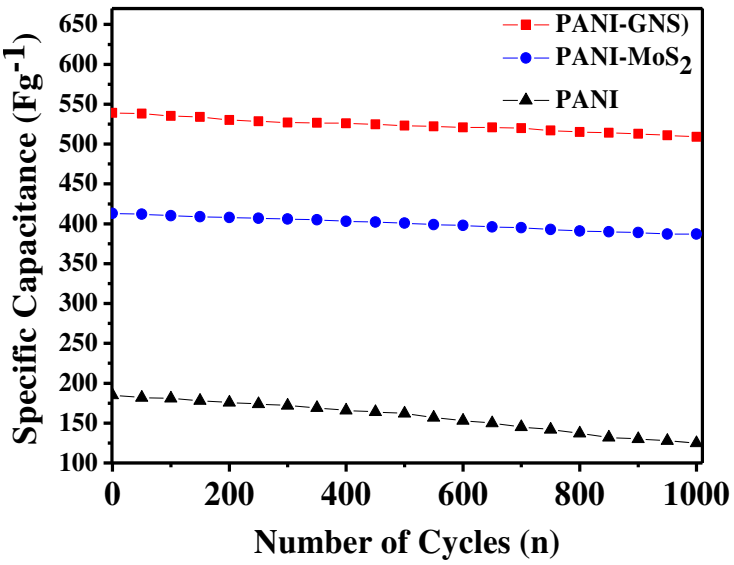

Figure 4.21 Cycle performance of PANI, PANI-GNS and PANI-MoS_2 at current density of 20 µA, for 1000 cycles.

1000 cycles of charge-discharge processes (Figure 4.21) have been studied to establish the stability of the performance of the composite and it is found that there is

retention of C_{sp} up to 94% at high current density of 20 µA. PANI-MoS_2 composite showed retention of capacitance up to 93% which is also achieved because of the present LbL architecture.

The bare PANI electrode showed 67% retention of specific capacitance which is also better than earlier reports. PANI is known to get degraded and is an obvious conclusion of the earlier reports. Thus, the LbL composites are relatively more stable at higher current density as well as on large number of cycling and therefore can be useful for specific applications. It is suggested that the large capacitance for PANI-GNS/MoS_2 can be rationally explained by 1) the complete separation of GNS/MoS_2 sheets from PANI nanoparticulate thin film as a spacer in the composite, 2) fast charge transfer at the interface between the electrode and 3) electrolyte ions and large surface area due to GNS/MoS_2.

4.5 Conclusions

We have successfully synthesized and characterized high performance super capacitive electrodes composed of a PANI, PANI-GNS and PANI-MoS_2 thin films containing PANI nanoparticulate sizes in the range of 5 to15 nm by using modified LLIRT. An additional feature of the present technique is the applicability of LbL technique to fabricate PANI-GNS and PANI-MoS_2 composite hybrid films with a well-defined architecture and tunable thickness on various substrates for applications such as supercapacitors. The obtained hybrid films having interconnected network prevented graphene sheets from stacking with one-another, thus assisting in the formation of nanocomposites. This is the proof of the concept of forming graphene semi-conductor composite by the reported technique and opens a new area for forming better capacitors. The CV results indicated good capacitive behavior for PANI-GNS and PANI-MoS_2composites. PANI-GNS composite showed excellent specific capacitance of 559 Fg^{-1} calculated from CV and 549.2 Fg^{-1} calculated from charge-discharge (CD) measurement. On the other hand PANI-MoS_2 composite showed specific capacitance of 426 and 413 Fg^{-1} calculated from CV and CD measurements respectively. A very good cycling stability 94% for PANI-GNS and 93% for PANI-MoS_2 up to charge discharge 1000 cycles at 20 µA current density is an indication that nanocomposite thin film formed with the present technique is a possible candidate for super-capacitor application and in an energy storage

technology. The excellent electrochemical performance of the composite as supercapacitor electrodes is due to the synergistic effects among the components in the composites.

4.6 References

[1] M. D. Stoller, S. Park, Y. Zhu, J. An and R. S. Ruoff, *Nano Lett*., 2008, **8 (10)**, 3498–3502.

[2] L. L. Zhang and X. S. Zhao, *Chem. Soc. Rev*., 2009, **38(9)**, 2520–2531.

[3] A. G. Pandolfo and A. F. Hollenkamp, *J. Power Sources,* 2006, **157(1)**, 11–27.

[4] L.-Z. Fan and J. Maier, *Electrochem. Commun.,* 2006, **8(6)**, 937–940.

[5] K. Keiichi, M. MacRae, P. N. David, G. M. Alan and J. H. Alan, *J. Chem. Soc., Faraday Trans. I,* 1982, **78**, 3417.

[6] C. Arbizzani, A. M. Marinangeli, M. Mastragostino, T. Hamaide and A. Guyot, Synth. *Metals*, 1991, **41**, 1147.

[7] O. Tetsuya, N. Katsuhiko, S. Hiroshi, and O. Satoshi, J. *Electrochem. Society*, 1987, **134**, 285.

[8] F. Trinidad, J. Alonso-Lopez and M. Nebot, *J. Appl. Electrochem.*, 1987, **17**, 215.

[9] W. P. Elizabeth, J. R. Antonio and S.W. Mark, *J. Phys. Chem.,* 1985, **89**, 1441.

[10] K. Tetsuhiko, Y. Hiroshi and T. Hideo, *J. Electroanaly. Chem. Interfac. Electrochem*., 1984, **161**, 419.

[11] K. Masao, N. Hideki and S. Takeshi, *Macromol.Chem. Rapid Comm.,* 1987, **8**, 179.

[12] B. E. Conway, Electrochemical Supercapacitors: scientific fundamentals and technological applications, *Kluwer* Academia/Plenum Publishers, New York, 1999.

[13] A. Bohler, S. Dirr, H. H. Johannes, D. Ammermann and W. Kowalsky, *Synth. Metals*, 1997, **91**, 95.

[14] Y. Gang, *Synth. Metals*, 1996, **80**, 143.

[15] Z. Ruifeng, Z. Haipeng and S. Jiacong, *Synth. Metals*, 1999, **106**, 157.

[16] O.Y. Yu and V. F. Zolin, *Synth. Metats*, 1997, **91**, 205.

[17] G. M. Alan, *Synth. Metals*, 1997, **84**, 27.

[18] F. Garten, J. Vrijmoeth, A. R. Schlatmann, R. E. Gill, T. M. Klapwijk and G. Hadziioannou, *Synth. Metals*, 1996, **76**, 85.

[19] B. Hua and S. Gaoquan, *Sensors,* 2007, **7**, 267.

[20] M. S. Halper and J. C. Ellenbogen, Mitre Corporation, Virginia, 2006.

[21] S. Elisabeth, I. Olle and L. Ingemar, *Science*, 1995, **268**, 1735.

[22] K. Lota, V. Khomenko and E. Frackowiak, *J. Phys. Chem. Solids*, 2004, **65**, 295.

[23] L. Alvarez-Mejia, H. Salgado-Ceballos, R. Olayo, G.J. Cruz, M.G. Olayo, A. Diaz-Ruiz, C. Rios, R. Mondragon-ozano, A. Morales-Guadarrama, S. Sanchez-Torres and J. Morales, *Revista Mexicana de Ingenieria Biomedica*,10/2014, **36(1)**, 7.

[24] J. Jiang and A.Kucernak, *J. Electroanal. Chem*., 2000, **490**, 17.

[25] E. Frackowiak, K. Jurewicz, S. Delpeux and F. Beguin, *J. Pow. Sources*, 2001, **822**, 97.

[26] K. Jurewicz, S. Delpeux, V. Bertagna, F. Beguin and E. Frackowiak, *Chem. Phys. Lett.,* 2001, **347**, 36.

[27] S. Yongchao and T. S. Edward,*Nano Lett*., 2008, **8**, 1679.

[28] H. Wenjing, X. Yuxi, L. Gewu, L. Chun and S. Gaoquan, *Electrochem. Comm.,* 2008, **10**, 1555.

[29] Y. K. Tae, W. L. Hyun, S. Meryl, R. D. Daniel, W. B. Christopher, S. R. Rodney, and S. S. Kwang, *ACS Nano*, 2011, **5**, 436.

[30] C. N. R. Rao, A. K. Sood, K. S. Subrahmanyam and A. Govindaraj, *Angew. Chem. Int. Ed*., 2009, **48**, 7752.

[31] P. Sharma and T. S. Bhatti, *Energy Convers. Management*, 2010, **51**, 2901.

[32] W. Jie, X. Youlong, C. Xi and D. Xianfeng, *J. Power Sources*, 2007, **163**, 1120.

[33] B. J. Waghmode, S. H. Patil, M. M. Jahagirdar, V. S. Patil, R. P. Waichal, D. D. Malkhede, S. D. Sathaye and K. R. Patil *Colloid and Polymer Science*, 2014, **292(5)**, 1079.

[34] S. Patil, V. Patil, S. Sathaye and K. Patil, *RSC Advances*, 2014, **4 (8)**, 4094.

[35] a) C. D. Lokhande, D. P. Dubal and J. Oh-Shim, Curr. Appl. Phys., 2011, **11**,

255. b) S. Patil, A. Harle, S. Sathaye and K. Patil, *CrystEngComm*, 2014, **16 (47)**, 10845.

[36] a) J. Widlarzm, *J. Polymer*, 2005, **46**, 1485. (b)Y. Xis, J. M. Wiesinger, and A. G. MacDiarmid, *Chem. Mater.,* 1995, **7**, 443.

[37] a) H. Nalwa, *Journal of Mater. Sci.*, 1991**, 26**, 1683. b) M. Shahadat, S. A. Nabi, R.Bushra, A. S. Raeissi, K. Umaraand M-O. Ansarib*, RSC Advances,* 2012, **2**, 7207.

[38] W. R. Salaneck, I. Lundstrom, T. Hjertberg, C. B. Duke, E. Conwell, A. Paton, A. G. MacDiarmid, N. L. D. Somasiri, W. S. Huang, and A. F. Richter, *Synth. Metals*, 1987,**18**, 291.

[39] P. Snauwaert, R. Lazzaroni, J. Riga and J. J. Verbist, *Synth. Metals*, 1987, **18**, 335.

[40] D. Gui, C. Liu, F. Chen and J. Liu, Applied Surface *Science*, 2014, **307**, 172.

[41] Z. Tong, Y. Yang, J. Wang, J. Zhao, B-L. Su and Y. Li, *Journal of Mater. Chem. A: Materials for Energy and Sustainability*, 2014, **2(13)**, 4642.

[42] Z-F. Li, H. Zhang, Q. Liu, Y. Liu, L. Stanciu and J. Xie, *Carbon* 2014, **71**, 257.

[43] S. Montree, S. Montakan, K. Kawita, K. Jakkrit, S. Pattarachai, S. Yanisa, K. Panupong, S. Phansiri and C. Poramane, *Journal of Mater. Chem. A, Materials for Energy and Sustainability*, 2013, **1(34)**, 9630.

[44] M. Liu, Y-E. Miao, Z. Chao; W. W. Tjiu, Z. Yang, H. Peng and T. Liu, *Nanoscale*, 2013, **5(16)**, 7312.

[45] L. Hu, J. Tu, S. Jiao, J. Hou, H. Zhu and D. Fray, *Physical Chemistry Chemical Physics*, 2012, **14(45)**, 15652.

[46] M. Liu, Y-E. Miao, C. Zhang, W. W. Tjiu, Z. Yang, H. Peng and T. Liu *Nanoscale*, 2013, **5(16)**, 7312.

[47] X. Li , H. Song, Y. Zhang, H. Wang, K. Du, H. Li, Y. Yuan and J. Huang, *Int. J. Electrochem. Sci.,* 2012, **7,**5163.

[48] K-J. Huang, L. Wang, Y-J Liu, H-B. Wang, Y-M. Liu and L-L. Wang, *Electrochimica Acta*, 2013, **109**, 587.

[49] J. Wang, Z. Wu, K. Hu, X. Chen and H. Yin, *Journal of Alloys and Compounds*, 2015, **619**, 38.

Chapter-5

Architecturally designed Pt-MoS_2 and Pt-graphene composites for electrocatalytic methanol oxidation

Thin films consisting of platinum nanoparticles (Pt NPs) with uniform size and distribution have been successfully prepared at the Liquid-Liquid interface and subsequently transferred on suitable substrates. Apart from the usual substrates like glass, Si etc. the films were also deposited on the substrates coated with MoS_2 thin film and graphene nanosheets (GNS) thin film respectively, by using Layer-by-Layer (LbL) deposition technique to form Pt-MoS_2 and Pt-GNS composites. The architecture of the composite and loading concentration of Pt nanoparticles on MoS_2 and GNS can be adjusted by selecting the number and sequence of component layers during LbL deposition. Pt thin films, Pt-MoS_2 and Pt-GNS nanocomposite thin films are characterized by transmission electron microscopy (TEM), high resolution transmission electron microscopy (HRTEM), energy dispersive X-ray spectrometry (EDX), X-ray diffraction (XRD) and X-ray photoelectron spectroscopy (XPS). TEM results of the composites show that Pt nanoparticles with sizes in the range of 1 to 3 nm are uniformly dispersed on MoS_2/GNS surface. The catalytic activity of Pt and Pt-composites for the reaction of methanol oxidation is studied by cyclic voltammetry and chronoamperometry. Electrochemical studies reveal that both Pt-MoS_2 and Pt-GNS nanocomposites show excellent electrocatalytic activity towards methanol oxidation. Pt-MoS_2 and Pt-GNS nanocomposite electrodes show excellent stability for reuse of catalyst. Probable mechanism of catalysis has been discussed. It is proposed that the architecture presented in this Chapter, would be promising for the synthesis of high performance catalysts for fuel cells, gas phase reactions, and other applications such as sensors.

Content in this Chapter is published in the following article,
Phys. Chem. Chem. Phys., 2015, 17, 26101-26110.
http://pubs.rsc.org/en/Content/ArticleLanding/2015/CP/C5CP04141D#!divAbstract

5.1. Introduction

The energy transformation along with energy storage has become a very important issue worldwide. In previous Chapters we have dealt with mainly energy

storage problems. However our objective of the thesis work is to deal with various aspects of energy problem faced by the whole mankind. Among these problems, energy conversion is an important one. It is reported that high efficiency energy conversion from the stored energy in methanol for utilization of other applications would be an important step forward.[1] Apart from these, other energy conversion problems are studied all over the world, namely, solar energy, wind energy, geothermal energy etc. A development of efficient, low cost fuel cells (FC) is one of the most focused areas in current science research. Fuel cells are used to convert chemical energy into electric energy. Methanol has several advantages including the simplicity of transportation and storage and high theoretical energy density over hydrogen as a fuel in fuel cells. The methanol oxidation reaction occurs at the anode in direct methanol fuel cells (DMFCs). Pt electrode has a high activity toward the dissociative adsorption of methanol; therefore, most of the DMFC's use Pt electrode as an electrochemical catalyst.[2-5] Despite many of the advantages of Pt as a catalyst in fuel cells, there are some challenges namely a) higher costs of Pt catalysts,[5] b) poor utilization of surface in case of bigger particles[6] and c) surface poisoning due to by-product carbon monoxide (CO).[7] To overcome the above challenges, it is a need to manoeuvre the physical properties of the Pt catalysts. The efficiency of Pt catalyst can be improved by using a) lower size nanoparticles to increase the effective surface area and b) bi or tri metallic alloys or Pt based composite materials. Use of materials having high surface area as a support for nanoparticle Pt electrode shows improvement in catalytic activity. However, support material may get oxidized in harsh chemical environment in the cell reaction causing performance loss.[8-11] The drawback of using uncapped, unsupported smaller particles of Pt involves a possibility of their agglomeration during the fuel cells reaction.

Extensive work has been reported in the literature to achieve better performance of Pt catalysts in fuel cells. Accompanying platinum, other metals such as ruthenium,[12] palladium,[13] and gold-platinum nanocrystals[14] have been used to improve catalyst efficiency. Efficient removal of CO from Pt electrode is designated as CO tolerance of the electrode. To get rid of this issue, researchers have reported that Pt-based alloys with transition metals Co, [15] Ni, [16] Cr, [17] etc. are supportive to advance the kinetics of the oxygen reduction reaction (ORR).[18, 19] Currently, the most effective way of increasing CO tolerance is the use of oxophilic elements such as Ru,

Pd, Au, and so forth, to form alloys with Pt.[20-24] However, this is an extremely costly solution as all these elements are also quite expensive. Furthermore, it is well-known that at least three adjacent Pt sites should be properly placed in crystallographic arrangement of bimetallic structures to activate the chemisorption of methanol during methanol oxidation.[23] In case of bi-metallic M-Pt catalyst; it becomes a study in itself to obtain right composition and suitable structure to fulfil the above condition. Apart from this, dissolution of oxidized form of the base metal from the surface of bimetallic catalysts in the acidic fuel cell environment remains a major problem of concern in this field.[7–10] Both theoretical predictions and experimental observations have shown that a strong metal leaching can occur during the fuel cell operation.[11, 12] Therefore, use of bare Pt metal with small particle size and appropriate environment of support of the catalyst suits the reaction of methanol oxidation at the electrode.

The most appropriate particle size for Pt-based electro-catalysts is in the range of 2–4 nm.[20-22] To achieve cost reduction of fuel cells through enhanced surface utilization of electrode, it is necessary to further decrease the particle size of Pt-based electro catalysts. A recent study reveals that for Pt nanoparticles' size of 1 nm or even smaller is better for Pt surface exploitation in electro-catalysts.[6] The support material can complement the catalytic properties of Pt nanoparticles. Carbon based supports for Pt electrodes are preferred considering their inertness toward chemical environment, low cost etc. Apart from porous carbon as supporting material for Pt nanoparticles, carbon nanotubes,[24] polypyrrole,[25] carbon nanofibers,[26] carbon spheres,[27] coin-like carbon materials,[28] carbon nanorods,[29] spherical carbon capsules[30] and GNS[31] are reported in recent years. However, normally, synthesis of such supports is expensive and involves many steps.

Graphene nanosheets (GNS) exhibit a 2D structure composed of sp^2-bonded carbon atoms. Graphene has a layered structure consisting of a few atom thicknesses. Mono/few layer graphene has high surface area, superior electrical conductivities, and an excellent mechanical strength and elasticity.[31] It therefore, proves to be a good component among carbon-metal nanocomposite materials for the next generation catalysts in general and fuel cells in particular. Various methods of preparation of graphene-based composites have been studied so far.[32-36] Most of the studies report GNS-supported Pt catalysts wherein graphene oxide (GO) is used as a precursor to GNS.[37, 38] Uniform dispersion and stabilization of Pt nanoparticles by getting bound to

GO via plentiful oxygen-containing functional groups on GO surface could have been considered a superior support to Pt anode in methanol fuel cells; but for the lower electrical conductivity of GO due to loss of conjugated sp2 network. Therefore, GO is needed to be reduced to GNS, which leads to restoring the hybridized sp^2 network and consequently increase its electronic conductivity and restore structural stability.[39] Such GNS-Pt nanocomposites have been reported recently for better electrocatalytic performance and stability.[40-43] Apart from GNS, other Carbon materials doped with non-metal elements such as nitrogen, phosphorus, boron and sulphur atoms have pronounced catalytic activity.[44-46]

Similar to GNS, the layer-structure di-chalcogenides of transition metals like W and Mo have 2D structure and can be used as support for metal catalysts.[46-49] Recently, Lithui Yuwen et al. reported noble metal modified MoS_2 nanocrystals/nanosheets, especially MoS_2-Pd composite for electrocatalytic activity[50a] shows higher catalytic performance, however, method of preparation involves use of surfactants/dispersing agents which makes the synthesis procedure lengthy and multi-stepped. Also, the presence of surfactants and dispersing agents may affect catalytic activity unfavourably. Chunyang Zhai et al. reported the formation of MoS_2-Pt and Pt-MoS_2/RGO composites wherein matrix MoS_2 and MoS_2/RGO is formed by hydrothermal method followed by Pt nanoparticals (3-4 nm) deposited on it by an electro-chemical deposition method.[50b]

On this background, we choose to study GNS/Pt and MoS_2/Pt composites as electrochemical catalysts for methanol oxidation for their possible use in fuel cells application. Here, we report an easy, inexpensive, one step and surfactant free method to prepare nanoparticulate film consisting of Pt-nanoparticles at liquid-liquid interface and subsequently transferred on suitable substrates. These films can be directly deposited/ transferred on the suitable substrate like glass slides, Si wafers/ layered graphene/MoS_2 etc. Moreover, 'Pt' in these films is shown to be present mostly in zero oxidation state as is preferred for methanol fuel cells catalyst application. We have recently reported facile methods to prepare mono/few layered graphene[51] and mono/few layered MoS_2[52] thin films. We further demonstrate the use of layer-by layer (LbL) technique to make hybrid composites of Pt nanoparticles on MoS_2/GNS with controlled deposition. This would prove to be a significant development for the

synthesis of electrode for methanol fuel cells. Further, we show that the resulting composite films thus formed are effective catalysts for methanol oxidation.

5.2 Experimental Section

5.2.1 Chemicals

All of the reagents used herein were of analytical grade and used as received without any further purification. Chloroplatinic acid (H_2PtCl_6), Molybdenum disulfide (MoS_2, 99.9%) and graphite rod (99.99 %) were purchased from Sigma-Aldrich Ltd. Concentrated Sulfuric acid (H_2SO_4, 98%), Sodium borohydrate ($NaBH_4$) and Oleic acid (99% by GC) were purchased from Merck chemicals. Carbon tetrachloride (CCl_4, 99.5%) was purchased from Loba Chemie and water used in this process was doubly distilled de-ionized.

5.2.2 Preparation of nanoparticulate thin films of Pt and its composites

Highly dispersed Pt nano particles thin films have been prepared using Liquid-Liquid Interface Reaction Technique (LLIRT).[51-53] A detailed process of formation and transferring the film to a suitable substrate is described in earlier Chapters. However, for a better understanding; a short schematic of Pt nanoparticulate film formation is given in Scheme 5.1. In a typical procedure, 10^{-3} M $NaBH_4$ solution was prepared in deionised water in a teflon tray (15 cm x 15 cm x 2 cm) so that it forms a meniscus at the edges of the tray (sub phase). The surface of the solution in tray (subphase), was divided into two compartments by a Teflon thread barrier which was conveniently fixed on the opposite edges of the tray keeping an allowance for its contraction/expansion on the surface. Spreading solution was prepared by mixing 0.1 mL 0.023 M H_2PtCl_6, 0.2 mL ethanol and 0.2 mL CCl_4 to make final volume 0.5 mL. A few drops of spreading solution were allowed to spread over the surface of subphase in the compartment on one side of the thread with the help of a micro-syringe until the drop makes lens or simply stops spreading. The solvents were allowed to evaporate. A drop of oleic acid was allowed to spread on the surface of subphase in the other compartment. The spreading oleic acid exerts a lateral pressure 30 dynes cm^{-1} on the film. The as-formed compressed film on the subphase surface was transferred on a glass/quartz/silicon wafer substrate by immersing in the subphase where the compressed Pt nanoparticles film floats and lifting it vertically at a constant

rate of 0.5 cm min^{-1} with the help of coating unit, so that the film covers the dipped area of the substrate (Langmuir-Blodgett technique).

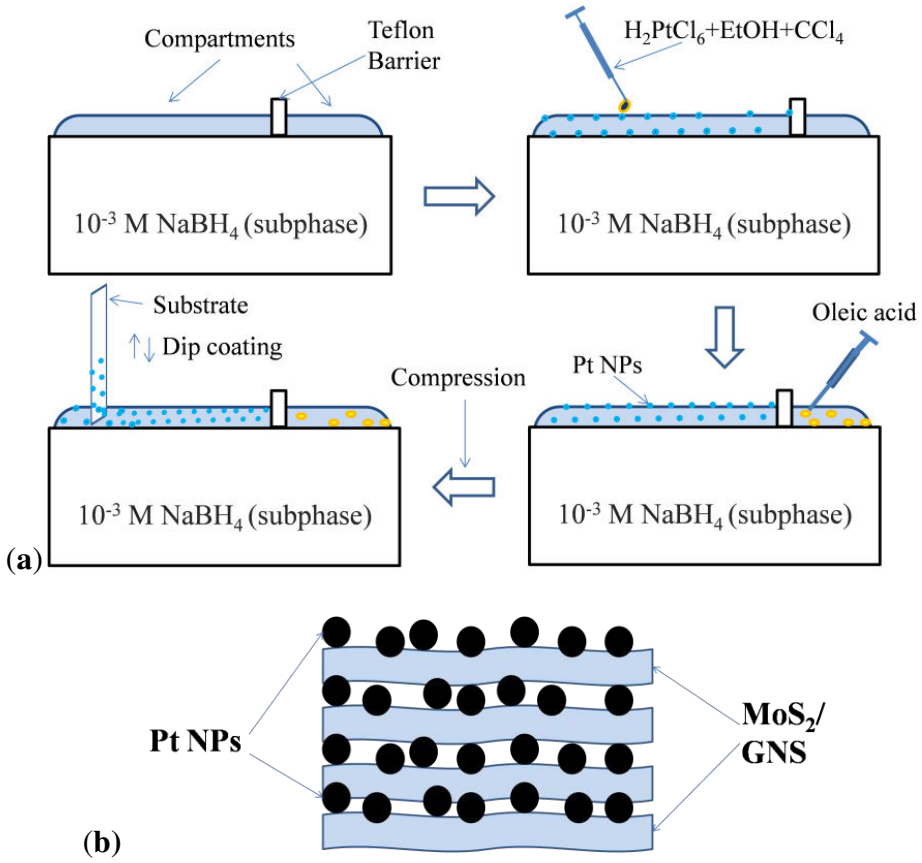

Scheme 5.1 Schematic representation of (a) Preparation and transfer mechanism of Pt Nanoparticulate thin film by using LLIRT technique. (b) The L-b-L composite.

A procedurally similar technique was tailored to obtained graphene and MoS_2 films[51, 52] as narrated in earlier Chapters. The operation of transferring the film from subphase surface to substrate was repeated required number of times to get a desired film thickness/mass for specific applications and characterization. The film was then washed with deionised water several times. This film was then used for characterization. Furthermore, this technique can be useful for the growth of the composite thin film consisting of MoS_2-Pt or GNS-Pt by LbL technique. A few-layered MoS_2/GNS nanosheets thin film was obtained on the surface of water in a separate tray.[51, 52] Stacked composite films of Pt-MoS_2 and Pt-GNS were deposited on the substrate by forming a layer of each component (Pt and MoS_2/GNS) alternately from two independent trays. Thus, a layer, say Pt, is deposited on a substrate by dipping the substrate in one of the trays, and subsequently the same substrate was

dipped in the other tray to deposit the film of say MoS_2 to form Pt-MoS_2 and so on to form a film of desired thickness. The composition of the composite can be manoeuvred by monitoring of number of dips of each layer before the other component layer/s is deposited. A similar procedure is adapted for other composition namely Pt-GNS. The film of above mentioned composite catalysts with desired thickness/mass was deposited on the fluorine doped tin oxide deposited glass (FTO) substrate. The films were further annealed at 400^0C to increase the crystalline active sites on Pt surface. Scheme 5.1b shows the schematic of desired composite layer film formation. The Pt-MoS_2 and Pt-GNS hybrid electrode of the desired thickness are obtained by depositing the number of layers of each component alternately in a premeditated sequence.

Here, it may be noted that deposition of alternate single dip of Pt nanopartices and MoS_2/GNS on the substrate would establish a close contact between Pt nanoparticles with MoS_2 or GNS layer. As each MoS_2 and GNS has 2D structure, such an arrangement is proposed to be suitable to compact catalyst composite having desired loading of Pt nanoparticles on the surface.

5.2.3 Sample Characterization

The crystal structure of the materials was determined using Cu Kα radiation (λ=1.54A^o) (PAN analytical X'Pert pro X-ray diffractometer). Transmission electron microscopy (TEM) images were taken on a JEOL 1200-EX instrument with an accelerating voltage of 100 kV and high-resolution transmission electron microscopy (HRTEM-JEOL 2010F) at an acceleration voltage of 300 kV. The electron diffraction facility was employed during the morphological characterization of the film for assessment of the structure and the phases present. The thickness of the cast film on silicon wafer was examined by an atomic force microscope (AFM, Digital Instrument Environ Scope) using a tapping mode, with tip made up of silicon nitride. Environ-SEM (E-SEM, Quanta 200 3D) was used to get the additional information of morphology. XPS analysis was performed on a ESCA-3000 VG Scientific UK, using non-monochromatic, Al Kα radiation (1486.6 eV) operating at 150 W with a spectral resolution of 0.2 eV. Cyclic voltammetry (CV) and chronoamperometry (CA) tests for methanol oxidation at varying potentials in 0.5 M H_2SO_4 aqueous solution at room temperature were performed using an Autolab PGSTAT 30 (Ecochemie)

electrochemical workstation. Electrochemical impedance spectroscopy (EIS) was carried out in the frequency range from 0.1 Hz to 100 kHz and AC bias voltage of 10 mV.

5.2.4 Electrochemical measurements

In a typical experiment 40 mL 0.5 M H_2SO_4 solution was taken as an electrolyte and blank FTO coated glass having dimensions (1cm X 3cm) was used as an electrode for initial analysis of I-V characteristic at a scan rate of 50 mV/s. The FTO substrate of same dimension was used for the deposition of thin film of Pt nanoparticles by dip coating unit (Holmark). As a working cell, three-electrode system was employed wherein Pt wire and SCE electrodes, were used as counter and reference electrode respectively. For working electrode, a known weight of sample, namely, Pt nanoparticles / Pt-MoS_2 / Pt-GNS was deposited over the FTO coated glass by using dip coating unit and estimating weight of the coated film by separate experiments. The weight of catalysts present over the FTO substrate/electrode was estimated by using quartz crystal microbalance.[51, 52] Estimated mass loading of Pt nanoparticles for each phase was kept nearly constant with an instrumental error ±0.05 µg. For better comparison, the area of deposition was also kept constant i.e. $1cm^2$. The estimated masses were 17.3 µg, 18.9 µg, 17.6 µg and 23.1µg for Pt-MoS_2, Pt-GNS, Pure Pt nanoparticles thin film and commercial Pt/C, electrodes respectively.

5.3 Results and Discussion

5.3.1 X-ray diffraction study (XRD)

The XRD pattern of the Pt nanoparticles (Figure 5.1a) exhibits the characteristic line pattern assignable to fcc platinum lattice. Diffraction peaks at 39.7, 46.4 and 67.2 match with those reported for Pt (111), Pt (200), and Pt (220) planes respectively (JCPDS-PDF#040802), confirming that the platinum precursor has been chemically reduced to Pt nanoparticles by $NaBH_4$. The XRD analysis of the other components namely GNS and MoS_2, when deposited separately, has been discussed in the earlier Chapters of this thesis. Therefore, it is presumed that the same structures are reproduced. The composite structure inferred from XRD is just an overlapping of Pt-XRD and MoS_2/GNS XRD.

The effect of temperature on XRD patterns of (a) Pt nanoparticles (b) Pt-graphene and Pt-MoS_2 nanocomposites with different loading of Pt are shown in

Figure 5.1 Better crystallinity of Pt nanoparticles at higher temperatures leads to increase in the intensity of Pt-XRD peaks. The X-ray peak of the GNS in Pt-GNS composite is observed at 2θ value of 26.7 for (002) plane, confirms GNS to be multi-layered.[51] The diffraction peak for Pt (111) was used to estimate the Pt crystallite size since there is no interference from other component's diffraction peaks. Calculation using the Scherer equation yields an average crystallite size of Pt on graphene of 2.0 nm, which is in close agreement with the crystallite size shown in TEM below. The Pt-MoS_2 nanocomposite shows diffraction peaks for Pt at 39.7^0 (111), 46.4^0 (200) and 67.2^0 (220) as well as peaks for MoS_2 polycrystals at 14.1^0 (200), 44.2^0 (104). In the present method, the Pt loading density can be adjusted by varying the number of dips over the support (MoS_2 and GNS). Furthermore, the composites with varying Pt layers (1:1 and 3:1) were formed and analysed as shown in Figure 5.1b. It is important to note that the feature of present method is that Pt nanoparticles size does not vary with the increasing number of Pt layers on support semiconductor. Such exceptional distribution of dispersed Pt nanoparticles on MoS_2/GNS can be obtained with 3:1 ratio of Pt: MoS_2/GNS.

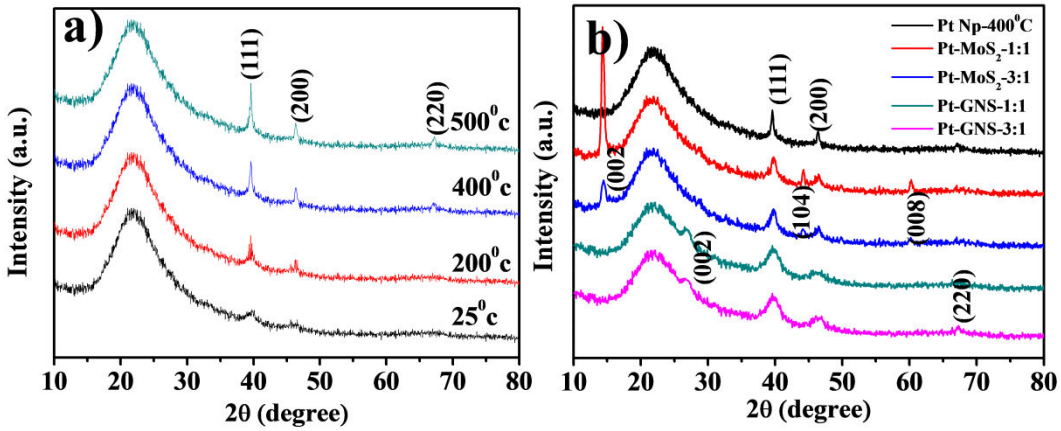

Figure 5.1 (a) XRD spectra for Pt nanoparticles thin film at different elevated temperatures. (b) XRD spectra for Pt nanoparticles composites with GNS and MoS_2 with 1:1 and 3:1 ratios.

5.3.2 X-ray Photoelectron spectroscopy (XPS)

X-ray Photoelectron spectroscopy (XPS) can be helpful to throw light on the species present on the surface of the samples and their respective oxidation states which are likely to be electrochemically active for the reaction under study. Therefore, Pt nanoparticles, Pt-MoS_2 and Pt-GNS nanocomposite samples were

subjected to XPS analysis, importantly, closely analysing Pt 4f, Mo 3d and C 1s peaks. The general survey scan spectrum for the Pt nanoparticles film and composites, Pt-MoS_2 and Pt-GNS (Figure 5.2) clearly reveals the presence of Mo/C and Pt in the respective samples. An XPS spectrum for Pt nanoparticles shows the Pt 4f levels i.e. $4f_{7/2}$ at binding energy (BE) 70.7 eV and $4f_{5/2}$ at 74.0 eV with spin orbit splitting of ~3.3 eV as shown in Figure 5.3.

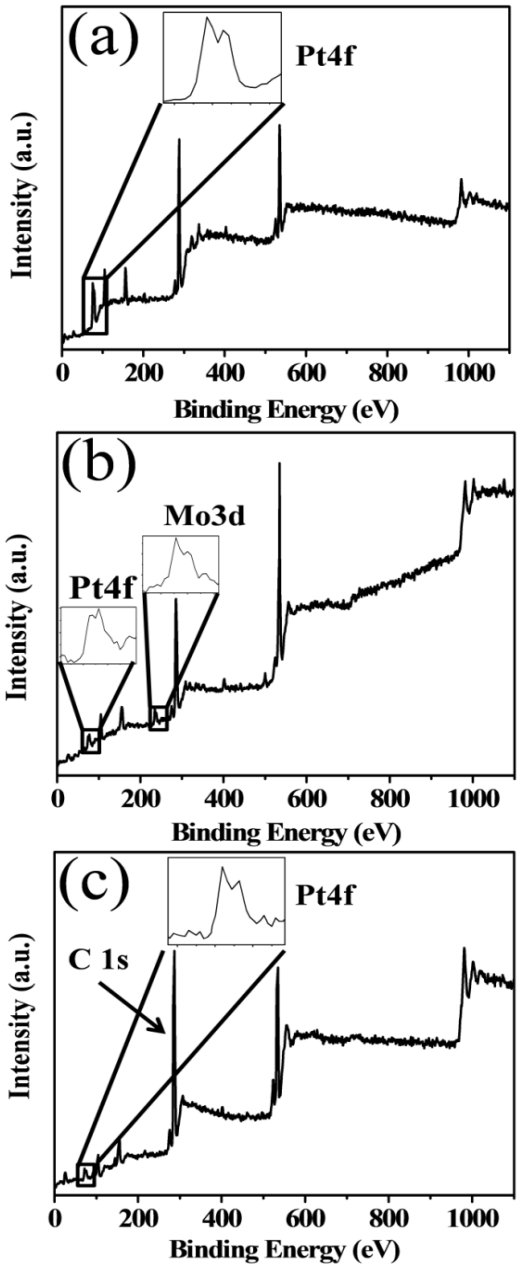

Figure 5.2 General XPS spectra for a) bare Pt nanoparticles catalyst, inset Pt 4f , b) Pt-MoS_2 catalyst inset Pt 4f, Mo 3d and c) Pt-GNS catalyst.

These observations suggest the conversion of Pt^{4+} in H_2PtCl_6 into Pt^0 due to reduction by $NaBH_4$ added to the subphase, during the reaction. Moreover, the peaks were deconvoluted to check the different oxidation states of Pt after the reaction. The respective high binding energy doublet with low intensity peaks of $4f_{7/2}$ at 72.7eV and $4f_{5/2}$ at 75.9eV with spin orbit splitting of ~3.3 eV which fall between Pt^0 and PtO_2 (BE for PtO_2 74.8 and 78.1 eV) is attributed to the slight oxidation of Pt to PtO*x*. The negligible presence of 'O' on the surface is understandable and can be attributed to the surface oxidation by X-ray source during XPS measurement or oxygen adsorption during the exposure of samples to atmosphere.

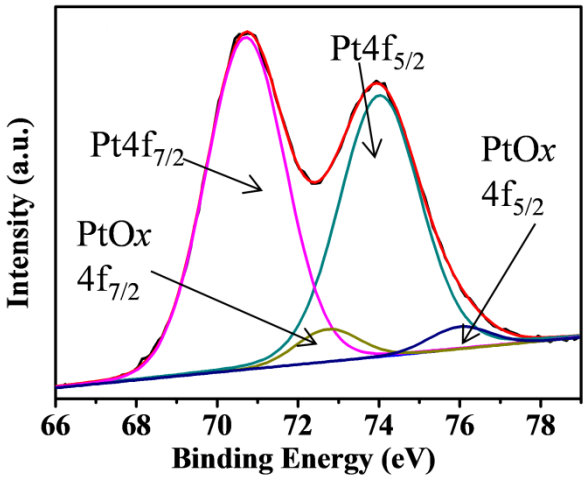

Figure 5.3 XPS spectrum of Pt nanoparticles: Pt 4f

Moreover, this surface layer gets removed during electrochemical reactions. Figure 5.4a shows Mo 3d level in which peaks at 230.14 eV and 233.29 eV with spin orbit splitting of ~3.2 eV corresponds to Mo $3d_{5/2}$ and Mo $3d_{3/2}$ respectively which suggest the presence of Mo in 4^+ oxidation state.[51]

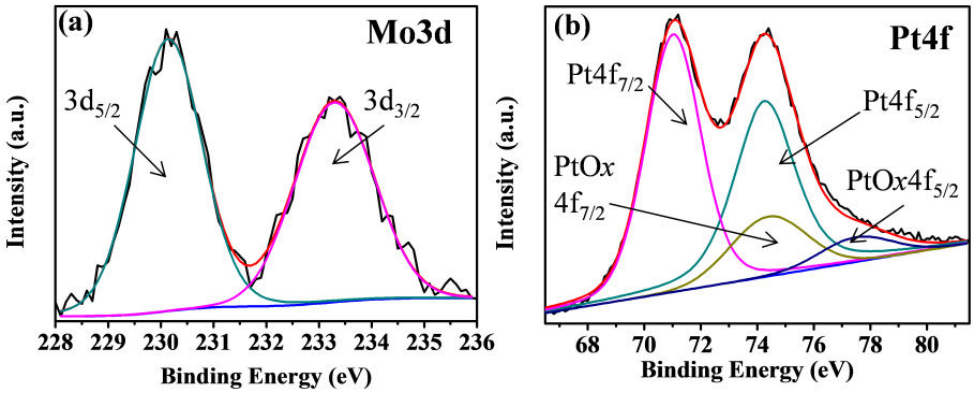

Figure 5.4 XPS spectra of Pt-MoS_2 composite. (a) Mo3d in Pt-MoS_2 catalyst and (b) Pt4f.

Pt-4f level (Figure 5.4b) shows two doublets due to Pt^0 and Pt 2^+ moieties. Peak at 70.47 eV and 73.73 eV correspond to Pt $4f_{7/2}$ and Pt $4f_{5/2}$ levels respectively with spin orbit splitting of ~3.3 eV attributed to the presence of Pt^0. Moreover peak at 73.4 eV and 76.7 eV with spin orbit splitting ~3.3 eV corresponds to PtO*x* 4f levels namely Pt $4f_{7/2}$ and Pt $4f_{5/2}$ respectively. Pt-GNS composite (Figure 5.5a) shows C1s peak at 284.6 eV, however, the peak is asymmetric and therefore deconvoluted. The deconvoluted peaks at 284.6, 285.62, 286.89 and 288.28 eV can be attributed to graphitic C-C, C-O, C=O and COO^- moieties respectively. Pt 4f levels (Figure 5.5) namely $4f_{7/2}$ at 70.8 and $4f_{5/2}$ 74.1 eV are obtained with spin orbit splitting of ~3.3 eV which shows that during the process of composite formation conserves the presence of Pt in zero oxidation state. Peaks at 72.5 eV and 75.9 eV with spin orbit splitting ~3.4 eV corresponds to PtO*x* 4f levels namely Pt $4f_{7/2}$ and Pt $4f_{5/2}$ respectively.

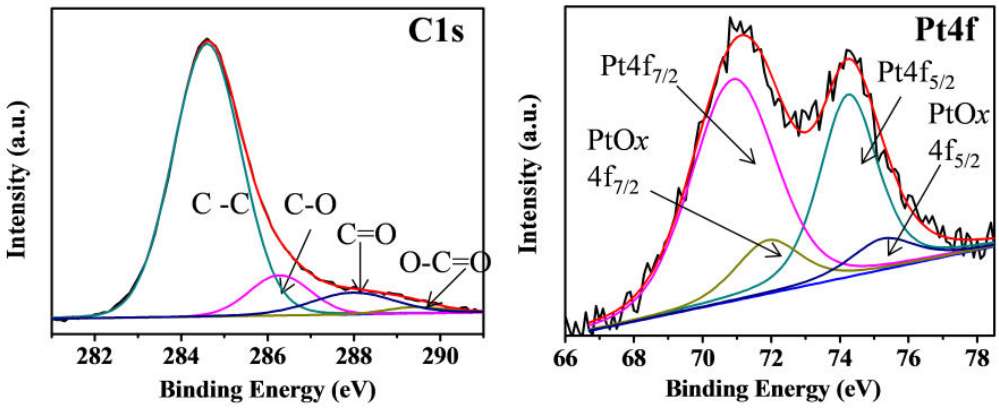

Figure5.5 XPS spectra of Pt-GNS composite (a) C1s and (b) Pt4f.

5.3.3 Transmission electron microscopy (TEM)

The morphology and structure of Pt nanoparticles, Pt-MoS_2 and Pt-GNS were studied by TEM, HRTEM and SAED facility therein. Figure 5.6 shows typical TEM images of the Pt nanoparticles thin film. The particle size is in the range of 1-3 nm. The mean size of particles is 1.9 nm which is reflected in a histogram as shown in the inset of Figure 5.6. Another inset of Figure 5.6a shows the electron diffraction wherein ring pattern is observed. The calculated d values from the diffraction ring pattern are 2.21Å (111), 1.89Å (200), 1.31Å (220) and 1.18Å (311) which match with those reported for pure Pt metal (JCPDS, PDF#040802). The HRTEM image in Figure 5.6b shows that the spacing between lattice fringes is 0.22 nm, corresponding with the (111) planes of crystalline Pt. It is observed that there is no aggregation or

growth of particle with respect to time of aging at the air water interface as shown in figure 5.7.

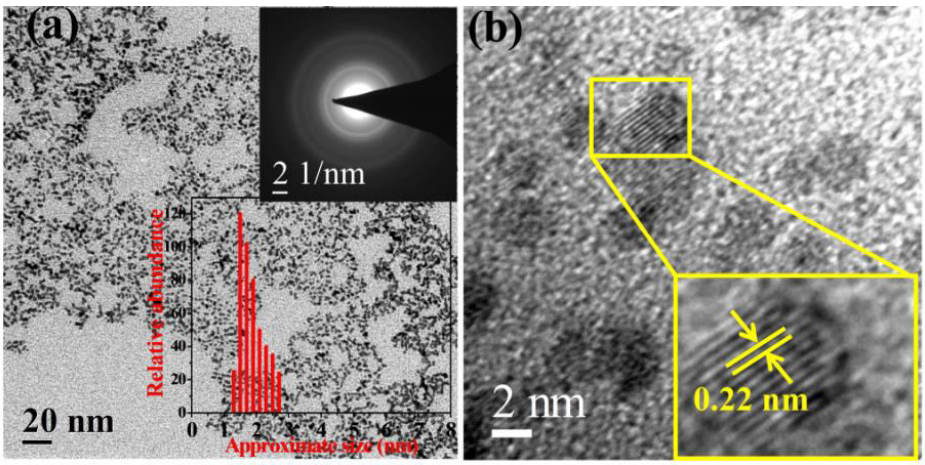

Figure 5.6 (a) TEM image of as-synthesized Pt nanoparticles, inset shows electron diffraction pattern and histogram of particle size distribution for the same. (b) HRTEM image of Pt nanoparticles, inset showing lattice fringe distance of 0.22 nm corresponding (111) plane of Pt.

Figure 5.8 and 5.9 show typical TEM images of the Pt nanoparticles supported on MoS_2 and GNS i.e. Pt-MoS_2 and Pt-GNS respectively. These hybrids were prepared by depositing alternately a layer of Pt nanoparticles and or Pt nanoparticles with MoS_2/GNS and so on.

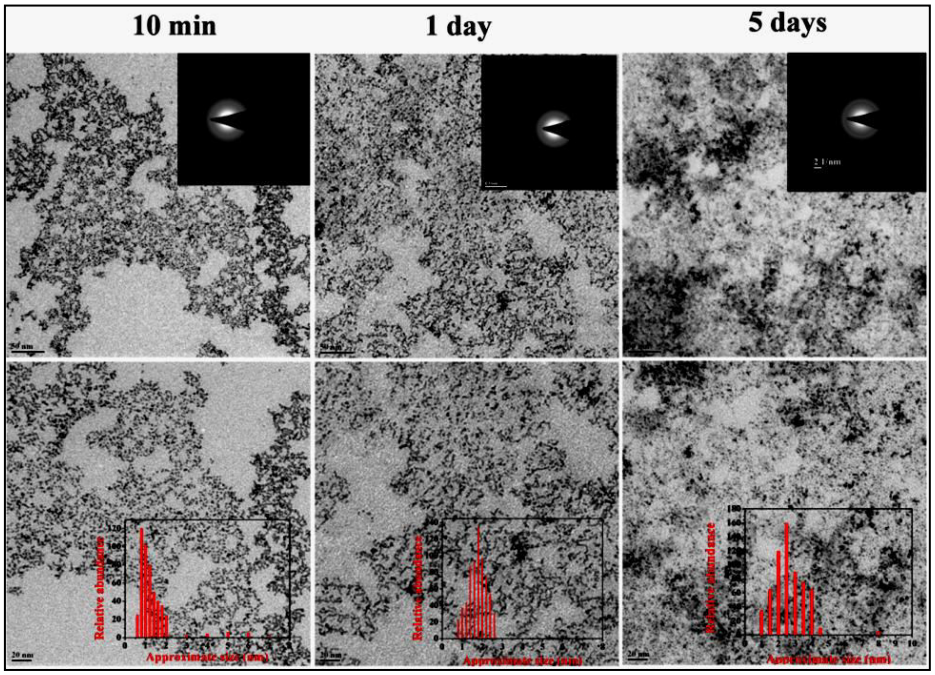

Figure 5.7 Study of kinetics of growth of Pt nanoparticles with respect to the reaction time, inset shows respective electron diffractions and size distribution histograms.

TEM clearly shows that Pt nanoparticles with uniform size are stabilized on the surface of MoS_2/GNS. The average particle size of the Pt nanoparticles on both graphene and MoS_2 is 1.9 nm. Thus, an end result signifies that Pt metal nanoparticles are dispersed on the MoS_2/GNS surface uniformly.

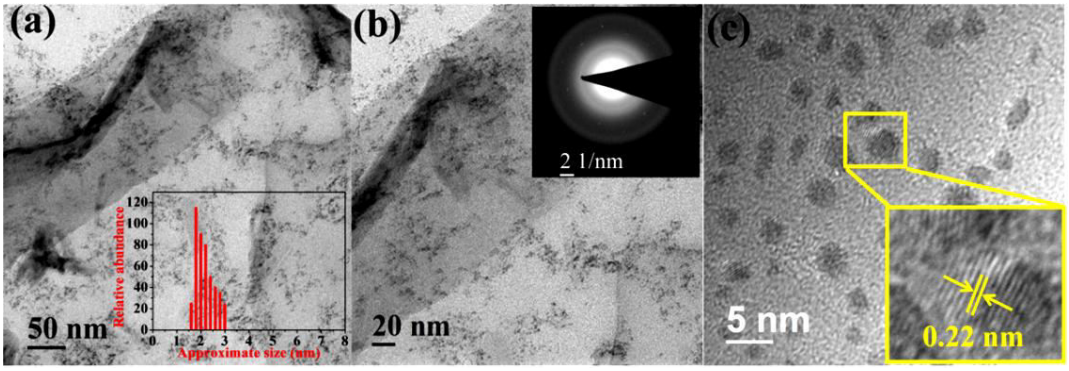

Figure 5.8 (a) TEM image of Pt nanoparticles distributed over MoS_2nanosheets. (b) TEM image at higher magnification, inset shows electron diffraction pattern for Pt-MoS_2. (c) HRTEM image of Pt-MoS_2, inset showing lattice fringe distance of 0.22 nm corresponding (111) plane of Pt.

The calculated d values from the ring pattern in both Pt-MoS_2 and Pt-GNS are 2.22Å (111) and 1.17Å (311) which match with those reported for pure Pt metal (JCPDS, PDF#040802). HRTEM images of the Pt-MoS_2 and Pt-GNS are shown in Figure 5.8c and 5.9c respectively. It shows lattice fringes for Pt nanoparticles. The lattice fringe distance of 0.22 nm matches with that of face centred cubic (fcc) Pt (111) plane (JCPDS, PDF#040802).

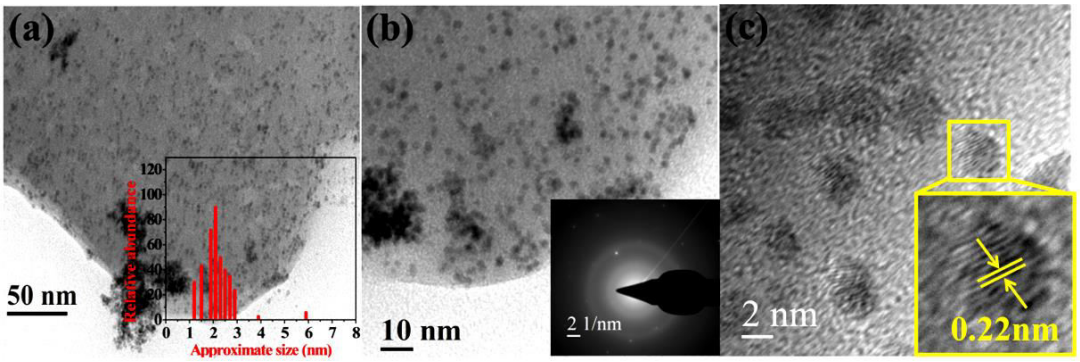

Figure 5.9 (a) TEM image of Pt nanoparticles distributed over GNS. (b) TEM image at higher magnification, inset shows electron diffraction pattern for Pt-GNS and (c) HRTEM image of Pt-GNS, inset showing lattice fringe distance of 0.22 nm corresponding (111) plane of Pt.

5.3.4 Scanning electron microscopy (SEM) and EDS

The presence of respective elements in the Pt nanoparticles, Pt-MoS_2 and Pt-GNS nanocomposites were further confirmed by energy dispersive spectroscopy (EDS) as shown in Figure 5.10 and Figure 5.11ab.

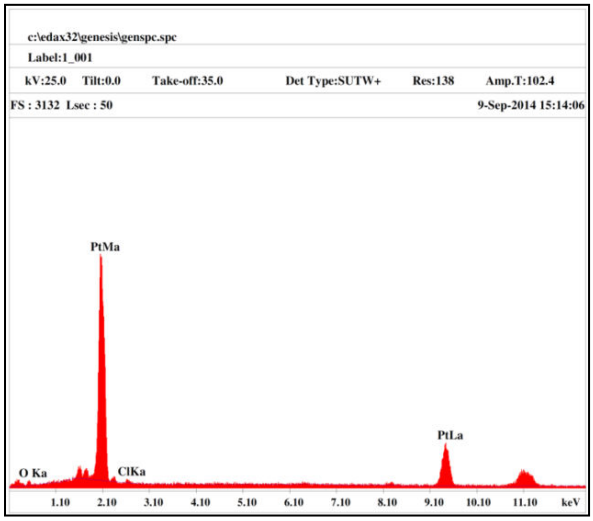

Figure 5.10 EDX for Pt nanoparticles thin film over silicon wafer.

The EDS spectrum shows the peaks corresponding to C, O, Pt, Mo and S elements, confirming the formation and deposition of Pt nanoparticles on MoS_2 and GNS in the respective samples.

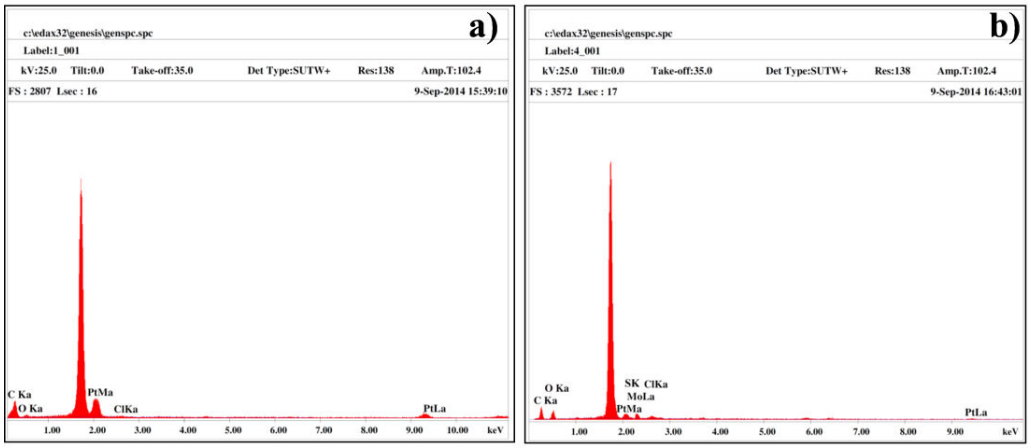

Figure 5.11 EDX for a) Pt-GNS and b) Pt-MoS_2 composite over silicon wafer.

Effect of chemical environment on the surface morphology of catalysts composites for the duration of the electrochemical study was also revealed through the SEM imaging before and after the electrochemical experiment (ECE).

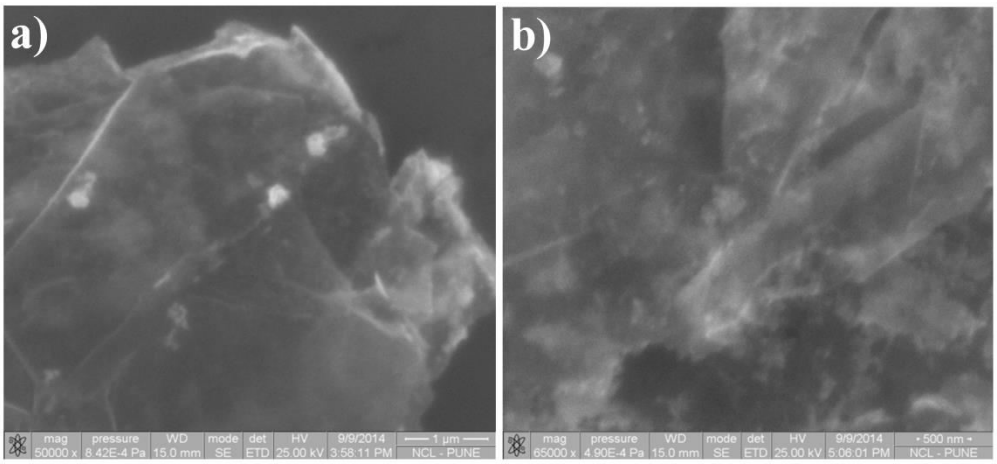

Figure 5.12 SEM image for a) Pt-GNS and Pt-MoS_2composite before electrochemical measurements.

From Figure 5.12ab and Figure 5.13ab, it is seen that both the catalysts remain intact morphologically.

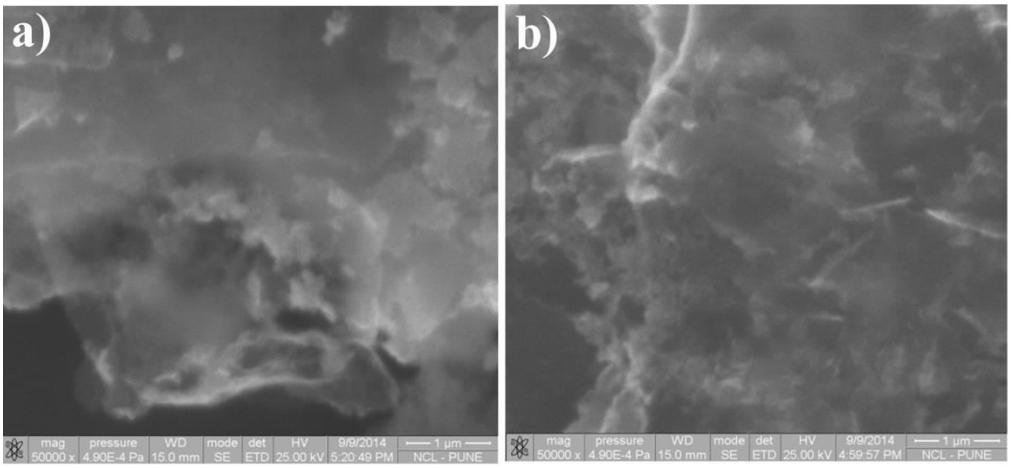

Figure 5.13 SEM image of a) Pt-GNS and b) Pt-MoS_2after the electrocatalytic experiment in 0.5 M H_2SO_4 + 2M methanol at a scan rate of 500 mV/s after the chronoamperometry study for 3600s.

5.3.4 Atomic Force Microscopy (AFM) study

To see actual thickness of the thin film and effect of LbL deposition on interlayer spacing of GNS and MoS_2, an AFM study was employed. As an example the effect of Pt loading over the interlayer spacing of GNS was studied by AFM as shown in Figure 5.14. The samples were coated over the cleaned Si-wafer by using dip coating method described in the experimental section. For an example, 20 dips of GNS were coated over one Si wafer and 20-20 alternated dips of GNS and Pt over another Si

wafer. The height profile in AFM gives the thickness of the film. The height for the 20 dips of GNS is 19.4 nm which gives the average thickness of 0.9 nm for each GNS layer. On the other hand the thickness for Pt-GNS LbL composite of 20-20 alternate dips is 85.8 nm which means the average separation between two graphene layers is 3 nm. Thus, Interlayer spacing has increased. From this study it can be concluded that there is an increase of thickness by one order of size due to Pt nanoparticles in the composite.

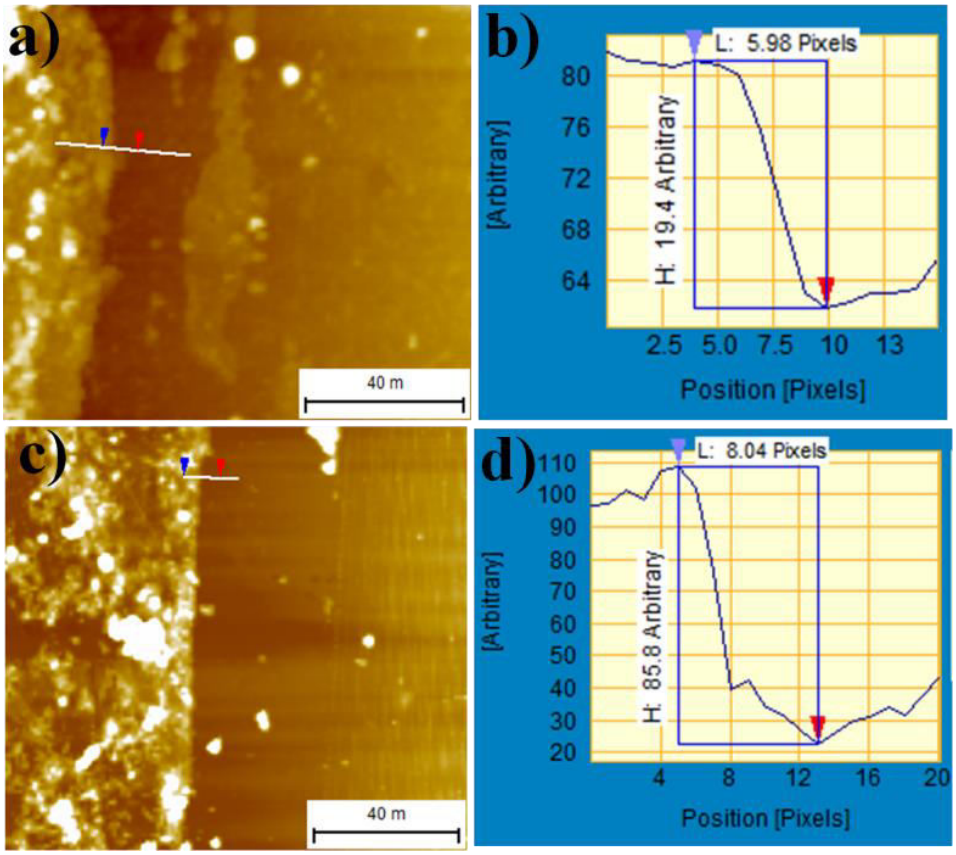

Figure 5.14 (a&c) Atomic force microscopy (AFM) images for the 20 dips coated graphene nanosheets (GNS) and 20-20 alternate Pt-GNS coated LbL composite, (b&d) height profile for a and b respevtively.

5.4 Electrochemical characterization.

5.4.1 Cyclic Voltametry (CV)

For the formation of hybrid electrodes, Pt nanoparticulate thin films were deposited on FTO coated glasses along with MoS_2 and GNS respectively. CV curves observed for Pt and Pt composite hybrid electrodes are shown in Figure 5.15. CV

curves for Pt-GNS, Pt-MoS_2, Pt nanoparticles thin film and commercial Pt/C electrodes show similar features to those shown by CV of Polycrystalline Pt electrode. From the Figure 5.15, an electrochemical active surface area (ECSA) was calculated from the equation,[54] by integrating the charge under the hydrogen desorption curve as explained bellow,

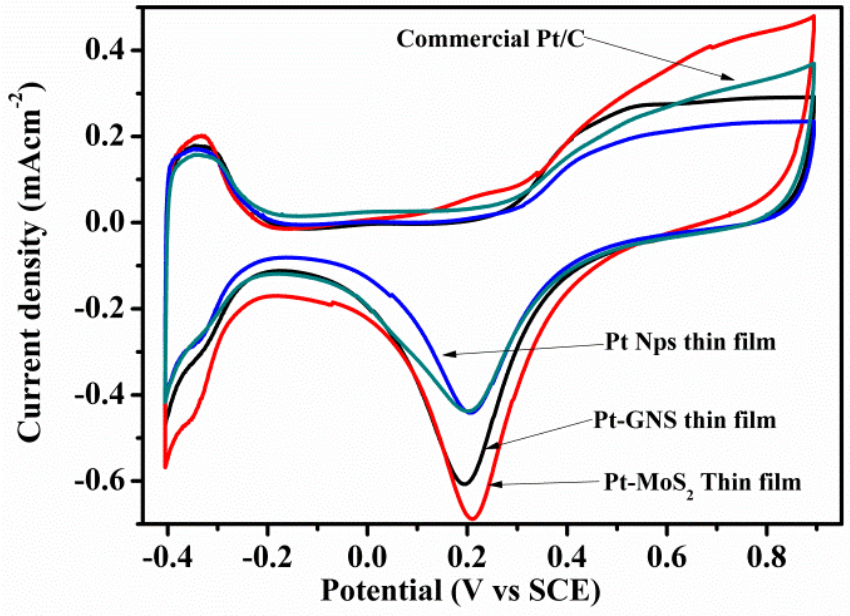

Figure 5.15 Cyclic voltammogram of Pt-MoS_2, Pt-GNS, Pt nanoparticles, and commercial Pt/C catalyst, coated over FTO glass and in 0.5 M H_2SO_4 solution at scanning rate 50 mV/s vs. SCE.

$$\textbf{ECSA}\ (cm^2Pt/gPt) = qPt / \Gamma * L \qquad (1)$$

Where,

qPt is the charge density,

Γ = 210 $\mu C/cm^2$ and L = gPt/cm^2 (the Pt content or loading in the electrode).

ECSA values were found to be 13.4, 13, 10.8 and 10.4m^2/g, for Pt-MoS_2, Pt-GNS, Pt nanoparticles thin film and Pt/C respectively.

By using the ECSA values and the actual mass of Pt in the electrodes, Intensities for methanol oxidation peaks (mA/cm^2 and mA/mg) were calculated and are tabulated in following table-5.1.

Table 5.1 Relative study between the intensities calculated from geometrical area of the electrodes, an ECSA value for electrodes and by considering the Pt mass in active electrodes.

Sr. No.	Sample	Intensities of Methanol oxidation peak calculated by considering geometrical area of the electrode (mA/cm^2)	Intensities calculated by considering ECSA of electrodes. mA/cm^2	Intensities calculated by considering the Pt mass in active electrodes (mA/mg)
1	Pt-MoS_2	3.07	13.23	177.4
2	Pt-GNS	2.61	10.53	137.5
3	Pt-nanoparticles	0.977	5.13	55.51
4	PT/C	0.772	3.18	33.16

5.4.2 Electrochemical impedance spectroscopy (EIS)

Electrochemical Impedance Spectroscopy (EIS) gives information concerning the internal resistance of an electrode material as well as the resistance between the electrode and electrolyte. Impedance spectra for Pt-MoS_2 and Pt-GNS are shown in Figure 5.16. The spectra are analyzed using Nyquist plots.

A semicircle in high frequency region is related to the charge transfer resistance and a straight line in low frequency region represents an ideal capacitive behaviour. The diameter of the fitted circle is equal to the electrode resistance arising from the charge transfer resistance (Rct) in the cell.[51, 55]

The resistance (Rs) for the Pt-GNS composite and Pt-MoS_2 composite was found to be 8.6 and 10.94 Ω respectively. The charge transfer resistance (Rct) was measured to be 5.3 and 6.7 Ω for Pt-GNS and Pt-MoS_2 respectively.

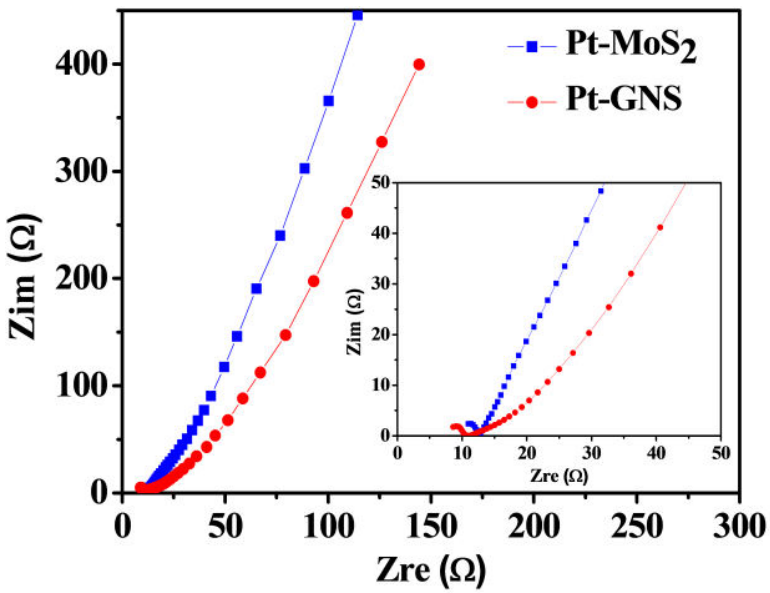

Figure 5.16 Electrochemical Impedance Spectroscopic results for Pt-GNS and Pt-MoS_2 electrode in 0.5 M H_2SO_4. Inset shows magnified portion in the high frequency region.

5.4.3 Cyclic voltammetry (CV) and linear sweep voltammetry (LSV) and chronoamperometry/ durability study of catalysts for methanol oxidation.

The electrocatalytic performance of Pt-GNS and Pt-MoS_2 for methanol oxidation was investigated by cyclic voltamogram (CV) in an electrolyte 0.5 M H_2SO_4 solution containing 1.0 M CH_3OH. As shown in Figure 5.17, bare FTO electrode does not show any electrocatalytic activity toward the oxidation of methanol. On the other hand, CV using Pt-MoS_2 nanocomposite electrode shows remarkable catalytic activity, displaying prominent methanol oxidation peaks in both positive and reverse potential scans at 0.53 V and 0.33 V respectively (versus SCE). It is attention grabbing to observe lower onset potentials for methanol oxidation at 0.17 V and 0.25 V for Pt-MoS_2 and Pt-GNS respectively; as against the onset potentials for methanol oxidation for bare Pt electrode > 0.31 V and commercial Pt/C electrode (0.35V). The importance of the 'on set potential' is discussed in the literatures like, Pt/CCG,[56] Pt/RGO,[57] Pt nanoflowers/RGO/CC[58] and Pt/graphene.[41] The importance of the present architecture of Pt-MoS_2 and Pt-GNS nanocomposites in improving electrochemical catalytic activity toward the methanol oxidation proves to be meritorious. For the Pt-GNS composite, in the forward potential scan, the methanol

oxidation peak is observed at about 0.53 V (versus SCE). The current density is observed to be at 2.6 mA.

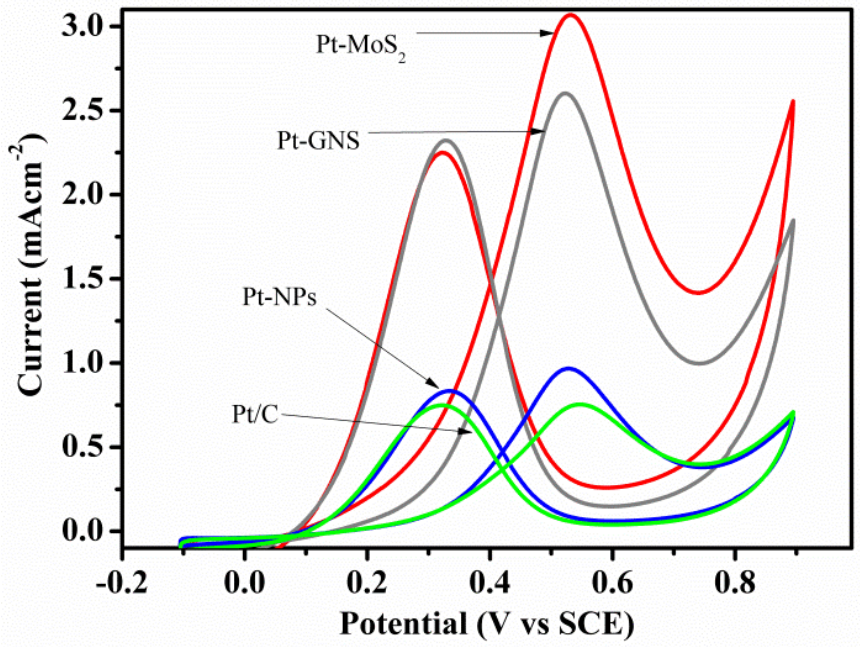

Figure 5.17 CV of Pt-MoS_2, Pt-GNS, Pt nanoparticles and commercial Pt/C catalyst substrate in 0.5 M H_2SO_4 solution + 1M methanol solution at scanning rate of 50 mV/s.

In the reverse potential scan, oxidation peak is observed at ~0.35 V (versus SCE), having a current density of 2.2 mA. Furthermore, most interestingly, for Pt-MoS_2 composite, the peak current densities and potentials are 3.12 mA at 0.53 V and for Pt-GNS; it is 2.16 mA at 0.33 V (versus SCE) in the forward and reverse potential scans respectively. The current intensity/cm^2 was calculated by considering actual geometric areas as shown in Figure 5.17 of the electrode as well as by ECSA. The comparison is given in Table 5.1. All these results were further reproduced with linear sweep voltammetry as shown in Figure 5.18.

In the forward cycle, the desired reaction of oxidation of methanol occurs on Pt surface which is reflected by I_f. However, one of the decomposition products, namely, CO or/and similar carbonaceous matter has affinity towards Pt surface so that it gets adsorbed on it. In its presence, further oxidation would be prevented; poisoning the catalyst. Incidentally, in the reverse cycle, these 'poisoning' species get oxidized in presence of adsorbed H_2O, with the regeneration of active sites for further reaction, reflected by I_b. The efficiency of such regeneration of active sites is reflected by the

ratio I_f/I_b, provided methanol is uninterruptedly available to get adsorbed on Pt active sites. In other words, ratio I_f/I_b indicates the tolerance of catalyst towards 'poisoning.'[59, 60]

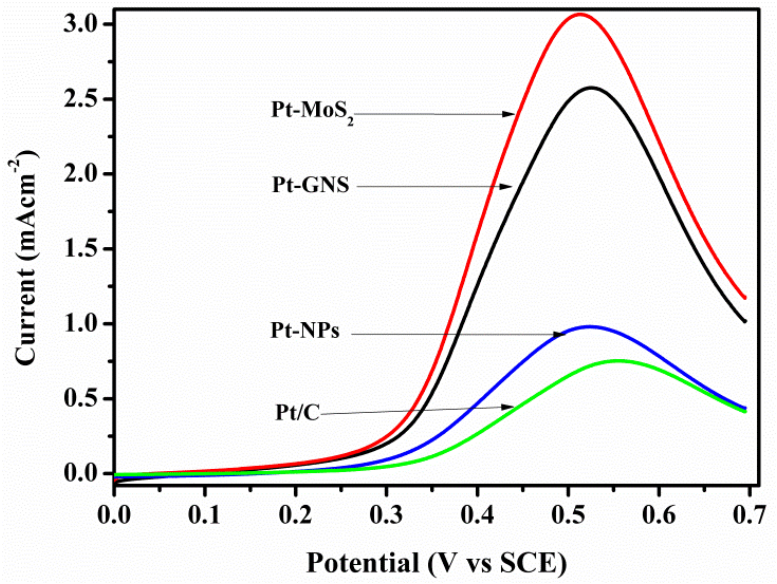

Figure 5.18 Linear sweep voltammograms (LSV) for Pt-MoS2, Pt-GNS, Pt nanoparticles thin film and commercial Pt/C catalyst for the electrocatalytic oxidation of 0.1 M methanol in 0.5 M H_2SO_4 solution with reference to SCE.

The mechanism is represented by the equations as given below. A higher ratio implies more effective removal of the poisoning species from the catalysts surface. The I_f/I_b ratio is about 1.10, 1.18 and 1.44 for Pt nanoparticles, Pt-GNS and Pt-MoS_2 respectively. Such a high value of I_f/I_b indicates that the Pt-MoS_2 has less retention of carbon containing moieties formed during the catalytic reaction and hence is proves to be much more tolerant toward 'CO poisoning'. It indicates that the composite catalyst with the reported architecture is highly efficient for the desired methanol oxidation reaction. However, some inherent by-products of the reactions consisting of mainly CO and other carbonaceous species are likely to 'poison' the course of further reaction. These 'poisoning' species would lower I_f/I_b ratio. For Pt/MoS_2 composite, I_f/I_b ratio is the highest, indicating that poisoning species mostly get eliminated during the complete scan-cycle.[61] It is clear that the composite electrode of present study reports one of the highest ratios I_f/I_b reported so far for methanol oxidation; from the comparison of data given in the following Table 5.2.

Table 5.2 Summarised I_f/I_b values for different electrodes.

Electrode type	I_f/I_b	Reference
Pt-MoS_2	1.44	Present work
Pt-GNS	1.18	Present work
Pure Pt nanoparticles	1.10	Present work
Commercial Pt/C	0.95	Present work
Pt/Chemically converted GNS	0.83	55
Commercial ETEK catalyst	0.74	59
Pt-on-Pd bimetallic nanodendrites supported on graphene nanosheets	1.25	60
Pt/CNT	1.4	61

The same arguments hold good for Pt/GNS also. The other factors that help efficient catalytic activity are ascribed to the uniformly dispersed small Pt particles in the composites.[62]The elimination of adsorbed CO/'C' containing intermediates can be described through the following reactions.[63-65] Possible mechanism of CO electro-oxidation on the Pt-MoS_2 and Pt-GNS catalyst can be explained by equations (2- 5).

$$\text{Pt-MoS}_2 + \text{H}_2\text{O} \longrightarrow [\text{Pt-MoS}_2]\,(\text{OH})_{ads} + \text{H}^+ + \text{e}^- \quad (2)$$

$$\text{Pt-GNS} + \text{H}_2\text{O} \longrightarrow [\text{Pt-GNS}]\,(\text{OH})_{ads} + \text{H}^+ + \text{e}^- \quad (3)$$

$$\text{Pt-CO}_{ads} + [\text{Pt-MoS}_2]\,(\text{OH})_{ads} \longrightarrow 2\text{Pt} + \text{CO}_2 + \text{H}^+ + \text{e}^- \quad (4)$$

$$\text{Pt-CO}_{ads} + [\text{Pt-GNS}]\,(\text{OH})_{ads} \longrightarrow 2\text{Pt} + \text{CO}_2 + \text{H}^+ + \text{e}^- \quad (5)$$

We propose that the maximum interface formed by the LbL architecture is responsible for the CO tolerance improvement. It is known that CO gets strongly adsorbed on Pt surface.[66] From equations 2 and 3, it is clear that H_2O be present at the site where CO is adsorbed on Pt to form the species [Pt-MoS_2] (OH) ads. These species further react with another Pt site where CO is adsorbed to regenerate active Pt sites (equation 4). The said catalytic process would be most favoured with maximum interface between MoS_2 and adequate density of Pt particles which exactly is the feature of the presented architecture.

5.4.4 XPS study of catalysts after the electrocatalytic experiments.

A very similar mechanism holds good for Pt-GNS composite.[67] The presence of oxygen moieties at the edges and defects of GNS and sulphur planes in MoS_2 structure promotes water adsorption on the composite catalyst surface through a hydrogen bond formation. Consequently, more OH_{ads} species are formed by dissociation of water on the composite catalyst surface as in equations 1 and 2. Subsequently, the formation of Pt-MoS_2 $(OH)_{ads}$ and Pt-GNS $(OH)_{ads}$ (equations 1 and 2) facilitate CO oxidation to CO_2 as in equations 3 and 4; ultimately resulting in the significantly decreasing amount of CO on Pt composite catalysts. This is well supported by the XPS study as shown in Figure 5.19 and 5.20.

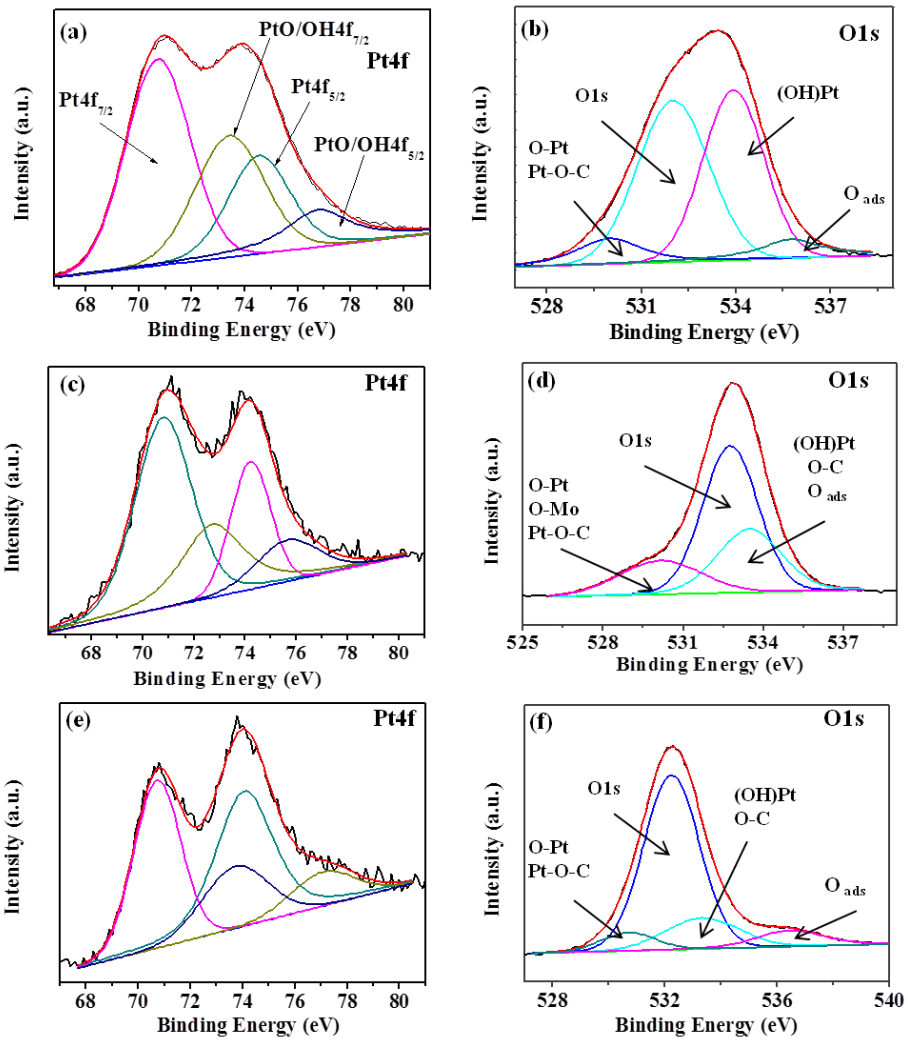

Figure 5.19 Pt4f and O1s respectively in (a,b) Pt nanoparticles, (c,d) Pt-MoS_2 (e,f) Pt-GNS, after the electrochemical reaction.

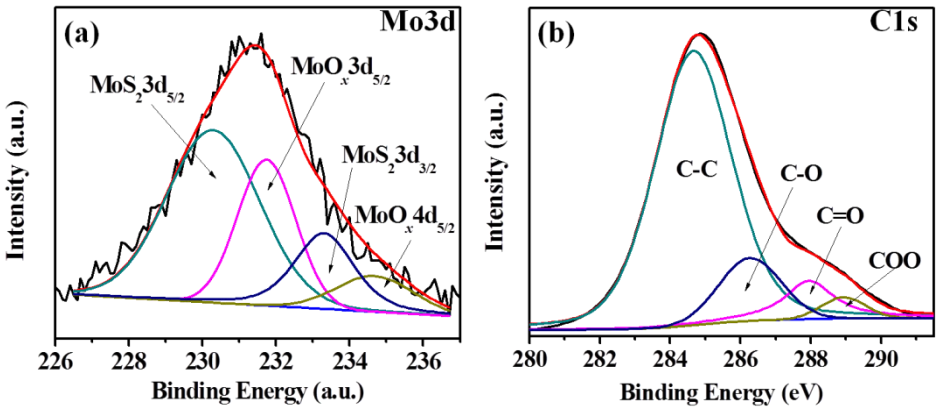

Figure 5.20 a) Mo 3d and b) C1s in MoS_2 and GNS respectively after the electrocatalytic oxidation of methanol and chronoamperometry study.

The quantitative estimation of elemental composition and different species formed at surfaces is rather very important factor in catalyst performance; therefore XPS spectra were deconvoluted and evaluated for the quantity of different species present at the surface. Following table 5.3 shows the detailed analysis of all the catalyst electrodes before and after the electrocatalytic reactions.

Table 5.3 Quantitative measurement of elemental and chemical composition for catalysts used before and after Electro-Chemical Experiment (ECE) by using an XPS.

Sample	Main peak	Deconvoluted peak(s)	Binding energy position (in eV)	Atomic %	FWHM	Species/ moiety
Pt nanoparticles (before ECE)	Pt4f	$4f_{7/2}$	70.70	93.6	2.36	Pt^0
		$4f_{5/2}$	74.01		2.31	
		$4f_{7/2}$	72.73	6.4	1.82	Pt-O*x*
		$4f_{5/2}$	75.99		1.75	
Pt nanoparticles (After ECE)	Pt4f	$4f_{7/2}$	70.87	65.5	2.36	Pt^0
		$4f_{5/2}$	75.09		3.03	
		$4f_{7/2}$	73.55	34.5	2.30	Pt-O*x*
		$4f_{5/2}$	77.32		3.08	
C in GNS	C1s	C1s	284.46	75.5	2.59	C-C
		C1s	287.75	9.1	1.68	C-O
		C1s	288.73	3.1	1.49	C=O

		C1s	286.07	12.4	2.09	COO
C in Pt-GNS (Before ECE)	C1s	C1s	284.6	86	1.90	C-C
		C1s	285.62	7.5	1.89	C-O
		C1s	286.89	4.4	1.89	C=O
		C1s	288.28	1.5	1.62	COO
C in Pt-GNS (after ECE)	C1s	C1s	284.61	83.8	2.83	C-C
		C1s	287.35	12.7	2.55	C=O
		C1s	288.96	3.3	1.60	COO
Pt in Pt-GNS (Before ECE)	Pt4f	$4f_{7/2}$	70.70	90.6	2.35	Pt^0
		$4f_{5/2}$	74.15		2.31	
		$4f_{7/2}$	72.73	9.4	1.82	Pt-O*x*
		$4f_{5/2}$	75.99		1.75	
Pt in Pt-GNS (After ECE)	Pt4f	$4f_{7/2}$	70.8	71.9	2.62	Pt^0
		$4f_{5/2}$	74.20		1.83	
		$4f_{7/2}$	72.71	28.1	2.88	Pt-O*x*
		$4f_{5/2}$	75.65		2.88	
Mo in MoS_2(Before ECE)	Mo3d	$3d_{5/2}$	230.14	99.9	1.51	Mo-S-Mo
		$3d_{3/2}$	233.29		1.78	
Mo in MoS_2(After ECE)	Mo3d	$3d_{5/2}$	230.29	66.2	2.98	Mo-S-Mo
		$3d_{3/2}$	231.74		1.86	
		$3d_{5/2}$	234.69	33.78	2.48	Mo-O*x*
		$3d_{3/2}$	233.31		1.90	
Pt in Pt-MoS_2 (Before ECE)	Pt 4f	$4f_{7/2}$	70.47	86.78	2.94	Pt^0
		$4f_{5/2}$	73.73		2.45	
		$4f_{7/2}$	73.42	13.21	1.59	Pt-O*x*
		$4f_{5/2}$	76.73		2.75	
Pt in Pt-MoS_2 (After ECE)	Pt 4f	$4f_{7/2}$	70.72	73.2	2.59	Pt^0
		$4f_{5/2}$	74.10		2.12	
		$4f_{7/2}$	73.72	26.8	2.88	Pt-O*x*
		$4f_{5/2}$	77.15		2.97	

Thus, the removal of species on the catalyst sites by electrocatalytic reaction as indicated in equations 4 and 5 become 'CO tolerance providing steps' in the overall process of methanol oxidation. In the absence of events of these reactions, the

catalysts would have been poisoned. The highest activity of Pt-MoS_2 shown in the present study can be attributed to more number of adsorption sites (Sulphur) for water molecule as compared to GNS.

It must be pointed out that 'S' species in MoS_2 would be present on the whole surfaces forming a layer of MoS_2 as against 'O' containing species in GNS would be present, mostly at the edges and defects of layered GNS, so that surface area of MoS_2 is more effectively used than that in the case of GNS. Also, as Mo in MoS_2 could bind with CO molecules, more Pt surface would be available for methanol oxidation.

The enhanced electrocatalytic activity may be attributed to following reasons, 1) The nanoparticles are ultra-small and well dispersed on MoS_2 or GNS surface which allows utilization of maximum surface area of metal atoms. 2) The use of LbL technique for synthesizing the composites have offered several advantages, namely, i) totally avoiding Pt particles aggregation/agglomeration, ii) the stacking of support layers is prevented by the presence of sandwiched Pt film, iii) an electrolyte has an easy access to catalyst particle surface, iv) the support layers are known to be good charge carriers which facilitate electrochemical reaction. 3) No surfactants or templates are used during the synthesis of composites so that the surfaces of metal component or supports are not covered by materials, not taking part in the catalytic reaction. 4) The architecture of the sample formed by present method is most suitable so that Pt and support have maximum interface which is known to be more active for CO oxidation;[63] which leads to maximize the efficiency and minimize the poisoning.

Figure 5.21 shows a plot of the current density for methanol electro-oxidation on Pt nanoparticles, Pt-MoS_2 and Pt-GNS catalyst electrodes as a function of time. The fall down of current density with the increased cycle numbers can be ascribed to the lowering of active area of the catalyst due to the adsorbed species formed as intermediates such as CO_{ads}, CH_3OH_{ads}, and CHO_{ads} on the catalyst surface during the methanol oxidation reaction,[37, 57, 68] i.e. poisoning the Pt nanoparticles catalyst for methanol oxidation. Figure 5.21 shows CA study which reveals the stability of various electrodes. From Figure 5.21 it can be seen that Pt-MoS_2 catalyst electrode shows higher current density as a function of time. Pt-GNS catalyst electrode shows reasonably stable current density over the time as against significant decrease in current density with time shown by bare Pt nanoparticles electrode.

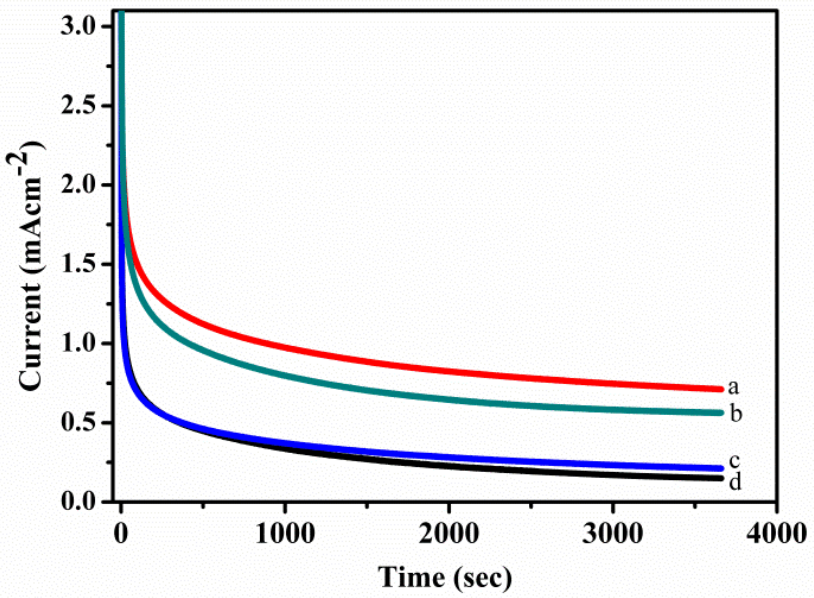

Figure 5.21 Chronoamperometric response of oxidation of 0.1 M methanol at the Pt-MoS_2 (a), Pt-GNS (b), commercial Pt/C catalyst (c) and Pt nanoparticles electrode (d) in 0.5 M H_2SO_4 solution under a constant potential of 0.5 V (versus SCE).

The retention of catalytic activity was found in order from of Pt-GNS >Pt-MoS_2> Commercial Pt/C catalyst >Pt nanoparticles electrode as shown in figure 5.21. However in cases of both the composites, the major fall occurred in initial 500 seconds which is due to the formation of intermediates during methanol oxidation reaction[69-71] and still retains comparable higher current than Pt nanoparticles thin film and Pt/C. On the other hand bare Pt nanoparticles and commercial Pt/C showed lower catalytic current after 3600 seconds also. These results are consistent with the observations in XPS study as shown earlier. To get the real insight of the mechanism of methanol oxidation, XPS study was further extended for the catalysts recovered after the electrochemical measurements. XPS spectra of Pt 4f in Pt nanoparticles, Pt-MoS_2 and Pt-GNS with their respective O1s (See, Figure 5.21) reveals that the extent of oxidation is higher in bare Pt nanoparticles catalyst as against both Pt-MoS_2 and Pt-GNS which show less oxidation. This confirms that these composite materials (Pt-MoS_2 and Pt-GNS) have higher stability than the bare Pt catalysts. Moreover the stability of supports was also revealed through careful observation of their corresponding deconvoluted XPS spectra. An XPS spectrum of Mo3d in MoS_2 and C1s in GNS after the electrocatalytic experiment is given in Figure 5.20. Both the supports showed broad asymmetric XPS peaks which can be attributed to bound bi-

product CO and adsorbed OH groups on supports (i.e. MoS_2 and GNS) surface. Table 5.3 shows the quantitative estimation of presence of different moieties in all the catalysts used before and after the electrocatalytic reaction. Thus, the data confirms that the support (MoS_2/GNS) shields Pt nanoparticles' surface and let it be free for methanol oxidation reaction. This proves the mechanism discussed earlier. Thus, this method offers better and stable catalysts than most of the conventional Pt based catalysts prepared and reported so far.

5.5 Conclusion

Using earlier reported methods of thin film formation of MoS_2 and GNS along with an elaborately described method of formation of Pt thin film consisting of particles of size in the range 1.5 to 2.5 nm and applying LbL technique, composite thin films namely Pt-MoS_2 and Pt-GNS are reported and used for electro-catalytic methanol oxidation. The suggested mechanism shows that MoS_2 and GNS not only act as a support to Pt nanoparticles but also complement enhanced electro-catalytic activity of Pt by improving CO tolerance. The electrochemical tests show that the Pt nanoparticles supported on MoS_2 and GNS have a higher catalytic activity than that of Pt/C. An important achievement in the present novel architectural design of the electrode is lower onset oxidation potential maintaining best I_f/I_b ratio reported so far. It is observed that the present composites showed better stability for reuse in comparison to stability shown by commercial Pt-C catalyst. The presently reported method of formation of composites displayed improved electrocatalytic activity for methanol oxidation which can widen the scope of fuel cell electrode fabrication.

5.5 References

[1] C. V. Rao and B. Viswanathan, *J. Phys. Chem. C,* 2010, **114**, 8661.

[2] X. Zhao, M. Yin, L. Ma, L. Liang, C. P. Liu, J. H. Liao, T. H. Lu and W. Xing *Energy Environ. Sci.*, 2011,**4**, 2736.

[3] D. X. Cao and S. H. Bergens, *Electrochim. Acta*, 2003, **48**, 4021.

[4] B. C. H. Steele and A. Heinzel, *Nature*, 2001, **414**, 345.

[5] E. Antolini, *Mater. Chem. Phys*. 2003, **78**, 563.

[6] D. Zhao and Bo-Qing. Xu, *Angew. Chem.*, 2006, **118**, 5077.

[7] H. A. Gasteiger, S. S. Kocha, B. Sompalli and F. T. Wagner, *Appl. Catal. B*, 2005, **56**, 9.

[8] Y. Mu, H. Liang, J. Hu, L. Jiang and L. Wan, *J. Phys. Chem. B,* 2005, **109**, 22212.

[9] J. L. Fernandez and A. J. Bard, *Anal. Chem.*, 2003,**75**, 2967.

[10] S. Cheng, R. E. Rettew, M. Sauerbrey and F. M. Alamgir, *ACS Appl. Mater. Interfaces*, 2011, **3**, 3948.

[11] R. Borup, J. Meyers, B. Pivovar, Y. S. Kim, R. Mukundan, N. Garland, D. Myers, M. Wilson, F. Garzon, D. Wood, P. Zelenay, K. More, K. Stroh, T. Zawodzinski, J. Boncella, J. E. McGrath, M. Inaba, K. Miyatake, M. Hori, K. Ota, Z. Ogumi, S. Miyata, A. Nishikata, Z. Siroma, Y. Uchimoto, K. Yasuda, K.-i. Kimijima and N. Iwashita, *Chem. Rev.*, 2007, **107**, 3904.

[12] H. Gao, S. Liao and J. Zeng, Y. Xie, *J. Power Sources,* 2011, **196**, 54.

[13] A. Galal, N. F. Atta, S. A. Darwish and S. M. Ali, *Top Catalysis*, 2008, **47**, 73.

[14] Y. Hu, H. Zhang, P. Wu, H. Zhang, B. Zhou and C. Cai, *Phys. Chem. Chem. Phys*., 2011,**13**, 4083.

[15] B. J. Hwang, S. M. S. Kumar, C. H. Chen, Monalisa, M. Y. Cheng, D. G. Liu, J. F. Lee, *J. Phys. Chem. C* 2007, **111**, 15267.

[16] F. H. B. Lima, E. A. Ticianelli, *Electrochim. Acta* 2004, **49**, 4091-4099.

[17] S. Mukerjee, S. Srinivasan, M. P. Soriaga, *J. Phys. Chem.* 1995, **99**, 4577-4589.

[18] F. J. Lucazk, D. A. Landsman, U.S. Patent 4447506, 1984.

[19] S. Mukerjee, S. Srinivasan, *J. Electroanal. Chem.* 1993, **357**, 201-224.

[20] Z. H. Zhou, S. Wang, Zhou, W. J. Wang, G. X. Jiang, L. H. Li, W. Z. Song, S. Q. Liu, J. G. Sun and G. Q. Xin, Q. *Chem. Commun*., 2003, 394.

[21] M. Arenz, J. Karl, K. J. J. Mayrhofer, V. Stamenkovic, B. B. Blizanac, T. Tomoyuki, P. N. Ross and N. M. Markovic, *J. Am. Chem. Soc*., 2005, **27**, 6819.

[22] H. Bonnemann and R. M. Richards, *Eur. J. Inorg. Chem.*, 2001, 2455.

[23] J. Zhao, H. Yu, Z. Liu, M. Ji, L. Zhang and G. Sun, *J. Phys. Chem. C*, 2014, **118**, 1182.

[24] M.Y. Wang, J. H. Chen, Z. Fan, H. Tang, G. H. Deng and D. L. He, *Carbon*, 2004, **42**, 3257.

[25] S.-Y. Huang, P. Ganesan and B. N. Popov, *Appl. Catal. B.*2009, **93**, 75.

[26] B. K. Balan and S. Kurungot, *Inorg. Chem.*, 2012, **51**, 9766.

[27] R. -Z. Yang, X. -P. Qiu, H. -R. Zhang, J. -Q. Li, W. -T. Zhu, Z. -X. Wang, X. -J. Huang and L.-Q. Chen, *Carbon*, 2005, **43**, 11.

[28] D. S. Yuan, C. W. Xu, Y. L. Liu, S. Z. Tan, X. Wang, Z. D. Wei and P. K. Shen, *Electrochem. Commun.*, 2007, **9**, 2473.

[29] G. F. Zou, J. Lu, D. B. Wang, L. Q. Xu and Y. T. Qian, *Inorg. Chem.*, 2004, **43**, 5432.

[30] G. S. Chai, S. B. Yoon, J. H. Kim and J. S. Yu, *Chem. Commun.,* 2004, **23**, 2766.

[31] K. S. Novoselov, A. K. Geim, S. V. Morozov, D. Jiang, M. I. Katsnelson, I. V. Grigorieva, S. V. Dubonos and A. A. Firsov, *Nature*, 2005, **438**, 197.

[32] G. Eda, G. Fanchini and M. Chhowalla, *Nat. Nanotechnol.*, 2008, **3**, 270.

[33] S. Stankovich, D. A. Dikin, G. H. B. Dommett, K. M. Kohlhaas, E. J. Zimney, E. A. Stach, R. D. Piner, S. T. Nguyen and R. S. Ruoff, *Nature,* 2006, **442**, 282.

[34] Z. L. Wang, D. Xu, Y. Huang, Z. Wu, L. M. Wang and X. B. Zhang, *Chem. Commun*., 2012,**48**, 976.

[35] Y. Wang, Z. Shi, Y. Huang, Y. Ma, C. Wang, M. Chen and Y. Chen, *J. Phys. Chem. C*, **113**, 2009, 13103.

[36] M. D. Stoller, S. Park, Y. Zhu, J. An and R. S. Ruoff, *Nano Lett*., 2008, **8**, 3498.

[37] Y. Li, L. Tang and J. Li, *Electrochem. Commun*., 2009, **11**, 846.

[38] L. Dong, R. R. S. Gari, Z. Li, M. M. Craig and S. Hou, *Carbon,*2010,**48**, 781.

[39] A. B. Bourlinos, D. Gournis, D. Petridis, T. Szabo and A. Szeri, *Langmuir*, 2003, **19**, 6050.

[40] B. Seger and P. V. Kamat, *J. Phys. Chem. C*, 2009, **113**, 7990.

[41] D. He, K. Cheng, H. Li, T. Peng, F. Xu, S. Mu and M. Pan, *Langmuir*, 2012, **28** 3979.

[42] E. Yoo, T. Okata, T. Akita, M. Kohyama and J. Nakamura, *Nano Lett*., 2009, **9**, 2255.

[43] S. M. Choi, M. H. Seo, H. J. Kim and W. B. Kim, *Carbon*, 2011, **49**, 904.

[44] K. P. Gong, F. Du, Z. Xia, Michael and L. Dai, *Science*, 2009,**323**, 760.

[45] H. Liu, Y. Liu and D. Zhu, *J. Mater. Chem.*, 2011,**21**, 3335.

[46] Ji-eun Park, Y. J. Jang, Y. J. Kim,Mi-sun Song, S. Yoon, D. H. Kim and S.-J. Kim, *Phys. Chem. Chem. Phys*., 2014, **16**, 103.

[47] J.-K. Lee, W. Lee, T.-J. Yoon, G.-S. Park and J.-H. Choy, *J. Mater. Chem*., 2002, **12**, 614.

[48] X. Huang, Z. Zeng, S. Bao, M. Wang, X. Qi, Z. Fan and H. Zhang, *Nat. Commun*., 2013,**4**, 1444.

[49] J. Kim, S. Byun, A. J. Smith, J. Yu and J. Huang, *J. Phys. Chem. Lett*.,2013,**4** 1227.

[50] (a) L. Yuwen, F. Xu, B. Xue, Z. Luo, Q. Zhang, B. Bao, S. Su, L. Weng, W. Huang and L. Wang, *Nanoscale*, 2014,**6**, 5762. (b) C. Zhai, M. Zhu, D. Bin, F. Ren and C. Wang, *J. Power Sources*, 2015, **275**, 483.

[51] S. Patil, V. Patil, S. Sathaye and K. Patil, *RSC Adv*., 2014,**4**, 4094.

[52] S. Patil, A. Harle, S. Sathaye and K. Patil, *CrystEngComm*., 2014, **16**, 10845.

[53] S. D. Sathaye, K. R. Patil, D. V. Paranjape, A. Mitra, S. V. Awate and A. B. Mandale, *Langmuir*,2000, **16**, 3487.

[54] K. Cooper, *Fuel Cell Magazine*, Jan/Feb 2009, 1.

[55] X. Wang, C. Hu, Y. Xiong, H. Liu, G. Du and X. He, *J. Power Sources*, 2011,**196**, 1904.

[56] Y. Li, W. Gao, L. Ci, C. Wang and P. M. Ajayan, *Carbon*, 2010,**48**, 1124.

[57] S. Sharma, A. Ganguly, P. Papakonstantinou, X. P. Miao, M. X. Li, J. L. Hutchison, M. Delichatsios and S. Ukleja, *J. Phys. Chem. C*, 2010, **114**, 19459.

[58] Z. Yao, M. Zhu, F. Jiang, Y. Du, C. Wang and P. Yang, *j. Mater. Chem.*, 2012, **22**, 13707.

[59] Y. Mu, H. Liang, , J. Hu, L. Jiang and L. Wan, *J. Phys. Chem. B*, 2005, **109**, 22212.

[60] S. Guo, S. Dong and E. Wang, *ACS Nano*, 2010, **4**, 547.

[61] Y. Lin, X. Cui, C. Yen and C. M. Wai, *J. Phys. Chem.B,* 2005, **109**, 14410.

[62] L. Wang and Y. Yamauchi, *Chem. Mater*., 2009, **21**, 3562.

[63] H. Igarashi, T. Fujino and M. Watanabe, *J. Electroanal. Chem*., 1995, **391**, 119.

[64] X. Cheng, Z. Shi, N. Glass, L. Zhang, J. Zhang, D. Song, Z.-S. Liu, H. Wang and J. Shen, *J. Power Sources,* 2007,**165**, 739.

[65] K. Sundmacher, T. Schultz, S. Zhou, K. Scott, M. Ginkel and E. D. Gilles, *Chemical Engneering Science*, 2001, **56**, 333.

[66] T. Ralph, G. Hards, J. Keating, S. Campbell, D. Wilkinson, M. Davis, J. St-Pierre and M. Johnson, *J. Electrochem. Soc*., 1997, **144**, 3845.

[67] C. V. Rao, C. R. Cabrera and Y. Ishikawa, *J. Phys. Chem. C*, 2011, **115**, 21963.

[68] Z. Wen, Q. Wang and J. Li, *Adv. Funct. Mater*., 2008, **18**, 959.

[69] Y. H. Xu and X. Q. Lin, J. Power Sources 2007, **170**, 13.

[70] K. Franaszczuk, E. Herrero, P. Zelenay and A. Wieckowski, *J. Phys. Chem*., 1992, **96**, 8509.

[71] Gasteiger, H.A.; Markovic, N.; Ross, P.N.; Cairns, E.J., J. Phys. Chem. 1993, **97**, 12020.

Chapter-6

6.1 Summery

Renewable alternatives for the fossil fuels are essential necessities of sustainable livelihood for a healthier future. However, uncontrollable nature of such renewable energy sources compels adaptation of highly proficient energy conversion and storage devices as an inevitable prerequisite for availing green-energy to next generation. Amongst a variety of energy storing devices, the electrochemical storage and conversion devices are most important, which comprise of supercapacitors, dye-sensitized solar cells (DSSCs), batteries etc. Such a system comprises of a highly active and efficient electrode-electrolyte interface, which requires simplistic ionic and electron transport throughout the materials to exploit. Making nanomaterials with extended interfaces in the above devices is promising at this perspective as it inflicts tunable physical and chemical properties.

Nanostructuring typically results in low electric and ionic conductivity in conjunction with stability. An inventive way to prevail over the low electric and ionic conductivity along with steadiness is with the help of a support material which offers high conductivity and high surface area. Among the various supported materials, 2-dimensional (2-D) structure seizes better advantages such as superior surface area with continuous electron path etc. Controlled conducting sheets can be utilized to grow active materials on it with tunable morphology and multifunctional properties together with enhanced conductivity, low charge transfer resistance and improved stability. Despite that, high surface area with the 2-D structure provides an easy ion flux and buffer volume changes between its layered-structures, due to expansion-contraction of materials and thus improves in the sustenance of mechanical stress of the materials. Also, no requirement of external binder or conducting ingredients is necessary which helps to reduce the cost of the devices.

The present thesis has addressed some of the issues related to the electrode-electrolyte interfaces of supercapacitors by utilizing various 2-D supporting nanomaterials. Further, efficient electrocatalysts could be fabricated with the same strategy by utilizing the 2-D support due to its ability to form suitable interfaces with the electrolytes. Finally, the future electronic devices require flexibility as an

important criterion for the above energy devices which demands highly efficient flexible electrode materials. An important progress in this direction is proposed to be made during the course of the work by developing a simple and facile method for preparing highly conducting and flexible films which when deposited on conducting substrates can form electrodes, of which usefulness would be proved by their application involving studies on supercapacitor and electrocatalysts. The major contributions of the present thesis are summarized as below:

Facile room temperature methods for formation of graphene thin films and nanoparticulate SnO_2 thin films and their use as prominent component of composite supercapacitor

In this chapter, a novel method to grow thin film of monolayer/few layer graphene is discussed. The method describes reaction, confined to air-water interface, leading to exfoliation of graphite to graphene. Such a reaction has following features. 1) Arrests restacking of graphene layers without using dispersing agents 2) Forms an ultra-thin film of graphene at air-water interface which can be conveniently transferred to substrates.

To effectively overcome the shortcoming of limited specific capacitance of graphene and nanomaterials, namely, SnO_2, MoS_2, PANI, etc; their composites have been considered for the supercapacitor application. Till date, there have been numerous reports on preparing graphene supported Sn-based materials to improve its electrochemical performance. Most of the composites are bulk mixtures of components wherein graphene is not fully exploited for its 2D structure. We proposed an architecture which overcomes such underutilization. There is still a requirement for an efficient and facile route to achieve satisfactory control of such architecture with graphene supported nanocomposites.

Second attractive aspect of this work is that we reported a versatile method to grow thin film of nanoparticulate crystalline SnO_2. The particle size in these films is in the range of 3-5 nm which is an achievement, rarely reported. Also; the method neither employs any dispersing agent to arrest the particle growth nor any capping

agent. Instead, the reaction of formation is confined to air-water interface. Procedurally, the methods to grow thin films of GNS and SnO_2 are similar.

Another feature of the present research is that the GNS and SnO_2 layers can be grown over each other in a desired sequence using LbL assembly (Figure 6.1), forming a matrix of the composite. One can decide the sequence so as to maximize the synergetic effect of components in the desired electrochemical application. Such an architectural structure would be useful in other applications such as, optoelectronic devices, dye-based solar cells, catalysts, gas sensors, electronic devices and electrode materials.

An additional feature of the presently developed technique is the applicability of modified LbL technique to fabricate SnO_2/GNS composite hybrid films with a well-defined architecture and tunable thickness on various substrates for applications such as supercapacitors. The obtained hybrid films having interconnected network prevented graphene sheets from stacking with one-another and simultaneously preventing the growth of SnO_2 particles.

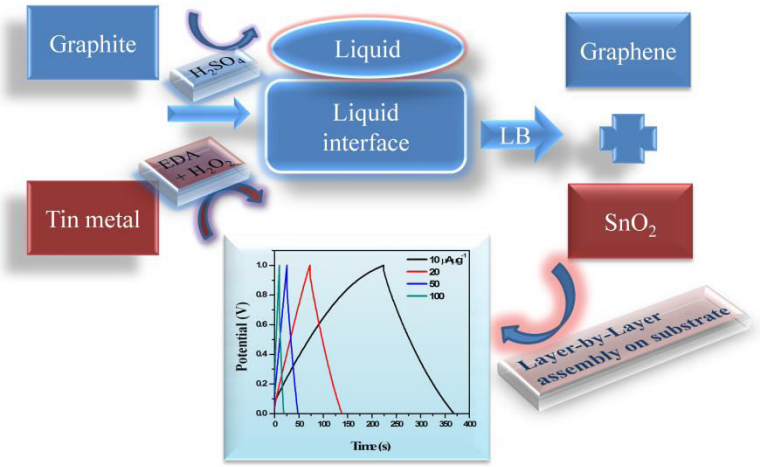

Figure 6.1. Schematic representation of SnO_2/GNS composite.

This is the proof of the concept of forming graphene semi-conductor composite with a predetermined architecture by the reported technique and opens a new area for forming better capacitors. The CV results indicated good capacitive behavior for SnO_2/GNS nanocomposites. The excellent specific capacitance of 472 Fg^{-1} calculated from CV and 471 Fg^{-1} calculated from charge-discharge measurement.

Also, composite has very good cycling stability. All these characteristics show that as-synthesized nanocomposite is a potential candidate for super-capacitor application and in an energy storage technology in future. The excellent electrochemical performance of the composite as supercapacitor electrodes is due to the synergistic effects among the components in the composites.

Development of a method to grow MoS_2 mono/few-layer films and MoS_2-graphene hybrid films for supercapacitor applications

It can be inferred from the available literature that bottom up of forming layered MoS_2 processes are energy intensive while top down processes necessarily need more than one step. Therefore, a 'top-down' single step process would be a desirable step forward in the research of layered MoS_2.

Composite's formation is shown to improve the energy storage capacity as compared to the capacity of singular components as in the case of graphene-SnO_2 composite discussed above.

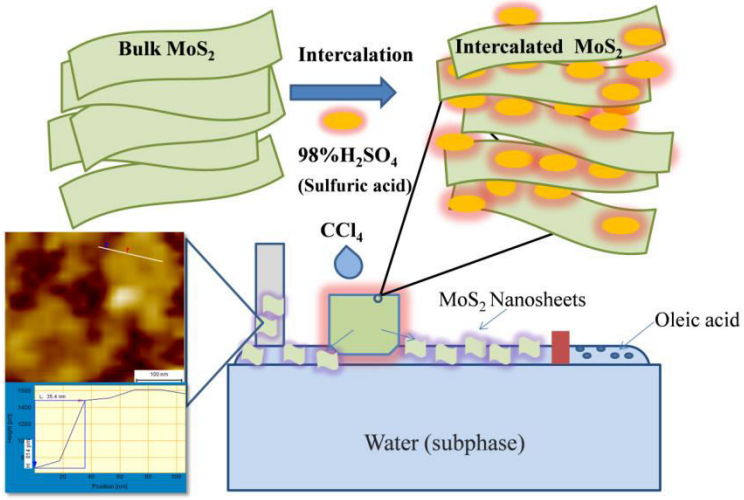

Figure 6.2. Schematic representation of MoS_2 thin layer formation.

Encouraged by this achievement, it was thought that semiconductor MoS_2 could be tried for the same underlying principle and if successful then claim that the underlying principle opens new avenues for research in energy conversion and storage.

Thus we developed a 'top down' method; using the same equipment used to grow graphene films reported earlier Chapter-1. The method is very similar in

principle (Figure 6.2) and practice to grow graphene layered thin films at liquid-liquid interface. It reports the formation of MoS_2 nanosheets in the form of thin films at room temperature at liquid-liquid interface, which can be suitably transferred on the substrates.

Furthermore, the resulting MoS_2nanosheetsfilm can be deposited on the surface of graphene nanosheets by Layer-by-Layer (LbL) assembly. Thus as-prepared MoS_2-graphene hybrid nanosheets not only prevent the agglomeration of graphene nanosheets but also restrict the growth of MoS_2 during LbL by the bond formed between MoS_2 nanosheets and graphene. Remarkably, the MoS_2-graphene hybrid demonstrates high capacity, superior rate capability and outstanding cycle life when evaluated as an anode material for super capacitor, showing a synergistic effect between MoS_2 nanosheets and graphene nanosheets.

Polyaniline (PANI)-Graphene, PANI-MoS_2 LbL composites for durable supercapacitors.

Development in conducting polymer research for in supercapacitor application has shown remarkable assurance due to their predisposition to form extremely porous films and reveal required reversible redox activity. Continuing progress in electrode performance demands new low cost materials that can assemble in composite structures and maintain transport pathways for the electrolyte and counter-ions. While the Faradic storage (redox activity) ultimately depends on the chemical structure of the polymer, the porosity and structure of the film determine EDLC contributions and fast scan-rate contribution (i.e. mass transport).

Recently, a great interest has been dedicated to the application of electronically conducting polymers (ECPs) in electrochemical capacitors because of its high specific capacitance to reach a maximum specific energy and power of the device. In this chapter we have given a method to form PANI thin film containing highly uniform film consisting of nanoparticulates of size in the range of 5 to15 nm by using modified LLIRT.

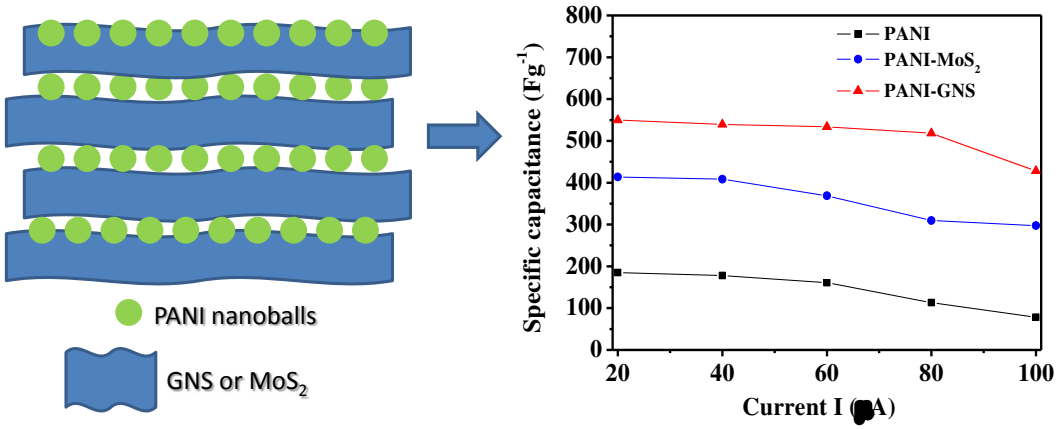

Figure 6.3. PANI/GNS and PANI/MoS_2 composite and relative specific capacitance.

The feature of applicability of LbL technique holds excellent the presently reported system of fabricating PANI-GNS and PANI-MoS_2 composite hybrid films with a well-defined architecture and tunable thickness on various substrates for applications such as supercapacitors (Figure 6.3). The obtained hybrid films having interconnected network prevented graphene sheets from stacking with one-another, thus assisting in the formation of nanocomposites. This is the proof of the concept of forming graphene semi-conductor composite by the reported technique and opens a new area for forming better capacitors. The CV results indicated good capacitive behavior for PANI-GNS nanocomposites. The excellent specific capacitance of 559 Fg^{-1} calculated from CV and 549.2 Fg^{-1} calculated from charge-discharge measurement and very good cycling stability is an indication that as-synthesized nanocomposite formed with the present technique is a potential candidate for super-capacitor application and in an energy storage technology in future. The excellent electrochemical performance of the composite as supercapacitor electrodes is due to the synergistic effects among the components in the composites.

Architecturally designed Pt-MoS_2 and Pt-graphene composites for electrocatalytic methanol oxidation.

Development of an efficient, low cost fuel cells (FC) is one of the most focused areas in current science research. FC's are used to convert chemical energy into electric energy. Methanol has several advantages including the simplicity of

transportation and storage and high theoretical energy density over hydrogen. The methanol oxidation electrochemical reaction occurs at the anode in direct methanol fuel cells (DMFCs). Pt electrode has a high activity toward the dissociative adsorption of methanol; therefore, most of the DMFC's use Pt electrode as an electrochemical catalyst.

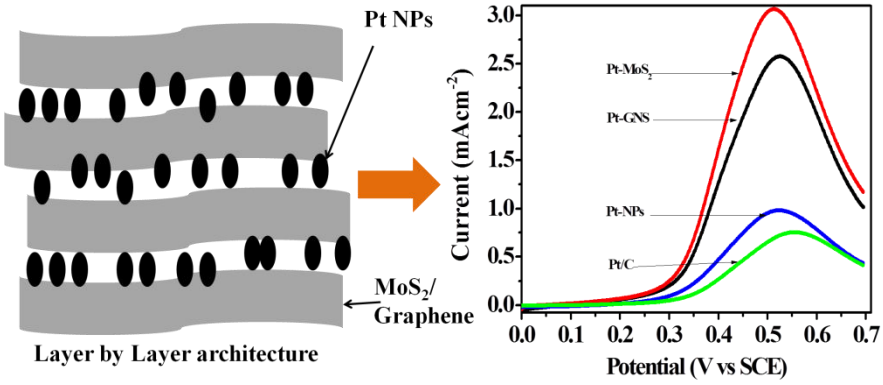

Figure 6.4. Pt-GNS and Pt-MoS_2 composite and its relative catalytic activity.

High cost of Pt metal necessitates its use at its highest efficiency. Therefore, the use of Pt nanoparticles, well dispersed on a suitable substrate or distributed in suitable matrix as electrochemical catalyst in FC is preferred. From the foregoing experience, it was thought that if one could have easy, inexpensive, one step and surfactant free method to grow Pt naoparticles on a substrate or a matrix consisting of Pt nanoparticles, then, it would be worth trying as electrochemical catalyst in FC. This background motivated us to develop a process of depositing Pt nanoparticulate film at liquid-liquid interface. Such a method is successfully developed during this thesis work.

These films could be directly transferred on the suitable substrates like glass slides, Si wafers, layered graphene/MoS_2, etc. Moreover, 'Pt' in these films is shown to be present mostly in zero oxidation state as is preferred for methanol FC catalyst application. We further demonstrate the use of layer-by layer (L-b-L) technique to make hybrid composites of Pt NPs on MoS_2/GNS with controllable deposition. This would prove a significant development for the formation of electrode for methanol FC. Further, we showed that the resulting composite films thus formed, are effective catalysts for methanol oxidation. Thus a method of formation of Pt thin film

consisting of particles of size in the range 1.5 to 2.5 nm and applying LbL technique (Figure 6.4), composite thin films namely Pt-MoS_2 and Pt-GNS are reported and used for electro-catalytic methanol oxidation. The suggested mechanism shows that MoS_2 and GNS not only act as a support to Pt NPs but also complement enhanced electro-catalytic activity of Pt by improving CO tolerance. The electrochemical tests show that the Pt NPs supported on MoS_2 and GNS have a higher catalytic activity than that of Pt/C. An important achievement in the present novel architectural design of the electrode is lower onset oxidation potential and maintaining best I_f/I_b ratio reported so far. It is observed that the present composites showed better stability for reuse in comparison to stability shown by commercial Pt-C catalyst. The presently reported method of formation of composites displayed improved electrocatalytic activity for methanol oxidation which can widen the scope of fuel cell electrode fabrication.

6.2 Future Prospects

The present thesis has wide potential impact in applied research, due to the unconventional use of interfaces through the development of unique methodologies to grow thin films of the nanomaterials which becomes responsible for the possible developments of devices and processes in applied research during the course of the research work.

Some of the key panoramas of the thesis are listed below. Although the current research activities on forming efficient electrode-electrolyte interface *via* 2-D hetero-structured materials as detailed in the thesis are restricted in applications to only supercapacitors and electrocatalysis, the observations, materials and methodologies would have wide impact and potential in other energy devices such as, fuel cells, Li-ion batteries photo electrochemical cells, sensors etc. 2-D confinement of GNS, MoS_2 and their association in a tandem are shown to have effect on surface area, conductivity, stability, etc. We believe this impact would be felt in its scenario for practical applications in other electrochemical devices such as a cathode material in Li-ion batteries and conductivity and humidity sensors. Such type of confinement can result in easier charge transport as proved in Chapter-2 and 3. However, more fundamental research is required to disentangle the synergic effect which helped in improving the Capacitance of the 2-D GNS/SnO_2 and 2D GNS-MoS_2 compared to the

individual materials. The methodologies used to make LbL supercapacitors with infiltrated polymer electrolyte can have potential applications in Li-ion battery as well. Especially, the polymer Li-ion battery is preferred over the liquid systems due to the safety issues. The strategy of usage of the porous electrode and intercalation of Li conducting polymer electrolyte can result in excellent efficiency and stability for the battery. Further, the method of thin films of conducting polymer PANI and 2D materials GNS and MoS_2 as showed in Chapter-4 can be utilized to various other group members of the polymers and 2D materials by LbL technique for energy applications. Especially, polypyrrole (PPy) and polythiophene (PT) have a potential or applications in the areas of fuel cells and supercapacitors. However, the architecture of the devices discussed in this work and the related background developments, we believe, throw light on the suitability of ionic dynamics of intercalation/de-intercalation as well as better stability on cycling in charge storage devices (supercapacitors) as one of the important contribution as described in Chapter 4.

Chapter 5 showed the potential application of a surfactant free method to grow Pt nanoparticles' film and its LbL composites having excellent catalytic activity towards a methanol oxidation. Such composites thin film on flexible substrate can have wide impact in various applications including photovoltaics, sensors, batteries etc. Further, enlarging the scope of method of growing thin films resulting from the 2D confinement to other materials will help to develop effective design strategies for nanomaterials to make use in various practical applications.

List of Publications

1) Facile room temperature methods for growing ultra thin films of graphene nanosheets, nanoparticulate tin oxide and preliminary assessment of graphene-tin oxide stacked layered composite structure for supercapacitor application.

S. Patil, V. Patil, S. Sathaye, K. Patil, *RSC Advances*, 2014, **4 (8)**, 4094.

2) Development of a novel method to grow MoS_2 mono/few-layer films and MoS_2-graphene hybrid films for supercapacitor applications.

S. Patil, A. Harle, S. Sathaye, K. Patil, *CrystEngComm*, 2014, **16 (47)**, 10845.

3) Architecturally Designed Pt-MoS_2 and Pt-Graphene Composites for Electrocatalytic Methanol Oxidation.

S. Patil, B. Anothumakkool, S. D. Sathaye and K. R. Patil , *Phys. Chem. Chem. Phys*., 2015, **17**, 26101.

4) Studies on morphology of polyaniline films formed at liquid–liquid and solid–liquid interfaces at 25 and 5 C, respectively, and effect of doping.

B. J. Waghmode, **S. H. Patil**, M. M. Jahagirdar, V. S. Patil, R. P. Waichal, D. D. Malkhede, S. D. Sathaye, K. R. Patil *Colloid and Polymer Science*, 2014, **292 (5)**, 1079.

5) A facile room temperature synthesis of ZnO nanoflower thin films grown at a solid–liquid interface.

A. H. Jadhav, **S. H. Patil**, S. D. Sathaye, K. R. Patil, *Journal of Materials Science*, 2014**, 49 (17)**, 5945.

6) A method to form semiconductor quantum dot (QD) thin films by igniting a flame at air–liquid interface: CdS and WO_3.

A. H. Jadhav, **S. H. Patil**, S. D. Sathaye, K. R. Patil, *Journal of colloid and interface science*, 2015, **439**, 121.

7) Spin Transport and Magnetic Correlation Parameters for Graphene-like Nanocarbon Sheets Doped with Nitrogen.

A. P. Alegaonkar, A. Kumar, **S. H. Patil**, K. R. Patil, S. K. Pardeshi, P. S. Alegaonkar ,The *Journal of Physical Chemistry C* , 2014, **117 (51),** 27105.

8) Solar photocatalytic degradation of methylene blue using doped TiO_2 nanoparticles.

R. R. Bhosale, S. R. Pujari, G.G. Muley, **S. H. Patil**, K. R. Patil, M. F. Shaikh, A. B. Gambhire, *Solar Energy*, 2014, **103**, 473.

9) Reduced Graphene Oxide Composite with Redoxible MnCo-oxide for p-cresol Oxidation using Molecular Oxygen.

A. Jha, **S. H. Patil**, A.P. C. Ribeiro, B. P. Solanki, C. N. A. Castro, K. R. Patil, A. Coronas and C. V. Rode, *Chem plus chem.*, 2015, **80(7)**, 1164.

10) Amelioration of excision wounds by topical application of green synthesized, formulated silver and gold nanoparticles in albino wistar rats.

S. Naraginti, P. L. Kumari, R. K. Das, A. Sivakumar, **S. H. Patil** and V. V. Andhalkar, *Materials Science and Engineering: C*, 2016, **62**, 293.

11) Polyaniline-Graphene and Polyaniline-MoS_2 LBL hybrid electrodes for durable supercapacitor.

S. H. Patil, B. J. Waghmode, A. H. Jadhav, I. Karbal, R. Gonnade, S. D. Sathaye, K. R. Patil ***Communicated***.

12) Novel process of assembly of Graphene-MnO_2 nano-3D-network/s composite gowned at Solid-Liquid interface for a promising supercapacitor.

S. Patil, A. Jadhav, B. Waghmode, R. Gonnade, S. Sathaye and K. Patil, ***Communicated***.

Conference Papers

1) Thermal Conductivity of Graphene based IoNANOFLUIDS

S. Patil, K. Patil, F. Reis, S. Vieira, S. M. S. Murshed, M. J. Lourenço, C. N. Castro. WLS-2013-Jan. CSIR-NCL, Pune-India.

2) Study of Anion effect and heat transfer properties of Ru-Ionanofluids

V. S. Patil, **S. H. Patil,** K. R. Patil, C.V. Rode, A. Coronas and C.N. Castro, Solar Absorption Refrigeration Systems Operating with Ionic Liquids, IIT-Madras, FEB-2014

Erratum